Title
Modeling the Cardiac Extracellular Matrix to Identify Age-specific Modulators of Cardiomyocyte Function

Author
Kauss, Mara Ariel

Publication Date
2020

Peer reviewed|Thesis/dissertation

Modeling the Cardiac Extracellular Matrix
to Identify Age-specific Modulators of Cardiomyocyte Function

by
Mara Ariel Kauss

DISSERTATION
Submitted in partial satisfaction of the requirements for degree of
DOCTOR OF PHILOSOPHY

in

Biomedical Sciences

in the

GRADUATE DIVISION
of the
UNIVERSITY OF CALIFORNIA, SAN FRANCISCO

Approved:

DocuSigned by:
Brian Black
BE1B184BD52347A...

Brian Black
Chair

DocuSigned by:
Todd C. McDevitt
DocuSigned by:
Deepak Srivastava
B06ED314924B4DE...

Todd C. McDevitt

Deepak Srivastava

Committee Members

Acknowledgements

I am incredibly fortunate to have completed my PhD at UCSF, at Gladstone, and in the McDevitt lab. Like many things, it takes a village, and there is an extensive community here whose support, encouragement and guidance made this degree possible.

I am especially grateful to my thesis advisor, Todd McDevitt, who is eternally generous about letting his trainees pursue the scientific avenues that excite them. He had faith in my project, and me, long before I did, and encouraged all of us to grow as leaders and community organizers. He has also established a lab culture that is one of the most connected and accepting I've ever experienced, which paved the way for a lot of personal growth during grad school, and set an example for the future. I am also grateful to Deepak Srivastava, who allowed me to share his resources and lab meetings, and benefit from the collective expertise of his lab. Beyond that, he has led by example to promote an unapologetically progressive and diverse community at Gladstone, which ensures us the bandwidth to make science our primary focus. Additionally, I want to thank Brian Black, who has provided years of scientific counsel with clarity and honesty that helped propel my research and my career path.

I also am very thankful for the other mentors who have helped guide me through this process. Hirdesh Uppal, my boss at Genentech, was the first mentor who really thought I was destined to succeed, and challenged me accordingly. His support changed the way I thought about myself as a scientist and a person, and I credit him with my acceptance to UCSF. I'm also grateful to the many UCSF mentors whose doors were always open, including Julie Sneddon and Po-Lin So. Julie's support and encouragement early on, and Po-Lin's frank and strategic discussions later, were so important to carving out my personal path through grad school. Additionally, one unexpected but invaluable mentor at Gladstone was Shannon Noonan. She was the best ally and enabler, no matter the context – science, activism, outreach, public speaking,

and professionalism. She also always called me on my shortcomings, which I appreciated most of all.

One of the most valuable aspects of graduate school has been the McDevitt lab itself. I'm not sure what exactly the secret ingredient is, but we have somehow amassed the most wonderful people who are all meme-savvy, rainbow-friendly kitchen gods with grade-A public speaking skills. I'm ashamed to admit that someone did end up barcoding cells before I left, but our (Lab Olympics, Halloween, Art Contest, etc.) record of awesomeness speaks for itself. Thank you to everyone who edited my endless drafts, watched practice talks, and cheered at the Grad Slam like it was a football game. Thank you, especially, to Tracy Hookway, for her mentorship and patience through my endless questions that could probably have been answered by re-reading Cardiac Fibroblast: Renaissance Cell. I also specifically want to thank Nik Mendoza for his flawless qPCR and never-ending Drag Race quotes, and Madelynn Whittaker for letting me cut my teeth as a mentor. To Ana Silva – long live the ECM! Thank you for dancing through our microscopy victories, and for generally brightening up our freezing cold bays with art and music. To Vaishaali Natarajan, I'm so grateful for your endless encouragement, dosas and chai, and those critical scope-room chats. I also want to thank Oriane Matthys, David Joy and Jasmine King for their time and support. Also, a special shout-out goes to my two benchmates, Serah Kang and Josh Zimmermann. So much living happens while we're in lab, and I owe them a very real thank you for making our bay pro-discussion, pro-sass, pro-politics, pro-representation, pro-sci-fi/fantasy, and generally accepting that sometimes feelings happen. To Serah, specifically, I am grateful for her thoughtful discussions on so (SO) many topics, for lending her voice to larger causes, and all those restorative boba runs.

Every single member of the McDevitt lab has made it the amazing place it is, and I'm honored to call you all lab family. I'm also grateful to the Zumba gang, Yvanka de Soysa, Bonnie Cole, and all the ladies of the Monthly Date Night for making time for fun and relaxation in between

the long lab hours. I know we are all navigating our own journeys – thank you for taking the time to listen to and share in mine. And lastly, I'm incredibly proud to be part of the LGBTQ+ Community Group, and am so appreciative for our members' willingness to speak out and push Gladstone forward.

Another separate, but essential, component of the last six years has been balancing out the weekends in lab with some non-science time to unwind. I want to thank the Half Pint Night crew for getting me through applications and the early years of grad school with monster sushi and DnD, despite continually thinking that I study fish cancer. And thank you to the Superfriends – Virginia, Sean, Greg, Lizzy and Darius – for normalizing the craziness of modern life, staying connected through a pandemic, and letting me practice my 3-Minute Thesis even when we were in the hot tub. I'm also so grateful to Jo Larsen for 11 years of transatlantic friendship and creativity. To Meg Tracz, our weekends to wine country have been a highlight of my time in SF – partially for Dutcher Crossing, but mostly because we can always pick up our friendship like no time has passed. And to Heli Ghandehari, BFF extraordinaire, taker of selfies since before it was cool – I'm not sure this is how we pictured adulting, but I couldn't have done it without you.

Most of all, I'm grateful for my Mom, Dad and brother, Noey. It's been a decade of growth for the Kauss-Andersons, each of us chipping away at our own (not-so-little) part, and I couldn't have completed mine without your steady support and love.

Contributions

Excerpts of the text from Chapters 1, 2, 3, 4, and 6 of this dissertation originally appeared in the following preprint:

M. A. Kauss, S. J. Rockwood, A. C. Silva, D. A. Joy, N. Mendoza-Camacho, M. N. Whittaker, Erica Stevenson, N. J. Krogan, D. L. Swaney, T. C. McDevitt. Cardiac Cell-Derived Matrices Impart Age-Specific Functional Properties to Human Cardiomyocytes. bioRxiv (2020).

doi: https://doi.org/10.1101/2020.07.31.231480

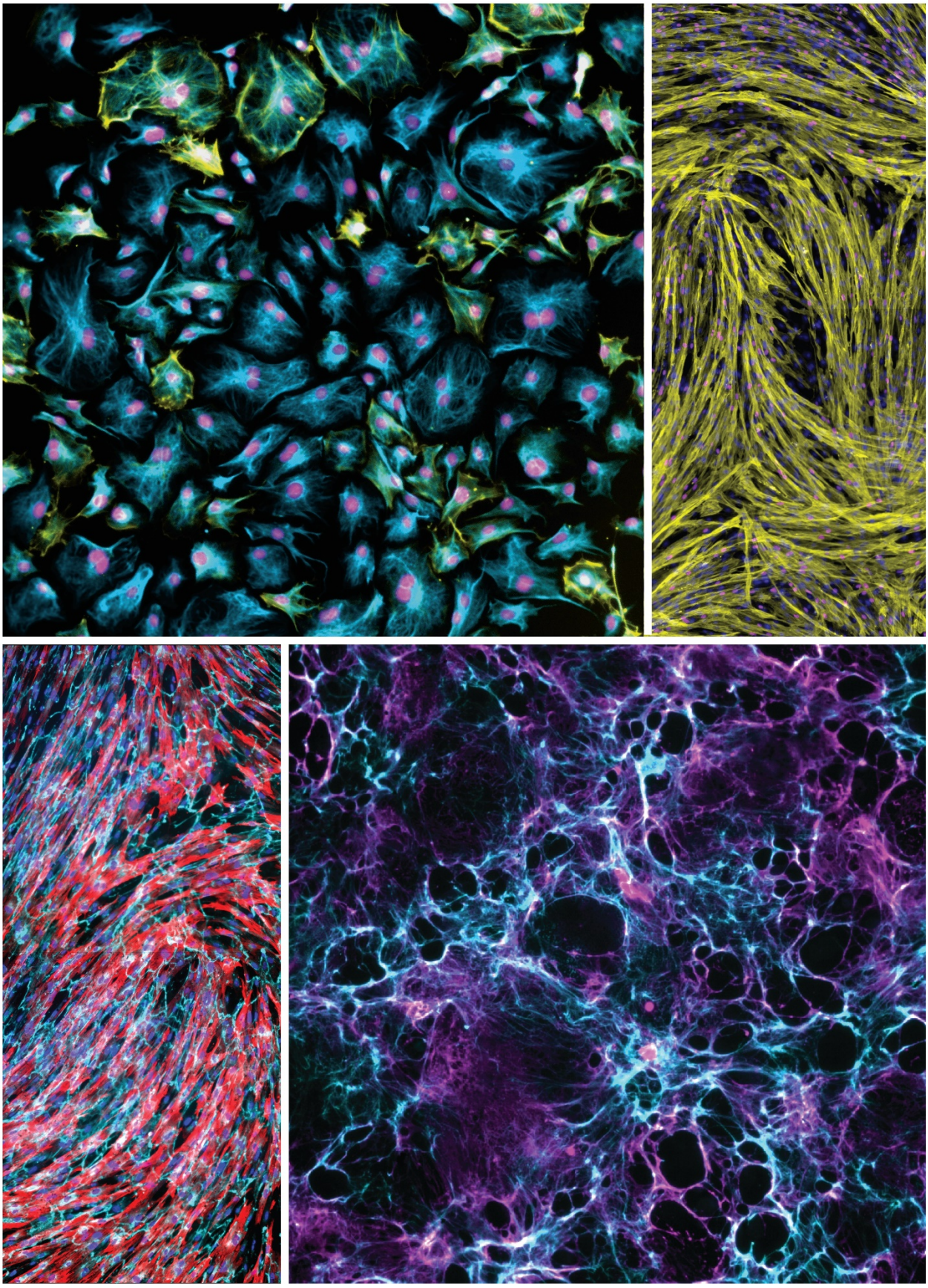

Modeling the Cardiac Extracellular Matrix

to Identify Age-specific Modulators of Cardiomyocyte Function

Mara Ariel Kauss

Abstract

The extracellular matrix (ECM) is a complex network of proteins that surrounds cells in all tissues, providing structural and biochemical cues that influence a multitude of cellular functions. In the heart, the ECM provides the local support and context for highly dynamic cardiomyocytes that are continuously contracting to pump blood throughout the body. However, the cardiac phenotype changes drastically throughout fetal development and postnatal maturation. Fetal cardiomyocytes are small, proliferative, glycolytic cells with disorganized sarcomeric structures. In the adult, however, cardiomyocytes become elongated, aligned, post-mitotic cells that rely on oxidative respiration and have highly organized sarcomeres. These ontogenic changes provide a dramatic increase in contractile efficiency, but sacrifice the heart's proliferation-dependent ability to regenerate after injury. As a result, heart disease is a major cause of death worldwide, and has warranted a wealth of research efforts to model cardiac tissue function and disease. During cardiac development and maturation, the ECM also undergoes age-dependent changes that can impact various cardiac functions, but the extent of its influence is poorly understood. To model the age-specific cardiac ECM in vitro, we created cell-derived matrices (CDMs) from cardiac fibroblasts to provide the structural, biophysical and chemical context of cardiac-specific ECM. In doing so, we sought to avoid certain caveats of established CDM protocols, which enhance matrix adhesion and thickness via introduction and promotion of singular matrix proteins, skewing the matrix composition, and confounding comparisons made between CDMs. We, therefore, developed a protocol that enhances matrix adhesion and deposition, respectively, by combining

an L-polydopamine coating and macromolecular crowding to produce CDMs composed of cell-produced ECM. This methodology was applied to the study of age-dependent phenotypic and functional changes observed in the heart by comparing the morphologic, metabolic and proliferative responses of cardiomyocytes to CDMs produced by fetal and adult cardiac fibroblasts. Additionally, mass spectrometry proteomics identified the enrichment of ECM proteins in fetal and adult CDMs, enabling loss-of-function studies via genetic silencing of enriched proteins during CDM production. Using this strategy, we identified collagen VI as necessary for maximal oxidative respiration in stem cell-derived cardiomyocytes, which is a key component of cardiomyocyte maturation. Furthermore, we conducted a screen of all age-specific enriched CDM proteins for their influence over DNA synthesis in cardiomyocytes, and found that laminin α2, plasmin-mediated signaling in fibroblasts, and fibrosis-associated proteins exerted inhibitory effects on proliferation. Overall, these results demonstrate the development and application of age-specific cardiac CDMs to dissecting the influence of ECM proteins on cardiomyocyte function.

Table of Contents

List of Figures

List of Tables

List of Abbreviations

αSMA - alpha-smooth muscle actin

BM - basement membrane

CDM - cell-derived matrix

CF - cardiac fibroblast

CM - cardiomyocyte

ColI - collagen

CsA - cyclosporin A

CSPG - chondroitin sulfate proteoglycan/Prolyl 3-Hydroxylase 1

CTGF - connective tissue growth factor/cellular communication network factor 2

dH_20 - deionized water

DMD - Duchenne's Muscular Dystrophy

DMSO - dimethyl sulfoxide

E(n) - embryonic day (n)

ECAR - extracellular acidification rate

ECM - extracellular matrix

FBS - fetal bovine serum

FN - fibronectin

GAG - glycosaminoglycan

HA - hyaluronic acid

Hu - human

IBAQ - Intensity Based Absolute Quantification

IGF - insulin-like growth factor

IGFBP - insulin-like growth factor binding protein

iPSC - induced pluripotent stem cell-derived

KD - knockdown

LAMA2 - laminin alpha 2

LAMA5 - laminin alpha 5

LOX - Lysyl oxidase

MEF - mouse embryonic fibroblast

MMC - macromolecular crowder

MMP - matrix metalloproteinase

MPTP - mitochondrial permeability transition pore

Ms - mouse

MS - mass spectrometry

NT - non-targeting

OCR - oxygen consumption rate

P(n) - postnatal day (n)

PBS - phosphate buffered saline

PenStrep - penicillin/streptomycin antibiotic

ROS - reactive oxygen species

RT - room temperature

SEM - scanning electron microscopy

TCP - tissue culture plastic

TGFβ - transforming growth factor beta

TGM2 - transglutaminase 2

tPA - tissue type plasminogen activator

uPA - urokinase plasminogen activator

Chapter 1. Introduction

The extracellular matrix (ECM) is a complex network of proteins that encases all cells, providing niche-specific physical and biological cues to each organ[1]. The heart, specifically, is an incredibly specialized organ that has evolved to efficiently meet high functional demands, but has lost the capacity to repair itself after acute or chronic injury. As a result, heart disease is a major cause of death worldwide[2]. However, prior to birth, mammalian hearts are able to regenerate after injury[3–6], and much of our understanding of cardiac repair mechanism and the maturation required for adult physiology are informed by comparative studies of fetal and adult hearts[3,7–9]. Of the many processes involved in this ontogenic shift, the ECM has been minimally explored. This thesis focusses on identifying aspects of fetal and adult cardiac function that are influenced by the ECM by modeling age-specific cardiac ECM *in vitro*.

1.1 Extracellular Matrix as a Regulator of Tissue Function

The (ECM) is the non-cellular component of all tissues that provides structural integrity and complex physiological cues that regulate developmental, homeostatic and pathological functions[1]. The ECM itself surrounds all cells as a bundled network of proteins, proteoglycans and polysaccharides that differ between tissues and across ages, thereby providing a context-dependent microenvironment to each tissue[10]. Among these ECM components are long, fibrillar proteins such as fibronectin (FN) and collagens (Col) that provide the foundation for the ECM[1,11,12], as well as proteoglycans[13]. Bound to these are smaller proteins such as morphogens[14,15] as well as glycosaminoglycans, a group of polysaccharides that are particularly abundant during morphogenesis[16,17], and bind numerous matrix components to modulate their functions and behavior[18–20]. The complex roles of the ECM in tissue biology can be categorized into three main functions: structure, adhesion and signaling, each of which are essential to tissue physiology.

The ECM is a largely fibrillar network of proteins bundled by precise interactions that make up both the interstitial tissue ECM[1,11] and basement membrane (BM)[1,21], each of which are characterized by specific matrix proteins. Interstitial matrix is present between cells, and is fundamentally composed of hydrated proteoglycans with minimal polarity, elastin, some collagens (I, III) and fibronectin[1,11,12]. The basement membrane, on the other hand, is produced by select cell types, and is specifically oriented lateral to the cell membrane[21,22]. In polarized cell types such and epithelium and endothelium, the BM is found on the basolateral surface[23]. However, both muscle and adipose cells produce BMs that are circumferential to each cell[21]. As a result, BM is found adjacent to the cell(s) it originated from, whereas interstitial matrix is produced and accessible to multiple cell types within a niche. Once deposited, these forms of ECM provide a structural basis for tissue organization, and must be degraded for any morphogenic or pathological alterations to tissue structure[24–27]. This continual deposition and removal of ECM is called remodeling, and reflects the homeostasis between ECM secretion/deposition and degradation by proteases including matrix metalloproteinases (MMPs), cathepsins and others[28,29]. The longevity of the ECM is also dictated by the extent of crosslinking between matrix proteins, which promotes the stability and stiffness of the ECM[12,30]. As a result, the half-life of individual matrix proteins can vary dramatically, from minutes[31] to years[32], and have long-standing effects on the tissue organization and function.

ECM proteins are essential for the adhesion of other ECM non-protein components and cells[1,11,21]. Fibronectin (FN), an exceptionally long glycoprotein, is one of the most widely expressed and adhesive ECM proteins[33]. Of its 32 domains, many regulate adhesion to itself, other matrix proteins including collagens and fibrin, and to heparin, each of which then bind to a multitude of other proteins and/or polysaccharides[34,35]. FN and collagens represent the basis of most interstitial matrices, and FN splice variants and collagen type has a large influence over which

additional ECM components are bound[34,36]. BMs, instead, are typically built on a foundation of Col IV and laminins, and provide adhesion for other BM-associated proteins[21–23].

Specific configurations of ECM proteins also play a large role in dictating cell adhesion. Cells primarily bind to the ECM via transmembrane receptors called integrins, which are heterodimers of non-covalently associated α and β subunits[37–39]. Specificity of cell adhesion to ECM proteins is determined by the combination of specific α/β dimer, of which there are 24 potential combinations in humans[38]. Another important adhesion unit is the dystroglycan complex, which binds the BM[40]. Importantly, both these adhesion complexes are comprised of transmembrane proteins that bind the ECM extracellularly and the cytoskeleton intracellularly[41,42]. The ECM-cytoskeleton interaction instructs several cellular processes that regulates cell morphology, stiffness, migration, mitosis, and multiple other functions[43–48].

The complex and niche-specific interaction of cells with their ECM microenvironment exert precise chemical and physical influences over a wide range of critical cell functions. FN is especially abundance during development, where its numerous binding domains promote enrichment for morphogenic molecules that influence cellular differentiation, migration and tissue formation[49–57]. However, FN is often replaced by collagens and laminins during adult homeostasis, which do not retain the same factors[58,59]. FN and the integrins that preferentially bind it, α5β1 are also associated binding dynamics that favor processing requiring cytoskeletal rearrangement such as migration and proliferation more than other ECM/integrin pairs[60–63]. Additionally, many potent signaling molecules bound to the ECM are regulated by other ECM properties, such as tension. For example, transforming growth factor β (TGFβ) is bound to the ECM in the form of a latent complex with its prodomain, and requires force exerted by integrins on a binding region within this prodomain to activate TGFβ[14]. Integrin clustering in response to matrix tension and binding domain availability has also been shown to augment local clustering of receptor tyrosine kinases, thereby recruiting these receptors to regions of the cell membrane held in close proximity to the

ECM and its bound signaling molecules[64–66]. A extensive list of signaling cascades respond to such cues originating from the ECM, including the Akt/PI3K, ERK, RhoA and Jnk pathways[67]. Another demonstration of the complexity inherent to these interactions is the mechanosensitive protein talin, which binds filamentous actin in focal adhesions at the intracellular domains of cell-matrix adhesions, and exhibits 14 different configurations dependent on the tension exerted at the cell membrane, thereby altering interactions with other intracellular proteins[68]. In these and related ways, ECM properties such as structure, composition and stiffness regulate signaling through membrane receptors and focal adhesions to influence a multitude of cell functions, including survival, proliferation, polarity, differentiation and migration.

These mechanisms of ECM-dependent cell behavior and signal transduction demonstrate the overt influence of the ECM over local tissue physiology and function. Modern analytical tools have improved our understanding of complex cell-ECM dynamics, but the numerous competing factors still necessitate the study of matrix-specific interactions within the context of specific tissues and stages of development.

1.2 Ontogenic Cardiac Function

The primary function of the heart is to pump oxygenated blood throughout the body. To do this, the heart contracts to expel blood from each of its four chambers in a coordinated, cyclical fashion, with enough force to delivery blood to the extremities[69]. This process is energy-intensive, and after birth the mammalian heart is subjected to heightened functional demands that necessitate significant adaptations in its contractile efficiency and responsiveness[70]. These adaptations arise through a number of characteristics that develop postnatally, including long, rod-shaped cardiomyocytes (CMs) with highly organized sarcomeres, which are the contractile unit of the CM

cytoskeleton, and metabolic efficiency driven by oxidative respiration[71]. However, these phenotypes are inversely correlated with the heart's ability to repair itself[3].

Insights into the ontogenic balance between maturation and regenerative capacity are available from comparative studies of fetal and adult mammalian hearts[3,4,72], and of non-mammalian vertebrates that retain this regenerative capacity into adulthood[8,73,74]. Fetal mice are capable of scarless repair after cardiac injury, though this ability wanes within the first 1-2 weeks after birth.[3,9] In humans this postnatal regenerative window lasts less than a year[75]. In non-mammalian vertebrates such as the zebrafish, the adult heart does not under undergo the same degree of maturation observed in mammals, and the regenerative capacity is never lost[74,76–78]. Comparative studies have demonstrated that this balance of repair and maturation occurs as a result of organism and tissue size[72,79,80], local oxygen concentrations[81,82] and metabolic substrate availability[70,83–86], among others[8,87–90].

The fundamental mechanism of cardiac regeneration is proliferation of pre-existing CMs[78] because, unlike many other tissues, the heart contains no resident stem cell or progenitor population[91,92]. During development, myocardial growth occurs by hyperplastic growth driven by CM proliferation, whereas postnatal growth occurs cellular hypertrophy with a concurrent loss of proliferative capacity[93]. CM proliferation is driven by multiple factors, including growth factors[90,94,95], regulators cell size[79,80] and the cell cycle[96,97], hormone signaling[8] and hypoxia[82,98]. As with all cells, this proliferative ability requires cytokinesis[3,99]. In many cell types, the synthesis of new DNA – an indicator of cells progressing through S phase of the cell cycle[100] – is used as a proxy for proliferation. However, in mice, mature CMs become multinucleated[6,101], decoupling the events of nuclear division (karyokinesis) with cytokinesis. Furthermore, mature human CMs often fail to progress through karyokinesis and become polyploid[99]. This is a potential indicator that while murine CMs experience inhibited cytokinesis, human CMs are inhibited at both karyokinesis and cytokinesis, although this has not been definitively demonstrated. Importantly, though,

induction of some fetal signaling in adult mice can rescue some of the regenerative capability[81,90,102], indicating the importance of fetal-specific processes and conditions to our understanding of CM proliferation and regeneration. Additionally, the balance between hyperplastic growth and functional efficiency represents a spectrum of CM behavior, and understanding both ends of that spectrum is crucial to dissecting the trade-offs between functional maturation and regenerative capacity.

A major regulator of CM size that has been linked to regenerative capacity is hippo signaling, which promotes cell and organ size[79,80]. The transcription factor YAP1, which drives CM proliferation, is present in fetal mouse hearts, but inactivated postnatally by hippo kinase signaling[7]. Additionally, heart size dictates certain dynamics during ischemic injury. In the presence of necrotic tissue that compromises myocardial integrity, the primary concern is hemorrhaging, which is handled differently depending on the size of an organism. The human heart beats 1-2 times per second – more in smaller vertebrates – and the hemorrhaging of blood from the contained chambers of the heart can lead to death long before there is time for any repair mechanisms. In small animals, this can be addressed fairly quickly by a blood clot[103], which may provide important signaling for cardiac regeneration[103], and prevents the loss of more blood. However, in adult mammals, blood clots may not be sufficient to stem the leak of blood, and the heart has developed adaptive processes to prevent hemorrhaging – specifically, activation of local stromal cells called cardiac fibroblasts (CFs) which proliferate and deposit collagen-rich ECM to patch the myocardium[104]. This occurs in both fetal and adult mice, though interestingly, in fetal/early neonatal mice this accumulation of ECM is resolved and replaced with functional myocardium, whereas in adults it develops into fibrotic tissue[105].

Cardiac regeneration and maturation is also dependent on oxygen saturation[82,98], as both zebrafish and fetal mammals exist in hypoxic conditions. Normoxic conditions promote aerobic respiration-mediated oxidative DNA damage via reactive oxygen species (ROS)[106], which inhibit

regenerative processes. Notably, though, acclimation of adult mice to hypoxic conditions is cardioprotective, and enables better repair after cardiac injury[81]. Normoxic conditions also contribute to the metabolic shift observed in adult mammals[70,107,108]. During embryogenesis and fetal development, glucose is a readily available substrate and the heart produces ATP via glycolysis, which occurs in the cytoplasm. After birth, there in a coordinated shift towards oxidative respiration that occurs in the mitochondria and heavily relies on oxidation of fatty acids. The normoxic oxygen tension present in adult physiology suppresses factors such as hypoxia inducible factor α, and consequently promotes the oxidative phosphorylation as the primary mechanism of ATP production[70]. This metabolic shift is also a response to availability of energy substrates, as glucose drops postnatally to be replaced primarily by fatty acids, as well as lactate and other substrates[84,86]. This shift from glycolysis to oxidative phosphorylation is crucial to the energy production and efficiency of the heart, as oxidative phosphorylation produces roughly 18 times more ATP than glycolysis[109].

During the ontogenic changes characteristic of cardiac development and maturation, the local ECM is also undergoing age-dependent shifts in composition and structure. The fetal cardiac ECM is loosely organized[110,111] and enriched with growth factors and GAGs[16,112] to support the developing myocardium and small, hyperplastic fetal CMs[58,59,113,114], whereas the adult ECM is a more fibrillar[110] and collagen-rich[115] environment intended to main homeostasis of aligned, energetically-demanding adult CMs undergoing significant contractile strain[84,116,117]. These collective changes are necessary for age-dependent cardiac functions, and understanding the reciprocal processes of regeneration and maturation are crucial to the design of effective cardiac tissue modeling and therapeutic strategies to address heart disease. The following sections will address the age-specific phenotypes and functions of CMs, and the role of the ECM in those processes.

1.3 Cardiomyocyte Morphology

CMs differentiation from induced pluripotent stem cells (iPSC-CMs) provide an *in vitro* model for the shifts in CM morphology and organization associated with the spectrum of maturity[118]. iPSC-CMs are naturally immature, and under standard culture conditions, iPSC-CMs that have been cultured for a year are only comparable to the maturity of fetal primary CMs[119]. There is ample evidence in tissue engineering and CM culture that the context and composition of the local ECM can dictate cell shape, orientation and function[120]. Immature fetal CMs are small and round, whereas mature adult CMs are large, rod-shaped cells organized parallel and end-to-end with other CMs to form highly-aligned myofibers[71,121]. Both developing and mature CMs contain sarcomeres – the cytoskeletal unit made up of actin and myosin, which generate contractile force by sliding along each other in an ATP- and calcium-dependent reaction[122]. Sarcomeres are also linked to the cell membrane and, thus, the ECM via specialized sarcomere/integrin complexes called costameres[123]. However, in fetal CMs these sarcomeres are disorganized, contain immature isoforms of some structural proteins, and do not produce contractions with much organized uniformity. In adult CMs, the sarcomeres are highly organized and regularly spaced parallel to the long width of the cell, producing uniaxial contractions that are directionally coordinated with adjacent CMs[124]. This unified axis of contraction is essential for ejection of blood from each of the heart's four chambers as efficiently as possible[125], and the high aspect ratio observed in adult CMs is associated with a greater contractile force generation than rounder cells typical of fetal hearts[126].

One of the primary factors determining mature CM function is their organization. Unlike fetal CMs, adult CMs are highly aligned, which promotes cell-cell adhesions that enable the synchronization of CM contractions. Specifically, mature CMs develop specialized adhesions between cells called intercalated discs that occur at the membrane of the short axis between longitudinally-adjacent CMs[127]. These structures contain gap junctions, which are comprised of connexins that allow the

passage of ions and small metabolites between CMs[128]. While immature CMs may express connexins, they are expressed circumferentially and not limited to distinct axes of the cells. Not only are the presence of gap junctions crucial for ion exchange and action potential propagation[129], but their diffuse localization can hinder the speed of signal propagation between CMs, and thus the coordination of CMs within the myocardium, as longitudinally localized gap junctions are expected to enable higher conduction velocities[130]. Intercalated discs also contain desmosomes and adhesion junctions, which anchor CMs to each other via transmembrane cadherins. These cadherins bind each other extracellularly and link to intermediate filaments of the cytoskeleton intracellularly[127]. The proteins involved in these junctions are not only important structural elements, but their presence is crucial for heart morphogenesis[131] and impacts transcriptional regulation of genes involved in contraction-related processes such as calcium cycling[132].

1.4 Cardiomyocyte Contraction Dynamics

The ECM is primarily implicated in CM contraction via its elasticity and stiffness[116,133], and in the disruption of cell-cell communication during excessive deposition associated with pathological conditions[134]. The ECM crosslinking prevalent in the adult heart leads to less compliant ECM, which can be perceived as stiffer substrates by the CMs. This enhanced stiffness in adulthood is further augmented by the isoform switching of the sarcomeric protein titin[135,136]. This increase in stiffness is correlated with increased force generation by CMs[126], although pathological stiffnesses are even higher and can impede CM function[137]. In cardiac tissue engineering, directional tension applied in microtissues from both physical (patterning), mechanical (stretching) and electrophysiological stimulation results in more aligned, more mature CMs[138–141]. However, the extent of the contributions of age-specific cardiac ECM to CM contractile properties has not been fully explored.

The electrophysiological properties of CM contractions also change with age, and are largely influenced by presence and abundance of ion channels that enable the flux of calcium, sodium and potassium in and out of the cell[125]. The propagation of electrical current termed the action potential triggers the opening L-type calcium channels on the cell membrane and the release of intracellular calcium from the sarcoplasmic reticulum that induces a rapid depolarization of the CM membrane[142]. This calcium binds the sarcomeric protein troponin C, enabling actin to slide along myosin, thus inducing the contraction of the cell[143]. Calcium channels then close, allowing repolarization of membrane, preparing the cell for to respond to future action potentials. There is an influx of sodium prior to the opening of the calcium channel, and an outflux of potassium during and after the calcium influx, that can mediate the speed of the depolarization and repolarization, respectively[144]. Together, these ions regulate dynamics of the action potential and CM contraction. The speed of the depolarization and repolarization phases, as well as the degree of ion influx into CMs, is associated with increased expression of ion channels and more mature CMs[125,145]. Fluorescent reporters of calcium flux into CMs, such as GCaMP, are a powerful tool to enable non-invasive assessments of calcium handling properties[146,147]. As calcium triggers the physical contraction of CMs, quantification of its dynamics can provide inferences about action potential dynamics[146].

1.5 Cardiomyocyte Proliferation

The loss of CM proliferation in adulthood is a primary driver of heart disease after an insult[9], though reactivation of fetal processes have been shown to rescue the proliferative ability. During development, CM proliferation is driven by multiple factors, including neuregulin[90], insulin-like growth factor 2 (IGF2) secreted by the adjacent epicardium[94,95] and hippo signaling[79,80], which regulates cell and tissue size, and hypoxia[82,98]. Additionally, the cytoskeleton is heavily implicated in CM cytokinesis, both in the fundamental mechanisms of mitosis and because it requires

disorganization of the sarcomeres that is sometimes associated with a 'de-differentiation' of CMs [74,148]. As the sarcomeres are linked to the ECM via integrins and the dystroglycan complex, ECM compliance of cytokinesis is a requirement for CM expansion[149–152].

The age-dependent contribution of the ECM to proliferative capacity has been demonstrated through the use of digested fetal, neonatal and adult cardiac ECM as a culture substrate for neonatal rat ventricular myocytes, which demonstrated increased expansion of CM number during culture on the fetal ECM[59,153]. Additionally, co-culture of mouse CMs and CFs revealed that fetal CFs secreted the matrix proteins FN and Col III, which promoted DNA synthesis in fetal CMs[114]. Over the duration of our own work, other groups have demonstrated that agrin, an fetal-enriched ECM protein associated with CM-matrix adhesions through the dystroglycan complex, is diminished in adulthood and can improve cardiac regeneration post-injury[102,154]. Additionally, another study has demonstrated the involvement of embryonic ECM proteins SLIT2 and nephronectin in enabling mitotic rounding in CMs, which is crucial to cytokinesis and promotes cardiac regeneration[155]. Both these findings highlight the role of CM-matrix adhesion dynamics as a fundamental ECM-derived influence on CM proliferation. However, both were performed with either digested or soluble matrix factors, which lack the structural context inherent to the ECM's influence on cell biology. Therefore, these studies definitively demonstrate the importance of the ECM in CM proliferation and regeneration, but also pose and open question about the possibility of additional, structure- or microenvironment-dependent ECM proteins the further influence CM proliferation.

1.6 Cardiomyocyte Metabolism

CMs undergo an age-dependent shift from glycolysis to oxidative respiration to utilize available energy substrates and enhance metabolic efficiency[85,86,125]. Oxidative respiration, but not

glycolysis, occurs in the mitochondria[156], and relative to fetal CMs, adult CMs contain dramatically increased mitochondrial numbers to meet energy demand[125]. Mitochondria are highly specialized double-membraned organelles that utilize oxygen and proton-derived membrane potential gradients to produce ATP. Metabolic shifts in cultured iPSC-CMs can be induced by altering the energy substrates, which can in turn promote other hallmarks of maturation[157,158]. However, CMs also respond to other strategies that promote maturation with an increase in oxidative respiration[138], demonstrating that maturation can be both the cause of, and responsive to, mechanisms of maturation.

While mitochondria do not directly interact with the ECM, deficiencies in the local ECM can induce metabolic dysfunction. This has been particularly demonstrated in skeletal muscle, where loss of the BM proteins Col VI and laminin α2 lead to muscular dystrophies characterized by reduced satellite cell proliferation and muscle regeneration[159], apoptosis and mitochondrial dysfunction[160,161]. Specifically, mitochondria exhibit decreased basal respiration, and a failure to reach the maximal respiration when exposed to stress. Although the skeletal muscle and cardiac tissues are both comprised of striated muscle and share numerous similarities in their physiology and disease pathologies, dystrophies induced by the loss of Col VI or laminin α2 do not demonstrate overt cardiac deficiencies. However, the direct influence of that ECM proteins on CM metabolic function has not been tested. There are other muscular dystrophies, however, that induce dysfunction in both skeletal muscle and cardiac tissue. Duchenne's muscular dystrophy (DMD) characterized by muscle weakness and dysfunction of the ventricle[162] – the cardiac chamber requiring the strongest contractions. DMD is caused by mutations in the protein dystrophin localized in the costamere, and was originally believed to be a metabolic disease based on its clinical presentation[163,164]. The involvement of these ECM and ECM-linked proteins underscore the role of cytoskeletal/ECM adhesion dynamics in proper cardiac function.

CM metabolism is inherently linked to maturation in *in vivo* and *in vitro* models, during which CM shape and contractility are both impacted. The ECM can both reinforce and destabilize the cell adhesions required to support ongoing contractile and metabolic demands. Additionally, it is currently unknown whether the loss of ECM proteins such as Col VI and laminin α2 directly impact CM physiology, and whether there are other age-specific ECM proteins that facilitate the shift towards adult metabolic respiration.

1.7 Cardiac Fibroblasts

CFs are the non-parenchymal cells that accompany CMs in the myocardium. They are derived from numerous cellular sources via epithelial-to-mesenchymal transition, primarily the pro-epicardium[165], though there is some evidence of CFs differentiated from the neural crest-derived endocardial cushion as well[166,167]. During injury and repair, fibroblasts become activated, and differentiate into myofibroblasts, which develop certain properties associated with smooth muscle, such as contractile behavior and expression of α-smooth muscle actin (αSMA)[168,169]. Lineage tracing studies have implicated myofibroblasts derived from several additional cell types, including epithelial cells and bone marrow, though these contributions are minor, at most, and have not been conclusively demonstrated[170]. A major confounding factor in the study of all fibroblasts is the lack of specific surface and intracellular markers, leaving the majority of CFs to be characterized by a concurrence of expressed proteins and their phenotypic and functional behavior. Primarily, CFs are associated with the production of ECM, both during development and pathological remodeling[104]. They produce the majority of non-basement membrane ECM in the heart[171], and this ECM profile changes with age and myocardial health[59,172].

Within the myocardium, CFs are abundant, but small, and every CM is believed to be in contact with at least one CF[166]. Not only do CFs contribute to myocardial structure via their ECM

deposition/maintenance, but they exhibit mechanical properties and stretch-dependent signaling that exerts a paracrine influence on surrounding CMs[173]. Unlike CMs, CFs do not become depolarized or exhibit action potentials; however, they do express ion channels and can function as transducers or as resistance between CMs[173], and their deposited ECM is capable of disrupting CM coupling, leading to arrythmias[134]. CFs also secrete numerous paracrine molecules that can influence CM proliferation[114], protein expression[174] and conductivity[175]. Thus, CFs are a dynamic and influence contributor to myocardial homeostasis.

1.8 Heart Fibrosis

Cardiac ECM is most commonly associated with its clinical presentation in heart disease, particularly in fibrosis[134,176]. Fibrosis is initiated by the activation of myofibroblasts which become highly proliferative, contractile, and deposit crosslink an excess of collagen-rich ECM[177,178]. In the heart, fibrosis can occur after acute injuries, such as myocardial infarctions, and chronic conditions, such as hypertension. If unchecked, the excessive expansion of CFs and their matrix production can interfere with the signaling and the deformability of the heart, inducing arrythmias and reducing the ejection fraction, or ratio of blood expelled from an individual heart chamber during contraction. Over time, these impaired functions lead to compensatory hypertrophy which results in the thickening of the myocardium, high blood pressure, and can eventually develop into heart failure[179].

CF-derived ECM is a necessary component of myocardial function under developmental and homeostatic conditions, and it is only once they are activated that this can become problematic[168,179]. However, CF expansion and matrix deposition is also an adaptive response[105], to replace myocardial tissue that has been damaged, and it is the failure to resolve this phenotype post-injury that poses the largest threat to cardiac function. Fibrosis and myofibroblasts are

canonically associated with TGFβ-signaling,[180] and the degradation of ECM and reversion back to the physiological fibroblast state is associated with the expression of MMPs and other matrix proteases. The most common collagens observed in fibrotic matrices are I and III, although those are also the types most commonly assayed, and other collagens present include Col IV and VI[172]. Therapeutic inhibitors of fibrosis exists, and largely target the myoactivation of fibroblasts to revert their phenotype, including TGFβ and PDGFRα[169,181,182], though this only halts the progression of fibrosis and does not mediate the existing ECM composition or the extent of its crosslinking. The presence of individual ECM proteins[183] and ECM protein subunits[184,185] can also mediate the severity of fibrosis. Thus, understanding the compositional and structural differences between physiological and fibrotic CF-derived ECM may provide the opportunity to address fibrosis via new mechanisms.

1.9 Traditional Models of the ECM

The complex biochemical and physical influences of the ECM significantly impact tissue function[1,186] that are sometimes apparent in tissue-level histological assessment and sometimes require more detailed investigation to detect. ECM proteins especially essential for tissue morphogenesis and integrity[50,186,187] – this has been demonstrated in animal studies containing global deletions of matrix proteins, many of which have proven to be embryonic lethal[50]. Such studies have identified the roles of numerous cardiac ECM proteins in cardiac development[50,58,188], including the necessity of FN for cardiac progenitor migration and heart tube fusion[189,190]. However, because production of matrix proteins is not often restricted to individual cell types, *in vivo* knock out and reporter studies often observe phenotypes arising from multiple cell lineages. CFs are frequently genetically labeled by expression of either COL1A1, TCF21 or periostin, which are not mutually exclusive to CFs or individual lineages[104,166,191]. Additionally, *in vivo* studies

subject all cell types to local matrix conditions, and preclude the ability to vary matrix conditions without impact all local cells.

In vitro experiments provide the flexibility lacking from *in vivo* experiments, and facilitate mechanistic studies of individual cell types. Monolayer cell culture systems often rely on ECM molecules as an adhesive for culture applications[192], and de-emphasize their influence as tissue-specific environmental cues. Many of the commonly used matrix coatings are comprised of individual, often recombinant, proteins[56], and others, such as Matrigel, have tumorigenic origins and offer no tissue specificity[193]. Additionally, monolayer culture is an inherently polarized system, with the cells exposed to ECM only basolaterally.

Some studies have adopted a simplistic approach to modelling the ECM, treating it primarily as a scaffold, but providing the three-dimensional structure typical of native tissues. In these applications, individual proteins such as Col I or fibrin[194], peptide fragment containing integrin binding domains[195], or Matrigel, are crosslinked into a hydrogel into which cells can be embedded[196]. This provide matrix proteins circumferentially, providing binding domains for integrins in all directions and promoting a more tissue-like adhesion profile[197]. However, in these configurations the matrix proteins predominantly serve the purpose of anchoring cells via integrin binding, and rely on cell-cell adhesions and *de novo* matrix production for a more niche-specific ECM composition.

A common approach to provide physiological ECM context *ex vivo* is the isolation of ECM from primary tissue. In these approaches, tissue sections are isolated by destabilizing and removing cellular components through a mixture of membrane bursting and detergents, following by a DNase treatment to remove nucleic acids[198,199]. Decellularized tissue has been used for numerous therapeutic purposes[200,201], and for the study of cell-ECM interactions[202]. In the latter case, the decellularized ECM provides a compositionally and structurally complex, tissue-specific scaffold for analysis, or the subsequent seeding of the desired cell type. These studies have been

informative in determining the response of cells to specific ECM composition[203], but have often been hindered by the tendency for reseeded cells to remodel the ECM, and have necessitated specialized methods of cell delivery[204,205]. As a result, these studies can sometimes be more informative regarding the influence of the cells on the ECM than of the ECM on the cells[110].

A more popular method of utilizing primary tissue ECM is to decellularize disrupt it, either by mechanical processing or enzymatic digestion, and potentially solubilizing it[202]. This creates a more homogenous and flexible matrix substance that can be adsorbed onto tissue culture plates for subsequent cell culture[59], added directly into culture media[102], or even injected into tissues[202,206,207], often promoting regenerative effects[208]. These methodologies have been incredibly useful in determining the interactions of cells with solubilized matrix proteins, and have been instrumental to identifying the ability of the fetal cardiac ECM[59] and its components[102] to promote CM proliferation. Although these applications have relied on destruction of ECM structure, they have provided invaluable information about cell-ECM behavior. However, the structure associated with the fibrillar, or insoluble, forms of ECM proteins have been shown to have unique properties[209,210], and the study of cell-ECM interactions in the context of physiological matrix structure may provide even further information about the influence of tissue-specific ECM over cellular function.

1.10 Cell-Derived Matrices

One ECM model that has emerged as a tractable *in vitro* model of the ECM is the use of cell-derived matrices (CDMs), which provide the complex composition of tissue-derived ECM as well as the efficient throughput of simple hydrogels. CDMs are comprised of the matrix produced by stromal cells from the tissue of interest[211,212], which produce a large proportion of interstitial ECM[171], and are then decellularized as is done for tissue-derived ECM. This methodology

preserves both the composition and the structure of the matrix produced *in vitro*. The source, age, and genetic background of the cells can be manipulated to tailor CDM properties to model specific tissue systems and address biological questions. Additionally, CDMs are an exceptionally flexible platform to model ECM because they are adaptable to a variety of culture formats, are highly amenable to genetic perturbation, and limit the paracrine influence of matrix-producing cells on additional cell types.

However, current methods for CDM matrix production and decellularization present caveats that limit CDM fidelity to natively produced ECM, with unknown influences on subsequent cell biology studies. Many protocols aim to improve the durability of ECM by promoting adhesion with pre-adsorbed and/or crosslinked matrix components, such as gelatin (denatured collagen) or fibronectin (FN)[211,213,214], and increasing matrix assembly and thickness by promoting Col I synthesis and secretion[212,213]. These types of approaches perturb the endogenous ECM composition by artificially increasing individual matrix proteins, sometimes to supraphysiological levels. Additionally, after ECM deposition, the method of decellularization can impact the composition and structure of the isolated matrix. Decellularization of tissues and CDMs often relies on the use of surfactants, such as SDS or Triton-X[211,213–215], which strip away a large fraction of the growth factors, proteoglycans and glycosaminoglycans (GAGs) that are non-covalently bound to the matrix[198], thereby significantly changing the relative composition of the ECM that had been produced. In addition, SDS has been shown to alter the stiffness and structure of collagens in decellularized tissues[216]. Thus, the susceptibility of CDMs to protocol-specific biases necessitates the need for careful methodological consideration in comparative matrix studies.

1.11 Approach

The role of the cardiac ECM in cardiac physiology and function is relatively unexplored, particularly as it pertains to the ontogenic shift undertaken by CMs to mature from disorganized, proliferative, glycolytic cells to efficiently contractile, post-mitotic cells utilizing oxidative respiration. The following studies aimed to model the age-specific cardiac ECM such that it was applicable to the study of CM morphology, metabolism and proliferation. To do so, we devised an improved strategy of CDM production from fetal and adult CFs that did not rely on exogenous matrix proteins, either as an adhesive substrate or as a culture media supplement, and preserved age-specific matrix structure. We then profiled the transcriptomic and proteomic composition of the CDMs by unbiased analyses, enabling the study of CM-ECM interactions in a defined system. Using this system, we characterized the morphology, contractility, metabolism and proliferation of cultured CMs in response to age-specific cardiac CDMs, and leveraged our knowledge of the CDM composition to selectively perturb individual matrix proteins. This enabled the mechanistic investigation into the functional CM responses to matrix composition in a structurally complex, tissue-like ECM environment.

These studies demonstrated the application of new and specialized CDM model to the interrogation of the ECM's influence over ontogenic cardiac function. Further, it emphasizes the importance of dissecting matrix biology in tissue- and age-specific contexts, and provides a model of tissue-specific niches for the interrogation of complex cell-matrix biology.

Chapter 2. Development of Unbiased Age- and Tissue-Specific Cell-Derived Matrices

The ECM represents a necessary and highly influential aspect of each tissue-specific niche. Not only does it maintain structural integrity and morphological context for all cells, it also mediates signaling that can have profound effects on cell migration, proliferation and metabolism[1,11,59]. It is also a dynamic component of tissue function – its components are not static over time, but constantly undergoing deposition and remodeling reflective of a tissue's developmental and disease state[58,59]. These conditions can be hard to define *in vivo*, and are often inferred from transcriptomic profiling. However, matrix proteins have incredibly variable half-lives, ranging from minutes[31] to years[32], which are not always reflected by transcript abundance. Proteomic profiling provides a more accurate depiction of matrix protein content, but relies heavily on dissection of *in vivo* tissue and the production of animal strains or pathological/pharmacological models, which are often hampered by issues of embryonic lethality, loss of structural integrity or confounding paracrine signaling[58].

We aimed to model the cardiac ECM *in vitro* to facilitate investigation of matrix chemical and structural properties at multiple developmental stages, and their influence on CM behavior. CMs undergo incredibly drastic shifts in almost all cell functions, including morphology, proliferation, metabolism, force production, regeneration and disease progression[58,172,186]. The ECM has been implicated in several of these processes from studies of tissue-derived matrix[102,178,183] but is, thus far, relatively understudied.

To model the cardiac ECM, we produced CDMs via culture of primary CFs, which synthesize and organize the majority of the ECM in the heart[171]. CDMs require successful matrix production and adhesion through decellularization and, to our knowledge, there were no pre-existing protocols for cardiac-specific CDMs. Additionally, in order to faithfully recapitulate fetal and adult matrices

and preserve the differences between them, we sought to avoid any methodology that would introduce compositional bias, such as the addition of L-ascorbic acid to promote matrix thickness specifically by collagen deposition[212,213], or the pre-coating of tissue culture surfaces with gelatin or fibronectin and the artificial crosslinking process to which they are often subjected[211,213,214]. Here, we present the development, optimization and characterization of *in vitro* cardiac CDMs derived from fetal and adult, mouse and human fibroblasts for the *in vitro* study of niche-specific cardiac ECM.

2.1 L-polydopamine

During optimization of the CDM production, each cell type was seeded at confluence and cultured for 10 days prior to decellularization. For the optimization phase of CDM retention testing, mouse embryonic fibroblasts (MEFs) were used, because of their ability to grow quickly and to high passage number. Initial attempts to decellularize CDMs cultured on tissue culture plastic (TCP) without any prior matrix coating invariable lead to matrix detachment, as the cells would respond to the initial steps of the decellularization process by contracting with enough force to detach the matrix from the plate (**Fig. 2.1A**). During subsequent efforts to optimize other aspects of the CDM decellularization, fibroblasts were cultured on gelatin-coated TCP, without any crosslinking. Though this enabled matrix retention through a salt-based decellularization[199] (**Fig. 2.1B**), CDMs still detached an appreciable amount of the time (estimated 30-50%), particularly on glass, necessitating better methods to anchor the matrix.

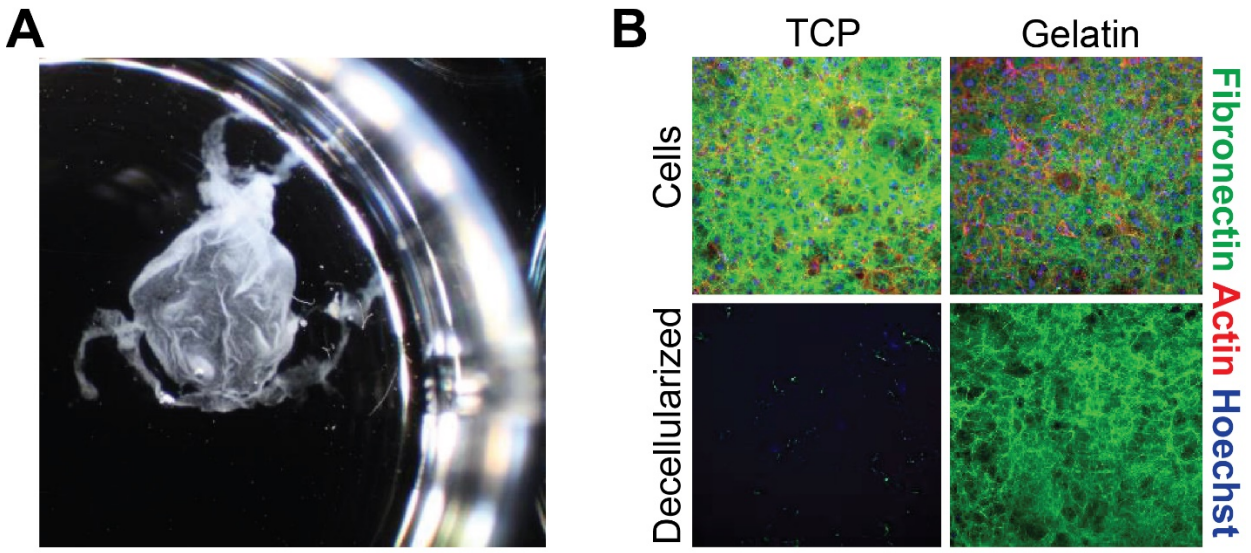

Fig. 2.1 CDM detachment. A) Detached layer of mouse embryonic fibroblasts (MEFs) in a 24 well plate during de-cellularization. B) Decellularization of MEFs on uncoated tissue culture plastic (TCP) and Gelatin-coated TCP.

L-polydopamine (dopa) is an inert biomolecule containing both catechol and amine functional groups which, together, promote adhesion on a wide spectrum of materials[217–219]. This functionality was discovered in the lab of a collaborator, Phil Messersmith, but had not yet applied to living cells. With the help of the Messersmith lab, we explored whether dopa-coated TCP could sustain cultured cells and promote matrix retention during decellularization. Dopa was solubilized in a solution of 100mM Bicine, pH 8.5 (a pH typical of marine environments[218]), added to standard plastic tissue culture plates at volumes sufficient to cover the wells, and incubated at room temperature (RT) overnight with agitation. Well were then washed sufficiently with deionized water (dH_20), allowed to dry, and sterilized by UV for 30 minutes (for more detail, see Ch. 2 Materials and Methods). Dopa solutions are initially clear, but quickly oxidize and turn a dark brown (**Fig. 2.2A left**), and high concentrations leave a residue on the TCP (**Fig. 2.2**A left, 2**.2B**).

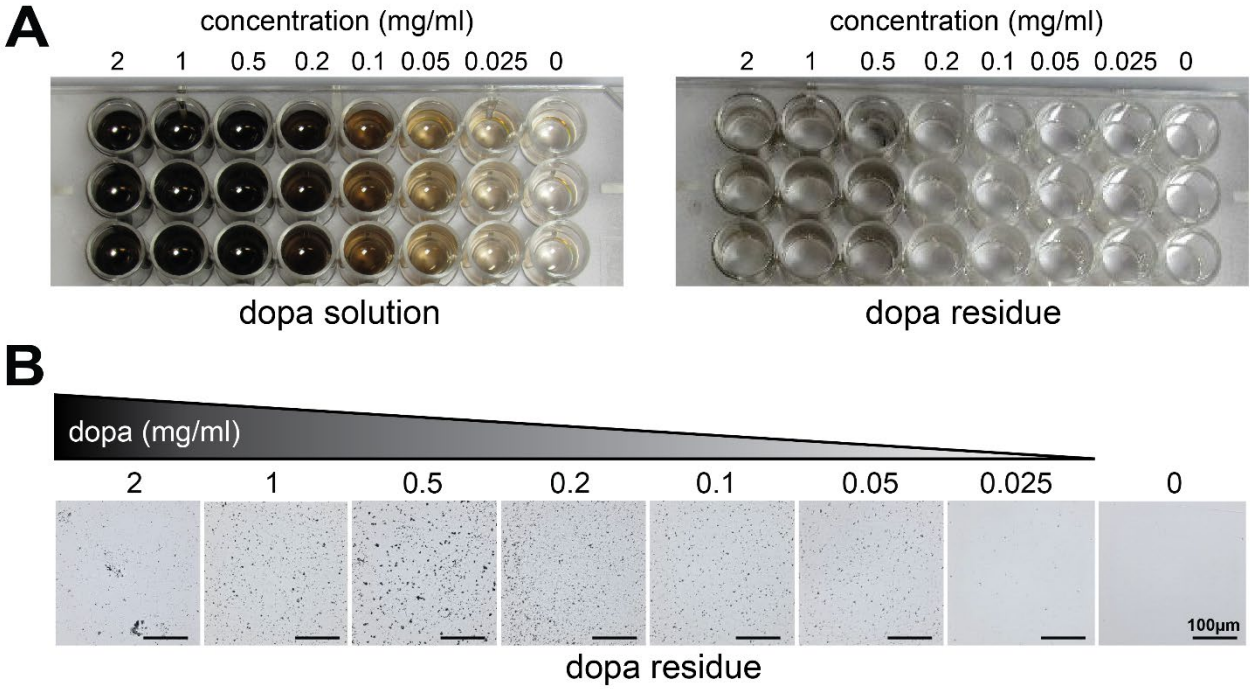

Fig. 2.2 L-polydopamine concentration curve. A) L-polydopamine solution (left) during plate coating oxidizes to form a concentration-dependent brown color. After washing, a residue is visibly left by high concentrations of dopa (right). B) L-polydopamine residue post-coating observed at high magnification.

In the context of CDM production, dopa coatings at multiple concentrations were tested for their abilty to support cell culture and retain ECM during decellularization with gentle, detergent-free salt-based methodology that relied on cycles of hypotonic bursting[199] (**Fig. 2.3A**). MEFs cultured easily and deposited matrix on dopa coatings of all concentrations. However, at dopa concentrations of 0.2mg/ml and below, matrix layers would become untethered at various positions – largely the edges, where cells likely exhibit anisotropic strain – and would detach. The matrix layers would then 'crumple' together, as a rubber band snapping, and would result in sheets of matrix with low tension loosely floating in the media. The higher concentrations tested – 2, 1 and 0.5 mg/ml – all retained CDMs produced on TCP through decellularization in fully-attached layers. Repeating this experiment with MEFs cultured on glass surfaces yielded similar results

(**Fig. 2.3B**). There were other substrates under investigation for adhesive properties by the Messersmith lab (tannic acid, pyrogallol, galic acid), that we tested for the retention of CDMs, but at the tested doses of 1 and 2 mg/ml, they were unable to retain CDMs (**Fig. 2.3C**).

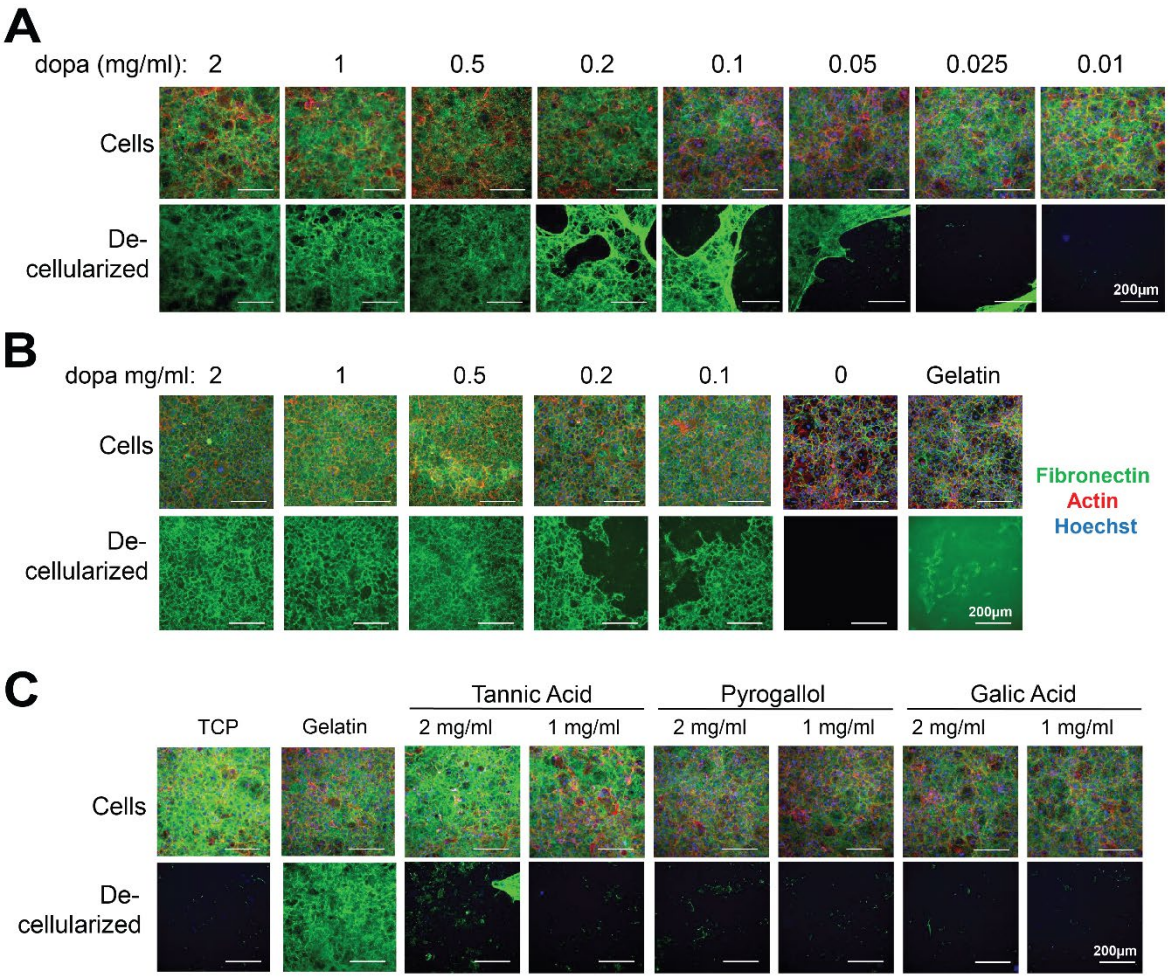

Fig. 2.3 CDM adhesion of culture surfaces and adhesive polymers. Fixed and decellularized MEF-derived CDMs on A) dopa-coated TCP and B) dopa-coated glass, and C) multiple adhesive polymers coating TCP.

The dopa concentration of 2mg/ml was selected for all future studies, because it maintained CDM adherence and initial testing indicated it left fewer dopa particulates on the tissue culture surface. The dopa particulates left behind were very dark and absorbed light during fluoresent imaging. As a result, images on dopa-coated plates were sometimes dimmer than on uncoated-plates, and

high magnification microscopy often included regions obscured by dopa preventing light transmission. Additionally, although the use of the salt-based decellularization method was used as a standard throughout all future studies, 2mg/ml dopa did retain matrices throughout classical detergent based decellularizations withTriton X-100- and SDS- as well[220].

2.2 Macromolecular Crowders

An existing method to enhance matrix production without ascorbic acid is the introduction of macromolecular crowders (MMCs) into the culture media of stromal cells[221–225]. MMCs provide steric and electrostatic hinderance to other molecules within a solution, thereby lowering the effective volume and increasing the effective concentration of all solutes. Along with the increase in perceived concentration, MMCs are also believed to reinforce the proximity of solutes (such as secreted growth factors or matrix proteins) to the cell membrane, as opposed to their typical diffusion through the full height of the culture media. This enhances signaling driven from molecules in solution, as well as an incorporation of secreted matrix proteins into the deposited and organized ECM. The primary MMCs investigated have been 37.5mg/ml 70 kDa Ficoll (Ficoll 70) and 25mg/ml 400kDa Ficoll (Ficoll 400), or a combination of both, 0.1mg/ml 500kDa dextran sulfate, and 0.1mg/ml 200 kDa polysodium-4-styrene sulfonate (polystyrene)[221–225]. Some sources have indicated that negatively charged MMCs have an advantageous effect on matrix deposition[222]; of these, dextran is negatively charged and Ficoll and polystyrene are neutral. The efficacy of these molecules as MMCs have been primarily investigated in fibroblasts of different origins[221,222,224,226] and mesenchymal stem cells[222,223,225], the latter of which are poorly defined but are potentially multipotent and often osteogenic, and largely in the presence of serum. Additionally, only minimal matrix parameters have been explored as a consequence of MMCs, and are typically limited to the presence/amount of collagens[221–225], fibronectin[221–224], GAGs[224,225],

and cell alignment[223], although some more recent studies have expanded to rheology, Raman spectroscopy and MMP quantification[227].

Dextran, polystyrene, and mixed Ficoll 70/Ficoll 400 were first tested on isolate primary murine CFs at the concentrations listed above (**Fig. 2.4A**). After 10 days of culture, cultures were fixed and immunolabeled for FN (green). Both dextran and polystyrene exhibited cytotoxicity at the doses tested, and although this may be addressed via dose testing and optimization, they were not pursued further. The Ficoll mixture (Ficoll 70/400), however, did promote a visible increase in FN deposition without evident cytotoxicity. Testing on human adult CFs also revealed comparable results of cytotoxicity with polystyrene and dextran MMCs, and good matrix coverage with the addition of Ficoll (**Fig. 2.4B**).

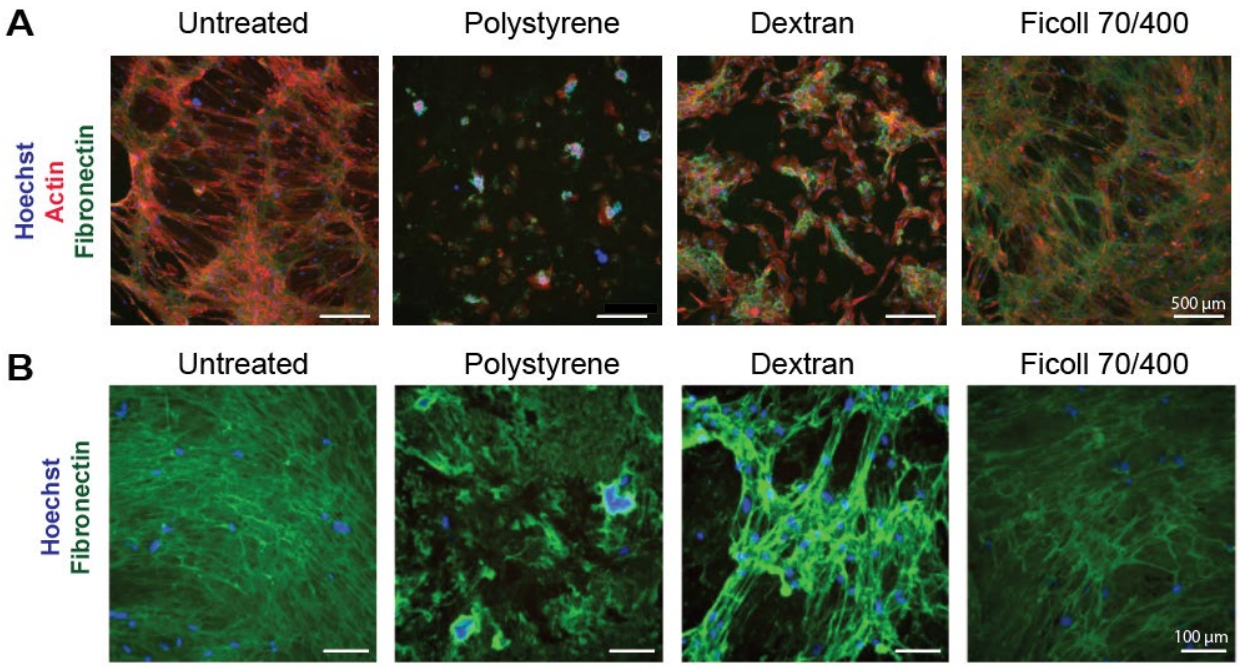

Figure 2.4 Matrix production with MMCs. Immunolabeling of adult (A) murine CFs (B) human CFs cultured for 10 days with MMCs. Fibronectin (green), actin (red) and nuclei (Hoechst, blue).

Thus, Ficoll 70/400 was established to be the only MMC tested capable of promoting matrix deposition without cytotoxicity, and has been commonly used in the field of matrix biology. For these reasons, Ficoll 70/400 was used as the MMC in all future studies. In combination with the

dopa pre-coating, Ficoll 70/400 enabled the production of thicker CDMs that were retained through decellularization (**Fig. 2.5A**). The method to produce CDMs was then standardized as follows, and is summarized in **Figure 2.5B**:

1) Coat tissue culture surface in 2mg/ml dopa in 100mM Bicine solution, pH 8.5
2) Rinse, dry and UV sterilize plate
3) Seed CFs at confluence and incubate overnight to allow attachment
4) Culture in DMEM + 10% FBS + PenStrep + 37.5mg/ml Ficoll 70 + 25mg/ml Ficoll 400
5) Refresh media with Ficoll 70/400 for 10 days of total culture time
6) Decellularize with 2 rounds of: 2X dH_20 rinse, 0.6M KCl (1hr), 1M KI (1hr)
7) Remove nucleic acids with 50U/ml DNase I
8) Store overnight at 4°C in $PBS^{(+/+)}$ + PenStrep + 1µl/ml Fungizone
9) Rinse 2X PBS
10) Seed subsequent cells (CMs) for testing, or fix in 4% paraformaldehyde for analysis

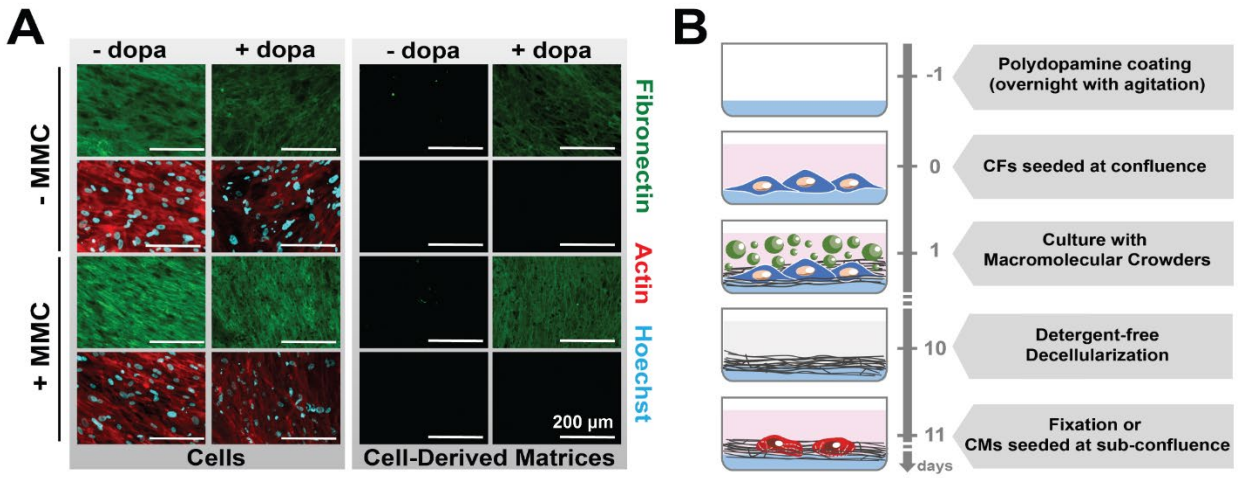

Fig. 2.5 Overview of CDM methodology. A) Successful isolation of CDMs with dopa and MMCs, visualized via fibronectin (green), actin (red) and DNA (Hoechst, blue). B) Summary of CDM production.

2.3 Impact of Ficoll as a Macromolecular Crowder on CFs and CDMs

Despite Ficoll's ability to promote CDM thickness and coverage, it was unknown what potential influence this MMC may have on CFs biology and resulting CDMs. To address this, we investigated a number of pertinent parameters. Ficoll molecules are small enough to be endocytosed, thus raising concerns about their impact on cellular function during CDM production. Examination by Zeigler, et al. observed only a minor uptake of Ficoll 70 and Ficoll 400 by MSCs, and that Ficoll molecules were retained within vesicles and not released to into the cytoplasm[223], thus remaining restricted from cellular processes. They further hypothesize that the cytoplasm is already so crowded, that the influx of Ficoll will not change intracellular pressure or density. To leverage these observations, we approached the question of whether molecules taken up by CFs would remain in the CDMs post-decellularization. Ficoll diameters are reported to be 4-14nm, which we modeled with the addition of 20nm fluorescent polystyrene beads (FluoSpheres Carboxylate-Modified Microspheres) to murine CF culture. While the beads were clearly taken up by CF (**Fig. 2.6**), all traces of fluorescent beads were removed with salt-based decellularization methods used throughout this thesis. Though this method of modeling Ficoll with polystyrene beads is not without caveats – largely the difference in charge, and the branched nature of Ficoll molecules, as opposed to uniform beads – it demonstrates that molecules endocytosed by CFs will be removed during decellularization,

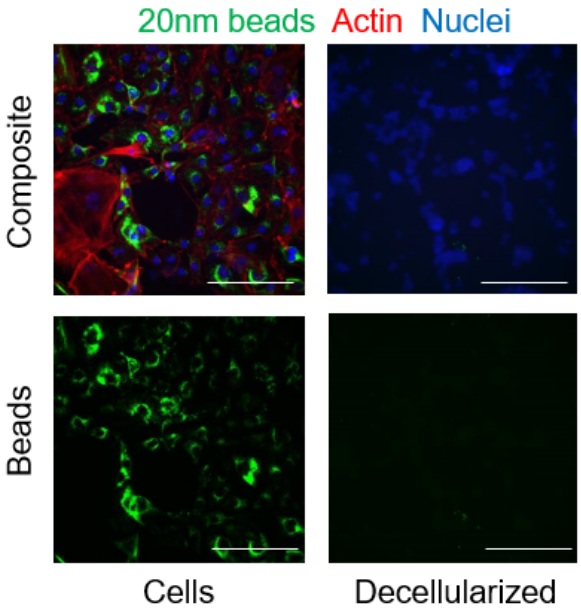

Fig. 2.6 CF uptake of 20nm FluoroSpheres. Beads cultured with murine CFs are internalized during culture, but removed during decellularization.

and not directly impact any subsequently cultured cells.

The addition of MMC has also been observed to promote stromal proliferation and cytoskeletal arrangement[223]. This corresponded with our visual observations that CFs cultured with MMC tended to adopt thin, tightly packed and aligned orientations, particularly human CFs. We ultimately adopted human CFs as the primary source of CDM models, to allow insight into human cardiac ECM, and unless noted, all following analysis was performed on human CFs and CDMs. Temporal imaging enabled us to track alignment of human CFs during the course of CDM production, as well as the alignment of the resulting CDMs, in fixed regions (**Fig. 2.7**). Though human CFs did exhibit some degree of alignment during prolonged culture, the presence of MMC in the culture media did promote further cellular alignment (**Fig. 2.7A**) and consequently the alignment of the resulting CDMs (**Fig. 2.7B**), as determined by orientational analysis of fibronectin (FN) fibrils using the Orientation J plugin[228] in FIJI image analysis software.

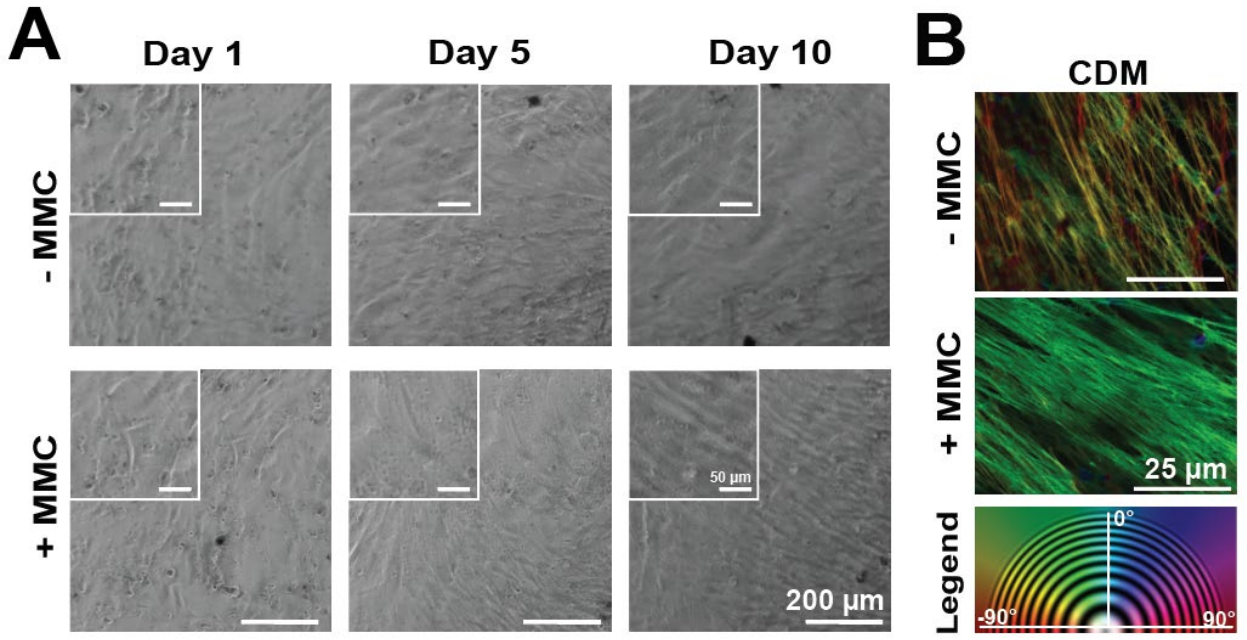

Fig. 2.7 Influence of Ficoll as an MMC on cell and CDM alignment. (A) Temporal imaging of adult human CFs during culture. (B) Alignment of fibronectin (FN) fibrils in CDMs, visualized by FN immunolabeling and assigned colorimetric values of alignment.

We also quantified the amount of matrix present post-decellularization with the addition of MMC. As standard BCA assays to quantify protein are noted for their inability to detect collagens, total matrix quantity was inferred from the dry weight of CDMs that had been scraped off the tissue culture surface and dried in a speed vacuum for equivalents amounts of time. MMC did, indeed, induce an increase in matrix production that was retained throughout the decellularization process by roughly 50% (**Fig. 2.8A**). Additionally, matrix thickness was assessed via optical sectioning of immunolabeled FN in CDMs post-decellularization. CDMs produced with MMC ranged from 5-10μm thick when assayed on glass (**Fig. 2.8B**). However, this was thinner than we'd previously observed in samples, and relative to published results from other labs. Though optical sectioning required the clarity achieved from confocal microscopy and, thus, a glass culture surface, we did approximate thickness with comparable optical sectioning of CDMs produced on TCP (**Fig. 2.8C**). CDMs produced on plastic ranged from 10-15μm, though were observed up to 25μm.

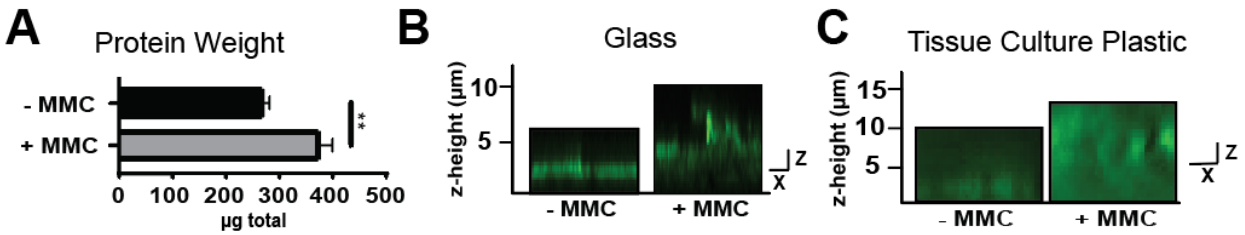

Fig. 2.8 Influence of Ficoll as an MMC on ECM quantity produced by adult human CFs. (A) Protein dry weight yielded from CDMs. (B-C) Reconstructed view of CDM thickness via optical sectioning of immunolabeled FN after production on (B) glass and (C) TCP.

The CDM thickness is relevant because there must be sufficient matrix to separate any subsequently cultured cells from the tissue culture surface, which has an incredibly high Young's Modulus that far exceeds physiological range and can have detrimental impacts on cell function[229], and represents an artificially flat environment. Some estimates suggest that cells require only ~5-6μm of matrix to behave as if they are in a 3D-like state, as interpreted by rearrangement of integrin and paxillin presentation and colocalization[197], and that neither

comparably thick matrices composed of single proteins, nor “2D” complex matrix coatings, which are closer to 1.5μm, are sufficient to promote “3D-like” integrin and paxillin colocalization[1]. These matrices produced on dopa coated plates and in the presence of Ficoll as an MMC, thus, reach the thickness required to support 3D-like interactions with the ECM, particular when CDMs are produced on TCP.

With the observed increase in matrix quantity with MMC, it became important to determine the extent of deviation in CDM composition with MMC. This had been minimally explored[221–225], with the observation that Ficoll, specifically, increases Matrix Metalloproteinase 2 (MMP2), but CDM composition had not yet been defined via unbiased methods. To do this, we subjected CDMs produced with and without MMC to unbiased proteomic analysis by liquid chromatography with tandem mass spectrometry (MS) and subsequent Intensity Based Absolute Quantification (IBAQ)[230] analysis and comparative analyses with statistical assessment using the MSstats[231]. To solubilize CDMs, methods established for the solubilization of native cardiac tissue ECM were adapted[232], and roughly equal fractions (volumetrically) of the -/+ MMC adult human CDM samples were prepared for MS. Extracellular matrix and matrix-associated proteins were filtered via reference to the annotated Matrisome Project[233]. The most commonly detected non-matrix proteins were cytoskeletal proteins and histones, as previously demonstrated[234]. Linear regression analysis of protein abundance in these samples revealed a Pearson’s correlation coefficient of R^2 = 0.96 between the two conditions (**Fig. 2.9**) indicating that MMC did not drastically alter the native matrix composition. FN, the foundational matrix protein required for binding and organization of many other matrix proteins[235,236], was the most abundant protein identified in CDMs, and was present at the same proportion regardless of the presence of MMCs, as was the basement membrane protein Collagen IV, alpha chain 1. Very few of the proteins detected deviated from the line of correlation, regardless of protein function. Interestingly, however, Col I and MMP2 were increased three-to-five fold with the addition of MMC, and may

reflect the more active remodeling required to produce thicker CDMs. Additionally, many of the proteins that deviated from the correlation are small secreted factors and ECM remodeling molecules (MMP2, S100A7, IL-1β, etc.) which fluctuate throughout time and are bound to the ECM more loosely than the bundled foundational matrix proteins, such as FN, collagens and laminins, many of which are present at or near the line of best fit.

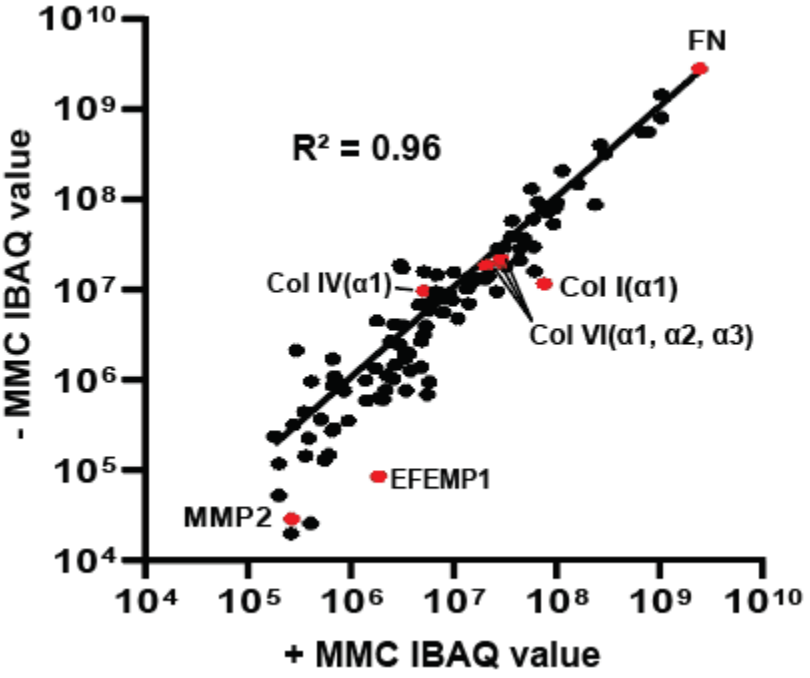

Fig. 2.9 Intensity Based Absolute Quantification (IBAQ) of adult human CDM proteins produced with and without MMC. Data was subjected to linear regression analysis, with line of best fit Y= 1.08X, Pearson's coefficient R^2 = 0.96.

Together, these analyses demonstrate that while MMC can increase the thickness and abundance of matrix and matrix-associated proteins, the majority of the matrix composition remains unaltered. Thus, the combination of dopa pre-coating and Ficoll as an MMC enabled the production of CDMs without exogenous matrix factors, and provided a platform for unbiased comparative studies of matrix biology.

2.4 Species-specific CF Characteristics

The characterization and optimization of cardiac CDMs was done with both murine and human CFs from both fetal and adult ages. In mice, these ages were standardized to E13.5-14.5 and 8wk old mice, respectively. Though each ontogenic cell stage has unique characteristics, the most stark morphological differences were observed between mouse and human CFs, and there are a number of potential sources for those discrepancies. Mouse CFs were smaller than human CFs, though both species exhibited slightly larger adult CFs, relative to fetal CFs. Additionally, mouse CFs were more circular but irregularly shaped, relative to human CFs, which were thin and elongated (**Fig. 2.10A**). Additionally, mouse and human CFs yielded CDMs with unique structural organizations (**Fig. 2.10B**), because the matrix deposited surrounds the cells, and that morphological structure is retained post-decellularization.

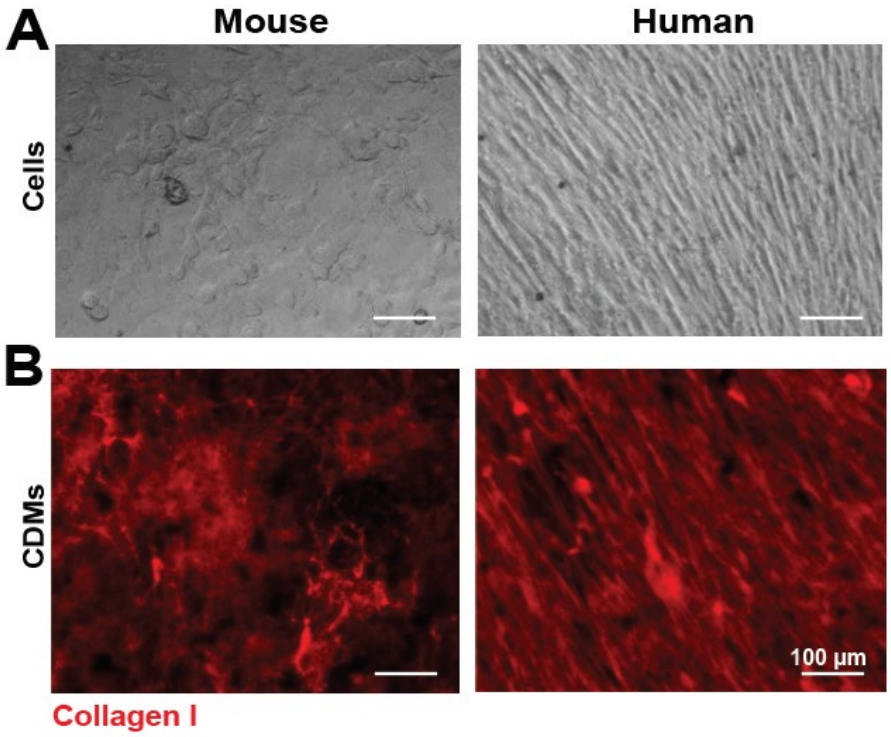

Fig. 2.10 Species-specific CF and CDM organization. Morphological differences between mouse and human A) CFs and B) CDMs, detected by brightfield imaging and fluorescent imaging of Col I (red), respectively.

There was also heterogeneity observed within mouse CF populations, whereas human CFs were very consistent, within each age. Of the several potential reasons for these differences, most are likely due to the fact that all murine CFs were isolated in-house and human CFs were all purchased commercially from Cell Applications. Mouse CF isolations were performed by letting minced fetal and adult heart tissue from CD1 mice onto uncoated tissue culture plates and selecting CFs via the preferential adhesion and outgrowth method[237], wherein fibroblasts are the best equipped cell type to adhere to uncoated TCP and migrate out of the tissue, producing colonies. This was a very robust method with fetal murine hearts, but inconsistent with adult hearts. The source of the variability with adult tissue was never determined, but likely due to the handling of the minced tissue. All mouse CFs were maintained in DMEM + 10% fetal bovine serum (FBS). Particularly in fetal mouse CFs, morphological heterogeneity indicated the presence of a non-cardiomyocyte (CM) cell type, because CMs are not migratory and no beating cells were observed after the first passage of isolated cells. Instead, the primary observed cell types were 1) flat with irregular shapes (likely CFs), 2) raised, more 'cobblestone'-like (likely endothelial cells, ECs) and 3) very small rounded cells that adhered to the surface of the culture (possibly immune cells). All 3 cell types propagated and expanded in colonies with each passage. Fetal mouse CFs were also isolated through enzymatic digestion of fetal hearts with collagenase and pancreatin, as a byproduct of fetal CM isolations, and this method also had visible morphological variability among cells (**Fig. 2.11**).

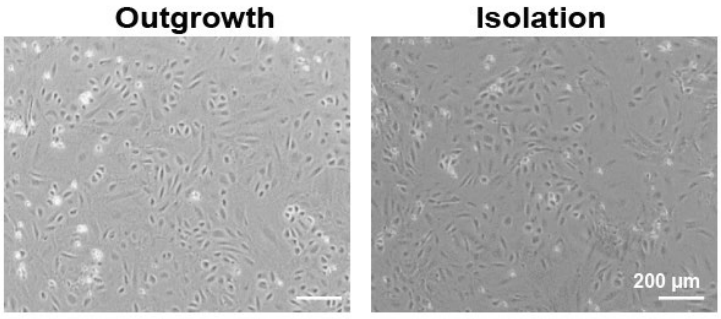

Fig. 2.11 CF cultures by isolation method. E14.5 fetal mouse CFs cultured isolated by preferential adhesion and outgrowth for 7 days (left) and from enzymatic digestion (right).

The presence of contaminating cell types, as well the prevalence of the preferential adhesion and outgrowth method of CF isolation, are derived from the fact that fibroblasts are a heterogeneous population[238,239], and surface markers for stromal cells are both poorly defined and unreliable. CFs originate from multiple progenitor sources, and attempts to label them depend on these origins[240] or their identity as matrix-producing cells[241]. Neither of these strategies have yet been able to successfully identify all CFs with within a heart, particularly across developmental timelines. Additionally, though there have been many attempts to identify surface markers for the isolation of stromal cells in general, and CFs in particular, many of these markers are not pan-stromal identifiers[242,243], or even specific to [167,170,191,238], and many surface markers are lost after even short term culture *ex vivo*. As such, the primary method of identifying isolated CFs without genetic tracing has been by the exclusion of other cell types.

We initially addressed the heterogeneity by quantifying the presence of CD31+ ECs in the fetal mouse CF cultures by flow cytometry (**Fig. 2.12A**), followed by microscopy (**Fig. 2.12B**). Flow cytometry detected mild increase in CD31+ signal in a subset of cells – more so in CFs isolated by outgrowth than by enzymatic digestion – but the intensity did not match that of the CD31+ signal observed in freshly isolated CD31+ cells. However, it is common for membrane receptors to dissipate after some time in culture, and so these results were inconclusive. We further attempted to quantify ECs by labeling them with a FITC-conjugated anti-lectin antibody, which detected lectins primary secreted by ECs. Lectin+ cells were detected in both cultures at very low levels, suggesting that while ECs were present in both cultures, they did not make up a significant amount of the non-CF contamination in either.

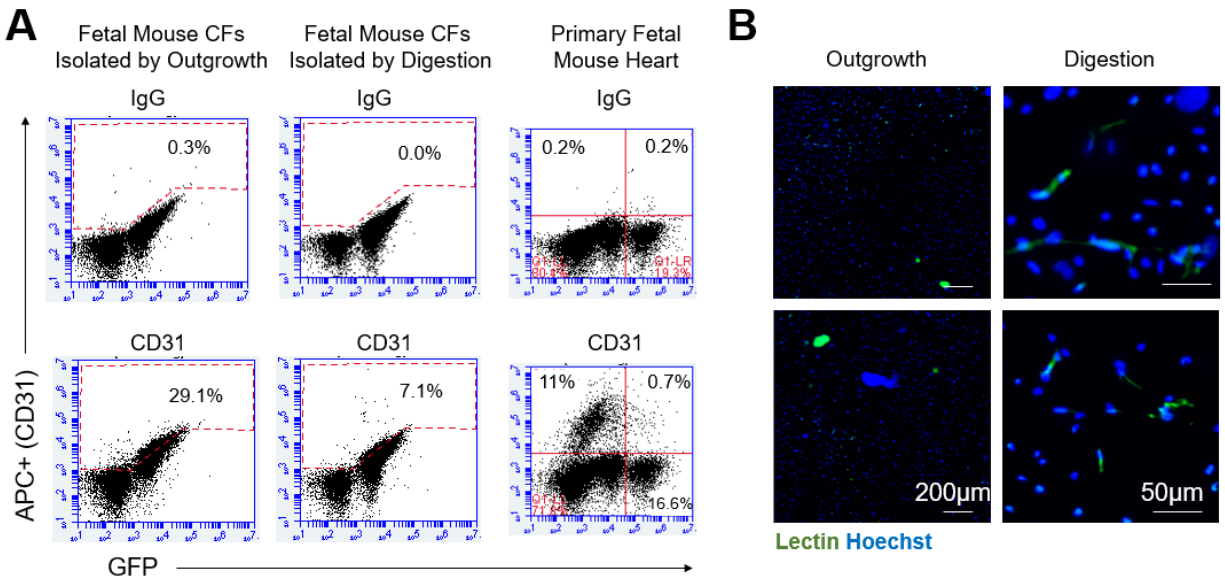

Fig. 2.12 Endothelial cell presence in fetal mouse CF cultures. A) Flow cytometric analysis of E14.5 fetal mouse CF cultures and freshly isolated fetal mouse cardiac cells immunolabeled for CD31. GFP is genetically encoded by a cardiomyocyte-specific αMHC promoter, and is detected in a negative (left) auto-fluorescent (middle) and positive (right) population. B) Fluorescent microscopy mouse CFs isolated by enzymatic digestion and outgrowth methods. Endothelial cells are labeled with anti-lectin:FITC (green) and DNA is labeled with Hoechst (blue).

Human CFs were obtained from Cell Applications from fetal (18 weeks of gestation) and adult (50-52 years) male donors and cultured in proprietary media (#316K-500, Cell Applications). Details about the isolation method and passage number prior to purchase are unknown, and may contribute to the differences observed between mouse and human CF cultures. The long, thin morphology of these CFs is often associated with myoactivation, in which CFs activate expression of αSMA and Col I, and become contractile. Myoactivation can be triggered by stress, as well as culture on stiff surfaces. αSMA was abundantly detectable in both fetal and adult human CFs when they reached confluence (**Fig. 2.13**), though notably higher in fetal CFs. Mouse CFs were not assessed for αSMA, although morphology is an indicator that they were not as activated as human CFs, and that human CFs were highly activated during CDM production. As both mouse and human CFs were cultured on TCP, there are likely additional factors impacting the activation state of human CFs. Although this is a caveat to our studies with human CFs, myoactivation is

the typical response of CFs to cardiac injury and hypertrophy[104], thus indicating that their use enables *ex vivo* study of human, disease-state CFs and ECM, which are otherwise very difficult to obtain.

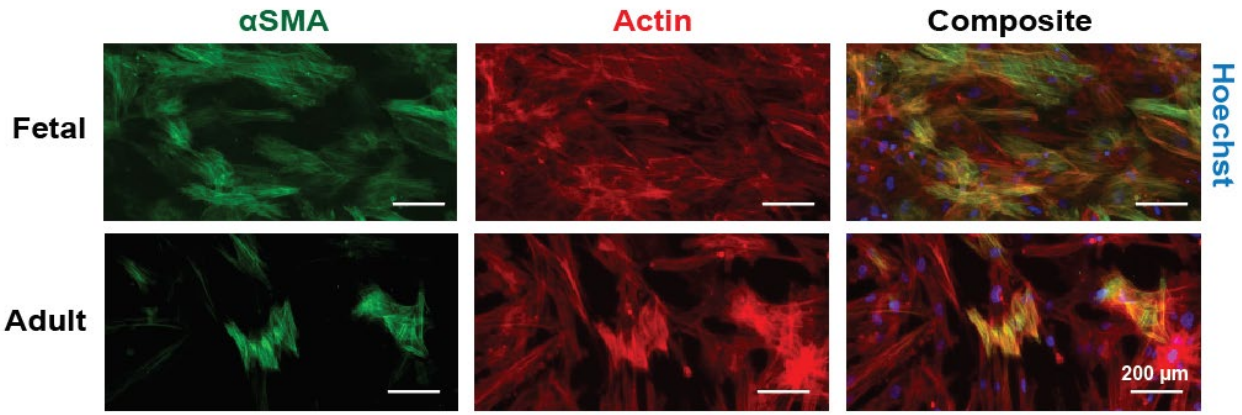

Fig. 2.13 Activation of human CFs. Fluorescent labeling of α-smooth muscle actin (αSMA, green), actin (red) and DNA (Hoechst, blue) in age-specific CFs

Pharmacological agents have been identified to counteract the activation of fibroblasts[239,244], largely for use in the treatment of clinical fibrosis. Both nintedanib and GLPG1690 were tested, alone and in combination. 1μM nintedanib alone was enough to significantly reduce αSMA (**Fig. 2.14A**), though the addition of 3μM GLPG1690 further reduced αSMA levels. Additionally, collagen deposition as detected by a picrosirius red stain was dramatically reduced in CFs cultured with nintedanib treatment during CDM production (**Fig. 2.14B**). However, the total matrix deposition was observed to be minimal in nintedanib- and nintedanib+GLPG1690-treated sample, such that no glossy matrix layers were present. Upon testing, these treated CDMs did not reliably withstand the gentle decellularization process, making them unsuitable for high-throughput modeling of the ECM.

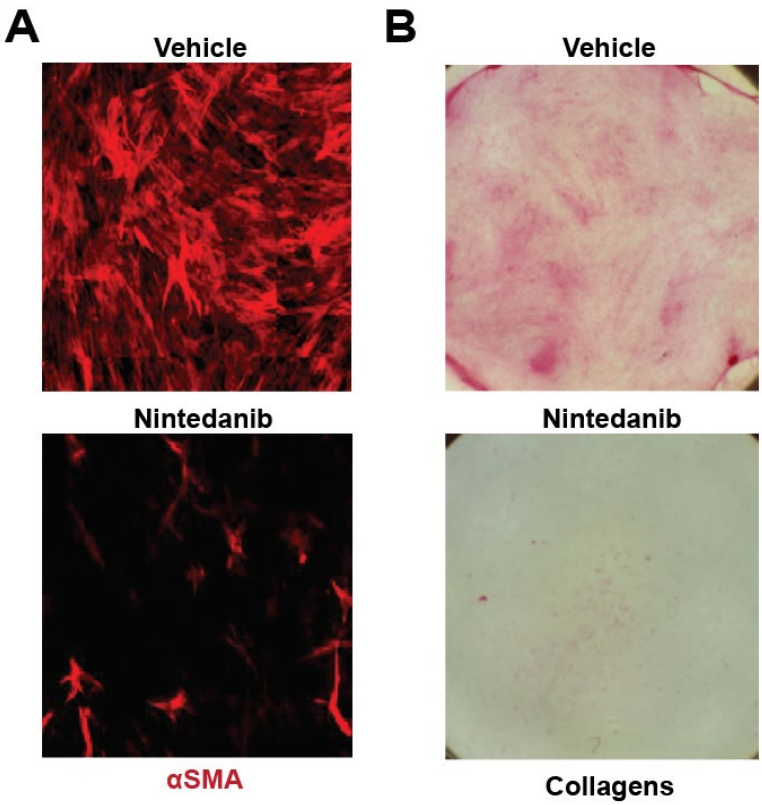

Fig. 2.14 Reversal of CF activation by nintedanib. Human CF culture for 10 days in the presence MMCs and DMSO or 1μM nintedanib. A) Immunolabeling of αSMA (red) B) Picrosirius red staining to detect collagen accumulation.

To normalize culture conditions, seeding densities between CF of different species were first normalized to reach confluence on day 1. This was determined empirically as 50K and 40K/cm^2 for fetal and adult mouse CFs, respectively, and 55 and 50K for fetal and adult human CFs, respectively. The differences in fetal and adult CF densities were dictated by their differences in cell size, but the differences between mouse and human CFs were derived from observed differences in packing densities – i.e., long, thin human CFs packed more tightly than the rounder mouse CFs (**Fig. 2.10**). These differences are attributable to the myoactivation observed in human CFs[245], and likely had consequences on the composition on the CDMs produced.

To determine species-specific compositional characteristics, IBAQ analysis was also performed on adult mouse and human CDMs subjected to MS (**Fig. 2.15**). Analysis was limited to proteins

detected in both mouse and human CDMs for which there was shared homology or clear analogs between species. Mouse and human CDMs had a poor correlation (Pearson's coefficient R^2 = 0.36), although FN was the one of the most abundant proteins in both, especially relative to other foundational matrix proteins, and well fitted to the line of correlation. This abundance of FN became a hallmark of CDMs in our hands, and became a very reliable marker for ECM visualization and normalization. Additionally, fibroblast specific protein 1 (FSP1/S100A4) was the highly enriched in mouse but not human CDMs. Despite the misnomer, this protein is strongly associated with immune cells[167,173], suggesting that the contaminating cell types in isolated mouse CFs may originate from the immune system.

Surprisingly, and inconsistent with the expectation of increased myoactivation in human CFs, Collagen I α1 was 2-fold higher in mouse CDMs than human CDMs. Col1 α2 and canonical collagen crosslinkers lysyloxidase (LOX) and lysyloxidase-like 1 (LOXL1) were similarly increased in mouse CDMs. However, the crosslinking protein transglutaminase 2 (TGM2) was increased in the human CDM, as were the hydrolyzing procollagen-lysine,2-oxoglutarate 5-dioxygenase (PLOD) 1 and 2, which serve to stabilize collagen secondary structure, and connective tissue growth factor (CTGF), which is canonically associated with fibrosis. This indicates that detection of collagen I and LOX at the proteomic level may not reliably demonstrate differences in CF activation, but that indicators of collagen hydrolysis and the fibrosis-associated CTGF are better markers of myoactivation in this culture system.

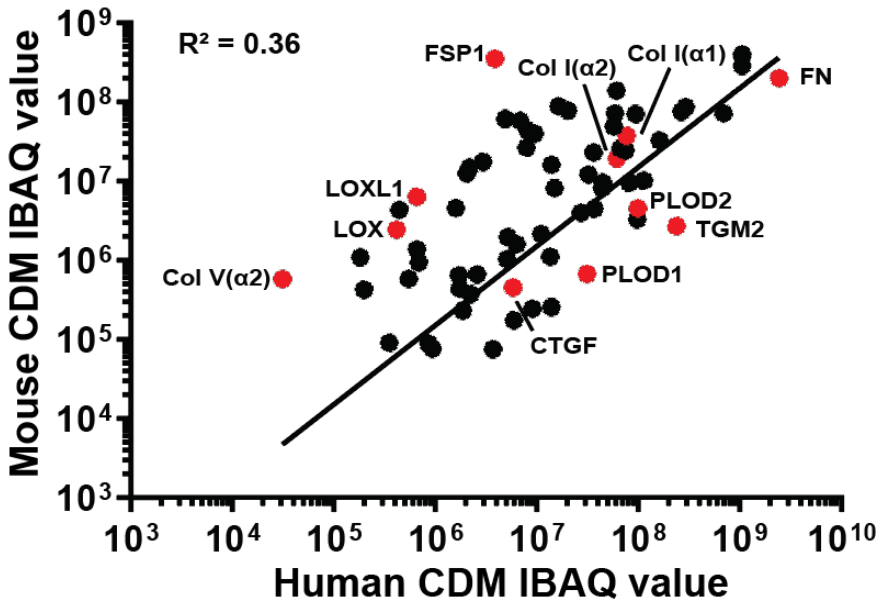

Fig. 2.15 IBAQ analysis of proteins in adult mouse and human CDMs. Data was subjected to linear regression analysis, with line of best fit Y= 0.15X, Pearson's coefficient R^2 = 0.36.

2.5 Influence of Culture Media on CDM Production

Standard CDM protocol, for both mouse and human CFs, was to culture in DMEM with L-glutamine + 10% FBS + antibiotics. However, FBS is known to contain matrix components, including fibronectin[246], but also many others. Additionally, there are occasionally needs for xeno-free culture practices, or the culture of CFs with other cell types that have more define media. For these reasons, we investigated the influence of media composition on CDM production, particularly exploring DMEM vs RPMI, and the replacement of serum with the supplement B27, which is integral to iPSC-CM culture. Human adult CFs were cultured with MMC prior to fixation and analysis in either DMEM or RPMI basal media with FBS or B27. Additionally, CFs were cultured in the proprietary CF culture media supplied from Cell Applications, which is used to passage the human CFs. Although the exact composition of the Cell Applications media is unknown, it is presumed to have a serum component, though potentially less than the 10% used

in CDM production. Surface area coverage was quantified at days 5 and 10 of culture (**Fig. 2.16A**), and final cell confluencies are shown at day 10 (**Fig. 2.16B**).

Under standard CDM conditions, the basal media of DMEM and the presence of FBS were required for confluence and sufficient matrix coverage. The presence of B27 instead of FBS prevented the alignment of CFs and caused irregular bundling of matrix fibrils. Notably, RPMI and the Cell Applications media with FBS did not produce confluent CFs or sufficient matrix coverage at day 10, although that is because the cells condensed and contracted, dislodging the matrix. This is likely due to the higher cell confluence and/or collagen production observed by day 5, than in the DMEM + FBS media. In those conditions, the matrix detected at day 10 is the result of the remaining CFs that remained and produced additional ECM. With optimization, it may be possible to replace FBS with B27, particularly if there is a need to disrupt the cellular and matrix alignment. However, it is likely that the matrix composition produced in medias containing either FBS or B27 would differ, and these differences would need to be quantified to interpret results of any comparative experiments.

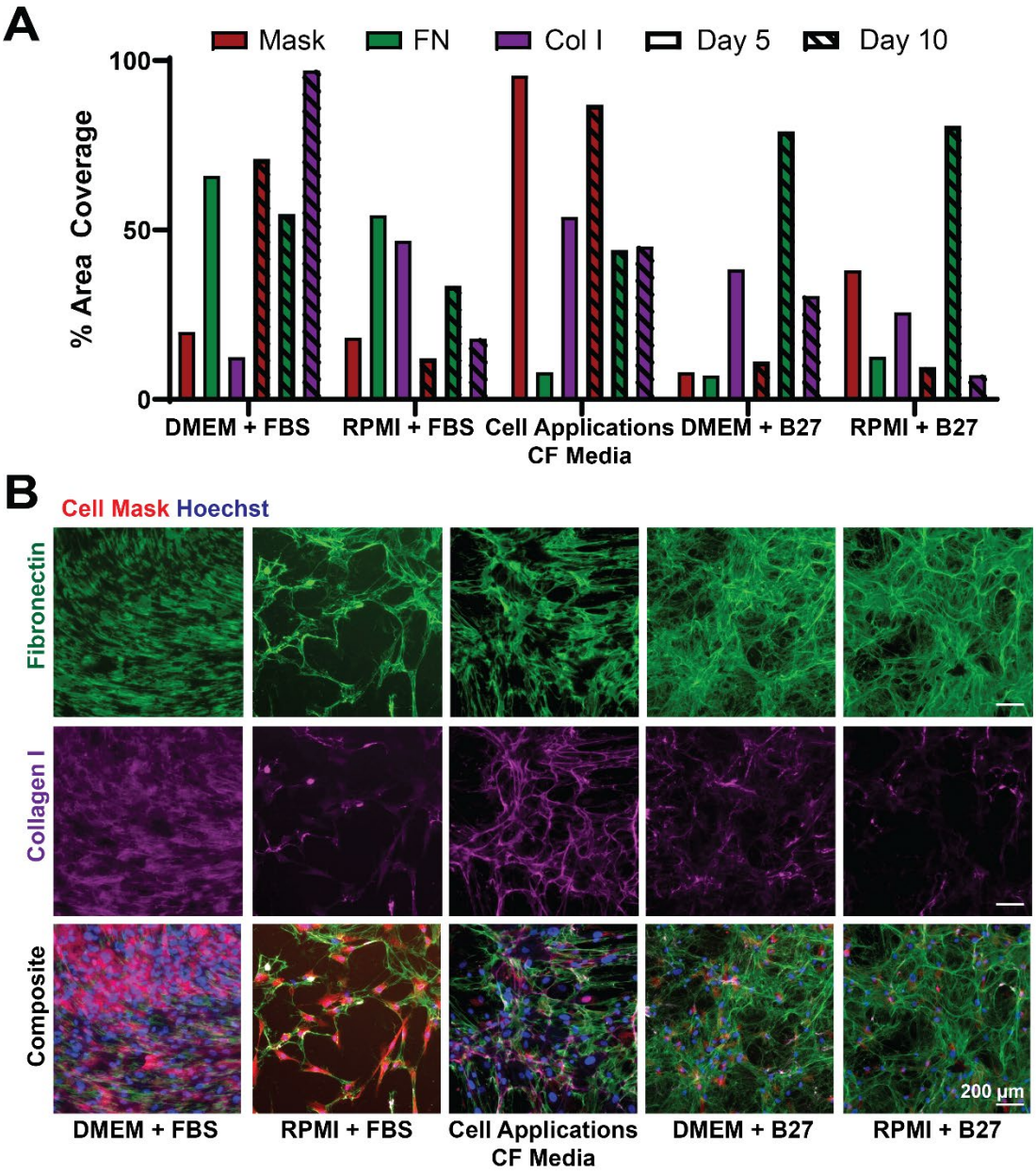

Fig. 2.16 Human CF confluence and coverage cultured with MMCs in various media conditions. A) Quantification of surface area coverage by cells and matrix proteins during culture. B) Visualization of CF cultures at day 10. CFs (Cell Mask, red), fibronectin (green) and collagen I (purple).

2.6 Preservation of CDMs

Our CDM methodology standardized CDM storage overnight at 4°C in $PBS^{+/+}$ with antibiotics and antifungals, and any subsequent cell seeding was performed the next day. However, there are advantages to long-term storage, particularly for the ability to streamline batch processing and quality control. We investigated two major storage strategies: lyophilization and freezing.

Lyophilization sublimates the liquid in samples, preserving their composition and, ideally, structure. Lyophilization had been successfully demonstrated to preserve ECM, and on substances in multi-well plates[247,248], but never in combination. Freezing, however, samples carries the risk of damaging ultrastructure with ice crystal formation[249]. To test these conditions, we cultured mouse CFs isolated from 3-week-old mice, cultured for 10 days with MMCs. Decellularized matrices were processed in one of the following ways: 1) stored overnight at 4°C, per the standard protocol, 2) snap-frozen and stored at -80°C overnight, or 3) snap-frozen and lyophilized overnight in a tray lyophilizer and rehydrated in dH_20 for 2 hours. Snap freezing was performed on parafilmed plates with PBS in all CDM wells. Dry ice was placed into a shallow Styrofoam container and covered with 100% ethanol. The plate was then submerged roughly 1cm into the ethanol. The edges of the wells were observed to freeze first, which caused the liquid to pulled to the edges, and 500µl was determined to be sufficient to maintain coverage of the whole well through freezing. Freezing required 2 minutes of submersion in ethanol. Freezing was also tested in plates containing no liquid (dry), and in 1:1 PBS:glycerol, as a possible method to supercool the wells without freezing. However, ice crystals were observed in the PBS:glycerol solution after ~1 minute, and the liquid did eventually freeze. CDMs subjected to these preservation techniques were then fixed and immunolabeled with FN to evaluate CDM coverage, as were fixed CFs from the same experiment as a reference (**Fig. 2.17**). Imaging of these CDMs revealed that lyophilization introduced cracking in the matrix topology (**Fig. 2.17A**), which is presumably due to the strain put on the matrix/dopa adhesions from the dehydration and

subsequent contraction of the matrices. However, freezing CDMs induced to matrix coverage or structure, expect when frozen dry (**Fig. 2.17A**). Freezing dry CDMs diminished the immunolabeling intensity of FN, likely indicating some compaction, or destruction of the FN structure or epitopes required for antibody binding. Estimates of cracking in lyophilized plates performed by creating channel masks in FIJI indicated that lyophilized CDMs had 16.5% uncovered surface, as opposed to the 0.00008% observed in CDMs frozen with PBS (**Fig. 2.17B**). The presence of GAGs were also investigated via staining with alcian blue, pH 2.5 (**Fig. 2.17C**), which detects sulfated GAGs and some hyaluronic acid, which is unsulfated. While GAGs were present in fixed CF cultures and only minimally detected in fixed CDMs, there was no overt loss of GAG presence with any preservation methods other than freezing plates dry.

Lyophilization was subsequently tried with a mixture of dH_20 and either 250mM trehalose[250] or 50% glycerol covering the CDMs. However, the trehalose did not prevent cracking, and the glycerol was not able to be sublimated and therefore prevented lyophilization. Cardiomyocytes were still able to adhere to CDMs post-preservation, both with lyophilization and freezing, but primary embryonic mouse CMs did adhere to the TCP in between regions of cracked CDM in lyophilized plates, therefore disrupting the influence of CDMs over the entirety of the seeded cell population. After these trials, lyophilization was deemed an unsuitable method for CDM preservation in multi-well plates, and while freezing CDMs remained a potential option for long-term preservation, it was not explored further. CDMs were routinely stored at 4°C in the presence of antibiotics and antifungals for one night and then utilized for subsequent seeding studies the next day. This is a more stringent protocol that used by some labs – many of which routinely store their CDM plates at 4°C for up to 2 weeks (word of mouth) – but we adhered to the maximum storage time of 1 day to minimize variability in downstream assays.

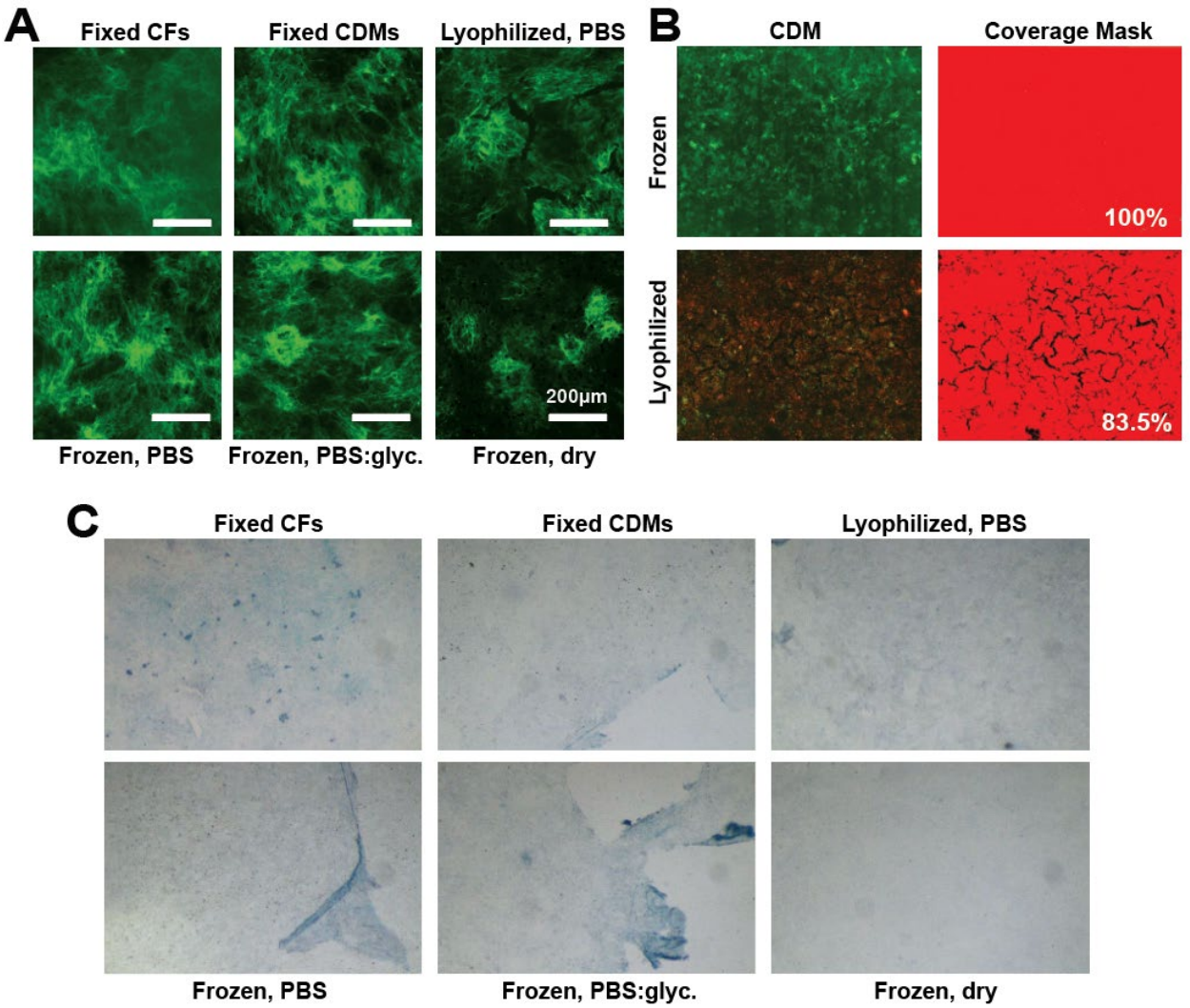

Fig. 2.17 Methods of CDM preservation. A) Matrix presence, visualized via fibronectin (green), in CFs and CDMs after overnight preservation. B) Summary of CDM production. Matrix coverage, labeled by fibronectin (green), Col IV (green) and laminin (red), and masked in FIJI. Percentages represent estimated coverage. C) Glycosaminoglycans (GAGs) labeled by alcian blue, pH 2.5 after various preservation techniques. PBS:glyc., 1:1 PBS:glycerol solution.

2.7 Selective Inhibition of Matrix Proteins

A key advantage of CDMs to model the extracellular matrix is that they are amenable to a wide range of perturbations. However, creating stable genetic modifications in isolated primary cells is compromised by the limited passage number. Thus, we sought to determine whether we could alter matrix composition by inhibiting the production of individual matrix proteins with siRNA-based

silencing. The challenge of this approach is that without genetic integration, transfections are transient. Additionally, CDMs contain the culmination of all proteins expressed and incorporated over the full culture duration, which indicates that intermittent failure to inhibit protein expression may result in protein accumulation in the CDMs. The efficiency and duration of siRNA-mediated silencing was optimized using an siRNA targeting FN, the most abundant protein in CDMs. Mouse CFs were transfected with either no siRNA, a non-targeting control, or a cocktail of 4 anti-FN siRNAs. The anti-FN siRNA was able to fully suppress FN transcripts by 48 hours post transfection, and suppression was waning but still >50% effective at 72 hours post transfection (**Fig. 2.18A**). However, the non-targeting siRNA alone had inconsistent effects on FN mRNA levels, first inhibiting and then enhancing expression at 48 and 72 hours, respectively. When tested under CDM conditions, siRNAs were transfected on days 1 and 4 of culture, and CFs were assessed for FN at the mRNA and protein level on day 7, to capture mid-CDM production dynamics. Although FN transcripts were 60% suppressed after 2 sequential transfections (**Fig. 2.18B**), the minimal presence of detectable FN protein (**Fig. 2.18C**) indicates that incomplete transcript inhibition is still capable of reducing protein levels dramatically. Additionally, despite the 4-fold increase in FN transcript resulting from the non-targeting siRNA control, protein abundance was not dramatically increased. Together, these data indicate that sequential transient transfections of siRNAs, delivered 3 days apart, are sufficient to prevent the majority of protein accumulation in CDMs, despite indications that some post-transcriptional regulation of FN dictates its abundance. Additionally, while inhibition of FN transcripts successfully prevented the accumulation of cellular FN after 10 days of culture, there was still robust detection in CDMs of FN originating from the serum used to culture the cells (plasma fibronectin, **Fig. 2.18D**), as distinguished by conformation-specific antibodies. Though the contribution of factors from serum will depend on the protein in question, this serves as a demonstration that culture in the presence of FBS may both contribute to, and confound, *in vitro* studies of the ECM.

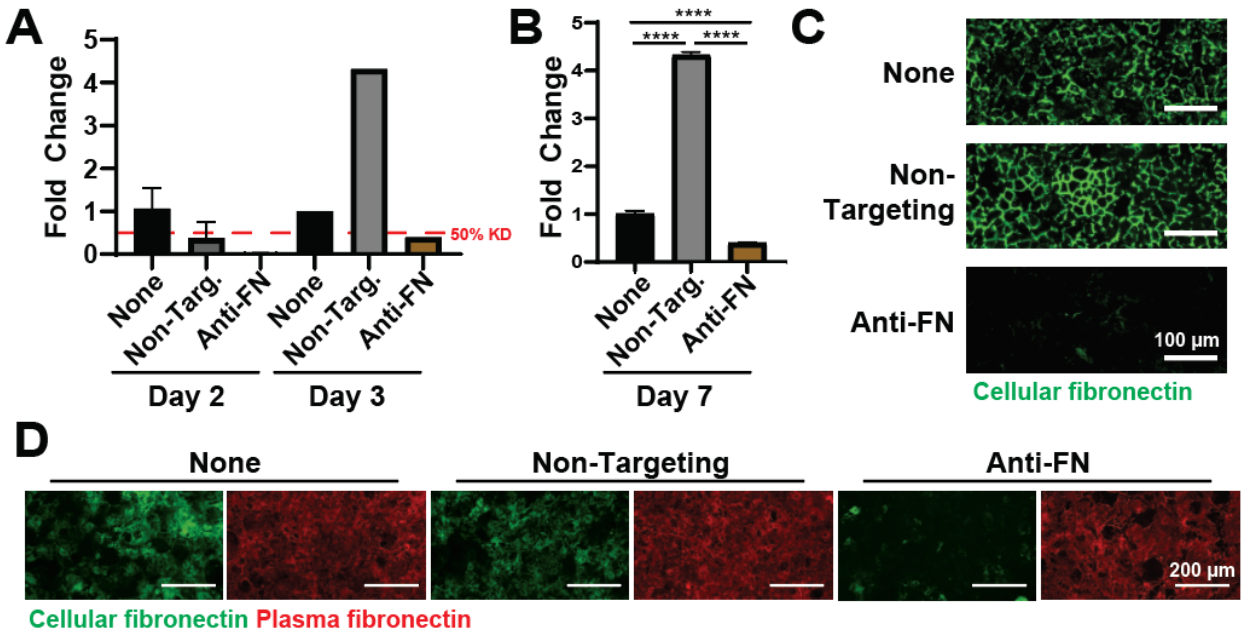

Fig. 2.18 Inhibition of FN by siRNA. Quantified FN mRNA A) 2- and 3-days post siRNA transfection, and B) after 7 days of CDM production. C) FN protein (green) was detected by immunolabeling at day 7 of CDM production. D) Both cell-derived FN (green) and serum-derived FN (plasma fibronectin, red), were detected after 10 days of CDM production by immunolabeling.

2.8 Human iPSC-CFs

Alternate approaches to creating human cardiac CDMs involve deriving cardiac fibroblasts from induced pluripotent stem cells (iPSCs)[251,252]. Not only does this circumvent the issues of accessibility and variability among CFs isolated from primary tissues, but it enables isogenic comparisons between CFs and other iPSC-derived cell types as well as permanent genetic or transgenic modifications. Though CFs from multiple origins may produce distinct ECM, many in the myocardium are transdifferentiated from epicardial and endocardial origins[167], which are derived from the second heart field[253,254]. Our lab primarily utilized the differentiation method that produced CFs via second heart field progenitors[251]. However, it was unknown whether these iPSC-CFs would form robust CDMs. Relative to primary human CFs, iPSC-CFs retained indicators of their cardiac lineage better (TCF21, GATA4), and expressed lower levels of genes associated with myoactivation (POSTN, ACTA2) (**Fig. 2.19A**), and inflammation (IL6, CXCL6)

(**Fig. 2.19B**). Additionally, while iPSC-CFs expressed comparable levels of collagens, they did not produce as much FN, LAMA1 or MMPs (**Fig. 2.19C**), which are essential for matrix adhesion and remodeling.

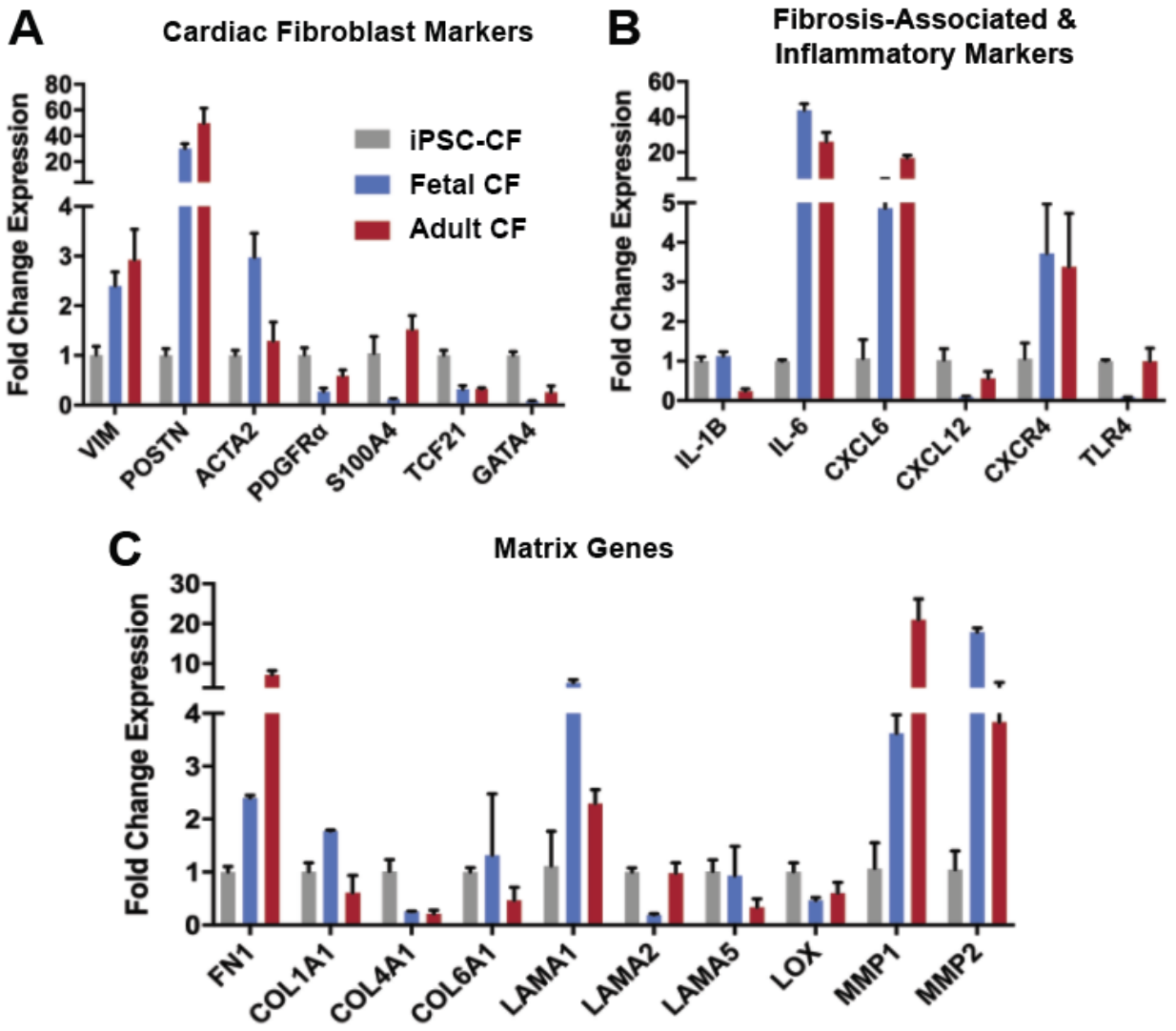

Fig. 2.19 Comparative gene expression of human iPSC-CFs and primary fetal and adult human CFs. A) Genes specific to cardiac fibroblasts. B) Fibrosis-and inflammation-associated genes. C) Genes involved in ECM production and remodeling.

In addition to deviations in the transcript signatures associated with primary CFs, iPSC-CFs seeded at confluence failed to adequately spread over the culture surface, even after 14 days of culture the presence of MMCs, and this could not be overcome by increasing the seeding density

to super-confluent levels (**Fig. 2.20**). To promote cell growth and matrix deposition, we tested a variety of parameters involving culturing at super-confluent densities and introducing factors known to promote proliferation (retinoic acid), collagen deposition (ascorbic acid, bFGF, FGF18), fibrotic responses (TGFβ, lipopolysaccharide (LPS), CHIR99021 (Wnt agonist)), and MMP inhibition (ONO-4817). All factors were added in addition to Ficoll 70/400 for 14 days, prior to CDM decellularization (**Fig. 2.21**). Factors that notably improved CDM coverage were TGFβ, ascorbic acid and ONO-4817, which selectively targets MMP-12, MMP-2, MMP-8, MMP-13, MMP-9, MMP-3 and MMP-7 with K_i values are 0.45, 0.73, 1.1, 1.1, 2.1, 42 and 2500 nM, respectively. While TGFβ acts as a positive control for fibrosis[255] and ascorbic acid is known to induce collagen production and synthesis[224], ONO-4817 is believe to promote matrix deposition and cell spreading by preventing MMPs from remodeling deposited matrix. When tested in combination, ascorbic acid and ONO-4817 were able to increase the FN and Col I abundance coverage most effectively, though still not to the extent that primary CFs did (**Fig. 2.22A-B**). Similarly, the addition of either ascorbic acid or ONO-4817 promoted a mild increase in GAGs in CDMs (**Fig. 2.22C**), as detected by staining with alcian blue, pH 2.5, but none of these conditions induced GAG retention to the level observed with primary human fetal and adult CDMs.

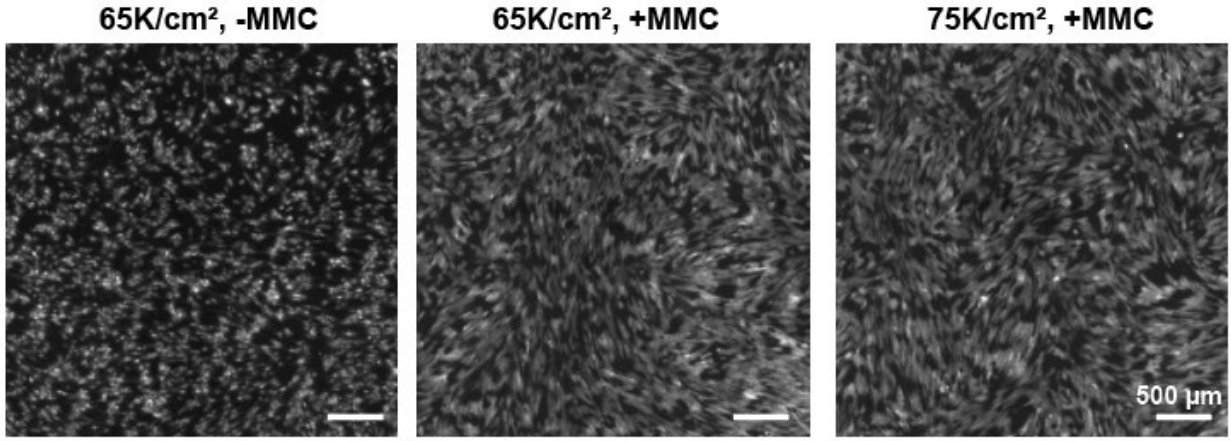

Fig. 2.20 Confluence of human iPSC-CFs cultured at multiple densities for 14 days. Cells are visualized by an endogenous red fluorescent protein. Uncovered areas are visible as black gaps between cells.

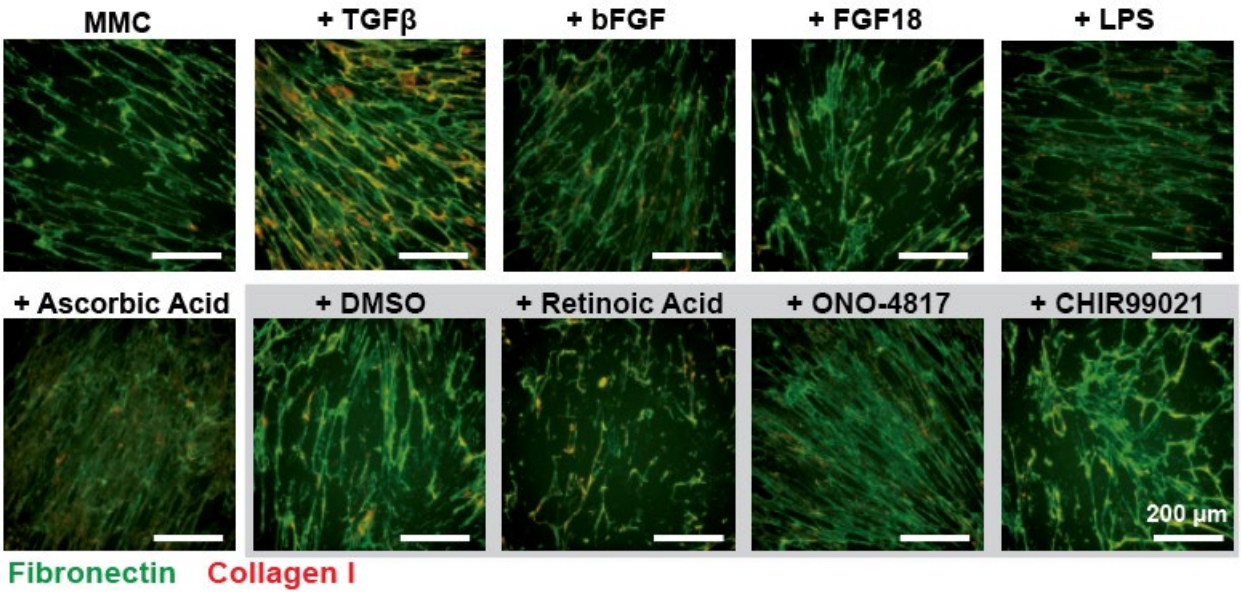

Fig. 2.21 Matrix retained in iPSC-CF derived CDMs cultured with MMCs and additional factors. ECM is visualized by immunolabeling of FN (green) and Col I (red). Conditions that received DMSO are shaded in grey. LPS, lipopolysaccharide. ONO-4817, MMP inhibitor. CHIR99021, Wnt agonist.

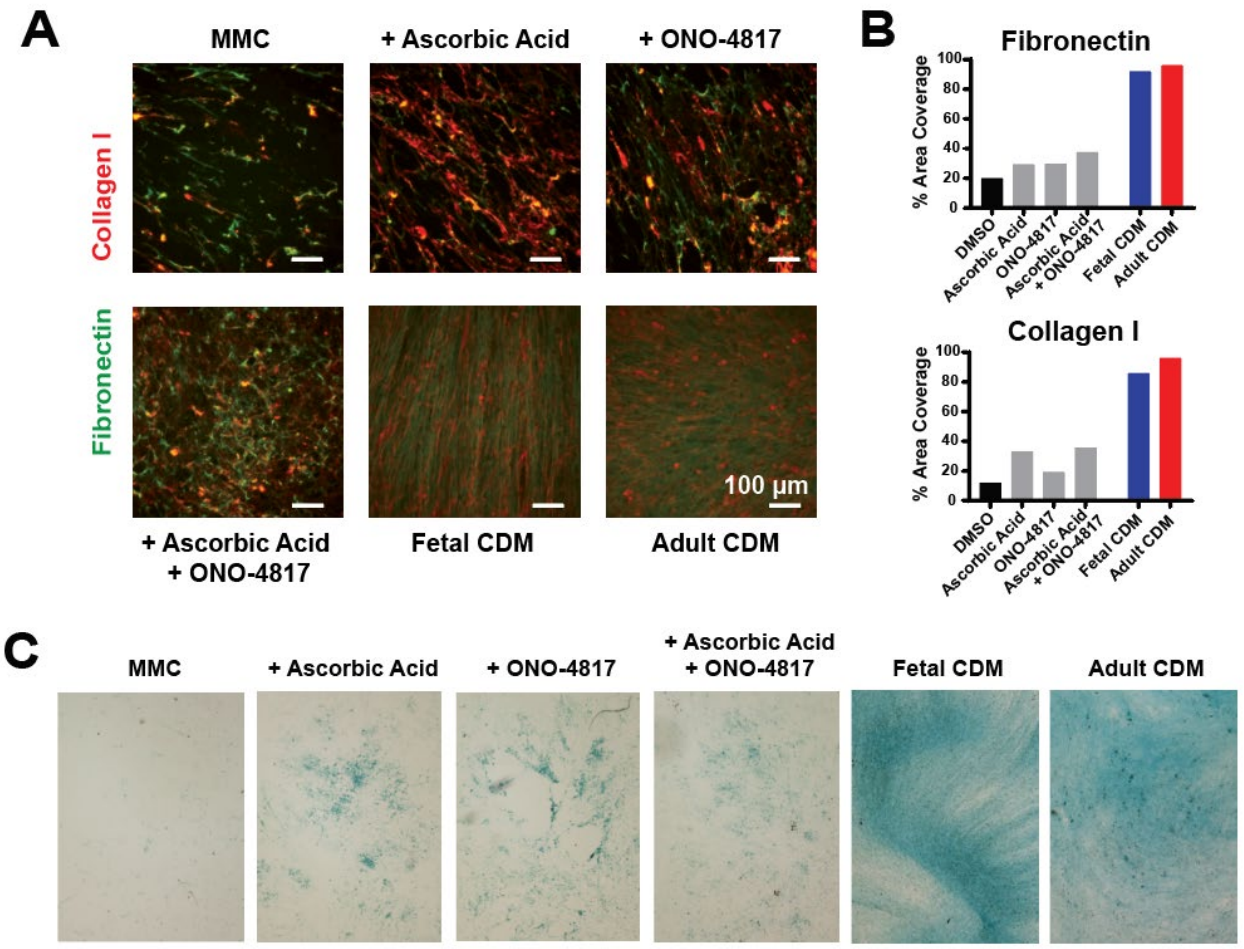

Fig. 2.22 Effect of ascorbic acid and/or ONO-4817 on iPSC-CF-derived CDMs. Comparative measurements in primary fetal and adult human CFs and CDMs are shown. Visualization (A) and quantification (B) of immunolabeling of FN (green) and Col I (red) in CDMs. C) GAGs retained in CDMs, detected by alcian blue staining, pH 2.5.

Future efforts with iPSC-CF-derived CDMs utilized the addition of ascorbic acid, solely, in CDM production, largely because it was already a common and standardized approach within the study of CDMs, and because the addition of ONO-4817 did not yield significant improvements on CDM characteristics. However, the evidence that the MMP inhibitor was able to promote matrix abundance similarly to ascorbic acid, which specifically drives collagen synthesis, is an indicator of the level of active remodeling the matrix undergoes during CDM production, and may be relevant to future studies of matrix dynamics performed with CDM models.

2.9 Troubleshooting

Underconfluence - The success of CDM formation depends on the seeding density of the CFs during CDM formation (**Fig. 2.23**). If cells are too sparse, CDMs will be thin and potentially not reach complete coverage. This is because all ECM remodeling and bundling into fibrils occurs adjacent to the cells, and gaps between cells will have minimal matrix deposition, if any. These gaps, then, cause uneven distribution of the tension applied across the CDM, whether from manual perturbations of the media or from cellular contractility, and increase the number of 'edges' where the matrix is more likely to start peeling. Additionally, sparse cells will take longer to produce as much matrix as dense cells, and after 10 days of culture may only produce thin CDMs that don't hold up well to further perturbations. Despite the striking adhesiveness of the dopa coating, it is possible for the matrix to detach, if enough force or stress is applied, and thin matrices are especially susceptible to this (**Fig. 2.24**, **middle**). The strategy of our CDM methodology is to seed CFs so that they begin at confluence, and produce as much matrix as possible right away. Other protocols seed at sub-confluence, or recommend waiting until confluence is reached before adding MMCs[213]. However, we have observed that CFs seeded on dopa at sub-confluence will never reach the packing density observed with cells seeded at confluent densities, with or without MMCs. Whether this is due to contact inhibition that limits cell expansion, or a failure to migrate/proliferate on dopa, is unknown. However, it underscores the necessity of optimizing seeding density for each cell type to produce sufficient matrix and robust CDMs. A starting density of 50K/cm^2 has been successful for CFs of many origins, but this is dependent on cell size and matrix production, and must be optimized for each cell type.

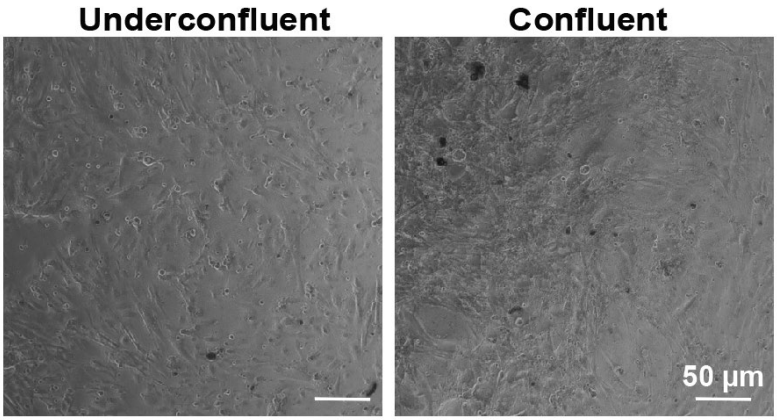

Fig. 2.23 Representative brightfield images CFs at subconfluent and confluent densities. Images shown are from 1 day post-seeding.

Overconfluence – CFs seeded too densely may also not yield functional CDMs, particularly if they have become myofibroblasts. Particularly because activated myofibroblasts are contractile, they will exert a considerable amount of force on the matrix, originating from where they are densest (**Fig. 2.24, right**). If this force is not evenly distributed, it risks dislodging or even tearing edges of the matrix. This will often be identifiable as one edge of the matrix bunching or bundling up – this region will appear very bright under fluorescent microscopy – but still contain loosely flowing/floating edges when subjected to the flow of media. Variations in tension across the CDM can also be introduced by raised portions of the culture surfaces, such as in the Seahorse XF plates which have 3 short posts on the culture surface for the upper plate to rest on, which will also lead to cell contraction and matrix peeling.

Matrix Peeling – Other than confluency issues, matrix peeling can be caused by a variety of factors. Drug additions and genetic perturbations to the CFs can increase or decrease their contractility and matrix production, which will impact CDM formation and integrity. In general, the peeling of CDMs is indicative of too many cells, or too much ECM or contractility, and peeling will often occur from one edge to relieve the tension across the rest of the CDM (**Fig. 2.24, right**). Conversely, the loss of cells or ECM will result in the sparse matrix that will appear to wash away

during decellularization. Through the testing of many drugs and siRNA targets, the majority of detrimental perturbations will result in a destabilization and loss of the CDM, rather than promoting the matrix abundance or contractility. Matrix loss, then, can be attributable to cell seeding density or treatment groups, but matrix peeling is almost always due to initial seeding density.

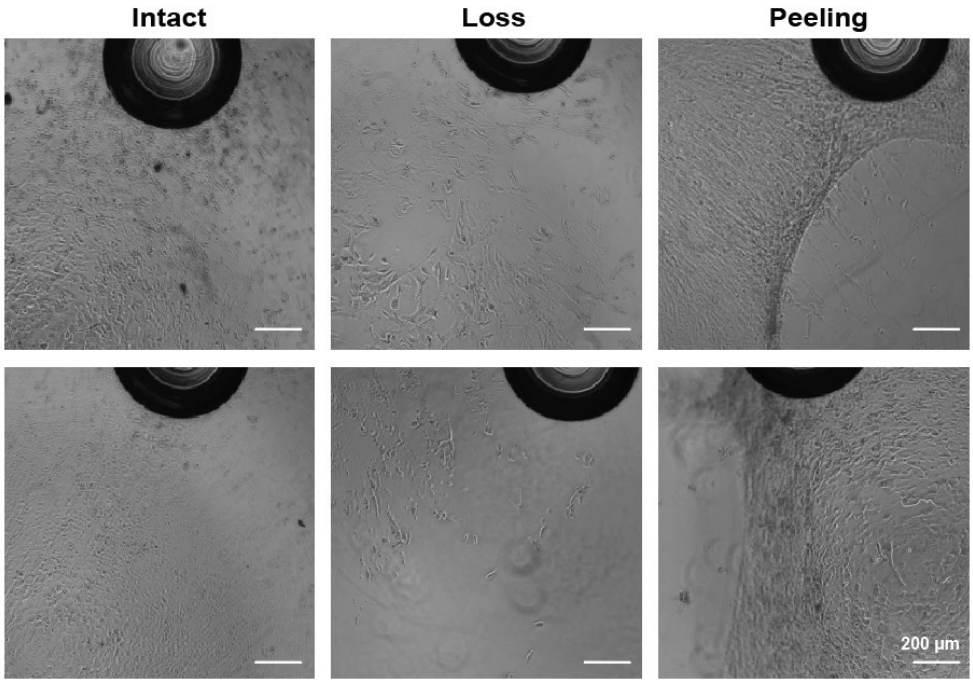

Fig. 2.24 Representative brightfield images of CDM loss. CDMs shown are intact (left), exhibiting loss due to insufficient coverage (middle) or peeling due to contraction (right).

Confirming decellularization – Due to the detergent-free decellularization technique used, some cell debris is often left behind. Under brightfield illumination, this can appear as if some cell bodies remain, or that the decellularization was not successful. However, even with some remaining debris, matrix organization can be clearly imaged, by both fluorescent microscopy and SEM, and cells seeded onto the CDMs can adhere easily. Prior to decellularization, immunolabeling of matrix proteins will not yield sharp images, because the cells bodies – and the cytoplasmic matrix proteins that have not yet been secreted – will refract the fluorescence of surrounding ECM. The best way to determine whether the decellularization is successful, is by visualization of Col I or

Col IV. In CDMs, Col I and Col IV are often enriched directly beneath CFs, as a 'footprint', and if the cells are not entirely decellularized Col I between the cell membrane and CDM will remain and be detected as a cellular shape on matrix fibrils. In general, Col I is detected beneath the FN layer of CDMs, and any irregular accumulation of Col I above the FN is indicative of remaining cell bodies and incomplete decellularization (**Fig. 2.25**). This can often be addressed by longer incubations during the decellularization process, which is currently standardized at 1 hour per solution. Despite the thin nature of CDMs, relative to tissue, decreasing this time has consistently led to incomplete decellularizations and should be avoided.

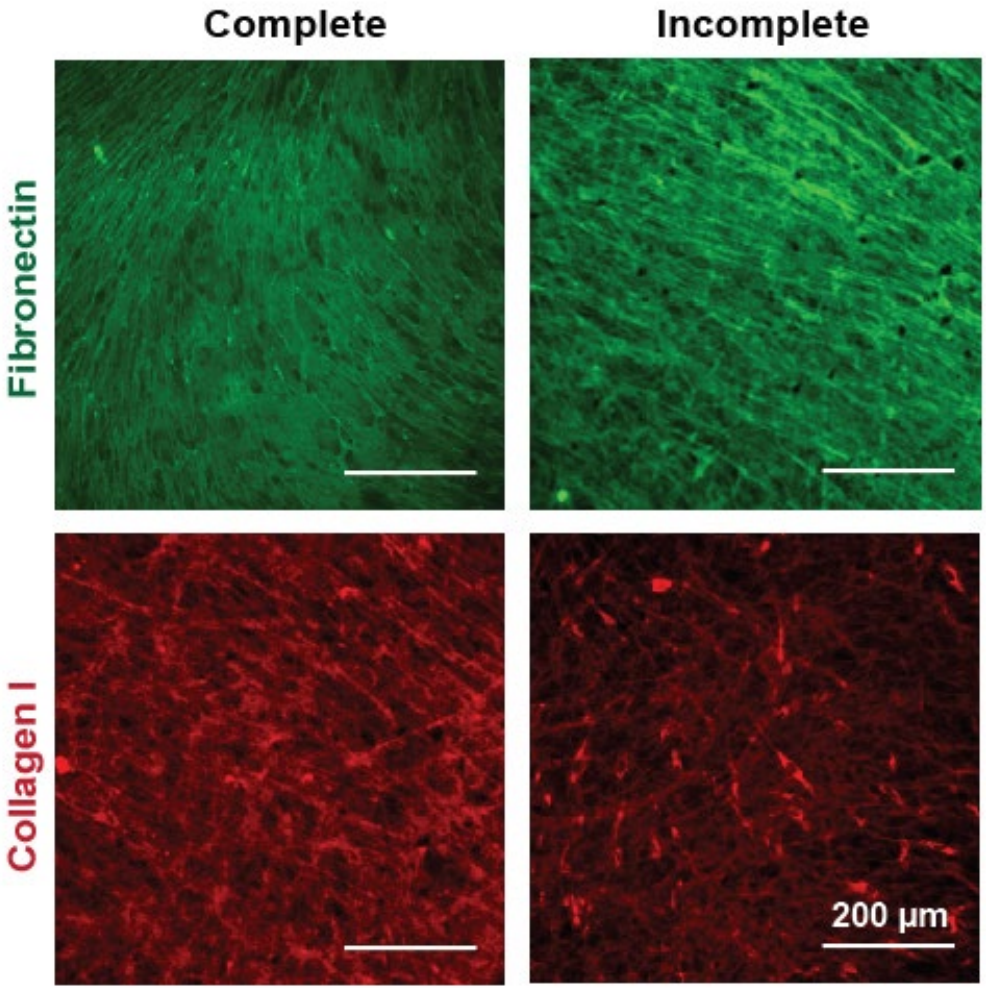

Fig. 2.25 Incomplete decellularization of CDMs. ECM is immunolabeled with FN (green) and Col I (red).

Inhibiting matrix proteins – The siRNA-mediated inhibition of individual transcripts does not always lead to consistent gene and protein suppression. Many matrix proteins are essential for cellular adherence and, therefore, survival, and cellular processes will promote their expression even in the presence of targeted siRNAs. In some cases, particularly among collagens (Col I, Col VI), attempts to knockdown individual components by siRNA caused a compensatory increase in transcription. This was also observed with other essential genes, such as the nuclear envelope component Lamin A/C. However, we also observed that even if the transcript level of a given gene was elevated at the time of analysis, it was still possible for the protein to be largely depleted in the final CDMs, as was the case when inhibiting Col VI production.

Serum-free media compositions – Although efforts to identify serum-free media for CDM production did not identify suitable alternatives, there are several avenues left unexplored. There is at least one commercial source of fibroblasts that use serum-free media (FibroGRO), indicating that is possible to culture stromal cells without serum. Additionally, discussions with their technical team alerted us to the fact that fibroblasts cultured without serum ultimate produce more matrix that those in serum-containing media, likely because they had adopted a senescent phenotype. This will have a negative impact on the speed and extent of culture expansion, but could be suitable for CDM production. One key factor in exploring any of these medias further is that CFs may need to be acclimated to serum-free media prior to CDM production, which was not the case in our studies.

Contamination – These CDMs were decellularized under non-sterile conditions on the benchtop. This, generally, had no detrimental effect on the CDM's utility for subsequent seeding with additional cells. We attribute this to the overnight incubation of CDMs with both antibiotics and antifungals, prior to subsequent seeding. We have seeded CDMs with both freshly isolated mouse primary CMs and human iPSC-CMs, and though both were seeded in the presence of antibiotics, we have only observed contamination with primary CMs coming from non-sterile environments.

When contamination did occur, it was often fungal, and not bacterial. The frequency of contamination with primary CMs on CDMs did not change when those CDMs were decellularized in tissue culture hoods with entirely sterile reagents, but did change when antibiotics and antifungals were included in the first day of CM culture, suggesting that the CDMs were not the source of contamination.

Alignment – The alignment of CDMs resulting from the activation level of myofibroblasts[256] are both a feature and a caveat of these CDMs. It may be advantageous for the study of CMs, particularly because mature CMs are naturally elongated and aligned, and the morphology and aspect ratio of CMs influences their physiology[126]. However, there is no doubt that matrix produced by activated myofibroblasts will differ from non-activated fibroblasts, and those differences must be taken into account when interpreting matricellular interactions.

2.10 Conclusions and Discussion

The use of CDMs to study fundamental principles of cell-matrix interactions is an attractive approach that has increasingly grown in popularity in recent years[212,213,227,257]. We applied this concept to the study of cardiac biology, which represents an incredibly dynamic tissue that undergoes both cellular and extracellular changes during development, maturation and disease progression. In particular, the ECM has only recently been implicated in the developmental and maturation processes that are so crucial for cardiac contractility to meet the metabolic demands of adult [84,258,259]. We present, here, an optimized method of cardiac CDM production in which we sought to address the two major challenges of CDM functionality – adhesion and thickness – without the introduction of exogenous matrix proteins. Crucial to that process was the use of dopa as an amine-binding adhesive substrate[218], which we show, for the first time, to facilitate cellular and matrix adhesion without adverse effects on cell culture. Additionally, we identified Ficoll as

the optimal MMC to promote matrix secretion and deposition. In combination with a gentle, hypotonic decellularization process[199], we aimed to capture matrix composition and structure with the most fidelity possible to native cell-produced ECM. This process successfully produced CDMs over 10μm thick, with only minimal alterations to the native matrix composition, and the successful retention of matrix through decellularizations. This methodology was applicable to fibroblasts from a variety of sources, including from mice and humans, fetal and adult tissues, and even iPSC-derived fibroblasts. While the characteristics of the CFs and resulting CDMs may have source-specific attributes, we found no source-specific variation in the ability to form CDMs. Overall, this study demonstrates the ability to produce CDMs without the introduction of exogenous matrix proteins or induction of collagen synthesis, and further characterizes the full proteomic composition of CDMs for the study of cell-matrix interactions in a defined culture system.

The introduction of MMCs during CDM production did influence some cellular and matrix properties. First, cells adopted an aligned organization during prolonged confluent culture and matrix deposition. While present even without MMCs, this was especially pronounced with their addition, and resulted in increased uniformity in matrix fibril orientation. Additionally, a few matrix components were more abundant in the presence of MMCs, including MMP2 and other secreted molecules. It is unknown whether this was a direct result of MMCs or a response to the altered cellular and matrix organization, but it is not unexpected that factors involved in matrix remodeling would be required at higher levels in response to increased matrix abundance.

Within CDMs, FN was the most abundant foundational matrix protein in both mouse and human CDMs. This is not surprising, because FN acts as a binding partner and anchor for vast number of ECM and ECM-associated molecules[18,260] including collagens[261] which form the basis of most assembled matrices. However, because it appears to be ubiquitously expressed at high levels, it promotes FN as a candidate for any CDM applications in which exogenous matrix proteins are desired for study-specific needs, though this abundance would need to be validated in non-

cardiac cells. Further, CDMs contained numerous basement membrane proteins, including collagen IV and laminins, which is notable because basement membrane proteins are thought to be largely produced by CMs and not CFs[104,262], and the production of these proteins in CDMs reflects a deviation from the expected tissue-specific composition. However, *ex vivo* culture represents an artificial environment for all cells, in both the stiffness of the culture surface and the polarized nature of monolayer culture. In the context of CDM production, CFs are required to produce the entirety of the matrix they require, and basement membrane proteins are not only crucial for cell adhesion, but also retention of other matrix proteins, proteoglycans, and GAGs[18,22]. It is, therefore, possible that CFs produce basement membrane proteins as an inherent caveat to *in vitro* cell culture.

In comparing the culture and CDM production of CFs derived from multiple sources, it became apparent that the isolation method and handling of the cells yielded demonstrable differences in cell culture and CDM properties. In murine CFs, the degree of non-CF presence in the cell culture was dictated by the method of cell isolation, and confounded by the fact that CFs have no reliable surface markers for positive selection. Additionally, there were stark differences between mouse and human CF morphology and organization of their matrices. Particularly because we isolated mouse CFs in house but purchased commercially available human CFs, it is unclear whether the morphological differences observed were purely species-based, or whether they are a result of cell handling during isolation and culture. However, because the human CFs exhibited morphology and protein expression canonically associated with myofibroblast activation indicative of cell stress[168], it is likely that the human CFs experienced some stress that induced the myofibroblast state prior to our use of them. It is unclear how human CFs could be procured without a similar mode of stress, particularly because human CFs procured from other companies had similar morphological phenotypes. The activation state, therefore, represents a caveat of human CDM production, particularly because our efforts to reverse the activation with established

small molecules abolished matrix production almost entirely. However, these cells present an opportunity to investigate human cardiac matrix with relevance to multiple disease states.

They key advantage of CDMs, particularly produced without exogenous matrix factors, is their flexibility and adaptability. Culture vessels were scaled up to 35mm (6 well plates, largest size tested) and down to 5.8mm (1/2 area 96 well plates, smallest size tested), with minimal optimization needed to successfully produce CDMs. Additionally, CDMs were successfully produced from all cell types tested, even iPSC-CFs, which are putatively immature and naturally produced less matrix that primary CFs. Despite the need for the addition of ascorbic acid in iPSC-CF-derived matrices in a timeframe comparable to primary CFs, they expand the potential for modeling CDMs with genetic perturbations. Our approach to modulating CF behavior and subsequent CDM characteristics was through the use of small molecule inhibitors and siRNA-mediated gene silencing. As with any cell culture, the inclusion of small molecules was a relatively straight-forward addition. However, siRNA transfections are transient, and required re-transfection every 3 days. This inherently introduces experimental variability, and was a cumbersome, though effective, process. The alternative approach of conditional or permanent genetic mutations is difficult to achieve in primary cells *ex vivo*, largely because the process of isolating clonal populations of genetically altered cells exceeds the passage number that most primary cells are capable of. iPSC-derived fibroblasts, on the other hand, can undergo genetic manipulation prior to differentiation, and stably express any genetic mutations without further oversight curing CDM production. As such, the introduction of iPSC-CFs may promote an already flexible model into an even more consistent and applicable system for the study of matrix biology.

This work is present an unbiased methodology and, to our knowledge, most detailed compositional investigation of CDMs. As such, it provides a platform for further studies of cardiac matrix biology in a defined system that is highly amenable to genetic and pharmacologic perturbation.

Chapter 3: Distinct Structural and Compositional Characteristics of Human Fetal and Adult CDMs

The mammalian heart undergoes dramatic shifts in composition and function during development and maturation[9,111,113,259], and the ECM both influences and reinforces a number of these processes[50,58,262]. The ECM itself undergoes dynamic structural[110] and compositional[59] changes during and after development. The fetal cardiac ECM is loosely organized[110,111] and enriched with growth factors and GAGs[16,112] to support the developing myocardium and small, proliferative fetal CMs[58,59,113,114], whereas the adult ECM is a more fibrillar[110] and collagen-rich[115] environment intended to main homeostasis of aligned, energetically-demanding adult CMs undergoing significant contractile strain[84,116,117]. However, the degree to which these CM characteristics are influenced by the local and age-specific ECM have only been minimally explored. There have been a number of efforts to create matrix scaffolds for the culture of CMs and cardiac tissues[139,205], often with the goal of promoting CM maturation. However, these engineered environments often utilize combinations of very few individual matrix proteins, such as collagen or fibrin hydrogels[263,264], or they use tissue-derived matrix such as Matrigel[193] or decellularized ECM from tissues[110]. These models have been useful to the study of ECM and cell-matrix interactions, but have certain limitations. In many cases, tissue-derived ECM has been digested, which removes all structural elements[102,139]. Further, reliance on tissue-derived ECM limits the ability to perturb matrix composition for the identification of individual proteins involved in driving cellular responses. A *in vitro* model of the cardiac ECM that contains both the composition and structure specific to a precise stage of cardiac development would enable mechanistic studies of matrix elements that are crucial to age-specific CM phenotypes and functions.

To facilitate study of the ECM's contribution to age-specific matrix-CM interactions, we created cardiac CDMs reflective of the developing and mature ECM using fetal and adult CFs, respectively. Fetal and adult CFs retain age-specific properties and influences over CMs[114] in an *ex vivo* murine system, including age-specific production of matrix components, but this phenomena has not been explored in the context of human biology. We, therefore, produced fetal and adult human cardiac CDMs, and subjected both CFs and CDMs to rigorous analysis of structure and composition to identify elements of cardiac matrix biology that are preserved in the CDM model.

3.1 Fetal and Adult Human Cardiac Fibroblasts

Fetal and adult human CFs had unique properties *ex vivo*, and were easily distinguishable in culture. Not only were fetal CFs slightly smaller, but they expanded faster than their adult counterparts, and could be maintained for more passages. Similar to what was observed with murine CFs, fetal human CFs were routinely cultured up to 10 passages, and often were still expanding after 12 passages. Adult CFs from both mice and humans, however, routinely exhibited delayed growth by passage 6, and often stopped expanding by passage 8. EdU labeling of human CFs during CDM production demonstrated that even under extreme confluence, DNA synthesis was still occurring in ~29% of fetal CFs, but only ~2% of adult CFs. Especially in adult CFs, one clear visual indicator of delayed growth was the observed morphological changes, wherein CFs exhibited pronounced spreading, losing their elongated morphology and refracting less light. Though this morphology is associated with senescence, β-galactosidase staining during CDM production was more abundant in fetal CFs than adult (**Fig. 3.1**). This is partially due to the fact that β-galactosidase frequently labeled densely cultured cells, and the fetal CFs are densely packed, but this suggested that senescence-associated signaling is not more prominent during

formation of adult CDMs than fetal CDMs. Instead, it suggested that the observed decrease in adult CF growth dynamics is due to alternate mechanisms.

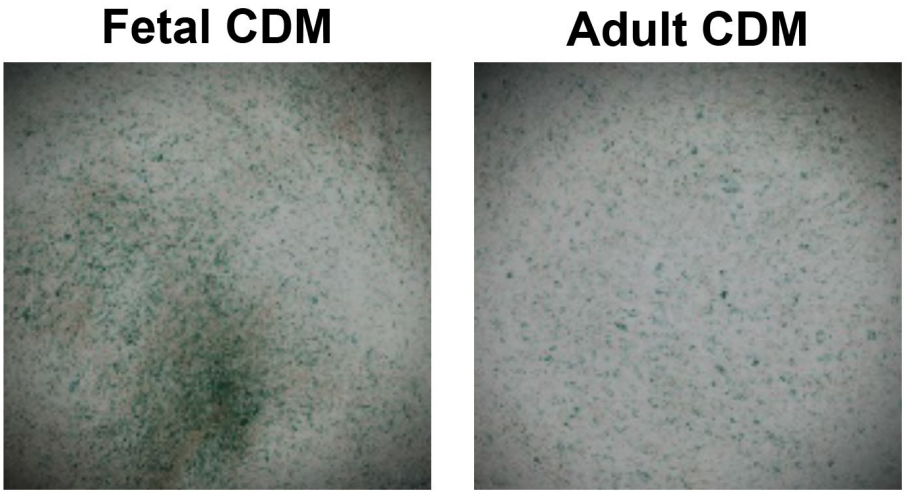

Fig. 3.1 β-galactosidase staining in fetal and adult human CFs under CDM conditions.

Given the unique growth properties of fetal and adult CFs, and myoactivation of CFs during CDM production, we investigated any age-dependent differences in activation level with immunofluorescent staining of αSMA after 5 days of culture. Images were taken across the width of the 16mm well to capture positional differences in cell behavior (**Fig. 3.2**). Strikingly, nearly all CFs of both ages contained strong αSMA signal, indicating that under CDM-producing conditions, CFs are in a myofibroblast state. Additionally, two phenomena were readily apparent – first, cells were condensed near the center of the plate in both cultures, but more so in fetal cultures, as evidenced by the high density of nuclei. Second, there were intermittent regions of adult CF cultures lacking αSMA, that were not observed in fetal CFs. The counter-label of Col I which, in this case, was still largely intracellular and served to mark a footprint of each cell, demonstrated that even areas with sparser αSMA contained confluent cells (**Fig. 3.2**). In a comparison of αSMA to Col I coverage, only 1% of fetal culture area containing cells lacked αSMA-positive CFs, as

opposed to only 5% of adult CF culture area. There are, therefore, mild age-specific differences in CF αSMA expression. However, the majority of both fetal and adult CFs were activated during CDM production, indicating that these CFs are more representative of myofibroblast biology and the associated pathological matrix deposition[104], as was noted in Chapter 2. Importantly, though, the age-specific differences in myoactivation were minor, and are unlikely to contribute to age-specific characteristics identified in further studies. Additionally, while the high degree of cellular alignment is indicative of myofibroblasts, this phenotype has been noted in multiple other CDM models, even from fibroblasts from non-pathological origins[213], and using non-Ficoll MMCs[227], and may be an inherent caveat of the CDM model.

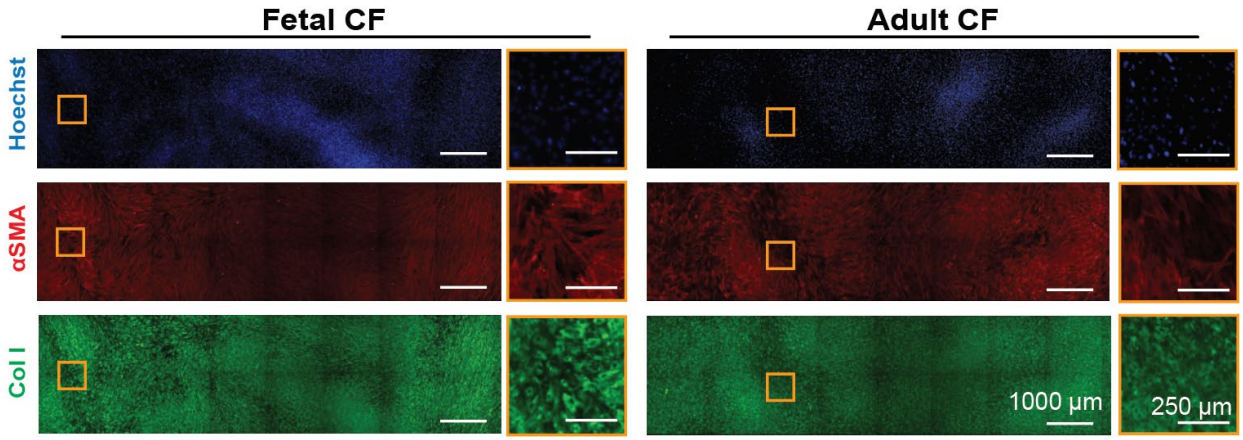

Fig. 3.2 αSMA (red) expression in age-specific human CFs during CDM production, counter-labeled with Col I (green) and Hoechst (blue). Images outlined in orange represent magnified regions indicated within the larger images, from regions of sparse αSMA detection.

Fetal and adult CFs also responded to CDM production differently. Both became highly aligned during dense culture with MMCs, but at different rates (**Fig. 3.3**). Fetal CFs aligned very quickly, adopting their final orientation by day 5 of culture. Adult CFs, however, were slower to respond to high culture confluence and only exhibited their final configuration by day 10 (**Fig. 3.3A**). The matrix deposited by these CFs exhibited the same pattern and alignment post-decellularization (**Fig. 3.3B**). These temporal changes are quantified in **Fig. 3.3C**.

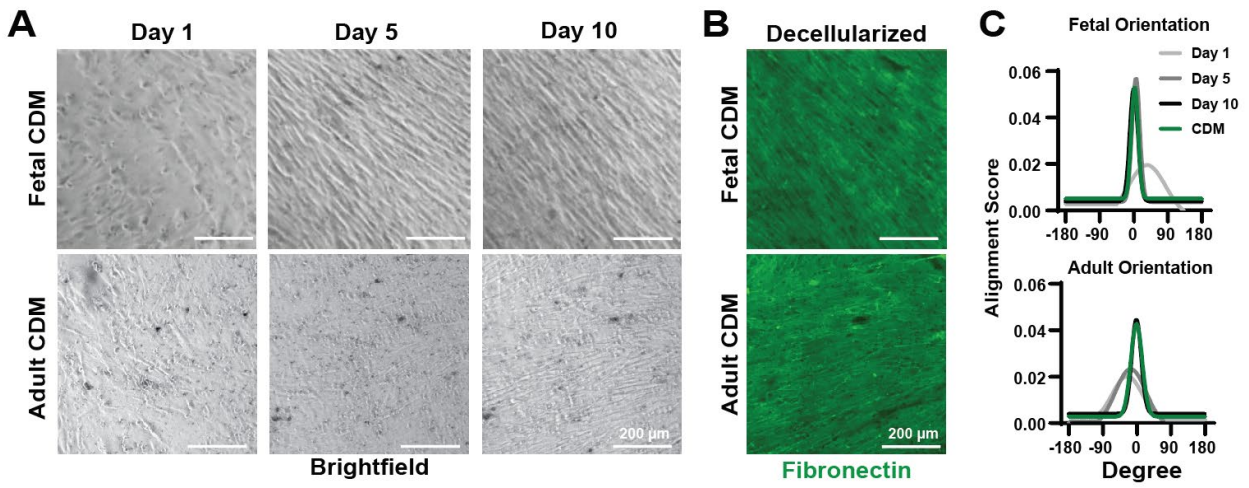

Fig. 3.3 Cellular and matrix alignment during CDM production. A) Longitudinal brightfield imaging of fetal and adult CFs. B) Resulting CDMs visualized by immunofluorescent labeling of fibronectin. C) Alignment of CFs and resulting ECM during CDM production.

We next sought to determine age-specific transcriptional signatures of fetal and adult CFs, particularly in the context of total transcript abundance during matrix deposition. Transcriptional analysis was performed by unbiased RNA sequencing of CFs collected longitudinally at culture day 0, 5 and 10 of CDM production. Total transcript accumulation was then assessed by calculating the geometric mean of transcript numbers, normalized against their abundance at day 0. This analysis revealed distinct temporal trends among the 497 matrix and matrix-associated genes (**Fig. 3.4A**). Genes encoding crucial matrix proteins responsible for the structural integrity and adhesion of the ECM (foundational genes) were expressed steadily throughout culture in both fetal and adult CFs, with less variation than other classes of transcripts. In comparing fetal and adult transcript abundance, often the genes most highly or lowly expressed in CFs of one age were also detected at high or low levels in CFs of the other age; for example, in both fetal and adult CFs, neuregulin (NRG1) is the most abundant growth factor and MMP3 is the most abundance protease. The presence of NRG1 is potentially unsurprising – it is strongly associated with promoting proliferation[90], which is ongoing in CFs *in vitro*, although of the cardiac cells, it has

not been explored extensively in non-CMs. However, it is expected that NRG1 would be more highly expressed in fetal CFs, which is the case, as neuregulin associated with the fetal heart, particularly in the context of the developing heart as a growth factor-rich, regenerative organ[90,112]. Similarly, another factor associated with cardiac regeneration, inhibin subunit beta B[265] (INHBB), was lowly expressed in both CFs, but was particularly depleted in adult CFs, which are derived from the post-regenerative stage. Additionally, the other growth factors most upregulated in fetal CFs over the duration of CDM production (epithelial mitogen, EPGN, glial cell line-derived neurotrophic factor, GDNF) are present but less abundant in adult CFs. This phenomenon is also observed in the higher abundance of multiple inflammatory molecules in adult CFs, including IL-1β[266], and increase in proteases in fetal CFs, both are which are consistent with the adult stage as more inflammation-prone[267] and the fetal stage as more plastic with active matrix remodeling[50,58]. These age-specific enrichments are better exemplified by the ratio of the fold change of each cumulative transcript abundance in fetal and adult CFs (**Fig. 3.4B**). Among foundational proteins, laminins were the most notably altered between ages, with the alpha 2 chain of laminin (LAMA2) upregulated in adult CFs and the gamma 1 chain (LAMC1) upregulated in fetal CFs. Numerous growth factors were also more enriched in fetal CFs, including epidermal growth factor (EGF) and nerve growth factor (NGF), which are involved in cardiac development[268] and repair[269], respectively. Additionally, no individual inflammation-associated genes were differentially associated with CFs of either age, but both did have age-specific proteases and protease inhibitors.

Temporal transcriptional analysis revealed multiple age-specific parameters that were consistent with known cardiac tissue biology, demonstrating that even after isolation and culture *ex vivo*, primary human CFs retain age-specific characteristics.

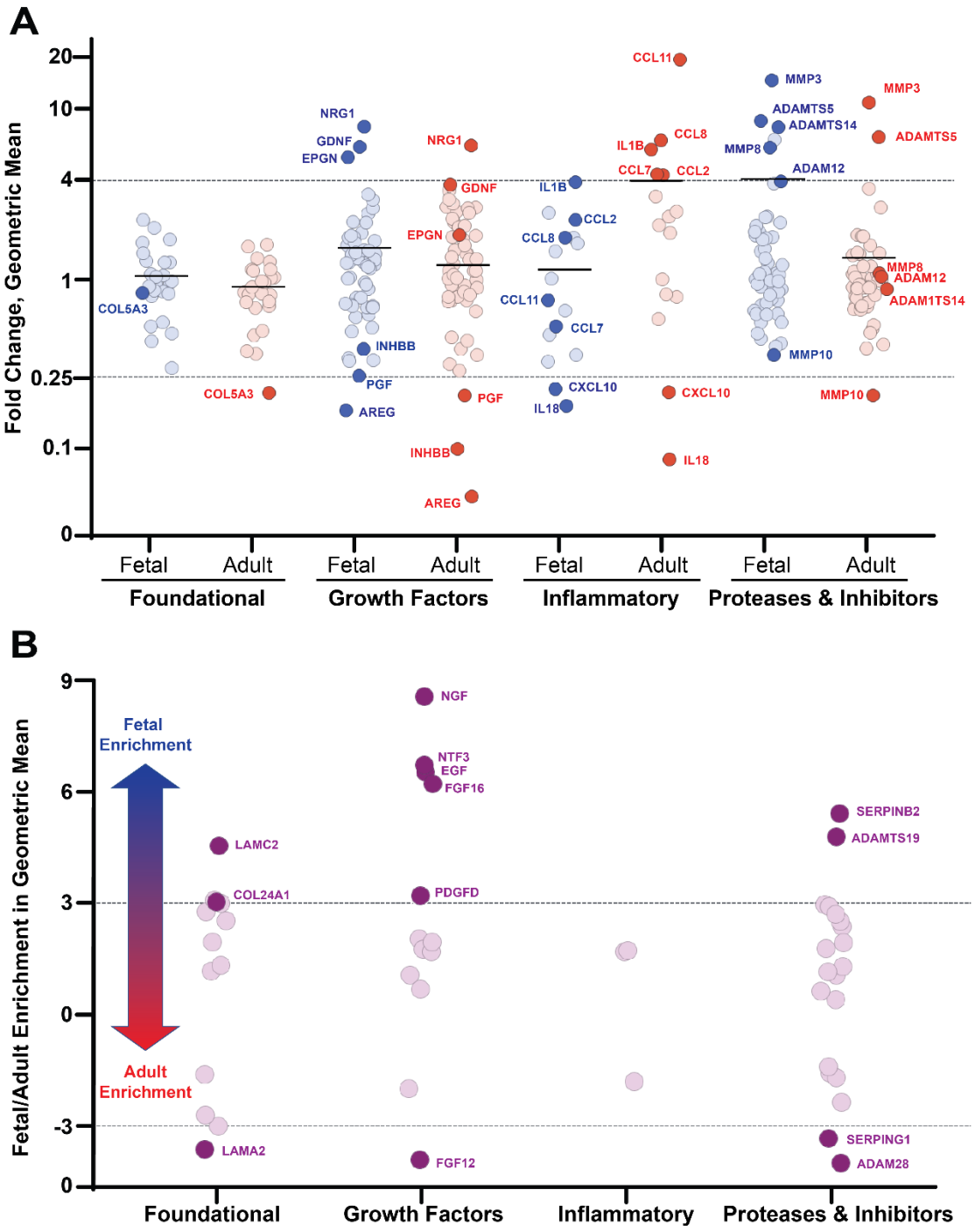

Fig. 3.4 Cumulative transcript abundance in fetal and adult human CFs. A) Individual transcript FC in fetal (blue) and adult (red) CFs, calculated as the geometric mean of temporal transcript fold change (FC) from expression at day 0. Genes that were more than 4-fold above or below 1 (denoted by dashed lines) were highlighted in both fetal and adult groups. The average value of each group is indicated with a solid line. B) Ratio of significantly different transcripts in fetal/adult CFs, more than 3-fold differentials highlighted (denoted by dashed lines).

3.2 Age-specific Characteristics of Cell-Derived Matrices

To determine whether age-specific transcriptional profiles of fetal and adult CFs impacted the deposition and contents of human CDMs, we characterized their structure and composition. First, we assess matrix structure and topology in fetal and adult decellularized CDMs by scanning electron microscopy (SEM). In native heart tissue assessed from mice, decellularized fetal ECM is more loosely arranged, with the coiled structure indicative of low matrix tension. Decellularized adult ECM, however, is organized into a more regular and fibrillar pattern, with larger and fewer coiled fibrils[110]. These age-specific structural differences were apparent in human CDMs as well (**Fig. 3.5A**), as seen in the smaller and more loosely coiled fibrils in the fetal CDM, relative to the bundled matrix fibers in the adult CDM. In the heart, this is associated with randomly oriented CFs of the fetal heart and the regimented alignment of CFs and CMs in the adult heart. These data suggest that age-specific human CFs faithfully recapitulate certain structural characteristics of age-specific matrix production, making them a suitable surrogate for the *ex vivo* modeling of some cardiac ECM structural elements.

To further investigate both structure and composition of age-specific CDMs, we employed histological stains common to tissue analysis. First, we assessed both collagen abundance and organization in fetal and adult CDMs (**Fig. 3.5B**) by picrosirius red staining, which detects Collagens I and III, which are the predominant collagens in the adult heart[59], and are more abundant in the adult murine heart, relative to fetal hearts. However, our fetal CDMs had enriched collagen accumulation, relative to adult CDMs, with regional differences dependent on CF growth patterns, resulting in a swirled pattern in fetal CDMs and more diffuse presence in adult CDMs. These patterns are reflective of the overall organization of confluent CFs, which show local alignment (**Fig. 3.4**) but do coalesce into broader swirling patterns, particularly in fetal CF cultures, as a result of cellular organization and condensation (**Fig. 3.2**). The collagens in these CDMs, then, are likely more a result of CF culture dynamics *ex vivo* than the age of the heart they

originated from. However, the consequences of this coalesced matrix also lead to the retention and unique distribution of GAGs in fetal and adult CDMs, as detected by staining alcian blue at a pH of 2.5 which indicates unsulfated GAGs and hyaluronic acid (HA). HA and other GAGs are particularly abundant during heart development, largely in the outflow tract and valves, but are also present throughout the developing myocardium, as they bind to not only matrix proteins but also enzymes, adhesion proteins and growth factors[18]. They also play a role in water retention, which lends unique biomechanical properties to various regions of cardiac tissue[270], as well as modulation of other matrix proteins. GAGs are expected to be enriched in the fetal heart, relative to the adult heart, which is reflected in human fetal and adult CDMs. Similar to the collagen accumulation, GAGs were more enriched in the fetal CDM, with heterogeneous distribution reflective of the original CF growth patterns, whereas they were more uniformly present in adult CDMs (**Fig. 3.5C**). Particularly in contrast to Matrigel, a common adhesive substrate for the culture of cardiac cells, the GAGs present in fetal and adult CDMs were highly abundant and more reflective of the levels and organization expected of native cardiac tissue[16] (**Fig. 3.5D**).

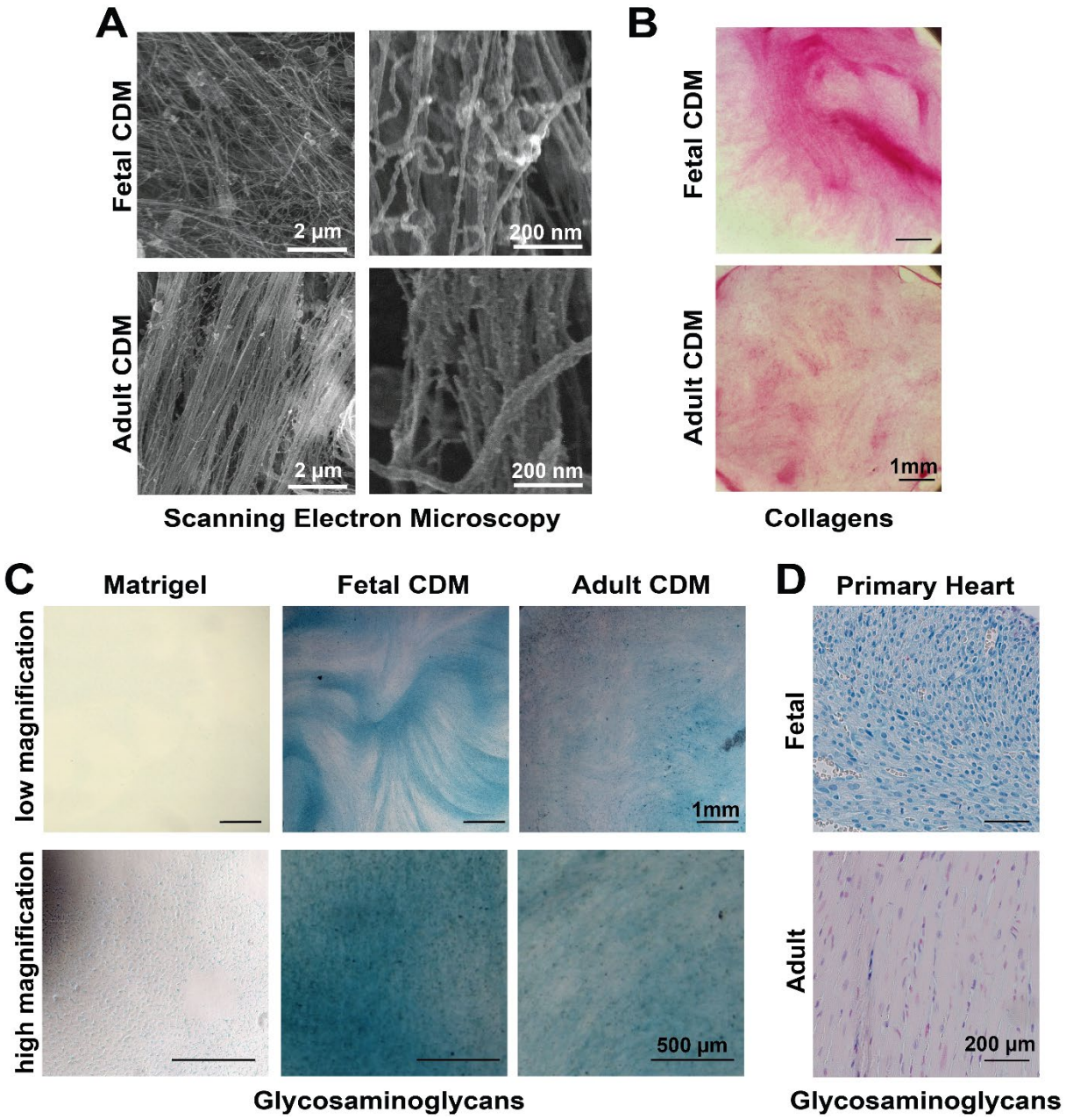

Fig. 3.5 Characterization of CDMs fibrils produced by fetal and adult human CFs. A) Ultrastructure detected by scanning electron microscopy, B) presence and distribution of Collagens I and III, detected by picrosirius red, C) GAGs detected by staining with alcian blue, pH 2.5 in CDMs and Matrigel, D) GAGs in primary heart tissue, detected by alcian blue, pH 2.5, counterstained with eosin.

These histological analyses indicate both age-specific retention and distribution of key matrix molecules in CDMs. However, a detailed account of compositional similarities and differences

required unbiased proteomic analysis. As such, we performed liquid chromatography tandem mass spec on 3 replicates of fetal and adult CDMs. Unique peptides were identified by MaxQuant[271] software referenced against the SwissProt human or mouse database. Data was subjected to comparative analyses with statistical assessment using the MSstats[231], and cross-references to the Matrisome database (http://web.mit.edu/hyneslab/matrisome/)[233] for the filtering of non-matrix proteins and for functional category assignments. Due to the nature of these analysis, non-proteins components such as GAGs were not detected or quantified.

First, we compared detected proteins in the CDMs to the transcriptional profile of CFs. Of the 397 matrix genes commonly expressed in both fetal and adult CFs, only 98 (25%) were detected at the protein level in both fetal and adult CDMs (**Fig. 3.6A**). In addition to the fact that several matrix-associated proteins are non-covalently bound to the ECM and therefore unlikely to be fully retained in CDMs through the decellularization process, this is also likely due to the transient nature of transcript expression that resulted in their loss during CF culture, even prior to decellularization. In total, 135 proteins were detected in decellularized CDMs by LC-MS/MS, with 109 proteins common to CDMs of both ages. These common proteins represented all major categories of fundamental matrix and matrix-associated proteins (**Fig. 3.6B**), as annotated by the Matrisome Project[233].

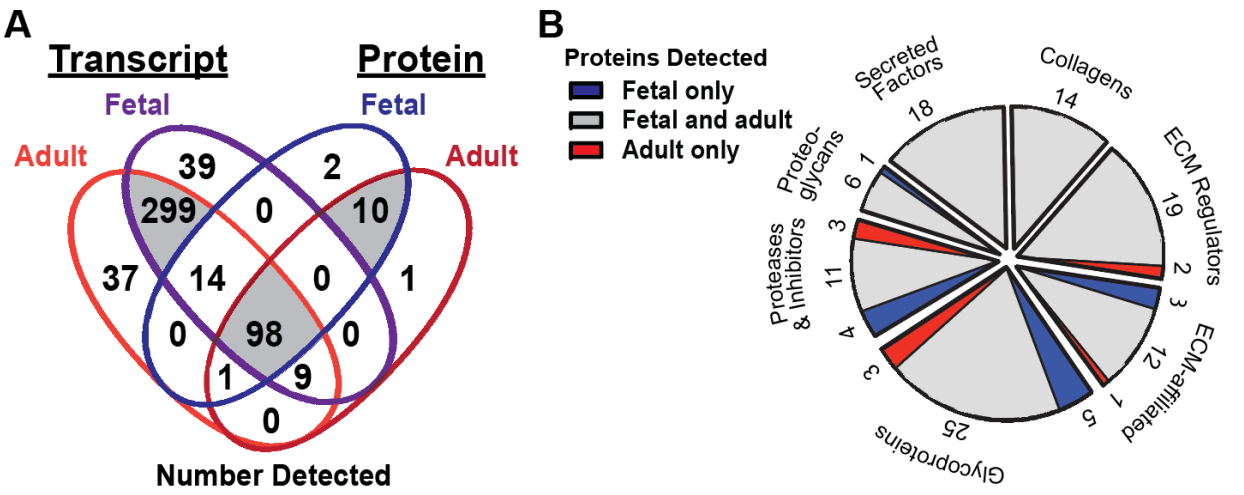

Fig. 3.6 Age-specific matrix and matrix-associated transcripts and proteins. A) Comparative Venn diagram of matrix-associated transcripts and proteins in fetal and adult CFs and CDMs, detected by RNA-Seq and LC-MS/MS. B) Proteins detected in fetal CDMs (blue), adult CDMs (red) or both (grey), per matrix protein categorization.

As was seen in the transcriptional analysis, CDMs from both fetal and adult CFs contained the expected foundational matrix proteins, including FN, Col I, Col IV, and laminins, with no significant age-specific differences in abundance (**Fig. 3.7A**). This is a departure from expected CDM composition, inferred from the lack of basement membrane produced by CFs *in vivo*[104,262]. However, not only are CFs in contact with BM proteins in the developing and adult heart, these foundational proteins are also necessary for cell adherence, as well as retention of other matrix proteins, proteoglycans, and GAGs, and are an essential component of all *in vitro* cell culture. Once isolated, primary CFs must produce these basement membrane proteins out of necessity. Additionally, many of the differences observed in age-specific cardiac tissue ECM are structural, and not reflected by transcriptional abundance.

Among non-foundational proteins, there were compositional features unique to age-specific CDMs. Nineteen proteins were significantly increased over two-fold in fetal CDMs relative to adult CDMs, and 10 were significantly decreased (**Fig. 3.7A**). Notably, many of the proteases transcriptionally enriched in fetal or adult CFs were either not detected or not significantly altered

between CDMs from different ages (**Table 3.1**). This underscores the unique profiles of matrix-associated proteins during stromal cell growth, as opposed to protein retained in decellularized matrices. However, similar to trends observed by transcriptional analysis, GO enrichment analysis via the STRING[272] database identified key processes in age-specific CDMs that reflect known ontogenic characteristics in mammalian cardiac tissue ECM and development (**Table 3.2**). Specifically, GO analysis identified fetal enrichment for collagen fibril organization and growth factor binding, whereas adult CDMs were enriched for peptide cross-linking and calcium-dependent protein binding.

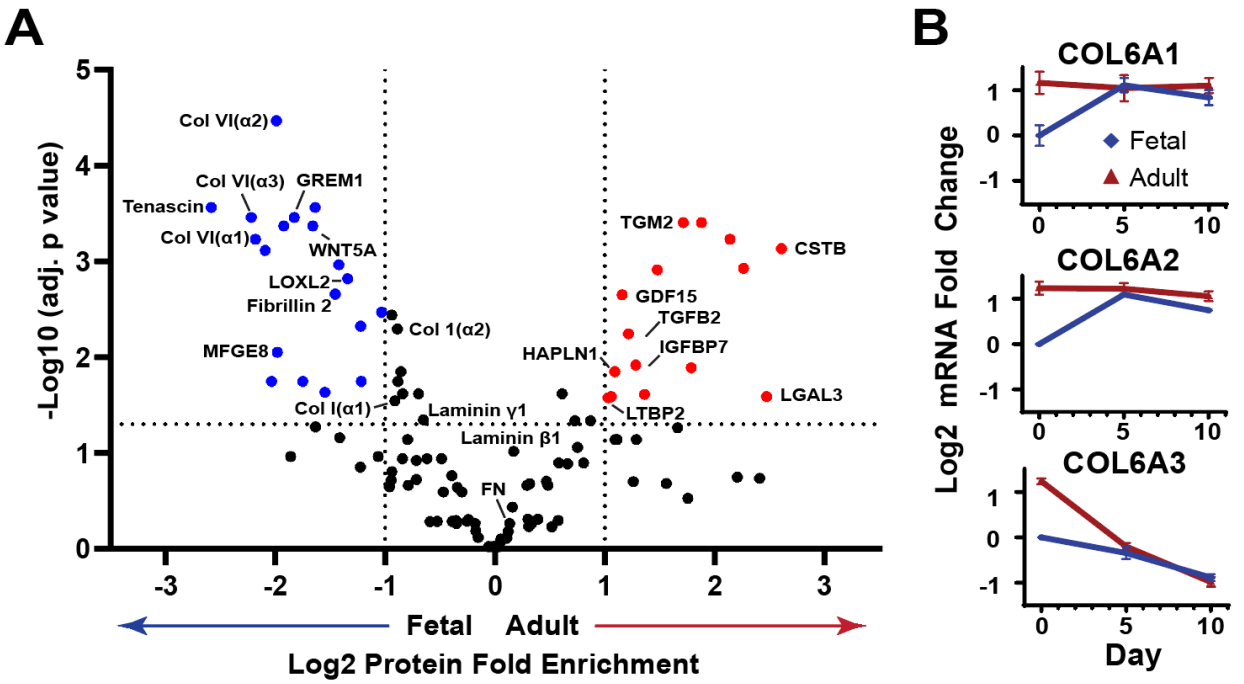

Fig. 3.7 Enriched CDM proteins. A) Age-specific enrichment of proteins in fetal and adult human CDMs. B) Temporal transcript expression of Collagen 6 chains in age-specific CFs during CDM production, normalized to fetal transcript abundance at day 0.

Some factors such as GDF15, which were enriched in adult CF transcripts, were also detected as significantly enriched in adult CDMs. However, other canonically age-specific factors observed in the CFs, such as the fetal abundance of IGFs, was not reflected by protein detection. Additionally, several matrix and matrix-associated proteins known to be abundant in fetal cardiac

ECM[273,274], such as fibrillin 2, tenascin and Col VI, were enriched in fetal CDMs, as were proteins known to influence multiple aspects of development such as morphogenesis (fibrillin 2)[188], specification of cardiac progenitors (Wnt5a and gremlin)[275,276]. Interestingly, milk fat globule-EGF factor 8 (MFGE8) is also enriched in fetal CDMs, which is known to be cardioprotective against hypertrophy[277] and inhibit fibrosis[278]. Adult CDMs, on the other hand, were enriched for several matrix-modulating proteins that promote matrix crosslinking and stabilization, such as transglutaminase 2[279,280] and hyaluronan and proteoglycan link protein 1[50,281], and proteins that are associated with fibrosis (transforming growth factor β2[282] and latent TGFβ-binding protein 2[283]) and heart failure (insulin-like growth factor-binding protein 7[284], growth differentiation factor 15[285], cathepsin B[286] and galectin 3[287]). This is consistent with adult cardiac biology, which exhibits increased ECM crosslinking[288] and organization[110] that promotes CM maturity[139].

It is worth noting that many biomarkers of heart failure in adults are often associated with the frequently concurrent clinical presentation of fibrosis[179], which presents as the overabundance of fibroblasts and deposited matrix. As such, it is not unexpected to find CDM proteins that correspond to fibroblast-associated disease states. However, several of the proteins enriched in adult CDMs are believed to be causative in several forms of heart disease, whether via canonical TGFβ-mediated fibrosis[180,282] or in that their inhibition reduces pathological severity[279,284,289,290], although the impact of these proteins may be context-dependent.

One of the most striking differences in fetal and adult CDM composition was the considerable enrichment of col VI chains in fetal CDMs. Col VI is unique in that it is not fully a fibrillar or non-fibrillar collagen, and instead presents as beaded microfilaments within an ECM network[291]. It is formed of three alpha chains – α1, α2 and α3 in a 1:1:1 stoichiometric ratio, although α3 can be replaced by α5 and α6. Another alpha chain with high homology to α3, α5 and α6 exists – α4 – though it is not functional due to a large chromosomal inversion. In our CDMs, only chains α1, α2 and α3 were detected. To investigate the fetal enrichment, we assessed the longitudinal

transcriptional data to determine whether the fetal enrichment was due solely to increased expression these Col VI genes in fetal CFs. In this case, data was normalized to transcriptional abundance in fetal CFs at day 0 of CDM production. However, although fetal expression of Col VI chains did increase over the time in culture, transcript abundance was less than or equal to that of adult expression at days 0, 5, and 10 of CF culture (**Fig. 3.7B**). This raises the possibility that Col VI is better retained in fetal CDMs due to other factors, such as its binding partners, Col I, Col IV, laminin[291] and FN[292]. Of these foundational matrix proteins, only Col I appeared to significantly enriched, though only mildly (**Fig. 3.7A**). It is therefore possible that subtle differences in Col I contributed to enhanced retention of Col 6 in fetal CDMs. However, this does not rule out the potential that Col 6 retention is influenced by other factors such as unique temporal matrix dynamics, matrix organization, or non-protein components of the CDMs.

This data, in conjunction with previously discussed proteins present in CDMs, underscores the non-linear relationship of matrix-associated transcripts and incorporation/retention into the ECM. In the case of Col VI, it suggests that binding profile, or other post-transcriptional influences, dictate Col VI abundance more than transcript production. Notably though, this fetal enrichment of Col VI is consistent with MS analyses of primary tissue-derived cardiac ECM[59]. As such, it will be explored in more detail in section 4.

Additionally, adult CDMs were notably enriched for S100 proteins and annexins (**Table 3.1**), which are calcium-sensitive proteins that influence both intracellular and extracellular functions. S100 proteins are a family of small proteins with diverse functions, united by structural similarities that typically include an EF-hand calcium binding domain[293]. Calcium is a common second messenger that interacts with many crucial EF-hand-containing proteins in the heart, such as calmodulin[294] and troponin C[295]. Of the many S100 proteins, subsets are associated with individual cell types and cell compartments, and can form both homo-dimers and hetero-dimers. This leads to wide range of potential configurations and influences multiple cell functions, including phosphorylation

events and signal transduction, as well as morphology and motility[293,296]. Similarly, annexins are a family of calcium-binding proteins that form a multitude of complexes to influence many cell behaviors[297]. They are unique from S100 proteins in that they can also bind cell membranes - canonically, annexins bind phospholipids and participate in membrane binding and vesicle formation. However, they also interact with cytoskeletal proteins, particularly at the internal cell membrane, and some annexins are reported to bind both DNA and RNA[297], and to be secreted extracellularly.

S100 proteins and annexins also complex with each other. The variety of reported S100 and annexin dimers leads to a multitude of potential complexes with a further variety of potential influences over cell function. The primary annexins in the heart are annexin A2, A5, A6 and A7[298] – each of which, except A5, are enriched in adult CDMs. Annexin A2, in particular, binds several S100 proteins[299] – of which S100A6 and S100A11 are also enriched in adult CDMs, and S100A10, which is common to both fetal and adult CDMs. Annexin A6 and its binding partner S100A11[300] are also both enriched in adult CDMs, as are several other S100 proteins (**Table 3.1**).

Notably, though, the extent and mechanism of secretion of annexins or annexin-S100 protein complexes is unknown. As annexins and S100 proteins are potentially secreted, they were included in the Matrisome[233] database that this data references. However, particularly because annexins are membrane-associated, and because the non-detergent decellularization of CDMs permits residual non-matrix proteins, this data does not provide clarity on whether the annexins and S100 proteins detected in CDMs were from the extracellular compartment or a co-contaminant of the residual cell membranes. However, they represent a minimally-explored class of proteins that are distinctly enriched in adult CDMs, which may influence cells that are later seeded onto these CDMs.

The concordance of fetal and adult enrichment of matrix-associated proteins in human cardiac CDMs with known cardiac developmentally- and functionally-relevant ECM demonstrates the

ability of human CF-derived matrix to recapitulate age-specific cardiac tissue ECM. Many of the age-specifically enriched CDM proteins listed in **Table 3.1** have been investigated in very few, if any, cardiac biological processes. They, therefore, represent potential candidates to further explore in the context of cardiac biology driven and reinforced by the ECM.

Table 3.1 Enrichment of proteins in fetal and adult human CDMs.

UniProt ID	Protein	Adult Enrichment	adj. p value
P02461	Collagen alpha-1 (III) chain	Fetal only	0.0000
P05997	Collagen alpha-2 (V) chain	Fetal only	0.0000
Q12805	EGF-containing fibulin-like extracellular matrix protein 1	Fetal only	0.0000
Q9Y6C2	EMILIN-1	Fetal only	0.0000
Q9Y625	Glypican-6 [Cleaved into: Secreted glypican-6]	Fetal only	0.0000
P24593	Insulin-like growth factor-binding protein 5	Fetal only	0.0000
P01584	Interleukin-1 beta	Fetal only	0.0000
Q08431	Lactadherin	Fetal only	0.0000
P01033	Metalloproteinase inhibitor 1	Fetal only	0.0000
P55001	Microfibrillar-associated protein 2	Fetal only	0.0000
P51888	Prolargin	Fetal only	0.0000
P28300	Protein-lysine 6-oxidase	Fetal only	0.0000
Q6UVK1	Chondroitin sulfate proteoglycan 4	Fetal only	0.0000
P02458	Collagen alpha-1 (II) chain	Fetal only	0.0000
Q02388	Collagen alpha-1 (VII) chain	Fetal only	0.0000
Q5KU26	Collectin-12	Fetal only	0.0000
Q6UXH1	Cysteine-rich with EGF-like domain protein 2	Fetal only	0.0000
P53634	Dipeptidyl peptidase 1	Fetal only	0.0000
Q9UHF1	Epidermal growth factor-like protein 7	Fetal only	0.0000
Q14393	Growth arrest-specific protein 6	Fetal only	0.0000
P10145	Interleukin-8	Fetal only	0.0000
P55268	Laminin subunit beta-2	Fetal only	0.0000
P05120	Plasminogen activator inhibitor 2	Fetal only	0.0000
Q6ZMP0	Thrombospondin type-1 domain-containing protein 4	Fetal only	0.0000
P00750	Tissue-type plasminogen activator	Fetal only	0.0000
P00749	Urokinase-type plasminogen activator	Fetal only	0.0000
P29279	Connective tissue growth factor	Adult only	0.0000
P07585	Decorin	Adult only	0.0000
Q13443	Disintegrin and metalloproteinase domain-containing protein 9	Adult only	0.0000
Q4ZHG4	Fibronectin type III domain-containing protein 1	Adult only	0.0000

Table 3.1 continued

UniProt ID	Protein	Adult Enrichment	adj. p value
Q13361	Microfibrillar-associated protein 5	Adult only	0.0000
P22735	Protein-glutamine gamma-glutamyltransferase K	Adult only	0.0000
P48061	Stromal cell-derived factor 1	Adult only	0.0000
P61812	Transforming growth factor beta-2	Adult only	0.0000
P09525	Annexin A4	Adult only	0.0000
Q96HD1	Cysteine-rich with EGF-like domain protein 1	Adult only	0.0000
Q8IWU6	Extracellular sulfatase Sulf-1	Adult only	0.0000
P30740	Leukocyte elastase inhibitor	Adult only	0.0000
P08493	Matrix Gla protein	Adult only	0.0000
P26447	Protein S100-A4	Adult only	0.0000
P50453	Serpin B9	Adult only	0.0000
P35442	Thrombospondin-2	Adult only	0.0000
P12110	Collagen alpha-2 (VI) chain	-1.99	0.0000
P12109	Collagen alpha-1 (VI chain)	-3.10	0.0000
P50281	Matrix metalloproteinase-14	-1.64	0.0003
P24821	Tenascin	-2.58	0.0003
O60565	Gremlin-1	-1.83	0.0003
P12111	Collagen alpha-3 (VI) chain	-2.22	0.0003
P31949	Protein S100-A11	1.88	0.0004
P21980	Protein-glutamine gamma-glutamyltransferase 2	1.71	0.0004
P41221	Protein Wnt-5a	-1.66	0.0004
Q99715	Collagen alpha-1 (XII) chain	-1.92	0.0004
P08133	Annexin A6	2.14	0.0006
P04080	Cystatin-B	2.61	0.0007
Q15582	Transforming growth factor-beta-induced protein ig-h3	-2.09	0.0008
P07858	Cathepsin B	-1.42	0.0011
P06703	Protein S100-A6	2.26	0.0012
P50995	Annexin A11	1.48	0.0012
Q9Y4K0	Lysyl oxidase homolog 2	-1.34	0.0015
P35556	Fibrillin-2	-1.45	0.0022
Q99988	Growth/differentiation factor 15	1.16	0.0022
Q92626	Peroxidasin homolog	-1.03	0.0034
Q14766	Latent-transforming growth factor beta-binding protein 1	-1.22	0.0047
P08123	Collagen alpha-2 (I) chain	-0.89	0.0051
P13611	Versican core protein	-1.15	0.0074
Q16270	Insulin-like growth factor-binding protein 7	1.28	0.0120
P49257	Protein ERGIC-53	-1.40	0.0124
P20073	Annexin A7	1.79	0.0129

Table 3.1 continued

UniProt ID	Protein	Adult Enrichment	adj. p value
P10915	Hyaluronan and proteoglycan link protein 1	1.09	0.0142
O60687	Sushi repeat-containing protein SRPX2	-0.86	0.0142
O43854	EGF-like repeat and discoidin I-like domain-containing protein 3	-1.22	0.0180
P08253	72 kDa type IV collagenase	-1.75	0.0180
P50454	Serpin H1	-1.55	0.0233
P80162	C-X-C motif chemokine 6	1.75	0.0236
O00469	Procollagen-lysine,2-oxoglutarate 5-dioxygenase 2	0.61	0.0241
Q96CG8	Collagen triple helix repeat-containing protein 1	-0.70	0.0241
P07355	Annexin A2	1.36	0.0244
P17931	Galectin-3	2.47	0.0258
Q14767	Latent-transforming growth factor beta-binding protein 2	1.06	0.0258
P05121	Plasminogen activator inhibitor 1	1.03	0.0265
P02452	Collagen alpha-1 (I) chain	-0.91	0.0284
Q99584	Protein S100-A13	1.11	0.0356
P11047	Laminin subunit gamma-1	-0.65	0.0453
P04083	Annexin A1	0.87	0.0462
P00488	Coagulation factor XIII A chain	0.73	0.0462
P08758	Annexin A5	0.51	0.0488
P09486	SPARC	-1.63	0.0532
P13674	Prolyl 4-hydroxylase subunit alpha-1	-0.80	0.0621
P22692	Insulin-like growth factor-binding protein 4	0.68	0.0625
Q02809	Procollagen-lysine,2-oxoglutarate 5-dioxygenase 1	-0.92	0.0625
P02751	Fibronectin	0.81	0.0630
P02462	Collagen alpha-1 (IV) chain	-1.41	0.0693
Q08397	Lysyl oxidase homolog 1	1.11	0.0726
Q15063	Periostin	-0.80	0.0726
O60568	Procollagen-lysine,2-oxoglutarate 5-dioxygenase 3	-0.84	0.0805
Q96FQ6	Protein S100-A16	0.75	0.0874
P07942	Laminin subunit beta-1	0.17	0.0962
P78539	Sushi repeat-containing protein SRPX	-1.06	0.1086
P35555	Fibrillin-1	-1.86	0.1086
P20908	Collagen alpha-1 (V) chain	-0.49	0.1144
Q8IVL6	Prolyl 3-hydroxylase 3	-0.72	0.1197
P35237	Serpin B6	0.81	0.1266
Q9NS15	Latent-transforming growth factor beta-binding protein 3	0.58	0.1266
P27658	Collagen alpha-1 (VIII) chain	0.66	0.1293
Q14112	Nidogen-2	-1.23	0.1409

Table 3.1 continued

UniProt ID	Protein	Adult Enrichment	adj. p value
P60903	Protein S100-A10	-0.94	0.1569
P07339	Cathepsin D	0.86	0.1603
P01040	Cystatin-A	2.21	0.1783
P50452	Serpin B8	0.47	0.1982
P02679	Fibrinogen gamma chain	1.26	0.1999
P07093	Glia-derived nexin	0.32	0.2092
O15460	Prolyl 4-hydroxylase subunit alpha-2	0.29	0.2176
P07996	Thrombospondin-1	-0.79	0.2176
P01344	Insulin-like growth factor II	-0.96	0.2253
Q12841	Follistatin-related protein 1	-0.34	0.2281
Q92743	Serine protease HTRA1	-0.47	0.2547
P05109	Protein S100-A8	1.75	0.2967
Q13219	Pappalysin-1	0.68	0.3277
O00622	Protein CYR61	0.50	0.3378
P09382	Galectin-1	-0.55	0.3378
Q32P28	Prolyl 3-hydroxylase 1	0.43	0.4793
P08572	Collagen alpha-2 (IV) chain	-0.38	0.4793
P21810	Biglycan	0.39	0.4914
Q7Z4N8	Prolyl 4-hydroxylase subunit alpha-3	0.30	0.4914
P13497	Bone morphogenetic protein 1	-1.21	0.4987
P06702	Protein S100-A9	0.57	0.5061
O15031	Plexin-B2	-0.39	0.5188
P35030	Trypsin-3	0.31	0.5863
P09341	Growth-regulated alpha protein	0.52	0.5901
Q9BY76	Angiopoietin-related protein 4	-0.17	0.6509
P98160	Basement membrane-specific heparan sulfate proteoglycan core protein	0.12	0.6566
Q07092	Collagen alpha-1 (XVI) chain)	0.13	0.9259
P09038	Fibroblast growth factor 2	N/A	N/A
P47929	Galectin-7	1.38	N/A
Q15113	Procollagen C-endopeptidase enhancer 1	-1.03	N/A

Table 3.2 GO enrichment analysis of fetal and adult human CDM protein composition.

CDM	Biological Process			Molecular Function		
	GO term	***Description***	***FDR***	***GO term***	***Description***	***FDR***
Fetal	GO:0030198	extracellular matrix organization	5.93E-29	GO:0019838	growth factor binding	8.63E-08
	GO:0009653	anatomical structure morphogenesis	5.85E-14	GO:0005201	extracellular matrix structural constituent	1.80E-06
	GO:0048646	anatomical structure formation involved in morphogenesis	2.41E-11	GO:0048407	platelet-derived growth factor binding	1.80E-06
	GO:0030199	collagen fibril organization	2.90E-11	GO:0005102	signaling receptor binding	1.63E-05
	GO:0072359	circulatory system development	2.25E-09	GO:0005178	integrin binding	1.63E-05
Adult	GO:0032940	secretion by cell	0.00044	GO:0048306	calcium-dependent protein binding	3.37E-14
	GO:0018149	peptide cross-linking	0.00073	GO:0005509	calcium ion binding	6.48E-12
	GO:0045055	regulated exocytosis	0.001	GO:0005544	calcium-dependent phospholipid binding	4.31E-09
	GO:0009888	tissue development	0.0013	GO:0044548	S100 protein binding	3.37E-07
	GO:0016192	vesicle-mediated transport	0.0016	GO:0046872	metal ion binding	1.19E-05

3.3 Conclusions and Discussion

The ontogenic changes undertaken by the cardiac ECM are complex and nuanced. They involve a shift from the ECM of the developing heart, which is loosely organized[110] and rich in factors[59] that promote morphogenesis[188,301] and proliferation[102], to the matrix of the adult heart, which is highly aligned, crosslinked, and rich in factors that support homeostasis and mechanical function[59,84,115,116]. The majority of studies that recognize the necessity of the ECM in cardiac function either rely on simplistic engineered environments[263,264] or native matrix with minimal means of *in situ* perturbation, which is often digested and therefore contains limited structural complexity[102,139,205]. Application of a tractable model of age-specific matrix environments enables a variety of mechanistic and engineering studies that tractably dissect and leverage the contribution of the native ECM to cardiac tissue function.

In this work, we demonstrate the ontogenic cardiac characteristics reflected by age-specific human cardiac CDMs. We subjected fetal and adult human CFs and CDMs to rigorous analysis of their structural and compositional attributes and found that they did retain a variety of age-dependent elements at the transcriptional, organizational and proteomic level. Fetal and adult CFs, themselves, displayed age-dependent growth dynamics and transcriptional profiles. Specifically, fetal CFs expressed more pro-mitotic factors matrix proteases, and adult CFs expression more chemokines and inflammation-related molecules. And while these categorical trends did carryover to the matrix produced by the CFs, it was not necessarily reflected by the exact same proteins enriched in fetal and adult CDMs being detectably upregulated in fetal or adult CFs. This emphasized the non-linear relationship of transcriptional and proteomic regulation of the ECM, and we, thus, focused our efforts of characterizing the fetal and adult CDMs.

Structurally, CDMs only recapitulated certain elements of age-specific cardiac tissue. When observing matrix fibrils, fetal CDMs demonstrated the thin, loosely coiled bundling expected of fetal tissue, and adult CDMs contained thick, highly-bundled fibrils indicative of the organized and

crosslinked adult tissue. However, the ultrastructure of the deposited matrix was highly aligned in CDMs of both ages, putatively due to the cellular organization resulting from the activated myofibroblast state[168] adopted by human CFs. Thus, these CDMS retain age-specific characteristics at the subcellular level, but both fetal and adult CDMs provide the enforced alignment that is typical of adult cardiac tissue and engineering strategies aimed at cardiac maturation[126,138,302]. This represents a confounding element of the CDMs for the study of some fetal-specific characteristics and cell-matrix interactions, but may also provide an advantage for the use of adult CDMs in studies of maturation, which is a major emphasis in iPSC-CM culture and tissue models[70,118,139]. Additionally, this common alignment between fetal and adult CDMs enables a more direct comparison of age-specific compositional differences and their impact on cardiac cells.

Compositionally, fetal and adult CDMs each contained over 100 matrix proteins belonging to all expected functional classes[233], which is indicative of the rich and complex matrix milieu presented the CDMs. Additionally, there were several hallmarks of developing and mature cardiac matrix identified in fetal and adult CDMs, respectively. Both retained sulfated GAGs, though they were particularly enriched in the fetal CDM, which would be expected of a matrix environment reflecting a developing tissue. Also enriched in fetal CDMs were numerous developmentally-associated proteoglycans and secreted morphogens, whereas the adult CDMs contained an abundance of matrix crosslinkers and secreted molecules associated with cardiac disease. As both fetal and adult CFs had adopted the myofibroblast state, this enrichment of fibrosis-related proteins in adult CDMs is more likely to reflect the natural propensities of adult CFs than an artifact of *in vitro* culture.

The age-specific enrichment of multiple classes of matrix and matrix-associated proteins in the human CDMs bolstered the applicability of fetal and adult CDMs to study ontogenic matrix environments and interactions, particularly when coupled with the evidence that they are being

presented in matrix structurally reminiscent of age-specific tissues. Additionally, it suggests that the enrichment of other proteins with no known age-specific or cardiac functions may also be indicative of genuine cardiac tissue biology, and are candidates for future studies of matrix-regulated CM behavior. This study's approach of creating a structural complex, yet defined, CDM represents an advancement in our approach to understanding matrix assembly and cell-matrix interactions in an easily perturbable model that can help identify nuances of ECM biology.

Chapter 4: Human iPSC-CM Phenotypic and Metabolic Response to Age-Specific Human CDMs

Throughout CM development and maturation, there are numerous morphological and functional changes that occur to promote their contractile efficiency. Characterization of these changes requires a battery of assays associated with the cytoskeleton, electrophysiology and metabolism, and specific metrics have become associated with these age-dependent changes as hallmarks of CM maturation. Adult CMs are characterized by regimented cytoskeletal organization and high metabolic demands to support ongoing oscillatory contractions[70,71,121,124,303]. Though fetal CMs are small with disorganized sarcomeres, postnatally they become elongated with regularly spaced, parallel sarcomeres[71,121]. This morphology and structure are crucial to perpetuate uniaxial contractions that coordinate the contraction of the heart to sustain blood flow. Also essential to this process is the synchronization of individual CM contractions, which is dictated by the propagation of electrical impulses that flow between cells via gap junctions. As the heart matures, these gap junction proteins localize to the intercalated discs that bridge adjected cardiomyocytes[304], along with ion channels and other cell-cell adhesion proteins, such as plakophilin-2 and cadherins[127,305]. This cellular arrangement and coupling is crucial for efficient propagation of electrical signal, and the aggregation of these junctional and adhesion proteins to the short axes between elongated CMs is a morphological hallmark of functional maturation[144].

There are many factors driving the elongation of developing CMs *in vivo*, including electrical stimulation[138] and mechanical stretch[306]. It has also been shown that enforced morphological constraints can promote electrophysiological properties associated with mature CMs[126]. As such, the morphological and contraction properties of CMs are inherently linked, though there is no single causative factor – each influences the other. The relationship between the cardiac ECM and cell morphology is equally ambiguous. The ECM surrounds all cells, both as interstitial matrix and, in the case of CMs, as basement membrane. As the heart develops into adulthood, the ECM

becomes aligned, mirroring the regular spacing and alignment of the CMs. It also becomes more abundant, more highly crosslinked and therefore stiffer, reinforcing the CM morphology and, thus, their axis of contraction.

The ECM also regulates other processes crucial to CM function, including metabolism, though this links have been primarily established in skeletal muscle; mutations in several ECM genes are associated with muscular dystrophies characterized by metabolic deficits[159–161]. Additionally, mutations in the protein dystrophin, which links the cytoskeleton to transmembrane ECM-adhesion complexes, induce contractile impairment in both skeletal and cardiac muscle[162] and has noted mitochondrial deficits[163,164]. Thus, the loss of certain elements in the ECM or cell-ECM adhesion can hinder mitochondrial function in striated muscle, implying that certain elements of the ECM are critical to metabolism.

We sought to determine whether age-specific human CDMs influenced structural, electrophysiological or metabolic elements of CM function, particularly those that were specific to pre- or post-natal physiology. We addressed this by seeding fetal and adult CDMs with iPSC-CMs which, though committed in their differentiation, are fairly immature and plastic. As such, they present the opportunity to study cardiac phenotypes associated with both development and maturation, allowing the investigation of the influence of fetal and adult cardiac ECM on a single, receptive cell source.

4.1 CDM Influence on iPSC-CM Morphology

To investigate the influence of CDMs on CM physiology, we first seeded primary fetal mouse CMs onto both mouse and human CDMs (**Fig. 4.1A**). CMs were able to adhere and remain viable, as indicated by visible contractions during culture durations of up to 7 days. The CMs were especially responsive to the matrix fibril orientations of each CDM, and displayed a fairly spread morphology

on mouse CDMs, which do not exhibit aligned matrix fibrils, but an incredibly thin, elongated morphology on human CDMs, which are highly aligned, thus demonstrating that CM morphology corresponds to the CDMs' respective organization. However, the patterning of fetal and adult CDMs are much more similar (Chapter 3). To determine whether the chemical composition of fetal and adult CDMs differentially impacted CMs, we worked in an entirely human system, and seeded human iPSC-CMs at day 15 of differentiation onto human fetal and adult CDMs for a minimum of 3 days at low densities. These parameters were specifically chosen because day 15 represents a committed but relatively immature stage of CM differentiation, and to allow the CDMs to be the predominant influence over CMs, rather than interactions dictate by cell-cell adhesions. Strikingly, we did observe distinct CM morphologies on age specific CDMs, particularly in the cellular width. On fetal CDMs, CMs were especially thin and elongated, whereas on adult CDMs they were notably wider and shorter (**Fig. 4.1B, upper**). Notably, the morphology of the CMs is readily apparent in the CDMs post-seeding, as demonstrated by the immunolabeling of FN (**Fig. 4.1B, middle**). Matrix fibrils in CDMs have regular spacing and consistent coverage (Chapter 2), but a clear negative space is observed in the FN where CMs have adhered. This phenomenon was observed throughout multiple experiments and is unlikely to be a technical artifact. Instead, it suggests that CMs are actively remodeling the FN beneath them, likely to migrate into the matrix itself, rather than adhering to it as merely a basal layer.

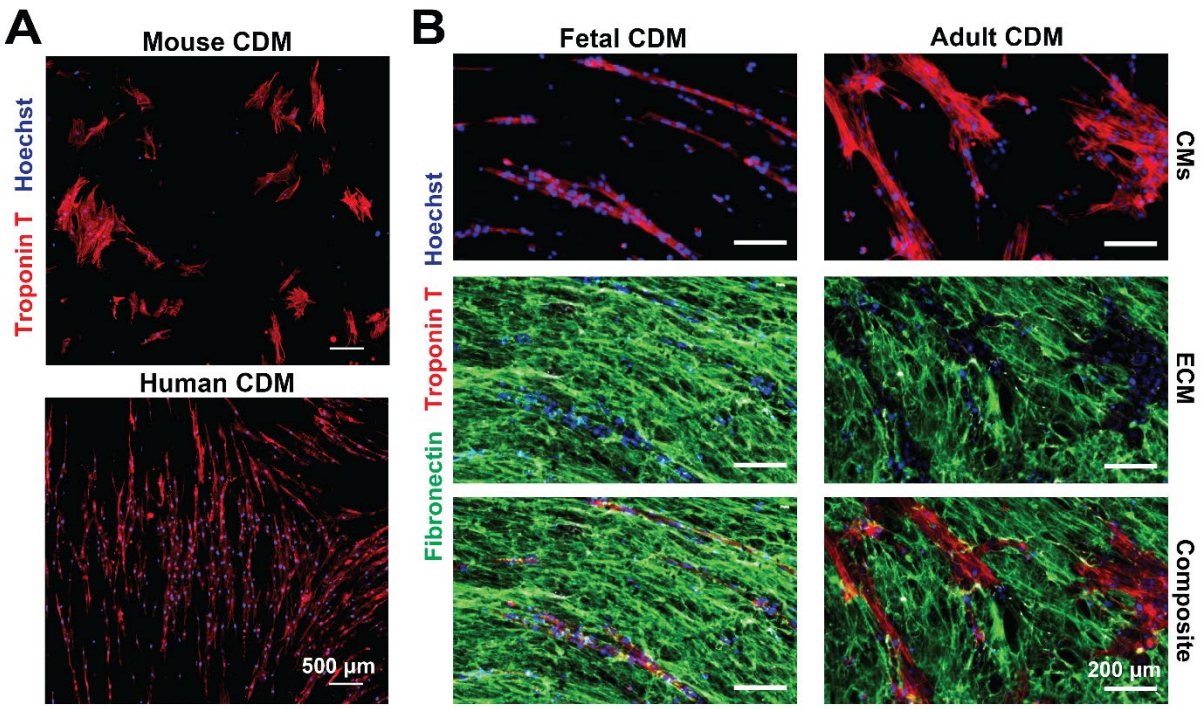

Fig. 4.1 Morphology of CMs seeded onto CDMs. A) Primary E14 murine CMs seeded onto mouse and human fetal CDMs. B) Human iPSC-CMs seeded onto human fetal and adult CDMs. Cardiac troponin T (red), fibronectin (green) and Hoechst (blue).

To further investigate the CM response to matrix structure, we performed high-resolution confocal imaging of human iPSC-CMs seeded onto human fetal and adult CDMs. We also seeded these CMs onto Matrigel at the same density to investigate potential advantages of thicker, tissue-like matrices over the common culture substrates used for iPSC-CMs. Confocal microscopy revealed that CMs did, indeed, embed themselves into the CDMs, enabling multidirectional matrix cues instead of the basally-restricted matrix cues provided by Matrigel (**Fig. 4.1A, XZ and YZ views**). This is more similar to the cell-matrix orientations found in tissue[110,262], and also promotes more tissue like matrix adhesions through integrin localization and binding[197]. Additionally, the variable orientation and morphology of CMs on CDMs, and lack of alignment when cultured on Matrigel, indicated that the alignment observed in CMs on human CDMs does correspond to the orientation of the matrix fibrils. In fact, cellular orientation was especially well-correlated to matrix, particularly

in CMs on fetal CDMs. (**Fig. 4.1B**). On adult CDMs, the majority but not all cells were oriented along the direction of matrix fibrils.

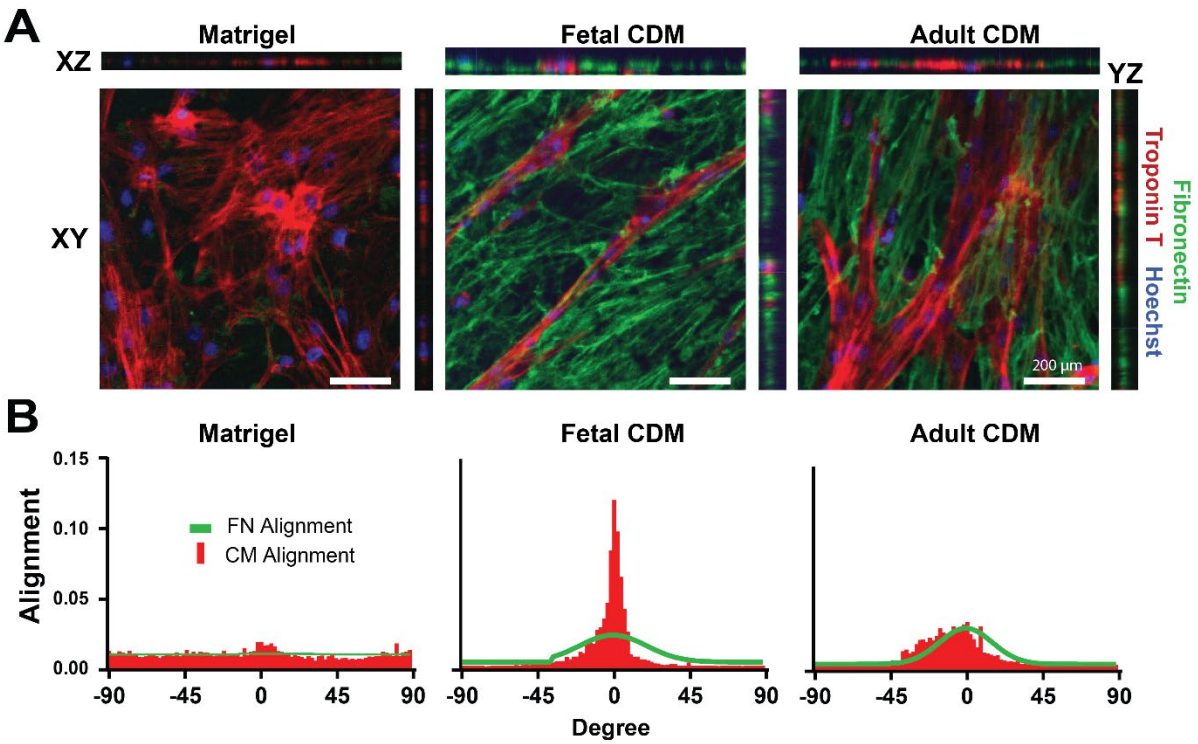

Fig. 4.2 Alignment of iPSC-CMs cultured on Matrigel and fetal and adult human CDMs. A) iPSC-CM morphology when cultured in XY, XZ and YZ planes. B) Alignment of fibronectin fibers in Matrigel and CDMs, and alignment of corresponding cultured iPSC-CMs.

We then assessed whether this alignment promoted any differences in cell-cell adhesions (**Fig. 4.3A**) and aspect ratio (**Fig. 4.3B**) by visualizing the presence and localization of the desmosome-associated protein plakophilin-2 via immunocytochemistry and measuring cell widths manually in FIJI. Many junctional proteins are enriched at the intercalated disc at the minor axis between CMs, with 30% distributed to the lateral cell borders[304]. Plakophilin-2 is also enriched at the intercalated discs in mature CMs, where it serves to promote electrophysiological coupling[131,132]. Additionally, CMs increase in size as they mature[93,307], and so while the combination of cell size, aspect ratio and desmosomal positioning are not demonstrable proof of CM maturation, they are visual indicators of various hallmarks associated with maturation. Upon examination, plakophilin-2 had

distinct positional phenotypes in CMs on each culture substrate (**Fig. 4.3A**). It was present but radially localized in CMs cultured on Matrigel, which had minimal indication of cell elongation and, consequently, a low aspect ratio (**Fig. 4.3B**), and did not exhibit the polarization of desmosomes to end-to-end CM connections that is observed in native adult tissue. CMs on fetal CDMs exhibited the smallest cellular area, and though plakophilin-2 was present at the CM borders, it was also diffusely localized over the entire CM area, which is indicative of desmosomes in immature CMs. Adult CDMs promoted the most notable localized enrichment of plakophilin-2 along the short axis of each CM at the putative intercalated discs, suggesting a cellular structure that is more mature than those of CMs on either the Matrigel or fetal CDMs. Notably though, CMs on adult CDMs did not have the highest aspect ratio, which was instead induced by the fetal CDMs. This is likely due to differences in the size of the CFs that produced these matrices, and the widths between the matrix fibrils they deposited, as expected. However, CMs on these matrices did not adhere to the pattern seen on in CMs cultured on stamped matrix substrates, wherein the highest aspect ratio promoted the most contractile force and velocity[126]. Instead, the combination of factors in the adult CDM promoted the most morphologically mature CM, based on the structural parameters tested, but this was not readily correlated to any single factor such as cell size of aspect ratio, but instead a combination of several factors, potentially including those not tested here.

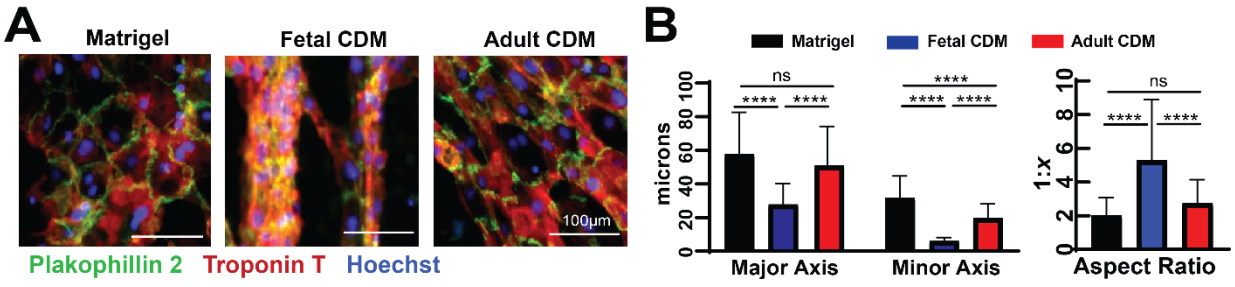

Fig. 4.3 Size of iPSC-CMs cultured on Matrigel and fetal and adult human CDMs. A) iPSC-CM morphology when cultured in XY, XZ and YZ planes. B) Alignment of fibronectin fibers in Matrigel and CDMs, and alignment of corresponding cultured iPSC-CMs.

We further found that the degree of alignment was not necessarily dependent on cell density. Instead, iPSC-CMs seeded at low (50K/cm^2), medium (250K/cm^2) and high (500K/cm^2) densities all responded to the alignment of adult human CDMs (**Fig. 4.4**). Additionally, at high densities, the configuration of densely-packed, aligned CMs began to resemble that of adult ventricular tissue; a feature that could potentially be exploited for the development of tissue-like cardiac/matrix constructs in the future. As a note, the adhesion efficiency of iPSC-CMs to CDMs was highly dependent on the presence of serum in the plating media. Serum contains an abundance of matrix proteins and is commonly used to promote adhesion in CM culture. The seeding densities listed above represent the numbers needed in the absence of serum. However, in the presence of 10% serum supplemented into the CM media upon plating, cell numbers could be reduced ten-fold.

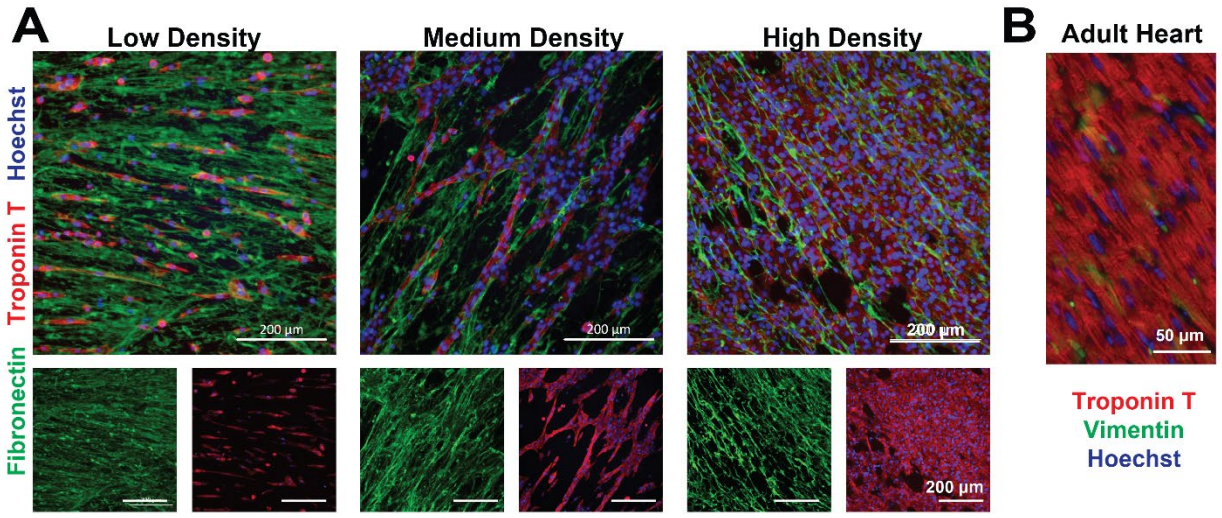

Fig. 4.4 CM alignment on CDMs. A) Human iPSC-CMs seeded onto human adult CDMs at low (50K/cm^2), medium (250K/cm^2) and high (500K/cm^2) densities, with ECM labeled via fibronectin (green). B) CM density and alignment in adult human heart tissue, with interspersed fibroblasts detected by vimentin (green). Cardiac troponin T (red) and Hoechst (blue).

CMs cultured on CDMs were especially sensitive to species- and age-dependent differences in matrix organization. CMs responded to topographical cues by adopting distinct morphologies and, when cultured on adult CDMs, desmosomal protein enrichment at putative intercalated discs. This

demonstrates the ability of CDM organization to instruct numerous structural hallmarks of CM maturity, which has been a major focus of engineered cardiac tissue.

4.2 CDM Influence on iPSC-CM Contraction Dynamics

Given the relationship between CM structure and contractile properties, we sough to determine whether fetal and adult CDMs influenced contraction and CM electrophysiology. Specifically, the uniaxial enrichment of plakophilin-2 observed in CMs on adult CDMs (**Fig. 4.2**) is important for the directional calcium signaling and consequent efficient force contraction in the adult heart, which results in increased displacement of contraction velocity of individual CMs[308]. What we found, instead, was that CMs were particularly receptive to the presence of matrices, as opposed to Matrigel, with only minimal differences in their contractile response to age-specific CDMs. We assessed CM contraction by two means – first, by optical flow analysis of live CMs spontaneously contracting, captured by live imaging in brightfield (**Fig. 4.5A-D**), and second by the genetically encoded calcium reporter, GCaMP6 (**Fig. 4.5D-F**), which fluoresces during the cyclical flux of calcium into CMs during action potential generation[146,147]. CMs grown on fetal and adult CDMs exhibited much more uniform axes of contraction compared to those cultured on Matrigel (**Fig. 4.5A**), though matrix substrates had no impact on CM beat rate (**Fig. 4.5B**). However, culture on fetal CDMs increased CM contraction velocity (**Fig. 4.5C**), which resulted in three-fold greater total displacement (**Fig. 4.5D**). CMs on adult CDMs, however, exhibited an average displacement and velocity that was between that of CMs on Matrigel and on fetal CDMs, and was not significantly different than either condition. This elevated velocity in CMs on fetal CDMs may be attributable to the abundance of GAGs in fetal CDMs, which can promote viscoelasticity[270]. Additionally, relative to CMs cultured on Matrigel, calcium handling analyses indicated that CMs grown on both fetal and adult CDMs had a much faster downstroke (t50 down), which is regulated by potassium and calcium channels (**Fig. 4.5E**), with no change in the upstroke (t50 up) that is

regulated by sodium channels (**Fig. 4.5F**)[309]. Given that calcium handling is not directly reliant on substrate elasticity, the faster observed downstroke reflects differences in CM function on CDMs, as opposed to Matrigel, and demonstrate the indirect impact of the ECM environment on cell function.

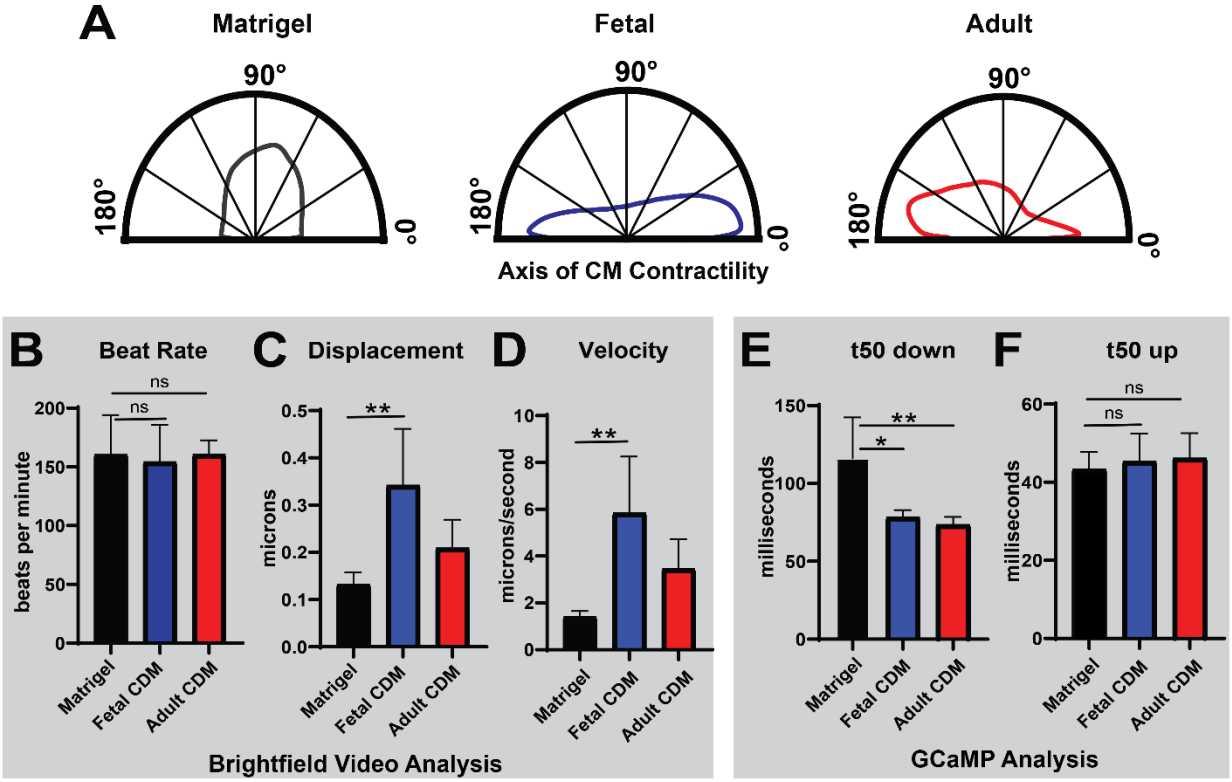

Fig. 4.5 Spontaneous contraction properties in human iPSC-CMs cultured on Matrigel and fetal and adult CDMs, assessed by optical flow analysis of brightfield (A-D) GCaMP indication of calcium flux (E-F) in live microscopy.

Collectively, these data indicate that CDMs improve the contractile function of CMs by promoting alignment, contraction velocity, and specific calcium handling properties that more closely resemble native heart tissue than those achieved by CMs cultured on Matrigel. These phenotypes appear largely correlated with the CM conformation to the structural alignment of age-specific matrices. The elongation of CMs observed enabled more uniform axes of contraction, as well increased speed of calcium handling correlated with enhanced calcium and potassium channels,

both of which are phenotypically associated with increased maturity. However, only the fetal CDM and not the adult CDM induced an increase in CM contractile displacement and velocity. While this is an inversion the phenotypes associated with age-specific environments, it is possible that the extreme elongation observed in CMs on fetal CDMs, and potential differences in viscoelasticity, contributed to the larger dynamic range of contraction displacement of CMs on fetal CDMs that was not matched by the relatively shorter CMs on adult CDMs (**Fig. 4.2B**). Similarly, ECM structure and composition exhibit specific viscoelastic properties which, while not measured here, may play a role in enabling CM contraction.

4.3 Contribution of Collagen VI to iPSC-CM Metabolism

Of the age-specific CDM properties previously identified (Chapter 3), one of the most striking was the enrichment of all three chains of Col VI in fetal CDMs. While this correlation has been noted in the ECM of fetal mouse hearts[59], Col VI is also crucial to metabolic function, and its loss impairs skeletal muscle regeneration[159] and induces muscular dystrophies characterized by metabolic deficiencies[160]. The genetic deletion of Col VI has been investigated in the context of cardiac injury[183], but revealed that the predominate phenotype of global Col VI loss influences the conversion of CFs to myofibroblasts in the adult heart, and therefore does not address whether cardiomyocytes, like skeletal myofibers[160], rely on the presence of Col 6 for physiological respiration.

We, therefore, chose to investigate the potential influence of fetal and adult cardiac CDMs on human iPSC-CMs in the context of Col VI loss. To do this, we leveraged the ability to specifically suppress individual transcripts during CDM production via siRNA-mediated silencing (Chapter 2). Fetal and adult CFs were transfected with non-targeting (NT) siRNAs, or a combination of siRNAs inhibiting COL6A1, COL6A2 and COL6A3 (KD) during culture. Since CDMs represent the

accumulation of protein production, Col VI was assessed in CFs after 10 days of culture with siRNA silencing by western blot (**Fig. 4.6A**) and in decellularized CDMs by immunofluorescent labeling (**Fig. 4.6B**). These analyses confirmed Col VI enrichment in un-silenced fetal CDMs, relative to adult CDMs, and showed that Col VI protein was dramatically reduced following Col VI KD. Notably, in some cases, suppression of Col VI destabilized the ECM to the point of CDM loss, and this was particularly frequent in the fetal CDMs, occurring in 4/6 replicates (**Fig. 4.6C**). The fetal CDMs that remained intact contained some residual Col VI protein, suggesting that the adult CDM, which innately has less Col VI, is better able to compensate for its absence. Additionally, this indicates that while the siRNA-treated adult CDMs represent a complete loss of Col VI protein, fetal CDMs have only a partial Col VI loss, which should be taken into account when interpreting the respective phenotypes cultured CMs.

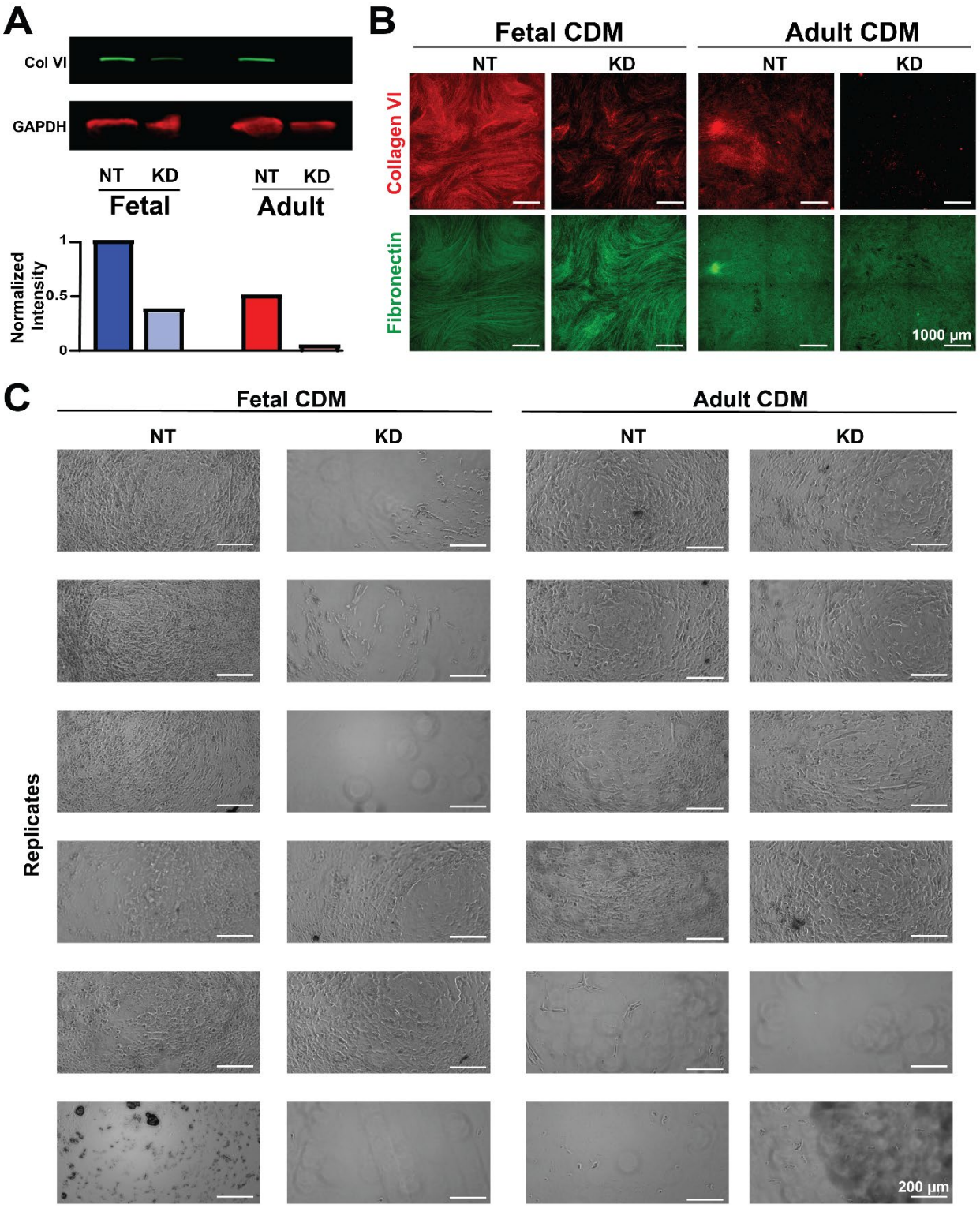

Fig. 4.6 Knockdown of Col VI (KD) protein in fetal and adult human CFs (A) and CDMs (B-C) by siRNA-mediated silencing. A) Western blot (upper) and intensity quantification (lower) of Col VI protein normalized to GAPDH. B) Immunofluorescent labeling of Col VI (red) and FN (green). C) Representative images of CDM replicates with Col VI KD.

To characterize the influence of Col VI on CM metabolism, CDM production was adapted to a 96-well plate format compatible with the Seahorse Extracellular Flux Analyzer. CM oxygen consumption rate (OCR) was assessed as a surrogate measurement for oxidative phosphorylation[310], an indicator of CM metabolic maturity[70], and extracellular acidification rate (ECAR) was assessed as measure of glycolysis[310], which is typical of immature CMs[70]. These properties were measured at basal levels and during induced metabolic stress (maximal levels) from the uncoupling key aspects of the electron transport chain. After 3 days of culture, CMs grown on adult CDMs had a higher maximal OCR than those on fetal CDMs (**Fig. 4.7A, C**), which is consistent with the increased oxidative phosphorylation observed in maturing CMs in the adult heart. Additionally, Col VI KD in fetal CDMs did not significantly alter OCR or ECAR properties, potentially due to the presence of residual Col VI protein. However, Col VI KD in adult CDMs reduced the maximal OCR achieved by CMs (**Fig. 4.7A, C, E**), without significantly altering basal OCR or ECAR (**Fig. 4.7A, B, D**).

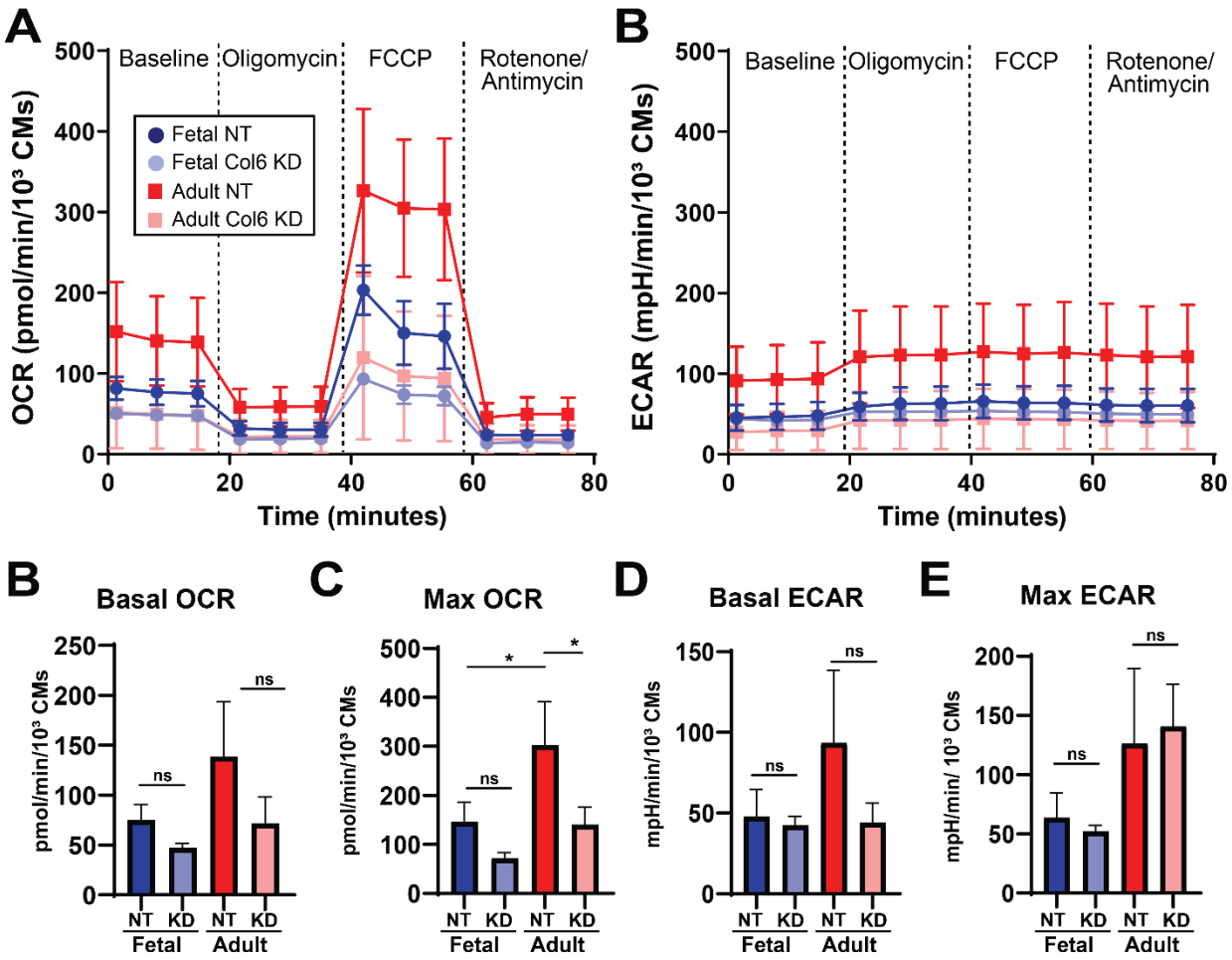

Fig. 4.7 Metabolic properties of CMs cultured on Col VI KD CDMs, normalized to CM number per well. Representative traces of oxygen consumption rate (OCR) (A) and extracellular acidification rate (ECAR) (B), quantified at the 3rd timepoint per treatment in B-C and D-E, respectively.

Given the relationship between metabolic demand and contraction in cardiomyocytes, particularly during peak demand simulated by the stress-inducing uncoupling of the electron transport chain, we investigated whether this reduced capacity for CM oxidative phosphorylation on adult KD CDMs influenced their contractile properties. We assessed both contraction dynamics and calcium flux, as was done previously (**Fig. 4.5**). The loss of Col VI from both fetal and adult CDMs had no impact on CM contractile properties, including beat rate, contractile displacement velocity, or downstroke time (**Fig. 4.8A-D**). While perhaps surprising, this is consistent with the lack of

reported cardiac dysfunction in Col VI-dependent muscular dystrophies[311] except during periods of physiological stress, such as pregnancy[312] or myocardial infarction[183].

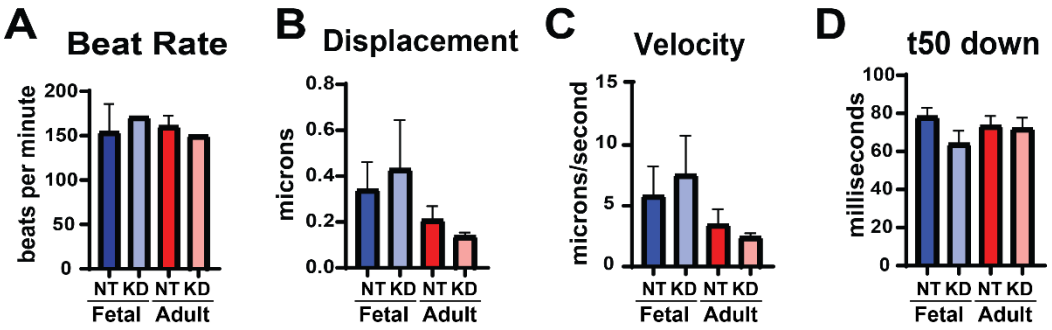

Fig. 4.8 CM contraction dynamics of iPSC-CMs on Col VI-deficient CDMs. Parameters measured by live imaging of A-C) spontaneous beating of brightfield and D) GCaMP fluorescence.

Thus, genetic suppression of Col VI had distinct influences on age-specific CDMs, and influences CM metabolism in the absence of additional cell types. Specifically, the loss of Col VI from adult CDMs influences CM metabolic respiration, specifically during simulated high energy demand, which is essential for metabolically active CMs to mature and respond to functional stressors and challenges, but this deficiency is not readily apparent in the contraction dynamics assessed here.

4.4 Conclusions and Discussion

The age-specific properties of CDMs had numerous influences on CM morphology and function. Notably, though, the correlation between CDM age and CM phenotype was not a direct correlation; adult CDMs did not unilaterally promote CM characteristics indicative of more advanced maturation than the characteristics of CMs on fetal CDMs. Instead, CMs responded to individual aspects of age-specific CDMs, which enabled a correlation between individual CM parameters and the CM response.

In particular, CMs responded to the structural organization of matrix fibrils of CDMs with distinctly age-dependent cell size, shape, cell-cell adhesions and contractile properties. Both fetal and adult human CDMs both promoted CM elongation and dictated the alignment and orientation of cultured CMs. However, CMs on fetal CDMs were more elongated, whereas CMs on adult CDMs exhibited uniaxial desmosomal protein localization at CM junctions. Notably, both of these phenotypes are associated with increased maturity in iPSC-CMs. However, elongation is expected to increase the contraction velocity and displacement, and putative electrical coupling observed in CMs on adult CDMs is associated with faster calcium flux in CMs. Instead, only fetal CDMs enabled faster CM contractions with higher displacement, and CDMs of both ages increased the action potential downstroke velocity. We interpret these phenotypic changes as responding to a combination of CDM-derived cues. Increased contraction displacement can result from higher elasticity of culture surfaces – which may be present in fetal CDMs as a result of both the coiled ECM fibrils and the hydration associated with GAG-rich tissues, providing more potential stretch of the matrix and, therefore, the cultured CMs[126]. The agnostic increase in calcium downstroke velocity on both fetal and adult CDMs also indicates that either a) plakophilin-2 enrichment at putative intercalated disks is not sufficient to promote electrical coupling requires to increase calcium flux rates, or b) that some other aspect of CDMs – possibly their alignment – is sufficient to increase calcium flux dynamics even without desmosomal formation, and that further maturity requires additional factors. The differential responses to age-specific CDMs also speaks to the inherent influence of the ECM on cardiac physiology, as these differences were observed after a relatively short culture duration, despite the observation that extended culture is often required to induce demonstrable maturation of stem cell-derived CMs on minimal ECM substrates[119].

Age-specific CDMs also influenced the maximal OCR of CMs, which is indicative of the peak oxidative phosphorylation possible during increased energy demand. This work demonstrates that culture on adult CDMs can promote greater respiratory capacity in CMs, thereby promoting

a major indicator of maturation, in a relative short time frame. It is, thus far, unexplored whether this is due to the correlated increase in putative intercalated disc formation in CMs on adult CDMs, but this age-specific property can be negated by the loss of an individual matrix protein – Col VI. In this case, the loss of Col VI had a detrimental impact on CM oxidative respiration without eliciting a compensatory increase in glycolysis, demonstrating the reliance of iPSC-CMs on Col VI for physiological respiration. Notably, though, this metabolic deficit on adult KD CDMs did not impair cardiac contractility or calcium handling, which is consistent with the lack of cardiac dysfunction in adult Col 6-deficient muscular dystrophies[311]. The differing metabolic and contractile responses further demonstrate that while the two functions are inherently linked in CMs by force-dependent bioenergetic demands[138,313], they can be uncoupled by intermediary steps.

It is notable that Col VI was particularly enriched in fetal CDMs, and yet the predominant influence of Col VI loss on CMs was observed in the context of adult CDMs. It is possible that Col VI has an equally important role in supporting CM respiration when cultured on fetal CDMs, and the inability to fully KD Col VI due to structural instability prevented us from fully exploring this phenotype. In the context of the developing heart, an abundance of Col VI might, then, serve to promote oxidative phosphorylation as the CMs are undergoing the maturation-associated metabolic shift away from glycolysis and towards oxidative respiration for increased ATP production[84,258] in the oxygen-rich environment associated adult physiology[259]. Additionally, it is also possible that the enrichment of Col VI in fetal CDMs accounts for a structural dependency that is not seen at later ages. However, the global deletion of Col VI is not associated with embryonic lethality, but instead associated with a reversion of the myofibroblast state[183]. Fetal development involves a similar, natural expansion of CFs that is not seen in adulthood except under pathological conditions[239], and it's possible that fetal matrices are especially reliant on a factor such as Col VI, which is associated with the CF proliferation and matrix production typical of development.

This work demonstrates that extracellular matrix reflective differential stages of development, modeled by CDMs, impart age-specific morphological and functional properties onto human cells. In this cardiac model, the influences of the ECM include CM shape, cell-cell adhesions, contraction dynamics and metabolism. The use of CDMs coupled with an atlas of their age-specific composition enabled the identification of Col VI as a crucial matrix protein for maximal metabolic respiration of iPSC-CMs. Furthermore, this work demonstrates the utility of age- and species-specific CDMs in dissecting complex cell-matrix biology.

Chapter 5. Influence of Age-specific CDMs on CM Proliferation

One of the most impactful ontogenic changes that occurs in the mammalian heart is the postnatal loss of regenerative capacity[3–6], which has lead to the prevalence of heart disease worldwide[2]. Cardiac regeneration occurs exclusively by proliferation of pre-existing CMs[78] in the fetal and early neonatal mammalian heart, after which the pathological response to injury such as hypertension and myocardial infarctions is via hypertrophy and fibrosis[93,314], which can develop to heart failure. Several key processes have been identified to regulate this age-dependent loss of proliferation in CMs[3,73], including hippo signaling[72,79,80], hypoxia and the postnatal increase reactive oxygen species[81,82], and the immune system[87–89]. CM proliferation involves a disorganization of existing sarcomeric structure[74,315], thereby implicating costameres and CM-ECM adhesion dynamics in the process. Recently, the individual components of the fetal ECM have been shown to promote CM proliferation[59] and cardiac regeneration[102,155,316]. As is the case for many developmental factors that promote CM proliferation, though they are less abundant after fetal development, the re-introduction of several of these factors can rescue the regenerative ability in adult mice[72,81,82,102,155]. As such, the identification of fetal factors that promote CM proliferation provide valuable information to ongoing therapeutic strategies for heart disease.

The ability of the fetal ECM to promote more CM proliferation than the adult ECM has been demonstrated *in vitro* with digested tissue-derived ECM[59,153]. However, to date, all studies exploring the contribution of the cardiac ECM to CM proliferation have done so with digested and/or solubilized ECM lacking the structurally-complex, tissue-like ECM demonstrated by our CDM system (Chapters 2-3). We, thus, sought to determine whether components of our fetal CDMs could support more CM proliferation than adult CDMs. To approach this, we investigated a broad number of fetal CDM proteins for their ability to promote DNA synthesis in CMs. Because DNA synthesis is decoupled from cytokinesis in mammalian CMs[3,6,99,101], this is not a definitive demonstration of proliferation. However, we perform these investigations in fetal mouse CMs,

which are still capable of cytokinesis, and impact on DNA synthesis is indicative of the ability to influence the cell cycle and, therefore, warrants further exploration.

5.1 Age-Specific CDMs are Differentially Permissive of DNA Synthesis in CMs

The fetal ECM has been demonstrated to support more CM proliferation than the neonatal or adult ECM. To determine whether our age-specific CDM model recapitulated this ontogenic function of the cardiac ECM, we seeded CMs onto fetal and adult CDMs and probed for DNA synthesis via labeling with EdU, which incorporates into newly synthesized DNA indicative of S-phase progression. We performed this experiment with both mouse and human CMs on CDMs from their respective species (**Fig. 5.1A, B**). Mouse CMs were isolated from fetal mouse hearts at E14 and labeled with EdU for 72h, and human CMs were differentiated from iPSCs for 15 days and EdU-labeled for 24 hours, to reflect the faster cycler time in human iPSC-CMs. Fetal mouse CMs and immature human CMs were specifically chosen because they possess a proliferative capacity to potentially be augmented/diminished by these studies and because, in the mouse, adult CMs are not able to be kept in culture. In both species, culture of CMs on fetal CDMs supported more progression through S phase than culture on adult CDMs. Next, we determined whether the pro-proliferative effect of fetal CDMs on CMs was species-specific by performing the inverse experiment, with mouse CMs on human CDMs and vice versa. Notably, we observed the same enrichment of EdU labeling in CMs on fetal CDMs (**Fig. 5.1C, D**) regardless of the species of origin. The majority of the structure and composition of mammalian ECM is conserved[317], and this data indicates that the proliferative response of CMs to the ECM is also conserved.

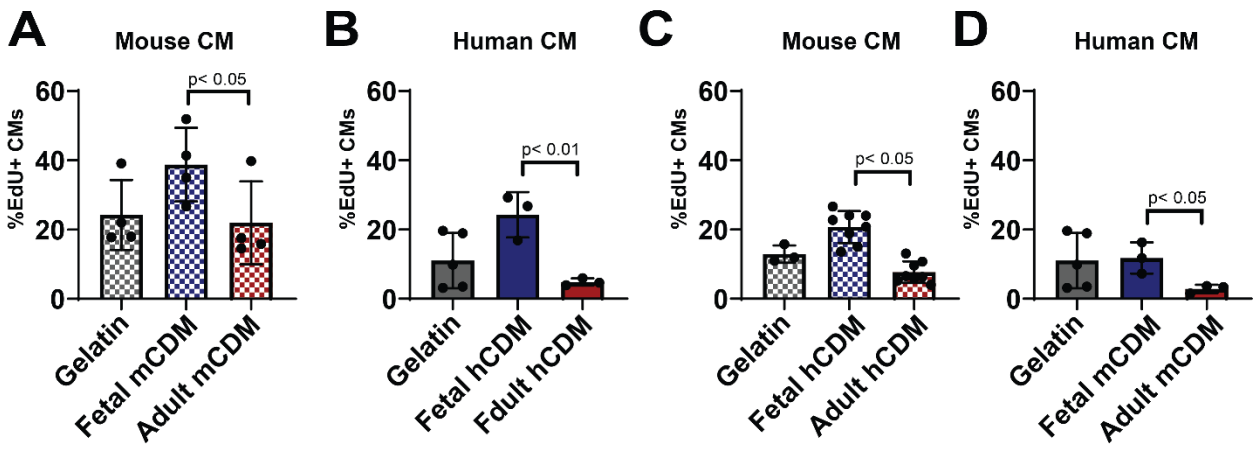

Fig. 5.1 DNA synthesis of CMs on species-specific CDMs. EdU incorporation into fetal (E14) mouse CMs and human iPSC-CMs (day 15) cultured on mouse CDMs (mCDM) and human (hCDM) age-specific CDMs. A) Mouse CM, mouse CDM. B) Human CM, human CDM. C) Mouse CM, human CDM. D) Human CM, mouse CDM.

5.2 Laminins as Regulators of CM Proliferation

The contrasting ability of fetal and adult CDMs to support CM DNA synthesis validates the use of CDMs as a model to explore the influence of cardiac ECM on CM proliferation. Coupled with our defined atlas of fetal and adult CDM compositions (**Fig. 3.7**, **Table 3.1**), this provided a list of candidate proteins potentially involved in the process. To augment this tool further, we assessed the composition of mouse fetal and adult CDMs by MS, although this was performed on single matrices and statistical analysis was not possible. Matrix proteins detected in mouse fetal and adult CDMs are listed in **Table 5.1**, alongside the age-specific enrichment found in human CDMs, if present. In mouse CDMs, 31 proteins were over 2-fold enriched in fetal CDMs, and 28 were over 2-fold enriched in adult CDMs. However, only 4 and 7 proteins were similarly upregulated in human fetal and adult CDMs, respectively. Among those with fetal enrichment in both species, 2 were laminin chains (laminin β2 and γ1), along with a Col V chain and the protease cathepsin B. Additionally, several other laminin chains (α5, β1) were enriched in fetal mouse CDMs, as well as the pro-regenerative fetal-associated protein agrin. Adult-enriched proteins in both mouse and

human CDMs were plasminogen activator inhibitor 1 (SerpinE1), IGFBP7, Matrix Gla protein, as well as annexins and S100 proteins.

Table 5.1 Age-specific enrichment of proteins in adult vs fetal mouse (Ms) CDMs, with correlating enrichment in human (Hu) CDMs and associated adjusted (adj.) p value. Enrichment is expressed as the log 2 Fold change (Log2FC). Proteins with matching age-specific enrichment in both Ms and Hu are bolded.

Ms UniProt ID	Protein	Ms Enrichment	Hu Enrichment	Hu adj. p value	Gene names
P02468	**Laminin subunit gamma-1**	**-20.50**	**-0.65**	**0.04526**	**Lamc1**
Q61292	**Laminin subunit beta-2**	**-16.65**	**Fetal Only**		**Lamb2**
P10605	**Cathepsin B**	**-2.00**	**-1.42**	**0.00108**	**Ctsb**
Q3U962	**Collagen alpha-2(V) chain**	**-1.47**	**-0.89**	**0.01795**	**Col5a2**
P10107	**Annexin A1**	**1.67**	**0.87**	**0.04620**	**Anxa1**
P19788	**Matrix Gla protein**	**2.08**	**Adult Only**		**Mgp**
Q07076	**Annexin A7**	**2.72**	**1.79**	**0.01293**	**Anxa7**
P22777	**Plasminogen activator inhibitor 1**	**17.10**	**1.03**	**0.02650**	**Serpine1**
Q61581	**Insulin-like growth factor-binding protein 7**	**19.15**	**1.28**	**0.01204**	**Igfbp7**
P07091	**Protein S100-A4**	**24.87**	**Adult Only**		**S100a4**
P14069	**Protein S100-A6**	**26.17**	**2.26**	**0.00118**	**S100a6**
P10493	Nidogen-1	-20.14	ND	ND	Nid1
Q61001	Laminin subunit alpha-5	-20.03	ND	ND	Lama5
P16110	Galectin-3	-19.88	2.47	0.02577	Lgals3
P08122	Collagen alpha-2(IV) chain	-19.03	0.11	0.76988	Col4a2
P18242	Cathepsin D	-18.93	-0.72	0.18912	Ctsd
P97384	Annexin A11	-18.74	1.48	0.00123	Anxa11
P02469	Laminin subunit beta-1	-18.44	0.17	0.09619	Lamb1
Q99JR5	Tubulointerstitial nephritis antigen-like	-17.75	ND	ND	Tinagl1
O88322	Nidogen-2	-17.56	-1.23	0.14095	Nid2
Q91WP6	Serine protease inhibitor A3N	-17.39	ND	ND	Serpina3n
P06797	Cathepsin L1	-17.37	ND	ND	Ctsl
A2ASQ1	Agrin	-16.11	ND	ND	Agrn
O35640	Annexin A8	-4.45	ND	ND	Anxa8
Q9R118	Serine protease HTRA1	-3.15	-0.47	0.25473	Htra1
P35441	Thrombospondin-1	-2.85	-0.79	0.21757	Thbs1
Q61702	Inter-alpha-trypsin inhibitor heavy chain H1	-2.42	ND	ND	Itih1
P02463	Collagen alpha-1(IV) chain	-2.39	-1.41	0.06926	Col4a1

Table 5.1 continued

Ms UniProt ID	Protein	Ms Enrichment	Hu Enrichment	Hu adj. p value
P21981	Protein-glutamine gamma-glutamyltransferase 2	-1.74	1.71	0.00039
Q3V1T4	Prolyl 3-hydroxylase 1	-1.57	-0.18	0.54377
P16675	Lysosomal protective protein	-1.41	ND	ND
O35639	Annexin A3	-0.98	ND	ND
Q99KC8	von Willebrand factor A domain-containing protein 5A	-0.85	ND	ND
Q62426	Cystatin-B	-0.72	2.61	0.00074
P50543	Protein S100-A11	-0.51	1.88	0.00039
Q05793	Basement membrane-specific heparan sulfate proteoglycan core protein	-0.39	0.12	0.65661
P11276	Fibronectin	-0.39	0.13	0.54377
Q91XD7	Cysteine-rich with EGF-like domain protein 1	-0.30	Adult Only	
P09535	Insulin-like growth factor II	-0.08	-0.96	0.22535
P14824	Annexin A6	-0.05	2.14	0.00059
P07214	SPARC	-0.02	-1.63	0.05318
P16045	Galectin-1	0.04	0.33	0.54377
Q9D0F3	Protein ERGIC-53	0.14	-0.84	0.02409
Q9R0B9	Procollagen-lysine,2-oxoglutarate 5-dioxygenase 2	0.19	0.61	0.02409
Q01149	Collagen alpha-2(I) chain	0.35	-0.89	0.00508
P19324	Serpin H1	0.41	-1.55	0.02326
Q9R0E1	Procollagen-lysine,2-oxoglutarate 5-dioxygenase 3	0.55	-0.30	0.25473
P97429	Annexin A4	0.70	Adult Only	
P07356	Annexin A2	0.91	1.36	0.02442
P11087	Collagen alpha-1(I) chain	1.03	-0.91	0.02844
Q61072	Disintegrin and metalloproteinase domain-containing protein 9	1.08	0.16	0.36716
P08207	Protein S100-A10	1.13	-0.94	0.15689
Q60854	Serpin B6	1.13	0.81	0.12655
Q60847	Collagen alpha-1(XII) chain	1.38	-1.92	0.00043
Q60715	Prolyl 4-hydroxylase subunit alpha-1	1.44	-0.39	0.17256
B2RXS4	Plexin-B2	1.47	-0.39	0.51881
P37889	Fibulin-2	1.94	ND	ND
Q9R0E2	Procollagen-lysine,2-oxoglutarate 5-dioxygenase 1	2.24	-0.26	0.51198

Table 5.1 continued

Ms UniProt ID	Protein	Ms Enrichment	Hu Enrichment	Hu adj. p value
Q99K41	EMILIN-1	2.89	-0.94	0.00364
Q5I2A0	Serine protease inhibitor A3G	2.90	ND	ND
Q60716	Prolyl 4-hydroxylase subunit alpha-2	4.43	0.29	0.21757
P08121	Collagen alpha-1(III) chain	4.52	-0.84	0.11442
Q61554	Fibrillin-1	7.88	-1.86	0.10862
Q62009	Periostin	18.33	-0.80	0.07261
O08573	Galectin-9	19.01	ND	ND
Q61398	Procollagen C-endopeptidase enhancer 1	19.02	-1.03	
Q9QZJ6	Microfibrillar-associated protein 5	19.29	2.41	0.18432
Q8VED9	Galectin-related protein	19.29	ND	ND
P51655	Glypican-4	19.52	ND	ND
P28653	Biglycan	20.82	0.39	0.49141

Given the prevalence of fetal-enriched laminins in both mouse and human CDMs, we first investigated whether individual laminins impact CM proliferation. Laminins are comprised of 3 chains – α, β and γ – that self-assemble to form a key component of basement membranes[33]. The majority of functional variation among laminins is derived from the α chains, because there are 5 α chains and only 2 β chains and 1 γ chain[318], and because exposed regions of the α chains bind individual integrins that are only expressed by certain cells[33]. Current annotation denotes laminins by the number associated with each chain, such that the laminin α5, β2 and γ1, would combine to form laminin 521. Multiple different laminins are associated with promoting specific cell behaviors, including proliferation or differentiation of progenitor populations[319,320], and laminin 521 has recently been shown to sustain pluripotency and promote expansion of stem cells[321,322]. In addition to the potential to promote DNA synthesis in CMs, we also explored whether laminin chains in the adult CDMs could potentially inhibit CM proliferation. The only alpha chain detected in CDMs was α5, which has noted as transcriptionally enriched in fetal mouse heart[155], but α2 is also present in the developing and adult heart[323]. We did, additionally, investigate the transcriptomic profiles of CFs during CDM production and determine that LAMA2, the gene

producing laminin α2, was in the top 10 might highly upregulated matrix genes in adult human CFs, relative to fetal CFs (p value = 0.000405), while no other laminins were enriched in adult CFs. Thus, the laminins we assessed for their contribution to CM proliferation included 211, 221, 511 and 521, as well as the commonly-used 111 as a reference. To perform these studies, we used primary murine CMs because they reflect native tissue biology that may not be recapitulated by immature iPSC-CMs[119].

When cultured on multiple laminins adsorbed directly onto TCP, we found that both laminins 511 and 521 supported more EdU incorporation into fetal mouse CMs than 211 or 221, suggesting that the α5 chain is a key component to promote CM proliferation. Further, it demonstrates that the identify of the β chain had no significant impact on DNA synthesis (**Fig. 5.2A**). CMs on laminin 211 also had a dampened proliferative response relative to laminin 111. To ensure that these differences were not due to adhesion – an important role of laminin - we quantified the number of CMs present in each condition (**Fig. 5.2B**). We observed only one significant difference in cell count between CMs on laminin 221 and 511, but in the inverse relationship of what would be expected if laminins containing the α2 chain compromised cell attachment. Instead, there were fewer CMs on laminin 511 than 221, despite supporting greater EdU incorporation. The potential causes for this are numerous; it is possible that laminin α2 enables the adhesion of a different subset of CMs that are less able to progress through the cell cycle, but equally possible that laminin α2 inhibits certain aspects of proliferation despite promoting adhesion. In fact, each matrix protein is preferentially bound by specific integrin pairs, and even minor differences in integrin/matrix dynamics can lead to differential adhesion and proliferation properties[324–326], due to mechanotransductive signals and because integrins link the matrix to the cardiac cytoskeletal[327], which must undergo dynamic rearrangement during the cell cycle.

Although the laminin α5 chain is associated with fetal CDMs and progenitor cells[319,320], cells are known to adapt their integrin expression and binding profiles over time, depending on the matrix

that is available to them. This raised the possibility that older CMs, representing a different maturational state, would respond differently to the different laminin chains. To test this, we isolated neonatal mouse CMs, and seeded them onto the same laminin combinations (**Fig. 5.2C**). The overall prevalence of DNA synthesis was low, as is typical of neonatal CMs. However, surprisingly, we saw the inverse relationship of DNA synthesis and laminins, wherein laminin 211 supported more EdU incorporation than 511, although once again the identify of the β chain had no influence of EdU levels. This suggests that while laminin α2 and α5 are capable of influencing CM proliferation, the cardiac response to individual laminins are dependent on the age or maturational state of the CMs.

Interestingly, laminin α2 is linked to muscle metabolism in a similar way to Col VI (Chapter 4). The loss of LAMA2 causes muscular dystrophy that is linked to metabolic dysfunction[161]. Specifically, this phenotype is a consequence of the opening of the mitochondrial permeability transition pore (MPTP), which sits in the inner mitochondrial membrane and allows the membrane to depolarize. When not properly regulated, it can cause mitochondrial swelling and apoptosis[328]. In CMs, the MPTP is detected as early as E9.5 and remains open by default until ~E13.5[329], when it's closure becomes regulated. Inhibition of the MPTP prevents dystrophic signaling in the absence of laminin α2, suggesting that one impact of laminin α2 is to promote MPTP closure which consequently promotes mitochondria integrity and homeostasis. This cardioprotective function associated with laminin α2 may be responsible for the lower CM numbers observed in culture on laminin 511 instead of 211. However, as laminin 511 also enhances CM cell cycling, it is possible that the laminin-specific regulation of the MPTP influences other developmentally-associated properties, such as proliferation. To address this, we cultured fetal CMs on laminin 111, 211 and 511 in the presence of a well-characterized MPTP inhibitor, cyclosporin A (CsA)[328], as well as on gelatin, as a non-laminin control (**Fig. 5.2D**). Under these conditions, MPTP inhibition suppressed the DNA synthesis observed in CMs cultured on laminin 511, but not on other laminins 211 or 111, or on

gelatin, and MPTP inhibition in CMs on laminin 511 suppressed the DNA synthesis to the level observed on laminin 211 (**Fig. 5.2D**). This suggests that the opening of the MPTP in fetal CMs is regulated by specific laminins, and enables CM proliferation.

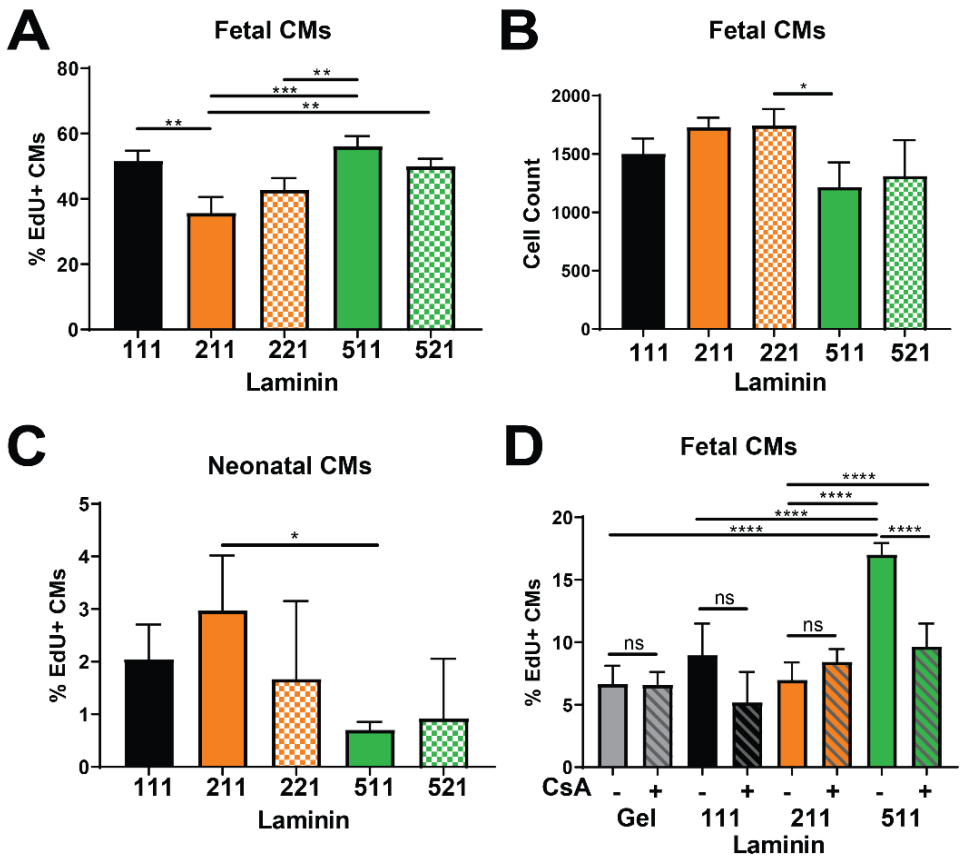

Fig. 5.2 EdU incorporation into CMs cultured on laminin-coated TCP, 10μg/cm^2. A) Fetal (E13) CMs, B) neonatal (P4) CMs, C) Fetal (E14) CMs in the presence of DMSO or the mitochondrial permeability transition pore inhibitor (CsA, 200μM). * $p < 0.05$, ** $p < 0.01$, *** $p < 0.005$, **** $p < 0.001$, as determined by one-way ANOVA.

5.3 Screening for Age-specific Modulators of CM Proliferation

Our ontogenic model of the cardiac ECM has, thus far, identified matrix proteins enriched in age-specific cardiac matrix that influence CM proliferation and mitochondrial function. Given the extensive list of other proteins enriched in age-specific CDM, we reasoned that there may be less-explored components of these CDMs that could also impact CM proliferation. To approach this,

we cast a wide net and compiled a list of all proteins that were significantly enriched in fetal and adult human CDMs, as well as enriched in fetal and adult mouse CDMs, and screened for their impact of EdU incorporation into mouse CMs on human CDMs. This resulted in a total of 115 proteins. To facilitate a screen of this size, we adopted a pooled-screen approached, wherein we group proteins into sets of 3 using a random number generator, and silenced each set of proteins in CFs by pooled siRNAs. To determine KD efficiency of siRNAs, transcript abundance of the targeted genes were assessed 24 hours after transfections and referenced to their abundance in CFs transfected with the NT siRNA control (**Table 5.2**).

Table 5.2. siRNA KD efficiency, determined by transcript abundance relative to non-targeting (NT) siRNA control 24 hours post-transfection.

Gene	KD	Gene	KD	Gene	KD	Gene	KD
VCAN	39.81	NID2	0.78	PLOD2	0.41	COL1A2	0.18
EGFL7	7.50	LGALS3	0.76	LOX	0.34	FBLN5	0.12
LAMA2	3.04	CTHRC1	0.76	PLOD1	0.34	PLXNB2	0.10
CSTB	2.76	CTGF	0.76	MGP	0.33	PAPPA	0.10
DCN	1.65	GAS6	0.72	IL1B	0.33	CRELD2	0.09
ANXA2	1.48	CXCL12	0.72	COL5A2	0.33	LOXL2	0.08
SULF1	1.47	COL7A1	0.72	COL12A1	0.33	HTRA1	0.07
TGFB2	1.45	THBS2	0.69	WNT5A	0.32	VWA5A	0.05
EFEMP1	1.41	TNC	0.68	NID1	0.31	EMILIN1	0.04
THSD4	1.39	IGF2	0.68	COL3A1	0.30	FGB	0.04
GPC6	1.36	LAMB2	0.68	LTBP2	0.30	LGALS1	0.03
F13A1	1.29	SERPINB2	0.66	AGRN	0.29	LMAN1	0.03
S100A11	1.26	SERPINE1	0.65	LAMA5	0.28	PLOD3	0.03
LTBP1	1.26	S100A13	0.61	CXCL8	0.28	SERPINA3	0.03
COL6A1	1.12	MFGE8	0.61	CTSL	0.27	COL4A1	0.02
TGFBI	1.11	MFAP2	0.61	ANXA5	0.27	EGF	0.02
TGM1	1.10	IGFBP7	0.60	P3H3	0.27	LAMB1	0.02
CXCL6	1.10	IGFBP5	0.57	CSPG	0.26	SERPINH1	0.01
MMP14	1.06	MFAP5	0.56	COL1A1	0.26	S100A6	0.01
SERPINB1	1.02	HAPLN1	0.56	LGALSL	0.25	HBEGF	0.01
PLAU	1.02	FGF2	0.55	LAMC1	0.25	CTSD	0.01
CSPG4	1.00	MMP2	0.54	EDIL3	0.24	ANXA4	0.00
ANXA1	0.98	IGF1	0.51	THBS1	0.24	S100A10	0.00

Table 5.2 continued

Gene	KD	Gene	KD	Gene	KD	Gene	KD
THBS1	0.95	S100A4	0.50	CTSC	0.23	TGM2	0.00
SRPX2	0.95	ANXA6	0.50	COL6A2	0.23	CTSB	0.00
ADAM9	0.95	PLAT	0.48	FN	0.22	ANXA11	0.00
FBN2	0.87	SERPINB9	0.47	LGALS9	0.21	CTSA	0.00
TIMP1	0.84	POSTN	0.46	CRELD1	0.21	GAPD	0.00
COL6A3	0.84	FBN1	0.46	COLEC12	0.21	FNDC1	0.00
ANXA7	0.81	SPARC	0.42	GDF15	0.21		

54% of siRNAs tested in human CFs achieved a KD of more than 50%. However, we noted that KD with siRNAs targeting COL6A1 and COL6A3 failed to reach this degree of transcript suppression, even though they had been demonstrated to successfully reduce Col VI protein almost completely. To determine whether this trend was observed across multiple proteins, we selected a few siRNAs and directly compared KD efficiency in RNA and the protein of corresponding CDMs (**Fig. 5.3**). Here, we noted that even in cases where protein transcript was not suppressed, as was the case for S100A10 KD in fetal CFs after 10 days of serial siRNA transfections, the protein was absent from the CDMs, indicating that transcript level at an individual timepoint is not a good indicator of total protein level. As such, we noted which siRNAs did not suppress transcripts efficiently (**Table 5.2**, KD > 0.5), but did not remove them from the screen.

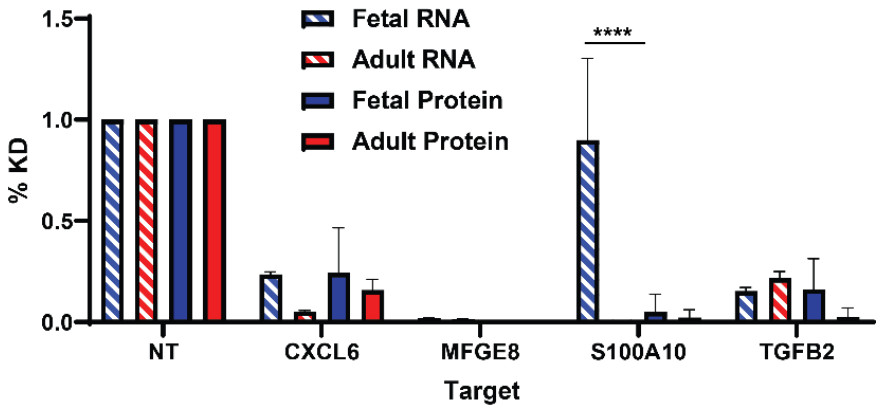

Fig. 5.3 Comparative KD efficiency in fetal and adult human CFs (striped) and CDMs (solid) after siRNA-mediated silencing of target genes in CFs. **** $p < 0.001$ as determined by one-way ANOVA.

To ensure quality control within the screen, siRNAs were pooled ahead of time and frozen in aliquots for individual use. As with previous studies, these pools of siRNAs were re-delivered every 3-4 days throughout the course of CDM production to maintain silencing. The inhibition of FN, the ubiquitous and abundant fundamental matrix protein, was used as a positive indicator of transfection efficiency on each experimental plate, as matrices without FN lack structural integrity and are not retained on the plate through decellularization. Furthermore, CMs were observed to undergo reduced DNA synthesis when cultured where the CDMs had been lost – i.e., TCP. Therefore, the anti-FN condition served as a positive control for transfection efficiency and a negative control for CM proliferation. Any plate on which this internal control did not behave as expected was discarded from the study. siRNA pools were annotated by alphabetic labeling (A-EE) and transfected into a minimum of two replicate wells across 3 experimental replicates. Each experimental replicate consisted of separate CDM preparations and CM isolations. Primary mouse CMs (E14) were cultured on the resulting CDMs in the presence of EdU for 72 hours, after which EdU+ CMs were quantified by fluorescent microscopy.

The results of the CDM target-inhibition screen are presented in **Fig. 5.4**. Representative levels of EdU incorporation in CMs on fetal and adult CDMs and gelatin are included for comparison,

and FN inhibition significantly decreased CM EdU levels in each set of CDMs. All values are shown relative to the NT control. Of the CDMs transfected with pooled siRNAs (**Fig. 5.4A, C**), there were 2 conditions in both fetal (**Fig. 5.4A**) and adult (**Fig. 5.4C**) that significantly increased EdU incorporation into CMs. There were, additionally, experimental conditions that destabilized the CDMs to the point of loss (§), and those with high variability, which potentially indicated that co-transfected had oppositional effects. As such, siRNAs from pools that induced significant changes in EdU incorporation, or were associated with CDM destabilization or variability, were further tested individually (**Fig. 5.4B, D**).

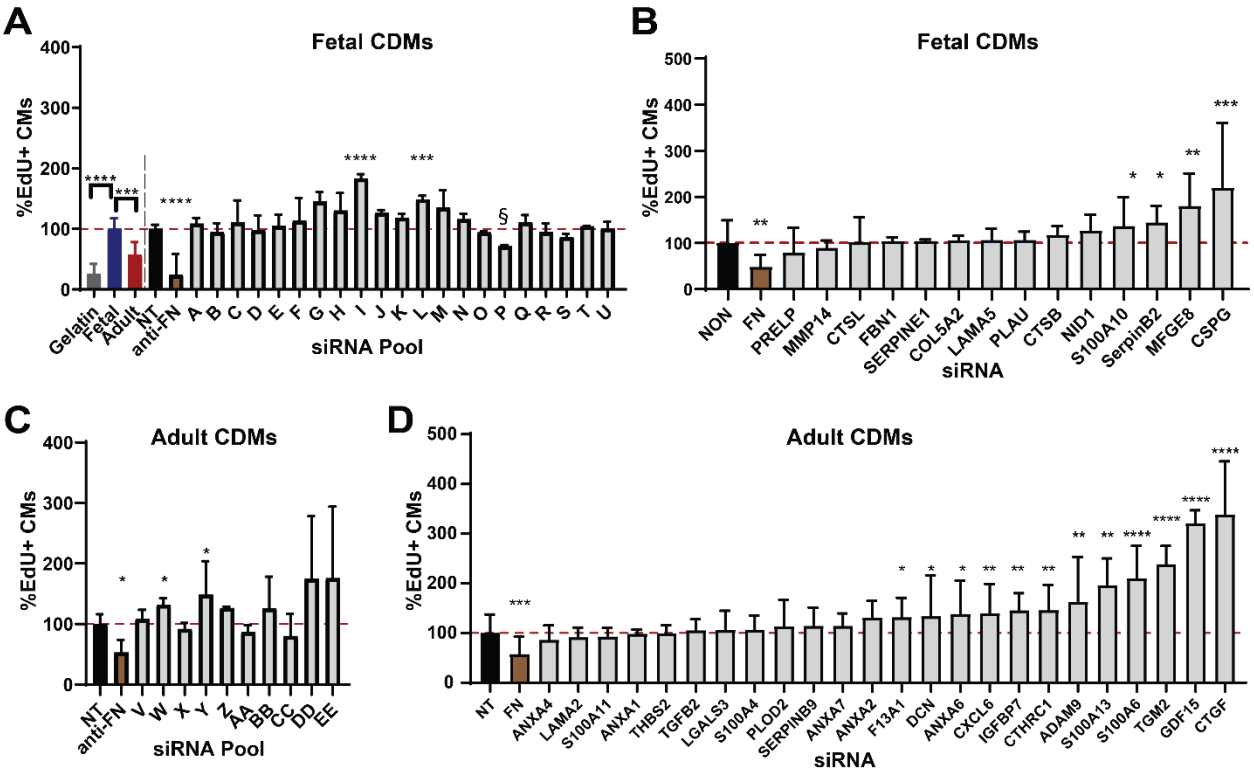

Fig. 5.4 Loss-of-function screen of age-specific CDM protein enrichment on CM proliferation. EdU incorporation into fetal (E14) mouse CMs was measured after culture on CDMs produced with siRNA-mediated silencing. EdU quantification in CMs on fetal (A-B) and adult CDMs (C-D) are shown relative to the NT control for each experimental group, after treatment with pooled A, C), and individual (B, D) siRNAs. * $p < 0.05$, ** $p < 0.01$, *** $p < 0.005$, **** $p < 0.001$, as determined by one-way ANOVA.

Our screen identified 3 and 12 proteins whose inhibition supported increased DNA synthesis in CMs on fetal and adult CDMs, respectively. Notably, we did not observe any conditions that resulted in a decrease in CM proliferation. According the paradigm of fetal ECM as permissive of CM proliferation and adult ECM as inhibitory to proliferation, the fetal CDMs were expected to contain pro-proliferative factors that, when removed, resulted in reduced EdU incorporation. This may still be the case; it is possible that the removal of individual factors is not sufficient to alter the pro-proliferative milieu contained within fetal CDMs. Additionally, these CDMs were prepared in the presence of FBS, which is known to contain pro-mitotic growth factors, which may negate the need for the matrix-bound reservoir of growth factors. These are caveats to this CDM model that may warrant future investigation. However, this model did identify that both fetal and adult CDMs contain factors that suppress DNA synthesis in CMs, and that these factors are 4 times more prevalent in adult CDMs.

5.4 Underlying Mechanisms

The identification of 15 protein 'hits' whose inhibition supported increased DNA synthesis in CMs, posed several potential avenues of further investigation. Focusing, first, on the targets that yielded the highest increase in CM EdU labeling (CSPG in fetal CDMs and CTGF in adult CDMs, **Fig. 5.4**), we noticed that both were involved in collagen production. CSPG, the basement membrane-associated chondroitin sulfate proteoglycan, catalyzes the 3-hydoxyproline formation required for proper collagen synthesis and assembly[330]. Additionally CTGF, connective tissue growth factor/cellular communication network factor 2 (CCN2), is a mitogen downstream of TGFβ signaling[282] that acts as an autocrine factor regulating cardiac fibrosis[331,332]. Given this functional correlation among the top hits in CDMs of both ages, we assessed the targets yielding significant changes in CM EdU labeling for overlapping functionalities. Among the significant hits in our screen, we found that several were associated fibrosis and/or plasmin signaling.

Fibrosis – Several of proteins involved in mediated CM proliferation, in both fetal and adult CDMs, were associated with the progression of tissue fibrosis, including CTGF, GDF15, TGM2, S100A6, CTHRC1 and CSPG. Specifically, CTGF, GDF15, CXCL6 and CTHRC1 are biomarkers of fibrosis in multiple tissues[331,333–335], whereas TGM2 is a transglutaminase that crosslinks matrix proteins to promote stability[336]. Fibrosis is characterized by conversion of fibroblasts to myofibroblasts and the excessive production and crosslinking of collagen-rich ECM that disrupts cell function[134]. We previously determined that our human CDMs were produced by activated CFs (**Figs. 2.13, 3.2**), which likely influenced the CDM composition. It has also previously been shown the prevention of cardiac fibrosis improves cardiac regeneration and recovery post-infarct[183,337], which requires an CM proliferation. To test whether this was broadly true of fibrotic signaling in the CDM model, we produced CDMs in the presence of angiotensin II, which is frequently used to induce tissue fibrosis in mouse models[338] (**Fig. 5.5A, B**). In both fetal and adult CDMs, the presence of angiotensin II significantly decreased the CDMs' ability to support CM proliferation. To then determine whether the pro-proliferative effects observed with KD of these proteins was due to their lower level of myofibroblast activation, we assessed αSMA expression in CFs during KD of target proteins (**Fig. 5.5C, D**). We observed that in some cases (CSPG, GDF15, TGM2), though not all, CFs exhibited a marked decrease in αSMA (**Fig. 5.5D**), suggesting a correlation between their reversion back to a physiological fibroblast state and their CDM's ability to support CM DNA synthesis.

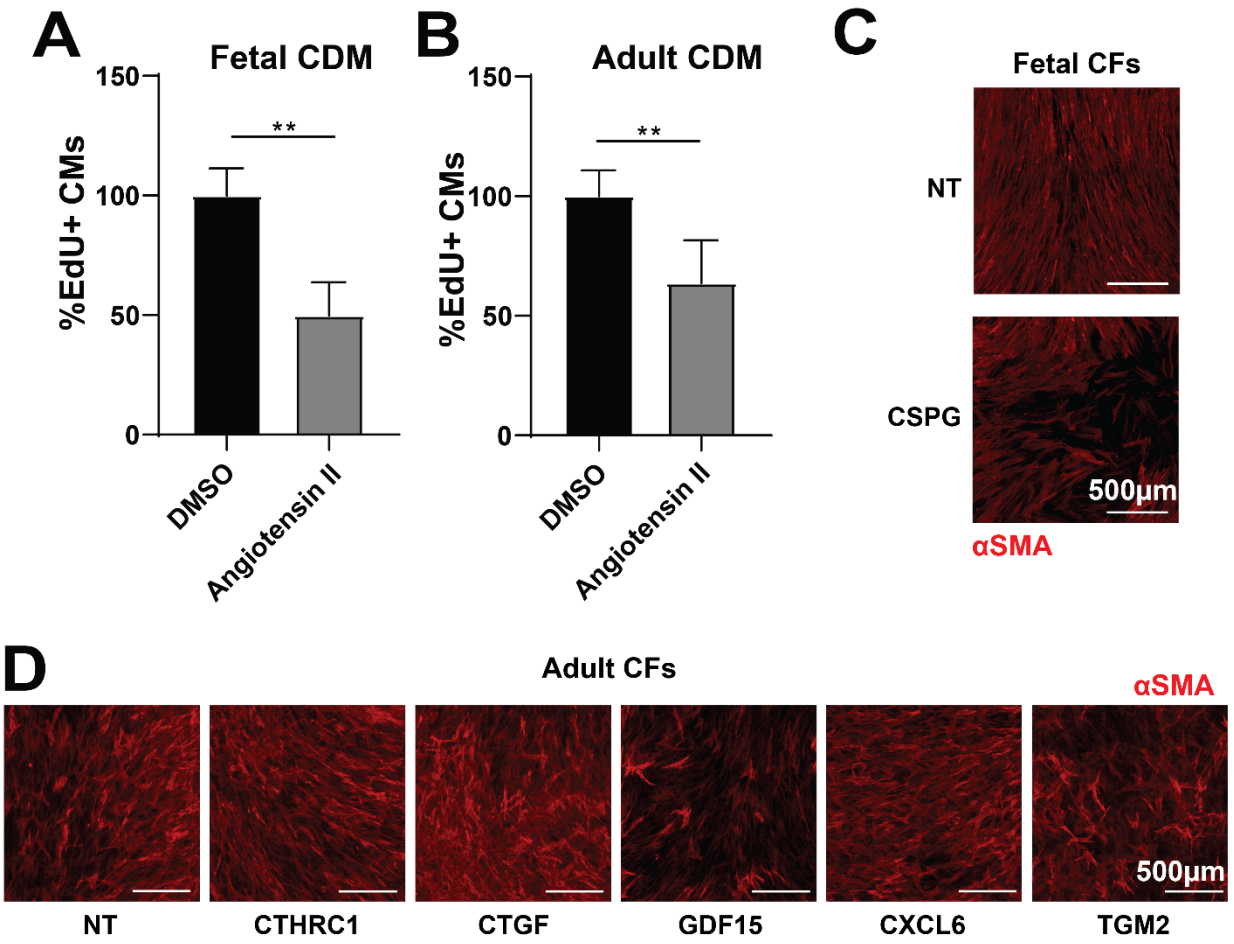

Fig. 5.5 Modulation of myoactivation and fibrosis in CDMs. EdU incorporation into fetal (E14) CMs cultured on A) fetal and B) adult CDMs produced in the presence of angiotensin II (250ng/ml). C-D) αSMA expression in C) fetal and D) adult CFs during silencing of fibrosis-associated genes. ** $p < 0.01$ as determined by ANOVA.

These findings indicate that 1) a selection of the fibrosis-associated proteins represent targets for the reduction of fibrosis signaling without destabilizing the total ECM, as was observed with small molecule inhibitor nintedanib (**Fig. 2.14**), and 2) that the matrix produced by activated, fibrosis-associated CFs directly inhibits CM proliferation.

Additionally, a major component of tissue fibrosis is the involvement of the immune system, which can act to either resolve or exacerbate the disease. CXCL6, for example, is a chemokine that promotes granulocyte chemotaxis and neutrophil recruitment[335]. In fact, multiple fibrosis-

associated proteins and others play a role in recruitment of immune cells. CTHRC1, ANXA1, MFGE8 and S100A10 recruit either monocytes or macrophages, which can be both pro- and anti-fibrotic, depending on a number of factors including local inflammatory signaling and timing. Although immune cells are not involved in CDM-CM interactions, this correlation between fibrosis, immune cell recruitment and CM proliferation raises the question of potential *in vivo* interplay during cardiac injury, which is known to respond to macrophage activation and infiltration[339].

Plasmin Signaling – Also well-represented among proteins involved in CM proliferation were several involved in plasmin signaling. Plasmin is a protease that is canonically involved in cleaving fibrin clots (fibrinolysis), but also cleaves other matrix proteins to activate MMPs and liberate growth factors[340]. Plasmin itself is cleaved from the zymogen plasminogen by urokinase and tissue-type plasminogen activator (uPA, tPA), which bind cell receptors uPA Receptor (uPAR) and the heterotetramer S100A10:annexin 2, thereby regulating the precise location of plasmin activity. This interaction is inhibited by upstream proteins plasminogen activation inhibitor 1 and 2 (PAI1/SerpinE1 and PAI2/SerpinB2). Fibrin clots are made up of insoluble fibrin crosslinked by multiple proteins including coagulation factor 13 (F13A1) and TGM2, a transglutaminase[336]. These interactions are summarized in **Fig. 5.6**, with the proteins identified in our loss-of-function screen shaded in with color (S100A10, SerpinB2, F13A1, TGM2).

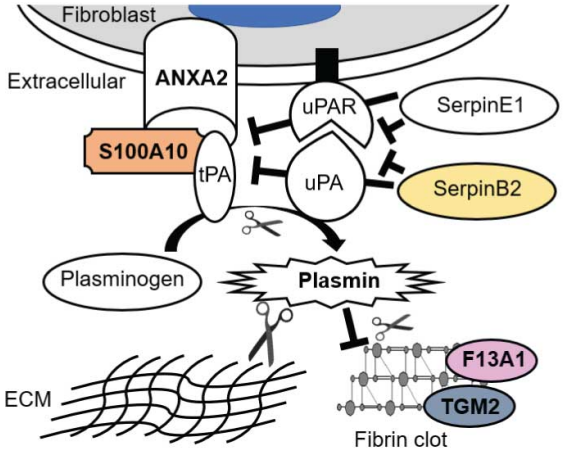

Fig. 5.6 Schematic of plasmin signaling.

The loss of plasminogen reduces regeneration in skeletal muscle[341,342], although in the heart the effects of plasmin signaling are disease- and context-specific. One inhibitor of plasmin activation, SerpinE1 both aggravates and ameliorates fibrosis in cardiac infarct[343] and hypertension[344] models, respectively. Plasmin(ogen) itself is required for macrophage recruitment to injury sites,

which are necessary for remodeling and resolving inflammation[340] and the plasmin activator uPA, specifically, is associated with cardioprotection from apoptosis[345]. Collectively, these data indicate the importance of plasmin regulation in the heart, though its role in proliferation, specifically, is unknown.

We first assessed whether mediating plasmin activation specifically in CDMs altered the CM proliferative response by producing CDMs in the presence of small molecules inhibitors against tPA and uPA (1μM PPACK and 10μM BC-11, respectively) and with the physiological direct inhibitor of plasmin, α2-antiplasmin (SerpinF2). We observed that when treated with α2-antiplasmin and anti-tPA, CDMs were able to support more CM DNA synthesis, though treatment with anti-uPA did not significantly alter CM proliferation, nor augment the increase observed with anti-tPA treatment (**Fig. 5.7A**). We reasoned, then, that if decreased plasmin activation enabled increased CM proliferation, suppressing plasmin activity during CM culture should have the same effect. To test this theory, we treated CMs cultured on Matrigel with the same inhibitors, as well as with free plasmin directly (**Fig. 5.7B**). Surprisingly, we saw the inverse effect – plasmin itself increased CM proliferation and inhibiting plasmin and its activators decreased proliferation. Further, unlike in the CDMs, inhibiting uPA had a more pronounced effect on EdU incorporation than anti-tPA, suggesting a different primary mechanism of plasmin in the CDM production vs CM culture. Additionally, we noted that the direct inhibition of plasmin activation in CM culture could not be rescued by the addition of free plasmin (**Fig. 5.7C**), but that it could be phenocopied by inhibiting a cell surface receptor, α-enolase[346], that recruits plasmin to the cell membrane to protect CMs from apoptosis during stress[347] (**Fig. 5.7D**).

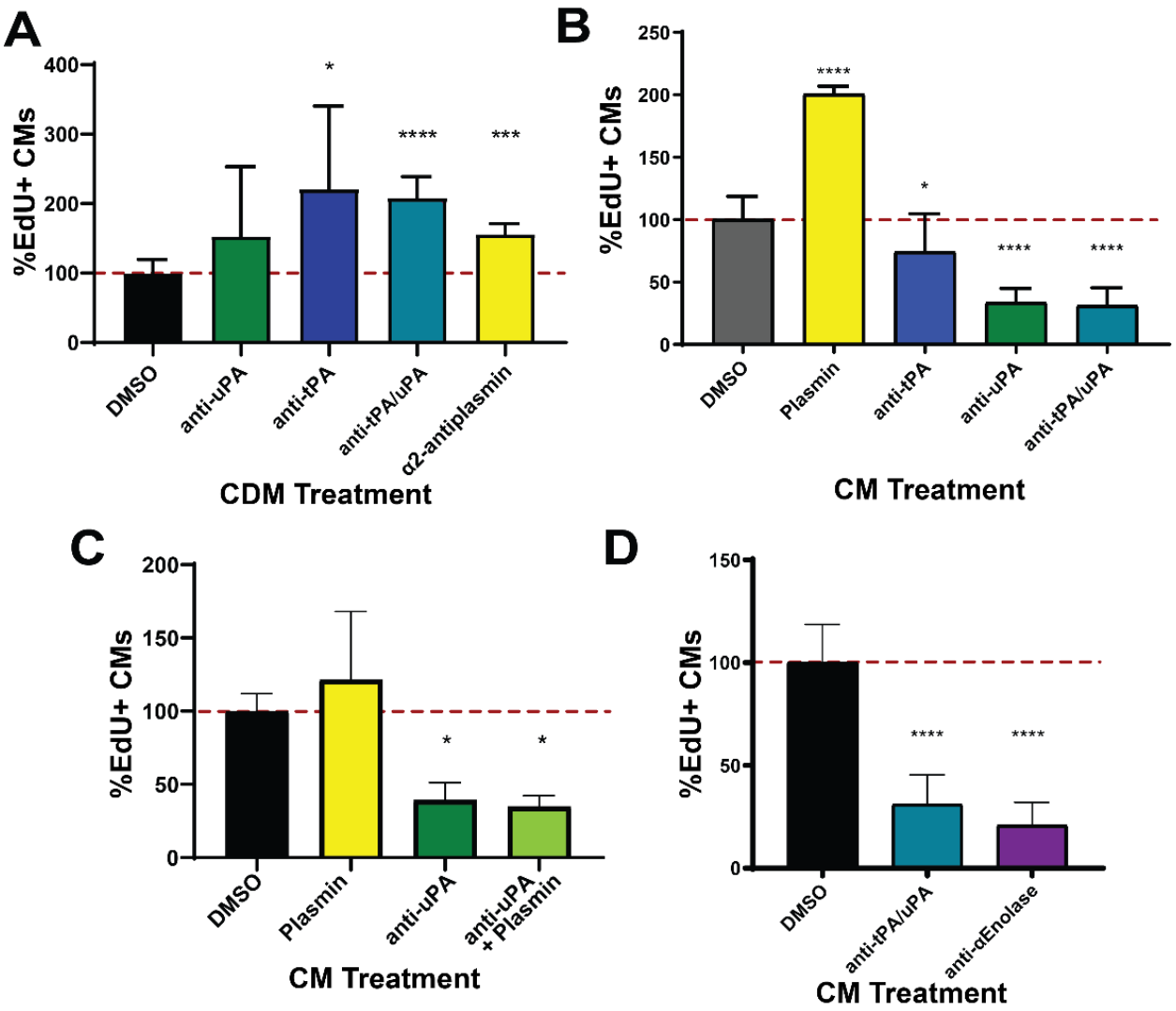

Fig. 5.7 Modulation of plasmin activation in CM culture. A) Inhibition of urokinase (uPA) and tissue-type (tPA) plasminogen activators with 1μM PPACK and 10μM BC-11, respectively, or combined, and α2-antiplasmin in fetal CDMs prior to CM culture. B-D) Inhibition of plasmin signaling directly in CMs cultured on Matrigel with B) inhibitors of plasmin and plasminogen activators, C) anti-uPA in the presence of plasmin, and D) inhibition of surface plasminogen receptor α-enolase. * $p < 0.05$, *** $p < 0.005$, **** $p < 0.001$, as determined by one-way ANOVA.

These results indicate that plasmin signaling have inverse effects during CDM production as opposed to CM culture. During CM culture, membrane receptors uPA and α-enolase that promote plasmin activity at the cell surface are crucial for DNA synthesis in CMs. However, during CDM production, plasmin activity is detrimental to the CDM's ability to support CM proliferation. It was unlikely, then, that inhibitors of plasmin activation in CDMs directly suppressing plasmin levels.

However, given that CDMs represent the accumulation of matrix protein during CF culture, we reasoned that suppression of plasmin activation during CDM production may leave more of the zymogen present for activation during CM culture. To address this first sought to determine whether inhibition of plasmin activation in CDMs altered the abundance of plasmin in the final CDM composition. Surprisingly, we were not able to detect any plasminogen in CDMs, with or without plasmin activity (**Fig. 5.8A**). Further attempts were made with high-sensitivity detection reagents, but no plasminogen was ever detected in CDMs.

The inhibition of plasmin activity, then, was not altering the level of plasmin available during CM culture. We next hypothesized that plasmin activity may be inducing systemic changes, as was observed with fibrotic agents (**Fig. 5.5**). Given the involvement of plasmin in cardiac fibrosis[343], we next assessed whether inhibition of plasmin activation was mediating indicators of fibrotic matrices, both by histology and transcriptional analysis. Staining of CDMs with picrosirius red (**Fig. 5.8B**) showed no overt changes in collagen accumulation with the inhibition of tPA and uPA. We then compared the transcriptional signature of CFs treated with inhibitors of plasmin activation with CFs receiving pro- or anti-fibrotic treatments (**Fig. 5.8C**). In doing so, we noted that anti-plasmin treatments did not cluster with anti-fibrotic treatments, but instead with TGFβ, which induces a fibrotic phenotype in fibroblasts[172]. However, the impact of plasmin inhibition in CDMs contrasted with the known influence of fibrotic CDMs on CM DNA synthesis, and we therefore reasoned the mediating the fibrotic state was not the primary function of plasmin signaling during CDM production. However, several other transcripts associated with plasmin signaling were notably altered. Specifically, in both fetal and adult CFs, multiple MMPs were downregulated during plasmin inhibition, which suggests a decrease in matrix remodeling, and several IGFs and IGFBPs were upregulated. One of the many function of plasmin is to cleave IGF1 and IGF2 from complexes with IGFBPs[348], and IGFs are well documented mitotic factors that promote CM proliferation during development and injury repair[94,95].

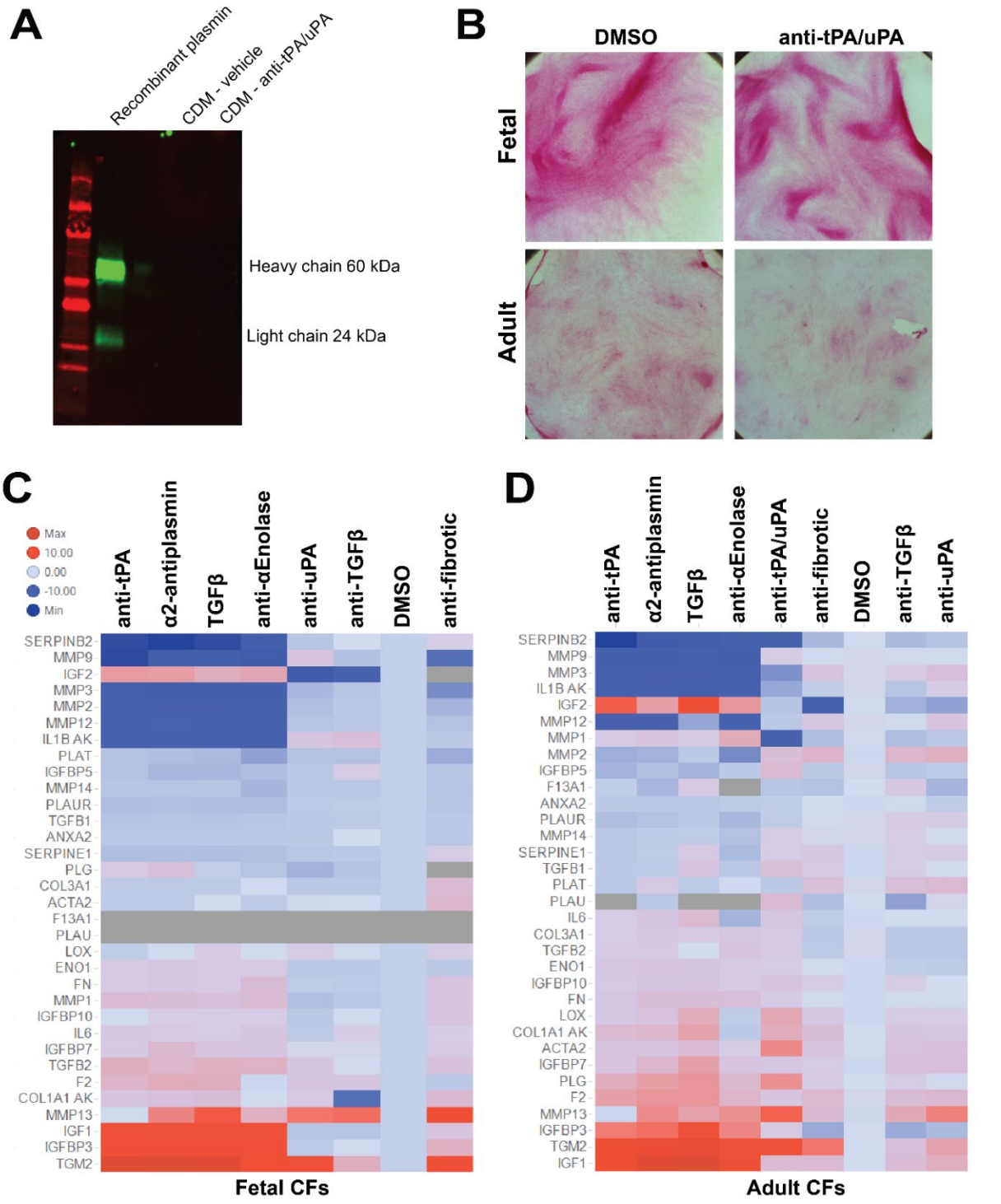

Fig. 5.8 Altered matrix transcription in CDMs induced by inhibition of plasmin activation. A) Immunodetection of plasminogen in CDMs by western blot. B) Collagen abundance in CDMs treated with plasminogen inhibitors, visualized by picrosirius red staining. C-D) Transcriptional analysis of genes associated with myofibroblasts and plasmin signaling in C) fetal and D) adult CFs after 10 days of treatment with anti-plasmin and pro-fibrotic (TGFβ 10ng/ml) or anti-fibrotic molecules (nintedanib 1μM + GLPG1690 3μM, or anti-TGFβ SB431542 1μM).

Inhibition of plasmin signaling enhanced expression of IFG1, IGF2 and IGFBP3 in fetal and adult CFs, suggesting that suppressing plasmin activation promotes the reservoir of potent mitogens for CMs. To determine whether enrichment of IGF protein was detectable in CDMs, we prepared western on CF lysates after treatment with anti-tPA and anti-uPA for 10 days and probed for IGF1 and IGFBP3 (**Fig. 5.9**). With the inhibition of plasmin activation, we noted a marked increase in free IGF1, both of the glycosylated form (2-fold) which has not yet been secreted, and of the deglycosylated form (~3-fold) (**Fig. 5.9A**), though a similar increase was not observed with IGFBP3 (**Fig. 5.9B**). Quantification of these band intensities shown in Table W were normalized to the cellular and matrix proteins GAPDH and FN, which were present in the samples at a ratio of 1:1.002 and 1:1.033, respectively. Surprisingly, there was not an increase in IGF1 bound to IGFBPs. However, IGF half-lives are quite short, even when bound to IGFBPs[31], and the treated CFs are cultured for a prolonged period and therefore represent the cumulation and compensatory response of any changes in IGF signaling dynamics. It stands to reason, then, that the increase in IGF production observed in plasmin-inhibited CFs may be a response to reduced bound and unbound IGF.

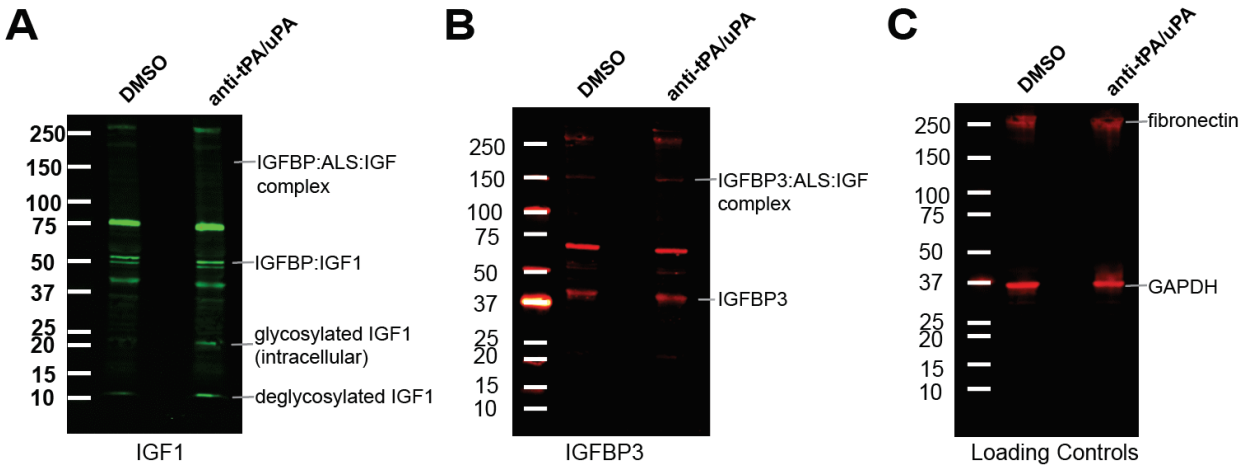

Fig. 5.9 IGF abundance in CFs after inhibition of plasmin activity. Lysates of CFs treated with either DMSO or a combination of anti-tPA and anti-uPA (1μM, 10μM) probed for A) IGF1, B) IGFBP3 and C) loading controls GAPDH and fibronectin.

Table 5.3 Abundance of IGF1 and IGFBP3 during inhibition of plasmin activation. Intensity of western blot bands, normalized to GAPDH and fibronectin.

Abundance Ratios	DMSO	anti-tPA/uPA
Free unglycosylated IGF1	1	1.98
Free glycosylated IGF1	1	3.3
IGF1:IGFBP	1	0.92
IGFBP3	1	1
IGFBP3:ALS:IGF	1	0.86

This data demonstrates the complex effect of plasmin signaling in both CDMs and CM culture. Plasmin activation is capable of promoting proliferation in CMs, but is heavily reliant on context. In CDMs, loss of plasmin activation promotes expression of IGFs, and ultimately leads to increased DNA synthesis in CMs subsequently cultured on those matrices. However, during CM culture, plasmin activity is required for maximal DNA synthesis, as are proteins that recruit plasmin to the cell membrane, uPA and α-enolase.

5.5 Conclusions and Discussion

Through this work we demonstrate that fetal and adult CDMs, which reflect many stage-specific characteristics of developing and mature cardiac ECM, impact the proliferative capacity of CMs through several distinct mechanisms. The ability of fetal CDMs to support more DNA synthesis in CMs is conserved between mice and humans, and is the result of several complementary mechanisms. Here, we leverage the known composition of fetal and adult CDMs to identify age-specifically enriched matrix proteins that contribute to their differential impact on CMs. We specifically investigated these interactions with primary fetal mouse CMs, which reflect native biology but still retain their proliferative capacity, thus providing a dynamic range to measure the influence of the CDM over aspects of the CM cell cycle. We demonstrate that the fetal-enriched laminin chain α5 enables more CM proliferation than laminin α2 via regulation of the mitochondrial permeability transition pore, and that a broad class of molecules associated with fibrosis induce CDMs with a suppressed ability to support CM proliferation. This is the first demonstration, to our knowledge, that matrix produced by myofibroblasts directly inhibits CM proliferations. Additionally, one of our most unexpected findings was the complex regulation of IGF expression during CDM production by inhibition of plasmin activation. Each of these findings represents opportunities for further exploration, both in the potential for these mechanisms to influence aspect of CM proliferation beyond DNA synthesis, and for potential therapeutic application during heart disease.

In particular, plasmin signaling is particularly relevant to the context of cardiac injury. Not only are plasmin activators and inhibitors upregulated during left ventricular hypertrophy[349], but any context in which there is a blood clot will required plasmin activity[350] and this activity could have multiple effects on CMs, depending on multiple contextual factors. One specific receptor of plasminogen – α-enolase – is heavily implicated in cardioprotection during hypertrophy[347] and in skeletal muscle regeneration[342], which shares many similarities with cardiac regeneration[351]. Our results also help distinguish signaling specific to CFs and the ECM from CM-specific biology. While

plasmin is an essential component of CM survival and proliferation, sequestering plasmin from CFs could induce and upregulation of IGFs, which would also promote CM proliferation, if this signaling could be limited to CMs and not allowed to promote pathological CF expansion. This balance between CF and CM signaling is an ongoing challenge in the treatment of cardiac disease, and requires a nuanced understanding of the balance between the two.

One paradigm that is pertinent to the study of multiple ECM-CM interactions is the concept of cardioprotection. In the context of plasmin signaling, activation at the CM membrane is cardioprotective against apoptosis and exclusively associated with positive outcomes[345,347]. However, in the context of laminins, laminin α2 induces a closure of the MPTP, and thereby suppresses a number of detrimental processes. However, we show that this closure is associated with decreased CM proliferation, and a switch to the laminin α5 prevalent during development increased DNA synthesis in CMs, but does so via an open MPTP, which poses a risk to CM stability[328]. Given this comparison, plasmin activation appears to be a more promising candidate for therapeutic application during cardiac injury; however, it is very difficult to restrict cardiac interventions to a single cell type, and unlike plasmin activation, laminin α5 is not associated with the promotion of fibrosis.

The question of CM proliferation is a complex challenge that requires insight into the heterotypic interactions of the heart's many cell populations. We provide, here, evidence that multiple aspects of the cardiac ECM influence the context-specific promotion of CM proliferation, and that leveraging knowledge of the developmental ECM can provide insights toward identifying the optimal extracellular environment for cardiac regeneration and resolution of pathological fibrosis.

Chapter 6. Concluding Remarks

6.1 Summary

The goal of this doctoral work was to further understand the influence of the ontogenic cardiac ECM on CM function. The mammalian heart undergoes a series of shifts throughout development and maturation[9] that coincide with significant changes to cardiac ECM structure, mechanical properties and composition[50,59]. These dynamic age-dependent properties have a significant impact on the prevalence of heart disease and the *in vitro* modeling of cardiac tissue[111,113,259]. Additionally, the cardiac ECM has been shown to influence multiple CM functions[59,102,155,159] but is still leveraged primarily for its structural properties[352,353]. We proposed that *in vitro* modeling of the age-specific cardiac ECM would enable systematic investigation of how its ontogenic properties support or initiate age-dependent CM characteristics, including morphology, metabolism and proliferation. The complex influences of the ECM can be difficult to study *in vivo*, and necessitate the careful application of *in vitro* modeling. To enable the mechanistic investigation of the age-specific cardiac ECM-CM interactions, we developed an improved CDM model from fetal and adult human CFs.

Our CDM system relies on a coating of the adhesive biopolymer L-polydopamine and macromolecular crowding to promote matrix retention and thickness, instead of the supplementation or promotion of individual matrix proteins that are common in other protocols, thereby maintaining compositional fidelity to the naturally cell-produced ECM (Chapter 2). We then systematically characterized the structure and composition of fetal and adult CDMs, which demonstrated the retention of numerous key hallmarks of age-specific cardiac ECM and validated the use of these matrices for *in vitro* ECM-CM mechanistic studies (Chapter 3).

We applied the fetal and adult cardiac CDMs to the culture of human iPSC-derived and mouse primary CMs, and observed a number of morphological and functional responses to the age-

specific matrices. Specifically, we found that both fetal and adult CDMs enhanced the alignment and speed of calcium handling in iPSC-CMs, but that only adult CDMs promoted morphology and desmosome localization to the putative intercalated discs in a pattern reminiscent of the adult myocardium (Chapter 4). Additionally, the defined composition and the accessibility of these CDMs enabled detailed loss-of-function studies into the influence of individual matrix proteins over CMs. Through this strategy we observed that Col VI is important for CM oxidative respiration when cultured on adult, but not fetal, CDMs (Chapter 4). We also identified a number of proteins enriched in adult matrices that are inhibitory to DNA synthesis in CMs, including laminin α2, pro-fibrotic agents and plasmin signaling (Chapter 5). In applying target-specific siRNA-mediated silencing to assays requiring multiple specialized formats, we demonstrated these CDMs to be a tractable, flexible platform that provides consistent methodology across numerous biological applications. Furthermore, it is, to our knowledge, the first ECM model to enable the pursuit of ontogenic research questions in an entirely *in vitro* system.

Together, these studies demonstrate the characterization and applicability of our CDM model to the mechanistic investigation of ECM-responsive cardiac functions, and identify ECM proteins capable of modulating age-specific proliferative and metabolic phenotypes in CMs.

6.2 CDMs as a Model

The development of CDMs[197,211] provides a powerful and flexible tool to study the ECM in a model providing the complexity and native organization of tissue-derived ECM and the simplicity of *in vitro* cell culture. They also enable the combination of ECM and cells from disparate origins, such as age-specific sources or healthy and diseased sources, which will aid in distinguishing matrix-derived influences from autocrine/paracrine influences. Additionally, CDMs are especially amenable to genetic and pharmacological perturbation without risking confounding cross-

signaling to parenchymal cells used in downstream studies, and have thus risen in popularity over recent years[212,213,227,257]. CDMs that reflect the native cell-derived matrix composition provide utility to study of ECM-related diseases involving multiple organs such as fibrosis, congenital disorders like Ehlers-Danlos and Marfan syndromes[354], and aspects of developmental biology, where embryonic cells and their derivatives migrate through various ECM environments while simultaneously undergoing concurrent lineage specification[253].

In approaching our study of the cardiac ECM, we noted that all CDM protocols cultured stromal cells on a substrate containing an sole matrix protein (often FN or denatured collagen)[211,213,214], or augmented the collagen secretion of the stromal cells with ascorbic acid[212,213], or both. Previous studies into the cardiac ECM proteomic composition had noted the age-specific enrichment of multiple fundamental proteins including FN (enriched in fetal ECM) and Col I (enriched in adult ECM)[59]. We were, therefore, reluctant to produce cardiac CDMs on these substrates, for fear the exogenous matrix protein would confound or negate age-specific compositional differences in the CDMs. We then identified L-polydopamine as an adhesive amine-binding substrate that could replace ECM substrates to retain the CDMs during decellularization[218,219], and augmented matrix production via the alternate strategy of Ficoll as an MMC[221], without significantly changing the composition of the CDMs (**Fig. 2.9**). The detailed proteomic analysis of the CDMs by MS provided an atlas of protein presence and abundance, and became a guide for the battery of mechanistic studies that would have been challengingly cumbersome to complete *in vivo*. During the optimization of this process, we identified a number of factors that influence the final CDMs, and therefore their downstream applications. The most notable of these factors were the isolation method and handling of the cells used to produce CDMs. Isolation of CFs from fetal mouse hearts enriched for different sub-populations (**Fig. 2.12**), and all commercially available human CFs expressed αSMA indicative of their conversion to myofibroblasts[168] (**Fig. 2.13**), likely due to their handling prior to purchase. The specific identity of the CFs producing CDMs undoubtedly had

consequences on the organization and composition of the CDMs, and must be considered when interpreting CDM-dependent results. However, the activation of the human CFs enabled the production of especially aligned matrices[256], which contributed to the CM alignment and functional response to age-specific CDMs. Additionally, it provided an opportunity to identify genes whose inhibition in CFs could revert the αSMA expression without compromising the integrity of the CDMs (**Fig. 5.5**) as was observed with a pharmacological inhibitor of myofibroblast activation (**Fig. 2.14**).

The defined protein composition of fetal and adult CDMs also allowed us to examine our assumptions about CDM composition. We found fetal and adult transcriptomes to generally reflect that classes of proteins enriched in age-specific CDMs, but to be poorly reflective of individual protein levels (**Fig. 3.4, 3.7A**), likely due to differential retention of proteins based on multiple parameters, including their half-lives, binding profiles and other protease activity. In many ways, the age-specific composition of CDMs matched expectations, based on proteomic analysis of cardiac tissue ECM (**Figs. 3.4, 3.6B, 3.7A**). However, the relative abundance of FN and Col I did not match that observed *in vivo*. FN, which is enriched in fetal heart ECM[59], was equally present in both fetal and adult human CDMs, and was the most highly detected matrix protein (**Fig. 2.9**). Col I, rather than being enriched in adult CDMs[59], was slightly, but significantly, more abundant in fetal CDMs (**Fig. 3.7A**). We attribute the deviation between CDM and ECM enrichment of these proteins to caveats of cell culture, in which CDMs are produced by only a single cell type, and must create their ECM *de novo* to ensure the adhesion required for their survival. However, we note that if future studies utilizing CDMs required the use of exogenous proteins, the addition of FN would likely not introduce any experimental biases between CDM conditions that did not already exist. Further, knowing the ways in which these CDMs differ from heart tissue ECM highlights the opportunity to further tailor CDM composition to better match that of native tissue.

6.3 ECM Applications for CM Maturation

An ongoing challenge in cardiac research is the relative immaturity of iPSC-CMs[139,144,355]. Many of the significant advances made in iPSC-CM maturity either promoted or enforced individual phenotypes associated with maturity[356], such as morphology/alignment[126,357], fatty acid oxidation[157], electrical stimulation[138], and three-dimensional tissue formation[138,141], and have observed a concomitant improvement in the maturity of other functions. However, very few of these studies have utilized the ECM for purposes beyond structural integrity or cell adhesion[352,353]. We demonstrate here that adult human CDMs naturally provide the structure to promote CM elongation and alignment in a 3D-like context without the need for specialized engineering culture vessels or surfaces, such as micropatterned polydimethylsiloxane (PDMS) substrates.

Further, we have identified certain age-specific ECM proteins that promote individual hallmarks of CM maturity, both in the context of complex CDMs and as individual proteins. Their application to ongoing efforts in cardiac modeling may augment maturation-associated phenotypes. For example, Col VI has not been previous linked to CM maturation but, in our system, Col VI-deficient CDMs were unable to support the maximal oxidative phosphorylation achieved by CMs cultured on CDMs containing Col VI (**Fig. 4.7**). Given the requirement for Col VI in the integrity of fetal CDMs, it is possible that the 3D, tissue-like structure of CDMs was required to isolate the influence of Col VI on CMs. It is also possible that the inclusion of Col VI in engineered cardiac tissue undergoing the stress of metabolic or electrical training may better support the function and ultimate maturation of these tissues. Additionally, multiple studies have observed that the pharmacological inhibition of the MPTP promotes mitochondrial maturity and iPSC-CM differentiation[358,359], though these studies were largely performed in differentiated CMs cultured on gelatin, i.e. denatured collagen. Our results demonstrate that CM culture on laminin 211 inhibits the proliferation of CMs associated with the opening of the MPTP (**Fig. 5.2D**) and, because proliferation is anti-correlated with CM maturity, culture of iPSC-CMs on laminin 211 may naturally

promote their mitochondrial function and augment their oxidative respiration. Currently, these proteins have not been implicated in the maturation of iPSC-CMs, and the potential of their impact and utility to the cardiac field is only speculative. However, the application of CDMs demonstrated that Col VI and laminin 211 are able to modulate maturation-associated phenotypes in CMs, and the other proteins enriched in age-specific CDMs have not yet been investigated for their impact to CM metabolism or maturation. Thus, these and other proteins enriched in the cardiac ECM and age-specific CDMs may have broader applications to advance efforts in iPSC-CM culture and tissue engineering.

6.4 ECM Implications for Cardiac Repair and Regeneration

In recent years, the ECM has been recognized as a contributing factor in CM proliferation and cardiac regeneration. This has led to the previous identification of 3 ECM proteins capable of regulating CM regeneration – agrin[102,154], nephronectin and slit 2[155]. One fundamental aspect common to these proteins is that they interact directly with transmembrane receptors and complexes. Agrin[154,360] and nephronectin[361], specifically, interact directly with the dystroglycan complex and integrin receptors, respectively, that bind both the ECM and the cytoskeleton. This is also true of laminins 511 and 211[39,362] and Col VI[291], which we identified as modulators of CM DNA synthesis and metabolism, respectively, and which both bind the dystroglycan complex and integrin receptors. Furthermore, while agrin did increase S phase cycling in CMs, nephronectin and slit 2 did not – they, instead, promoted mitotic cell rounding, which requires significant cytoskeletal rearrangement and dynamic interactions with cell-ECM binding complexes. Especially in light of the sarcomeric disorganization that accompanies CM proliferation[74,315], these studies and our data emphasize the importance of ECM adhesions as dynamic regulators of cell behavior, whose compliance is necessary for cell proliferation, particularly cytokinesis[149,150,363].

There are multiple factors that influence cell-ECM binding dynamics, including integrin[325,364] and ECM protein isoforms[365] and stiffness[363]. For example, FN is commonly associated with proliferation and migration, but FN containing the extra domain B (EDB) is more permissive of these processes[366,367], both of which require active cytoskeletal rearrangement. Thus, while EDB+ FN is not required for mitosis, it is more permissive of proliferation. Additionally, we observed laminin 511 to support more DNA synthesis than laminin 211. These proteins bind similar integrins but with different dissociation constants[368], which demonstrates the potential influence of binding dynamics in regulating CM proliferation. Given that CMs experience a significant block in proliferation and cytokinesis[3,99], specifically, there is merit in exploring the extracellular conditions that are most permissive of cell division.

One unexpected outcome of our studies was the identification of multiple factors involved in pathological fibrosis as associated with decreased CM proliferation. While fibrosis itself has typically been associated with reduced cardiac regeneration and poorer prognoses[169,178,179,183], the matrix itself produced under fibrotic conditions has not been directly show to impact CM proliferation. Based on this data, further studies are required identify which aspects of fibrotic ECM directly impact CM proliferation. Further, in combination with our studies suggestive of the ability of laminin 211 to suppress CM proliferation, these represent the first identification of ECM proteins that are inhibitory to CM proliferation, rather than fetal-associated proteins that promote proliferation. Additionally, our CDMs proved valuable in modeling the behavior of CFs from different ages and under different disease-associated conditions, and are applicable to the broad research focus of CF-targeted therapies addressing fibrosis and other aspects of heart disease.

Another phenomenon we observed is certain signaling being both advantageous in one context and detrimental in another. With plasmin, its presence is required for cardioprotection[345] and proliferation during CM culture, but CDMs produced in the presence of plasmin are inhibitory to CM proliferation (**Fig. 5.7**). Similar contrasting results are observed with plasmin signaling during

hypertension and infarct models[93,314]. However, this paradigm of conflicting functional consequences is not unique to plasmin[159,183], and represents a challenge in the therapeutic approaches to CM-ECM interactions. For example, injecting plasmin into a damaged myocardium may do more harm than good, but promoting plasmin receptors on CMs could selectively benefit CMs without impacting CF signaling. Similarly, laminin 511 may not enhance cardiac regeneration if laminin 211 is actively inhibiting CM proliferation, but laminin α2 blockade may be more effective.

Altogether, our work contributes to the growing evidence that fundamental ECM properties dictate CM proliferation, particularly in regulating ECM-CM-cytoskeletal binding dynamics that are more or less permissive of CM cytokinesis. Additionally, our findings identify proteins with potentially inhibitory influences to CM proliferation, including laminin 211, CTGF, CSPG, and plasmin-signaling in CFs (**Figs. 5.4B,D, 5.7**), and suppression of these proteins may provide a new therapeutic strategy in treating heart disease. Of the multiple protein candidates identified by our work, several warrant further investigation to identify the extent of their influence of CM cytokinesis and cardiac regeneration.

6.5 Conclusion

This work significantly contributes to the growing body of evidence that the cardiac ECM impacts the function of CMs in by dynamic and age-dependent mechanisms. A more thorough understanding of these ECM-CM interactions is necessary to recognize the influences guiding CM development and maturation, and to leverage the ECM as a biochemically instructive tool to model cardiac tissue behavior. Through the application and tailoring of CDMs to model the age-specific cardiac niche, we provide a defined and tractable platform for the mechanistic study of the ECM's role in tissue-specific biology that can, additionally, be applied to the study of all organ systems. Our investigation into CM metabolism and proliferation in the context of age-specific

ECM uncovered the impact of multiple matrix proteins in these processes, and identified numerous additional candidates for further investigation. Furthermore, we identified contrasting effects of signaling cascades in CFs and CMs, which provide important context for the role of multicellular interactions during cardiac homeostasis and injury. Together, this work demonstrates the nuanced and influential role of the ECM in multiple stages of CM function, and underscores the importance of the ECM as a fundamental component of niche-specific biology.

Materials and Methods

Cardiac Fibroblast Culture

Primary human fetal and adult CFs were obtained from Cell Applications and maintained in Human Cardiac Fibroblast Media (Cell Applications, 316K-500). Mouse CFs were isolated from CD1 murine hearts at fetal (E14) or adult (8 week) ages via outgrowth selection. Briefly, heart were extracted from euthanized mice, minced, and allowed to settle onto tissue culture-treated plastic. Cells that migrated out of heart sections were collected as CFs. Mouse CFs were maintained in CF Media, comprised of DMEM (Corning, 15-013-CV) + 10% Fetal Bovine Serum (FBS; Atlanta Biologicals, S11150 lot M16139).

Cell-Derived Matrix Production

Prior to cell seeding, tissue culture multi-well plates were dopa-coated with 2mg/ml poly L-dopamine hydrochloride (Sigma H8502) dissolved in a buffer of 100 mM Bicine (Sigma B3876), pH 8.5. Dopa stocks were stored under nitrogen before coating. Plates were allowed to incubate in dopa buffer overnight at room temperature (RT) with rotary agitation at 150rpm, and then washed with distilled water from a pressurized nozzle. After drying, plates were sterilized by UV for 30 minutes, and stored at RT until use. CFs were seeded at confluency, between 50-60K/cm^2 depending on well and cell size. Seeding was standardized to 55K (fetal) and 50K (adult) CFs in 24-well plates. Cells were cultured in CF media + 37.5mg/ml 70 kDa Ficoll (Fc; Sigma, F2878) and 25 mg/ml 400 kDa Ficoll PM (Sigma, F4375) (CF media + Fc) for 10 days with media refreshed every 2-3 days. Dextran and polystyrene were introduced to CF media at 100µg/ml, respectively.

Decellularization

CDMs were decellularized by first rinsing with H_20 twice, following by 2 rounds of the following: 0.6M KCl for 1hr, 1M KI for 1hr, 2X H_20 for 5 minutes at RT with rotary agitation at 150rpm. Matrices were then treated with 50u/ml DNase in 200mM Tris-HCl, pH 8.3 and 20mM $MgCl_2$ for 1 hour at 37°C with rotary agitation, and then rinsed 2X with H_20 for 5 minutes. CDMs were then either fixed for analysis, or stored overnight at 4°C in phosphate-buffered saline (PBS)+/+ with 1X Penicillin-Streptomycin (PenStrep) and fungizone at 0.25mg/ml. The following day, CDMs were rinsed 2X with PBS and allowed to equilibrate to RT prior to seeding with iPSC-CMs.

Mass Spectrometry

CDMs were rinsed overnight at 4°C in 0.5M NaCl in 10mM Tris at pH 7.5 + 1X cOmplete Protease Inhibitor Cocktail (PI), and subsequently solubilized with a 1% sodium dodecyl sulfate (SDS) solution in PBS + 1X PI at RT with agitation at 300rpm for 3-5 days until complete dissolution was achieved. Solubilized protein fractions were collected daily and replaced with fresh SDS + PI. Tris and SDS fractions were precipitated separately via chloroform/methanol separation and protein dry weight was quantified. Dry protein was then in 8M Urea with 100mM Ambic and 10mM dithiothreitol (DTT), reduced with 500mM iodoacetamide in HPLC-grade water and deglycosylated with 1000U PNGase F (P0704S, New England Biolabs). Solubilized protein was then be digested with 3ug trypsin at 37°C overnight with agitation at 1400rpm, and then desalted on C18 columns. 1µg of the protein (determined by volume/original protein weight) was then analyzed by LC-MS/MS. Unique peptides were identified by MaxQuant[271] software referenced against the SwissProt human or mouse database. Data was subjected to Intensity Based Absolute Quantification (IBAQ)[230] analysis and comparative analyses with statistical assessment using the MSstats[231]. A total of 3 distinct CDMs/condition were analyzed. Pearson's coefficient

was calculated assuming a Gaussian distribution from 109 data pairs. The mass spectrometry proteomics data have been deposited to the ProteomeXchange Consortium via the PRIDE[369] partner repository with the dataset identifier PXD020273. Identified proteins were cross-references to the Matrisome database (http://web.mit.edu/hyneslab/matrisome/)[233] for the filtering of non-matrix proteins and for functional category assignments.

Scanning Electron Microscopy

Decellularized CDMs were fixed with 2.5% (v/v) glutaraldehyde in 0.1 M sodium cacodylate and 0.03% aqueous eosin for 30 min with gentle agitation at RT. Then, samples were washed with 0.1 M sodium cacodylate buffer, progressively dehydrated in an ethanol series and stored in absolute ethanol until critical point drying. Dried samples were immobilized on carbon tape, sputter-coated with gold and imaged by a specialized technician at Electron Microscopy Lab (UC Berkeley).

Histological Stains

To detect glycosaminoglycans, CDMs produced in 24 well plates with 0.1% dimethyl sulfoxide (DMSO) were fixed, rinsed with distilled water, incubated with agitation in a 1% alcian blue solution in 3% acetic acid, pH 2.5, for 30 minutes at RT. Primary tissues were fixed in formalin for 6 hours (fetal) or 24 hours (adult), embedded into paraffin and sectioned. Individual sections were then deparaffinized with 3 incubations in xylene for 3 minutes, followed by rehydration in sequential solutions of 100% - 70% ethanol and then rinsed with tap water. Tissue sections were then stained with alcian blue for 30 minutes, followed by a 1 minute counterstain with eosin.

To detect collagens, CDMs produced in 24 well plates stained according to manufacturer's instructions (Polysciences, 24901). Briefly, fixed CDMs were rinsed with distilled water, incubated in solution A (Phosphomolybdic Acid) for 2 minutes, then rinsed in distilled water and incubated in solution B (Picrosirius Red F3BA Stain) for 60 minutes and then solution C (0.1 N Hydrochloride Acid) for 2 minutes. CDMs were then rinsed once more in distilled water.

To assess senescence, CFs were grown under conditions to produce CDMs and stained with a Senescence Detection Kit (Sigma Aldrich CS0030) according to manufacturer's instructions.

Histological stains were imaged on a Keyence BZ-X710 microscope.

Flow cytometry

Cells were removed from culture via trypsinization, and prepared for cytometry in a staining buffer containing 2% bovine serum albumin. Cells were blocked in staining buffer containing 2% FBS for 30 minutes prior, and then labeled for 30 minutes with the primary antibody against CD-31 (Santa Cruz Biotechnology SC-1506, 1:2500), followed by 3X washes with staining buffer. Cells were then incubated with an APC-conjugated anti-goat secondary antibody for 30 minutes, rinsed with PBS 3X and analyzed via cytometry on a BD Accuri.

Lyophilization

CDMs in 24 well plates were wrapped in parafilm and snap-frozen in PBS, 1:1 PBS:Glycerol, or dH_20 containing 250mM trehalose (Sigma T9449) by submerging plates into 100% ethanol super-cooled with dry ice. Pinholes were poked into the parafilm to allow sublimation, and plates were lyophilized overnight in a flask attached to a LABCONCO FreeZone 4.5 lyophilizer attached to an Adixen Pascal 2005SD vacuum.

RNA Sequencing

Cultured CFs were lysed with Trizol (Ambion), and all groups were collected in triplicate. RNA was extracted using the RNeasy Mini Kit (Qiagen 74104) and quantified using the NanoDrop 2000c (ThermoFisher Scientific). RNA-seq libraries were created using the SMARTer Stranded Total RNA Sample Prep Kit (Takara Bio) and sequenced on the NextSeq 500 (Illumina) to a minimum depth of 25 million reads per sample. Initial reads were aligned to GRCh37 human genome using HiSAT2 2.1.0[370]. Genes with low counts were filtered and gene expression levels normalized across samples using edgeR 3.28.1[371]. Counts were transformed to log2-counts per million (logCPM) using limma-voom 3.42.2[372]. Significantly different genes were assessed at a Benjamini & Hochberg adjusted $p < 0.05$ level and a minimum logCPM absolute difference of 1 between the gene and the mean expression level. GO term analysis was performed on significantly up and downregulated genes using enrichGO from clusterprofiler 3.14.3. To determine cumulative transcript abundance, Samples were normalized and converted to Log2Counts using the L2 transformation[373]. Log2FC differences between fetal and adult were compared using Welch's t-test with the bonferroni holm correction for multiple comparisons. Raw data will be available at GEO (Accession #:GSE155225).

Cardiomyocyte Differentiation

Human induced pluripotent stem cells (hiPSCs) (WTC11 cells modified with GCaMP6f reporter in the AAVS1 safe harbor locus; generously donated by Dr. Bruce Conklin) were seeded onto Matrigel-coated (80μg/mL; Corning, #354230) plates at a concentration of 3×10^4 cells/cm^2 in mTeSR1 medium (Stem Cell Technologies, #85850) supplemented with 10μM ROCK inhibitor, Y-27632 (SelleckChem, S1049) for 24h. Differentiation of hiPSCs to CMs was performed using a serum-free, chemically defined protocol. Briefly, once hiPSCs reached 100% confluence (~3-4

days; denoted as differentiation day 0), cells were fed with 12μM CHIR (SelleckChem, S2924) in RPMI1640 medium (Thermo Fisher, S2924) with B27 supplement without insulin (RPMI/B27-; Life Technologies, A1895602). After 24h, CHIR was removed by feeding with RPMI/B27- and on day 3, cells received a 48h-treatment with 5μM IWP2 (Tocris, #3533) in RPMI/B27-. On day 7, Medium was switched to RPMI1640 medium containing B27 supplement with insulin (RPMI/B27+; Life Technologies, 17504044) and fed every 3 days thereafter. On day 12-15 of differentiation, hiPSC-CMs were re-plated onto prepared CDMs in RPMI/B27+ with supplemented with 10μM ROCK inhibitor and 10% FBS and cultured in RPMI/B27+. Cultures were refreshed with RPMI/B27+ media after 2 days, and cultured for a minimum of another 1-4 days prior to functional assessment and/or fixation with 4% paraformaldehyde (PFA) for 15 minutes and 3X rinses with PBS.

Cardiac Fibroblast differentiation

Cardiac fibroblasts were differentiated from iPSCs following the GiFGF protocol, as previously published[251]. Briefly, hiPSCs were seeded at 1.5x104 cells/cm2 in mTeSR1 medium; once they reached 100% confluency, they were treated with 12μM CHIR99021 in R/B- medium (day 0). 24 hours later, media was changed to fresh R/B- (day 1). From days 2-20, cells were fed every 2 days with cardiac fibroblast basal media (CFBM) supplemented with 75ng/mL bFGF. On day 20, CFs were singularized with Accutase for 10 minutes and replated at ~7,000 cells/cm2 onto TCP plates in FibroGRO medium (MilliporeSigma SCMF001). Following this, FibroGRO media was changed every two days until the fibroblasts reached approximately 80-90% confluency when they were passaged with Accutase. iPSC-CFs were then cryopreserved in media containing 20% FBS and 10% DMSO prior to thawing and culturing for a minimum of 1 passage before use in any CDM experiments. iPSC-CFs were validated with the anti-stromal TE-7 antibody (MilliporeSigma

CBL271) by flow cytometry. Most replicates gave >80% TE-7+/Vimentin+, although the differentiation used to study CDM formation had very low TE-7+ detection (<10%).

Immunofluorescent Microscopy

Proteins were visualized by immunocytochemistry, wherein fixed CDMs and/or cells were blocked in 5% normal donkey serum (017-000-121, Jackson Immunoresearch Labs) and 0.3% Triton-X 100 (T8787, Sigma) in PBS for 1 hour at RT. Antibody dilution buffer (Ab Buffer) was comprised of PSB supplemented with 1% BSA (A4503, Sigma) and 0.3% Triton-X 100. Samples were incubated with primary antibodies in in Ab Buffer for 1 hour at RT or overnight at 4°C, followed by 3 washes with PBS and 1 hour of incubation with secondary antibodies at 1:300 in Ab Buffer at RT and 3 subsequent PBS washes. Primary antibodies and stains used are as follows: lectin (Sigma L9381), α-smooth muscle actin (DAKO M0851, 1:50), human-specific cardiac troponin T (Abcam ab45932, 1:400), mouse-specific cardiac troponin T (Abcam ab8295, 1:200), cellular fibronectin (used, unless otherwise noted, Sigma F6140, 1:400), plasma fibronectin (Abcam ab154211, 1:100), Collagen I (Abcam ab34710, 1:500), Plakophilin 2 (VWR 101981-232, 1:10), Col 6 (Abcam ab6588, 1:500), Hoescht 33342 (ThermoFisher 62249, 1:10,000), Phalloidin (ThermoFisher A34055, 1:100), and Cell Mask (ThermoFisher C10045, 1:5000). Samples were imaged on a Zeiss Z1 Inverted or Zeiss LSM880 Confocal Microscope.

Contractility and Calcium Handling

CM contraction and calcium handling properties were assessed via recorded live imaging of live CMs maintained at in Tyrode's solution (137 mM NaCl, 2.7 mM KCl, 1 mM $MgCl_2$, 0.2 mM Na_2HPO_4, 12 mM $NaHCO_3$, 5.5 mM D-glucose, 1.8 mM $CaCl_2$; Sigma–Aldrich) at physiological conditions (37°C, 5% CO_2, 80% humidity, OkoLab). Cells were placed into Tyrode's solution 1

hour prior to data acquisition. CM contraction frequency and speed were assessed from videos captured with brightfield illumination and assessed through the Pulse contractility analysis (Dana Solutions). Optical flow gradients of CM contractions were quantified by custom python scripts, available at https://github.com/david-a-joy/cm-disp-angle. Calcium handling properties were quantified by recording fluorescence intensity of the genetically encoded GCaMP6 calcium indicator. Stroke velocities were calculated using custom python scripts, available at https://github.com/david-a-joy/multilineage-organoid. A total of 4 experimental replicates were measured per condition, and video recordings were performed at 50ms (brightfield) or 10ms (fluorescence) exposure times through Zen software on a Zeiss Z1 Inverted Microscope.

siRNA-mediated silencing

Target KD in CDMs was achieved by serial lipid-mediated transient transfections of siRNAs in CFs during CDM production every 3-4 days. Complete CF media was refreshed at least 1 hour prior to transfection. All siRNAs were purchased from Dharmacon. siRNAs against the target(s) or a non-targeting control (D-001210-01) were diluted to a final concentration of 100nM in Opti-MEM Reduced Serum Medium (ThermoFisher, 31985070), and then mixed with an equal volume of Optimem:RNAiMax (ThermoFisher, 13778150) at a ratio of 50:1. The siRNA:RNAiMax mixture was allowed to complex at RT for 5 minutes, and was then added to cultures dropwise. Media was refreshed 6-18 hours later with CF media + Fc, and then cultured as normal. In 24 well plates, media was refreshed with 400µl CF media and transfected with a final volume of 100µl siRNA:RNAiMax. In the case of Col VI KD, siRNAs against COL6A1, Col6A2 and Col6A3 (Dharmacon, M-011620-01, M-011621-01, M-003646-02) were mixed at equal concentrations for a final combined concentration of 100nM. Other siRNAs pooled for screening purposes were mixed in the same manner, and stored as frozen aliquots for multiple uses without additional freeze-thaw cycles.

Cell Treatments

Both CFs and CMs were treated with a variety of biological agents and small molecules. In each case, control wells were treated with the same volume of the treatment's diluent. Treatments not addressed elsewhere are detailed below.

Treatment	Application	Conc.	Diluent	Distributor	Catalog #
fluorospheres	size-based uptake	100ug/ml	N/A	ThermoFisher	F8787
ascorbic acid	pro-collagen	100μM	Water	Sigma Aldrich	A8960
ONO-4817	anti-MMP	2uM	DMSO	R&D Systems	2628
bFGF	pro-fibroblast	75 ng/ml	Water	Stem Cell Technologies	78003
FGF18	pro-collagen	100 ng/ml	Water	Abcam	ab50129
LPS	inflammatory	1 ng/ml	DMSO	gift from Ott lab	
Retinoic acid	pro-growth	0.1 uM	DMSO	Sigma Aldrich	R2625
CHIR99021	Wnt agonist	1mM	DMSO	SelleckChem	S1263
cyclosporin A	MPTP inhibitor	200μM	DMSO	Sigma Aldrich	30024
PPACK	anti-tPA	1μM	Water	Sigma Aldrich	520222
BC 11 HCl	anti-uPA	10μM	DMSO	R&D Systems	4372
α2 antiplasmin	anti-plasmin	150μg/ml	Water	Sigma Aldrich	SRP6313
Plasmin	pro-plasmin	1μg/ml	Water	Sigma Aldrich	P1867
enoblock	anti-α enolase	10μM	DMSO	ThermoFisher	501364779
TGFβ	pro-fibrotic	10ng/ml	Water	R&D Systems	240-B-002
Angiotensin II	pro-fibrotic	250ng/ml	Water	Sigma Aldrich	A9525
SB431542	anti-TGFβ	1μM	DMSO	SelleckChem	S1067
Nintedanib	anti-fibrotic	1μM	DMSO	Cayman Chemicals	11022
GLPG1690	anti-fibrotic	3μM	DMSO	Cayman Chemicals	25498

Western Blot

CFs were incubated for 10 min on ice in RIPA Buffer (Sigma-Aldrich). Cell debris was pellet by centrifugation at 10,000Xg for 15 minutes, and supernatants were collected. Protein concentrations were determined using a Pierce BCA Protein Assay kit (Thermofisher Scientific, 23225) colorimetric reaction and quantified on a SpectraMax i3 Multi-Mode Platform (Molecular Devices). The protein concentration was determined by Bradford assay (Thermo Fisher, 23225). 17.5ug each lysates was suspended in 1X Sample buffer (BioRad) containing beta-mercaptoethanol, boiled for 5 minutes and separated on precast 12% SDS-PAGE TGX gels (BioRad, 465-1044). Proteins were then transferred to a nitrocellulose membrane, which was blocked in 1:1 PBS:Blocking Buffer (Rockland Inc, MB-070) for 1hr at RT and subsequently at 4°C overnight with primary antibodies anti-Col 6 (Abcam, ab182744, 1:2000), anti-plasminogen (Cell Signaling, #12657, 1:1000), anti-IGF1 (Bioss bs-0014R, 1:500), anti-IGFBP3 (Sigma Aldrich MA1-20185, 1:500), anti-FN (Abcam, ab194395, 1:200) and anti-GAPDH, (Invitrogen PA1-9046, 1:1,000). The membrane was washed with PBS containing 0.1% Tween, followed by incubation (45 min at RT) with infrared secondary antibodies: IRDye 800CW and IRDye 680CW (LI-COR 1:5,000) and imaged on an ChemiDoc MP Imaging System (BioRad). Band intensity was analyzed in Image Lab v2.4 (BioRad). Representative CDMs for each condition were assessed by western blot.

Seahorse Assay

For metabolic assays, fetal and adult CFs were seeded onto dopa-coated Seahorse XF96-well cell culture microplates (V3 PS, Agilent, 101085-004) at a density of 123k/cm^2 . XF96 plates were refreshed with 60µl CF media 1 hour prior to transfections, and transfected with a final volume of 20µl siRNA:RNAiMax pre-diluted with 20ul DMEM (Corning, 15-013-CV) following the 5 minute incubation. Transfections were repeated every 3-4 days for 10 days, and then decellularized. The

following day, iPSC-derived cardiomyocytes between day 12 and 15 of differentiation were dissociated with Trypsin supplemented with 10µM ROCK-Inhibitor for 30 min and seeded onto the decellularized Seahorse plate in RPMI/B27+ supplemented with 10µM ROCK inhibitor and 10% FBS at a density of 439k/cm^2 and cultured for 3 days. Before the metabolic assay, media was refreshed with Seahorse XF RPMI medium, pH 7.4 (Agilent, 103576-100) supplemented with 10mM Glucose (Agilent, 103577), 2mM Sodium Pyruvate (Agilent, 103578), and 1mM Glutamine (ThermoFisher, 35050061) pH 7.4, and incubated for one hour at 37°C without CO_2. Oxygen consumption rate (OCR) and extracellular acidification rate (ECAR) was measured using the Seahorse XF96 Extracellular Flux Analyzer (Agilent) during repeating cycles of 3x 3 minutes mix, 3 minutes measure, after sequential injection of the following mitochondrial inhibitors: ATP synthase inhibitor oligomycin (final concentration: 1.5uM), proton ionophore fluorocarbonyl cyanide phenylhydrazone (FCCP: 1uM), and complex I inhibitor rotenone/Antimycin A (0.5uM). Metabolic parameters were analyzed using Wave software version 2.6.1 and normalized per 10^3 iPSC-CMs. A total of 6-8 replicates were prepared per CDM condition, and 2-8 per experimental run were analyzed, depending on CDM integrity, which was assessed prior to CM seeding.

Primary CM Isolation

Embryonic CD1 mice from timed breedings were isolated at embryonic days 13.5-16.5. Briefly, pregnant mice were euthanized via CO_2 for a minimum of 5 minutes, followed by cervical dislocation. Embryos were then surgically extracted, after which their hearts were collected via a dissection microscopy. The atria and aorta were then removed, and the remaining ventricles and placed into cold isolation buffer containing 116.4mM NaCl, 20mM HEPES, 1mM NaH_2PO_4, 5.55mM glucose, 5.4mM KCl and 0.831mM $MgSO_4$. These procedures were performed with sterile tools in a non-sterile environment, and then ventricles were moved into sterile tissue culture hoods, minced, and transferred to sterile isolation buffer. CMs were then digested in 3-4 rounds

of sequential digestions with trituration at 37°C in sterile-filtered isolation buffer containing 50µg/20ml Collagenase A (Roche 10103586, 0.21U/mg) and 26mg/20ml pancreatin (Sigma P-3292). After each round, supernatant containing individual cells was diluted into DMEM containing 10% FBS. After the final digestion, all supernatants were passed through a 100µm filter and centrifuged at 350xg for 5 minutes to collect the cells. These cells were then resuspended in DMEM + 10% FBS and plated onto TCP for 1 hour, after which non-adhered cells were collected as the CM-enriched fraction. Adherent cells were saved as the stromal fraction. CMs were then collected via centrifugation at 350xg for 5 minutes, and resuspended in CM plating media containing a 4:1 mixture of M199 media (Gibco 21151-030) and DMEM + 10% horse serum (ThermoFisher 26050070), 5% FBS, 1X Glutamax, 1X Fungizone at 0.25mg/ml. Primary mouse CMs were seeded onto CDMs at 15-25K/cm^2, or onto substrate-coated TCP plates at 30-45K/cm^2, and allowed to adhere overnight prior to refreshing the media with CM maintenance media, containing 4:1 M199:DMEM + 1% FBS, 1X Glutamax and 1X PenStrep. A serum-free alterative to CM Maintenance Media was DMEM/F12 (ThermoFisher 10565018) containing 100uM L-ascorbic acid, 0.2% w/v BSA, 0.5% ITS-X (ThermoFisher 51500056) and 1X PenStrep.

Matrix Substrate Coatings

Laminins 111, 211, 221, 511, and 521 (Biolamina LN111-0,2 LN211-02, LN221-02, LN511-02, LN521-02) were diluted in PBS and added to tissue culture plates at a final concentration of 10µg/cm^2 and incubated 37°C for 3 hours. Plates were then rinsed with PBS, and cells suspended in culture media were added to the plates without letting the substrates dry.

Matrigel (Corning 354230) was diluted to a final concentration of 80µg/ml in Knock-out DMEM (ThermoFisher 10829018) and added to plates (100µl/well/96 well plate, 500µl/well/24 well plate).

Plates were then incubated in a 37°C tissue culture incubator overnight, or for a minimum of 2 hours. Immediately prior to use, Matrigel was removed from the plates without additional rinsing.

Gelatin (Stem Cell Technologies 07903) was applied to tissue culture surfaces with sufficient volume to cover the well and allowed to incubate at RT for 5-20 minutes. Immediately prior to use, gelatin was removed from the plates without additional rinsing.

qPCR

Transcriptional changes in CFs were assessed by quantitative polymerase chain reaction (qPCR). Treated CFs were lysed using RLT Buffer (Qiagen) containing 150mM beta-mercaptoethanol, and mRNA was isolated from treated CFs using the RNeasy Mini Kit (Qiagen, 74104) following the manufacturer's instructions. RNA was converted to cDNA using the iScript cDNA synthesis kit (Bio-Rad). Forward and reverse primers for genes were designed using NCBI's Primer-BLAST. To compare iPSC-CF CDM conditions, 50ng cDNA was diluted into Fast SYBR Green Master Mix (ThermoFisher 4385610) with primers listed below at a concentration of 200nM each. qPCR was run for 40 cycles on a QuantStudio 5 (ThermoFisher). CFs treated with modulators of plasmin signaling were assessed by high throughput qPCR using Fluidigm technology. Primers were pooled to 500 nM to enable specific-target amplification and cDNA was amplified with PreAmp Master Mix (Fluidigm 100-5580) and pooled primers for 15 cycles. Pre-amplified samples mixed with 2X SsoFast EvaGreen Supermix with low ROX (Bio-Rad SsoFast EvaGreen Supermix with low ROX) and 20X DNA Binding Dye Sample Loading Reagent (Fluidigm 100-7610), and 10 μM primer sets were mixed with 2X Assay Loading Reagent (Fluidigm 100-7611). 5 μl of diluted cDNA and primers and were loaded onto the IFC 48.48 Gene Expression chip per manufacturer's instructions and loaded into the chip using the IFC Controller MX (Fluidigm). qPCR was run for 40 cycles in the IFC chip using the BioMark HD in the BioMark HD Data Collection Software.

Resulting data was subjected to quality assessment in the Real-Time PCR Analysis Software. All instruments and software involved with the IFC chip were manufactured by Fluidigm.

Gene	Forward Primer	Reverse Primer
18S	CTC TAG TGA TCC CTG AGA AGT TCC	ACT CGC TCC ACC TCA TCC TC
ACTA2	AAA AGA CAG CTA CGT GGG TGA	GCC ATG TTC TAT CGG GTA CTT C
ANXA2	CAC GGC CCA GGT TAT CTT GT	CCA TAT GCA CTT GGG GGT GT
COL1A1	TTT GGA TGG TGC CAA GGG AG	CAC CAT CAT TTC CAC GAG CA
COL3A1	TGG AGG ATG GTT GCA CGA AA	AAA AGC AAA CAG GGC CAA CG
COL4A1	CCG GAT CAC ATT GAC ATG AAA CC	TGC TCG CAA AGC TCA GAA GA
CXCL12	TGC CCT TCA GAT TGT AGC CC	GCG TCT GAC CCT CTC ACA TC
CXCL6	CCC GGA AGC CCC TTT TCT AA	GTA GGC TTT CCC CCA CAC TC
CXCR4	CGT CTC AGT GCC CTT TTG TTC	CTG AAG TAG TGG GCT AAG GGC
ENO1	GCC GTG AAC GAG AAG TCC TG	ACG CCT GAA GAG ACT CGG T
F13A1	TCA GAA ACT TCC AGG ACC GC	AGG TGA ACG CTC GTG ACA TT
F2	CAC GGC TAC GGA TGT GTT CTG	ACC CTC AGC ACA GTT ACC TTC
FN1	CCCAATTGAGTGCTTCATGCC	CCTCCAGAGCAAAGGGCTTA
GATA4	ACCTGGGACTTGGAGGATAGC	CCATCAGCGTGTAAAGGCATCT
IGF1	AGA GCC TGC GCA ATG GAA TA	GGA GGA CAT GGT GTG CAT CT
IGF2	GTG GCG CCC TTC CCT C	ACA GCA CGG AGA GAA ACA GA
IGFBP10	CGC CTT GTG AAA GAA ACC CG	GGT TCG GGG GAT TTC TTG GT
IGFBP3	GCC AGC TCC AGG AAA TGC TA	TCG GAG GAG AAG TTC TGG GT
IGFBP5	TCC GTT TTC ACC CTT CTC CG	GCA GAA CAG GTA AGA GGC GT
IGFBP7	AAG GAC AGG CTT CAG CAT CA	ACT TAA TGC CCT TAT GGG TTG CT
IL1B	ATG ATG GCT TAT TAC AGT GGC AA	GTC GGA GAT TCG TAG CTG GA
IL6	CCT GAA CCT TCC AAA GAT GGC	TTC ACC AGG CAA GTC TCC TCA
IL6	CCT GAA CCT TCC AAA GAT GGC	TTC ACC AGG CAA GTC TCC TCA
LAMA1	CTC AGG TTA AGT GTT TCT GGG GA	ACG TTT AAA AAG AGA GCC AGG GAA
LAMA2	GGC TTC CGT TGT CAG CAA TC	TCA AGT TTC TCA GCG TTG GC
LAMA5	GGA CTG CAG GCC ACC G	AGG ATG CCC ACA AAC TCC AG
LOX	GCG AAG GGT GAG GAG TAA GG	GAC GCC TGG ATG TAG TAG GG
MMP1	TAT GCA CAG CTT TCC TCC ACT	GCC TCC CAT CAT TCT TCA GGT T
MMP12	GGA ATC CTA GCC CAT GCT TTT	CAT TAC GGC CTT TGG ATC ACT
MMP13	ACT GAG AGG CTC CGA GAA ATG	GAA CCC CGC ATC TTG GCT T
MMP14	ATC TGC CTC TGC CTC ACC TA	AAG CCC CAT CCA AGG CTA AC
MMP2	TCT GTG TTG TCC AGA GGC AA	GTG TTC AGG TAT TGC ATG TGC T
MMP3	CTG GAC TCC GAC ACT CTG GA	CAG GAA AGG TTC TGA AGT GAC C
MMP9	AGA CCT GGG CAG ATT CCA AAC	CGG CAA GTC TTC CGA GTA GT
PDGFRA	GAA GGC GCA ATC TGG ACA CT	AGT AAT GGG CTC AAA AAC CGC
PLAT	TCA GAA GCA ACC GGG TGG AAT A	ACG TGG CCC TGG TAT CTA TTT
PLAUR	TGT AAG ACC AAC GGG GAT TGC	AGC CAG TCC GAT AGC TCA GG
PLAUR	TCT GGT TTG TGG ATG CGT TT	AGA GGC TCT CCT TGA CCT GA

Gene	Forward Primer	Reverse Primer
PLG	TCT GGT TTG TGG ATG CGT TT	AGA GGC TCT CCT TGA CCT GA
POSTN	CCC GTG ACT GTC TAT AAG CC	CAC CTT CAA TGA ATT TGG TGA CCT
S100A4	TTC TTG GTT TGA TCC TGA CTG CT	CCT GTT GCT GTC CAA GTT GC
SERPINB2	GTA ACA ACT CTC AGA GGA GCA T	ACT CGG TGG TGC ATA GCT T
SERPINE1	GAC CGC AAC GTG GTT TTC TC	CTT GTA CAG ATG CCG GAG GG
TCF21	CTG ACG TGG CCC TTT ATG GT	ACA GAG AGA GGA GCA TTG CG
TGFB1	ATG GAG AGA GGA CTG CGG AT	TAG TGT TCC CCA CTG GTC CC
TGFB2	AGA AGA CTA TCC TGA GCC CGA	CTG AGC CAG AGG GTG TTG TAA
TGM2	TGT CTC TCC GGG AAC CCT TC	GAG ACC CTC CAA GTG CGA C
VIM	GGA CCA GCT AAC CAA CGA CA	AAG GTC AAG ACG TGC CAG AG

Statistical analysis

All results are shown as mean ± standard deviation. Unless otherwise stated, all statistical analysis of the data was performed using Prism 8 with statistical significance determined at $p < 0.05$ by a one way ANOVA with subsequent Dunnett's test to correct for multiple comparisons or a or student's t-test.

References

1. Frantz, C., Stewart, K. M. & Weaver, V. M. The extracellular matrix at a glance. *J. Cell Sci.* **123**, 4195–4200 (2010).

2. Virani, S. S. *et al.* Heart Disease and Stroke Statistics—2020 Update: A Report From the American Heart Association. *Circulation* **141**, 139–596 (2020).

3. Porrello, E. R. & Olson, E. N. A neonatal blueprint for cardiac regeneration. *Stem Cell Res.* **13**, 556–570 (2013).

4. Porrello, E. R. *et al.* Transient Regenerative Potential of the Neonatal Mouse Heart. *Science (80-.).* **331**, 1078–1080 (2011).

5. Ali, S. R. *et al.* Existing cardiomyocytes generate cardiomyocytes at a low rate after birth in mice. *PNAS* **111**, 8850–5 (2014).

6. Walsh, S., Ponten, A., Fleischmann, B. K. & Jovinge, S. Cardiomyocyte cell cycle control and growth estimation in vivo-An analysis based on cardiomyocyte nuclei. *Cardiovasc. Res.* **86**, 365–373 (2010).

7. Wang, J., Liu, S., Heallen, T. & Martin, J. F. The Hippo pathway in the heart: pivotal roles in development, disease, and regeneration. *Nat. Rev. Cardiol.* **15**, 672–684 (2018).

8. Hirose, K. *et al.* Evidence for hormonal control of heart regenerative capacity during endothermy acquisition. *Science (80-.).* **364**, 184–188 (2019).

9. Laflamme, M. A. & Murry, C. E. Heart Regeneration. *Nature* **29**, 997–1003 (2012).

10. Brizzi, M. F., Tarone, G. & Defilippi, P. Extracellular matrix, integrins, and growth factors as tailors of the stem cell niche. *Curr. Opin. Cell Biol.* **24**, 645–51 (2012).

11. Mouw, J. K., Ou, G. & Weaver, V. M. Extracellular matrix assembly: a multiscale

deconstruction. *Nat. Rev. Mol. Cell Biol.* **15**, 771–785 (2014).

12. Shoulders, M. D. & Raines, R. T. Collagen Structure and Stability. *Annu Rev Biochem* **78**, 929–958 (2010).

13. Sarrazin, S., Lamanna, W. C. & Esko, J. D. Heparan sulfate proteoglycans. *Cold Spring Harb. Perspect. Biol.* **3**, (2011).

14. Shi, M. *et al.* Latent TGF-Beta structure and activation. *Nature* **474**, 343–349 (2011).

15. Taipale, J. & Keski-Oja, J. Growth factors in the extracellular matrix. *FASEB J. Off. Publ. Fed. Am. Soc. Exp. Biol.* **11**, 51–9 (1997).

16. Markwald, R., Fitzharris, T. P., Bank, H. & Bernanke, D. H. Structural Analyses on the Matrical Organization of Glycosaminoglycans in Developing Endocardial Cushions. *Dev. Biol.* **62**, 292–316 (1978).

17. Toole, B. P. Glycosaminoglycans in Morphogenesis. in *Cell Biology of Extracellular Matrix* (ed. Hay, E. D.) 259–294 (Springer US, 1981).

18. Esko, J. D., Prestegard, J. H. & Linhardt., R. J. Proteins That Bind Sulfated Glycosaminoglycans. in *Essentials of Glycobiology* (eds. Varki A, RD, C. & JD, E.) (Cold Spring Harbor Laboratory Press, 2017).

19. Seyrek, E. & Dubin, P. Glycosaminoglycans as polyelectrolytes. *Adv. Colloid Interface Sci.* **158**, 119–129 (2010).

20. Tellier, L. E., Miller, T., McDevitt, T. C. & Temenoff, J. S. Hydrolysis and sulfation pattern effects on release of bioactive bone morphogenetic protein-2 from heparin-based microparticles. *J. Mater. Chem. B* (2015).

21. Jayadev, R. & Sherwood, D. R. Basement membranes. *Curr. Biol.* **27**, R207–R211

(2017).

22. Yurchenco, P. D. Basement membranes: Cell scaffoldings and signaling platforms. *Cold Spring Harb. Perspect. Biol.* **3**, 1–27 (2011).

23. LeBleu, V. S., MacDonald, B. & Kalluri, R. Structure and function of basement membranes. *Exp. Biol. Med.* **232**, 1121–1129 (2007).

24. Vu, T. H. Matrix metalloproteinases: effectors of development and normal physiology. *Genes Dev.* **14**, 2123–2133 (2000).

25. Jabłońska-Trypuć, A., Matejczyk, M. & Rosochacki, S. Matrix metalloproteinases (MMPs), the main extracellular matrix (ECM) enzymes in collagen degradation, as a target for anticancer drugs. *J. Enzyme Inhib. Med. Chem.* **31**, 177–183 (2016).

26. Klein, T. & Bischoff, R. Physiology and pathophysiology of matrix metalloproteases. *Amino Acids* **41**, 271–290 (2011).

27. Shi, F. & Sottile, J. MT1-MMP regulates the turnover and endocytosis of extracellular matrix fibronectin. *J. Cell Sci.* **124**, 4039–4050 (2011).

28. Cudic, M. & Fields, G. Extracellular Proteases as Targets for Drug Development. *Curr. Protein Pept. Sci.* **10**, 297–307 (2009).

29. Nagase, H., Visse, R. & Murphy, G. Structure and function of matrix metalloproteinases and TIMPs. *Cardiovasc. Res.* **69**, 562–573 (2006).

30. Mccormick, R. J. & Thomas, D. P. Collagen Crosslinking in the Heart: Relationship to Development and Function. *Basic Appl. Myol.* **8**, 143–150 (1998).

31. Allard, J. B. & Duan, C. IGF-binding proteins: Why do they exist and why are there so many? *Front. Endocrinol. (Lausanne).* **9**, 1–12 (2018).

32. Sherratt, M. J. Tissue elasticity and the ageing elastic fibre. *Age (Omaha).* **31**, 305–325 (2009).

33. Xu, J. & Mosher, D. Fibronectin and Other Adhesive Glycoproteins. in *The Extracellular Matrix: an Overview* (ed. Mecham, R. P.) 41–76 (Springer Berlin Heidelberg, 2011).

34. White, E. S. & Muro, A. F. Fibronectin splice variants: understanding their multiple roles in health and disease using engineered mouse models. *IUBMB Life* **63**, 538–46 (2011).

35. Pankov, R. & Yamada, K. M. Fibronectin at a glance. *J. Cell Sci.* **115**, 3861–3863 (2002).

36. Liu, X., Wu, H., Byrne, M., Krane, S. & Jaenisch, R. Type III collagen is crucial for collagen I fibrillogenesis and for normal cardiovascular development. *Proc. Natl. Acad. Sci. U. S. A.* **94**, 1852–6 (1997).

37. Hynes, R. O. Integrins: A family of cell surface receptors. *Cell* **48**, 549–554 (1987).

38. Takada, Y., Ye, X. & Simon, S. The integrins. *Genome Biol.* **8**, 215 (2007).

39. Belkin, A. M. & Stepp, M. A. Integrins as receptors for laminins. *Microsc. Res. Tech.* **51**, 280–301 (2000).

40. Adams, J. C. & Brancaccio, A. The evolution of the dystroglycan complex, a major mediator of muscle integrity. *Biol. Open* **4**, 1163–1179 (2015).

41. López-Colomé, A. M., Lee-Rivera, I., Benavides-Hidalgo, R. & López, E. Paxillin: a crossroad in pathological cell migration. *J. Hematol. Oncol.* **10**, 50 (2017).

42. Sieg, D. J. *et al.* FAK integrates growth-factor and integrin signals to promote cell migration. *Nat. Cell Biol.* **2**, 249–256 (2000).

43. Hammerschmidt, M. & Wedlich, D. Regulated adhesion as a driving force of gastrulation movements. *Development* **135**, 3625–3641 (2008).

44. Belkin, A. M. *et al.* Muscle β1D integrin reinforces the cytoskeleton-matrix link: Modulation of integrin adhesive function by alternative splicing. *J. Cell Biol.* **139**, 1583–1595 (1997).

45. Pham, C. G. *et al.* Striated muscle-specific beta(1D)-integrin and FAK are involved in cardiac myocyte hypertrophic response pathway. *Am. J. Physiol. Heart Circ. Physiol.* **279**, H2916–H2926 (2000).

46. Bourdoulous, S., Orend, G., MacKenna, D. a., Pasqualini, R. & Ruoslahti, E. Fibronectin matrix regulates activation of RHO and CDC42 GTPases and cell cycle progression. *J. Cell Biol.* **143**, 267–276 (1998).

47. Manso, A. M., Kang, S. & Ross, R. S. Integrins, focal adhesions, and cardiac fibroblasts. *J Investig Med* **57**, 856–860 (2009).

48. Gérard, C. & Goldbeter, A. The balance between cell cycle arrest and cell proliferation: control by the extracellular matrix and by contact inhibition. *Interface Focus* **4**, 20130075 (2014).

49. Heart, E. F. E., Jallerat, Q. & Feinberg, A. W. Extracellular Matrix Structure and Composition in the Early Four-Chambered Embryonic Heart. 1–14 (2020).

50. Lockhart, M., Wirrig, E., Phelps, A. & Wessells, A. Extracellular Matrix and Heart Development. *Birth Defects Res A Clin Mol Teratol* **91**, 535–550 (2011).

51. Muro, A. F. *et al.* Regulated splicing of the fibronectin EDA exon is essential for proper skin wound healing and normal lifespan. *J. Cell Biol.* **162**, 149–160 (2003).

52. Sottile, J., Hocking, D. C. & Swiatek, P. J. Fibronectin matrix assembly enhances adhesion-dependent cell growth. *J. Cell Sci.* **111 Pt 1**, 2933–2943 (1998).

53. Lukjanenko, L. *et al.* Loss of fibronectin from the aged stem cell niche affects the

regenerative capacity of skeletal muscle in mice. *Nat. Med.* **22**, 897–905 (2016).

54. Chen, D. *et al.* Fibronectin signals through integrin α5β1 to regulate cardiovascular development in a cell type-specific manner. *Dev. Biol.* **407**, 195–210 (2015).

55. Gomes de Almeida, P., Pinheiro, G. G., Nunes, A. M., Gonçalves, A. B. & Thorsteinsdóttir, S. Fibronectin assembly during early embryo development: A versatile communication system between cells and tissues. *Dev. Dyn.* 520–535 (2016).

56. Cooke, M. J. *et al.* Enhanced cell attachment using a novel cell culture surface presenting functional domains from extracellular matrix proteins. *Cytotechnology* **56**, 71–79 (2008).

57. Zhu, J. & Clark, R. A. F. Fibronectin at Select Sites Binds Multiple Growth Factors and Enhances their Activity: Expansion of the Collaborative ECM-GF Paradigm. *J. Invest. Dermatol.* **134**, 895–901 (2014).

58. Rienks, M., Papageorgiou, A. P., Frangogiannis, N. G. & Heymans, S. Myocardial extracellular matrix: An ever-changing and diverse entity. *Circ. Res.* **114**, 872–888 (2014).

59. Williams, C., Quinn, K. P., Georgakoudi, I. & Black, L. D. Young developmental age cardiac extracellular matrix promotes the expansion of neonatal cardiomyocytes in vitro. *Acta Biomater.* **10**, 194–204 (2014).

60. Lawson, C. *et al.* FAK promotes recruitment of talin to nascent adhesions to control cell motility. *J. Cell Biol.* **196**, 223–232 (2012).

61. Mittal, A., Pulina, M., Hou, S. Y. & Astrof, S. Fibronectin and integrin alpha 5 play requisite roles in cardiac morphogenesis. *Dev. Biol.* **381**, 73–82 (2013).

62. Li, R., Maminishkis, A., Zahn, G., Vossmeyer, D. & Miller, S. S. Integrin α5β1 mediates attachment, migration, and proliferation in human retinal pigment epithelium: Relevance

for proliferative retinal disease. *Investig. Ophthalmol. Vis. Sci.* **50**, 5988–5996 (2009).

63. Song, Y. *et al.* Effects of integrin α5β1 on the proliferation and migration of human aortic vascular smooth muscle cells. *Mol. Med. Rep.* **13**, 1147–1155 (2016).

64. Paszek, M. J., Boettiger, D., Weaver, V. M. & Hammer, D. A. Integrin clustering is driven by mechanical resistance from the glycocalyx and the substrate. *PLoS Comput. Biol.* **5**, (2009).

65. Yamada, K. M. & Even-ram, S. Integrin regulation of growth factor signalling and adhesion. *Nat. Cell Biol.* **4**, E75-76 (2002).

66. Woodside, D. G., Liu, S. & Ginsberg, M. H. Integrin activation. *Thromb. Haemost.* **86**, 316–323 (2001).

67. Miyamoto, S., Teramoto, H., Gutkind, J. S. & Yamada, K. M. Integrins can colaborate with growth factors for phosporylation of receptor tyrosine kinases and MAP kinase activation: roles of integrin aggregation and occupancy of receptors. *J. Cell Biol.* **135**, 1633–42. (1996).

68. Goult, B. T., Yan, J. & Schwartz, M. A. Talin as a mechanosensitive signaling hub. *J. Cell Biol.* **217**, 3776–3784 (2018).

69. Stephenson, A., Adams, J. W. & Vaccarezza, M. The vertebrate heart: an evolutionary perspective. *J. Anat.* **231**, 787–797 (2017).

70. Guo, Y. & Pu, W. T. Cardiomyocyte Maturation. *Circ. Res.* 1086–1106 (2020).

71. Bird, S. D. *et al.* The human adult cardiomyocyte phenotype. *Cardiovasc. Res.* **58**, 423–434 (2003).

72. Xin, M. *et al.* Hippo pathway effector Yap promotes cardiac regeneration. *Proc. Natl.*

Acad. Sci. **110**, 13839–13844 (2013).

73. Price, E. L., Vieira, J. M. & Riley, P. R. Model organisms at the heart of regeneration. *DMM Dis. Model. Mech.* **12**, (2019).

74. Jopling, C. *et al.* Zebrafish heart regeneration occurs by cardiomyocyte dedifferentiation and proliferation. *Nature* **464**, 606–609 (2010).

75. Mollova, M. *et al.* Cardiomyocyte proliferation contributes to heart growth in young humans. *Proc. Natl. Acad. Sci. U. S. A.* **110**, 1446–51 (2013).

76. Van Amerongen, M. J. & Engel, F. B. Features of cardiomyocyte proliferation and its potential for cardiac regeneration: Stem Cells Review Series. *J. Cell. Mol. Med.* **12**, 2233–2244 (2008).

77. Itou, J. *et al.* Migration of cardiomyocytes is essential for heart regeneration in zebrafish. *Development* **139**, 4133–42 (2012).

78. Poss, K. D., Wilson, L. G. & Keating, M. T. Heart regeneration in zebrafish. *Science* **298**, 2188–2190 (2002).

79. Heallen, T. *et al.* Hippo Pathway Inhibits Wnt Signaling to Restrain Cardiomyocyte Proliferation and Heart Size. *Science (80-.).* **332**, 458–461 (2011).

80. Xin, M. *et al.* Regulation of insulin-like growth factor signaling by Yap governs cardiomyocyte proliferation and embryonic heart size. *Sci. Signal.* **4**, (2011).

81. Nakada, Y. *et al.* Hypoxia induces heart regeneration in adult mice. *Nature* **20173**, 1–21 (2016).

82. Puente, B. N. *et al.* The oxygen-rich postnatal environment induces cardiomyocyte cell-cycle arrest through DNA damage response. *Cell* **157**, 565–579 (2014).

83. Chen, Y. *et al.* Enhanced Glycolysis Promotes Postnatal Cardiomyocyte Proliferation and Improves Cardiac Function. *J. Am. Coll. Cardiol.* **75**, 1042 (2020).

84. Lopaschuk, G. D. & Jaswal, J. S. Energy metabolic phenotype of the cardiomyocyte during development, differentiation, and postnatal maturation. *J. Cardiovasc. Pharmacol.* **56**, 130–140 (2010).

85. Bhute, V. J. *et al.* Metabolomics Identifies Metabolic Markers of Maturation in Human Pluripotent Stem Cell-Derived Cardiomyocytes. *Theranostics* **7**, 2078–2091 (2017).

86. Piquereau, J. & Ventura-Clapier, R. Maturation of cardiac energy metabolism during perinatal development. *Front. Physiol.* **9**, 1–10 (2018).

87. Aurora, A. B. *et al.* Macrophages are required for neonatal heart regeneration. *J. Clin. Invest.* **124**, 1382–1392 (2014).

88. Simões, F. C. *et al.* Macrophages directly contribute collagen to scar formation during zebrafish heart regeneration and mouse heart repair. *Nat. Commun.* 1–17 (2020).

89. Nahrendorf, M. Myeloid cell contributions to cardiovascular health and disease. *Nat. Med.* **24**, 711–720 (2018).

90. Bersell, K., Arab, S., Haring, B. & Kühn, B. Neuregulin1/ErbB4 Signaling Induces Cardiomyocyte Proliferation and Repair of Heart Injury. *Cell* **138**, 257–270 (2009).

91. Maliken, B. D. & Molkentin, J. D. Undeniable evidence that the adult mammalian heart lacks an endogenous regenerative stem cell. *Circulation* **138**, 806–808 (2018).

92. Eschenhagen, T. *et al.* Cardiomyocyte Regeneration. *Circulation* **136**, 680–686 (2017).

93. Frey, N. & Olson, E. N. Cardiac Hypertrophy: The Good, the Bad, and the Ugly. *Annu. Rev. Physiol.* **65**, 45–79 (2003).

94. Li, P. *et al.* IGF signaling directs ventricular cardiomyocyte proliferation during embryonic heart development. *Development* **138**, 1795–1805 (2011).

95. Brade, T. *et al.* Retinoic acid stimulates myocardial expansion by induction of hepatic erythropoietin which activates epicardial Igf2. *Development* **138**, 139–48 (2011).

96. Engel, F. B., Schebesta, M. & Keating, M. T. Anillin localization defect in cardiomyocyte binucleation. *J. Mol. Cell. Cardiol.* **41**, 601–612 (2006).

97. Mahmoud, A. I. *et al.* Meis1 regulates postnatal cardiomyocyte cell cycle arrest. *Nature* **497**, 249–253 (2013).

98. Kimura, W. *et al.* Hypoxia fate mapping identifies cycling cardiomyocytes in the adult heart. *Nature* **523**, 226–30 (2015).

99. Kikuchi, K. & Poss, K. D. Cardiac Regenerative Capacity and Mechanism. *Annu rev cell dev bio* 719–741 (2013).

100. Schafer, K, A. The Cell Cycle: A Review. *Vet. Pathol.* **35**, 461–478 (1998).

101. Soonpaa, M. H., Kim, K. K., Pajak, L., Franklin, M. & Field, L. J. Cardiomyocyte DNA synthesis and binucleation during murine development. *Am. J. Physiol.* **271**, H2183–H2189 (1996).

102. Bassat, E. *et al.* The extracellular matrix protein Agrin promotes heart regeneration in mice. *Nature* 1–20 (2017).

103. Chablais, F., Veit, J., Rainer, G. & Jawiska, A. The zebrafish heart regenerates after cryoinjury-induced myocardial infarction. *BMC Dev. Biol.* **11**, (2011).

104. Souders, C. A., Bowers, S. L. & Baudino, T. A. Cardiac fibroblast: the renaissance cell. *Circ Res* **105**, 1164–1176 (2009).

105. Sampaio-Pinto, V. *et al.* Neonatal Apex Resection Triggers Cardiomyocyte Proliferation, Neovascularization and Functional Recovery Despite Local Fibrosis. *Stem Cell Reports* **10**, (2018).

106. Adam-Vizi, V. & Chinopoulos, C. Bioenergetics and the formation of mitochondrial reactive oxygen species. *Trends Pharmacol. Sci.* **27**, 639–645 (2006).

107. Menendez-Montes, I. *et al.* Myocardial VHL-HIF Signaling Controls an Embryonic Metabolic Switch Essential for Cardiac Maturation. *Dev. Cell* **39**, 724–739 (2016).

108. Medley, T. L. *et al.* Effect of oxygen on cardiac differentiation in mouse iPS cells: Role of hypoxia inducible factor-1 and Wnt/beta-catenin signaling. *PLoS One* **8**, 1–8 (2013).

109. Lodish H, Berk A, Zipursky SL, E. Oxidation of Glucose and Fatty Acids to CO 2 Cytosolic Enzymes Convert Glucose to Pyruvate Substrate-Level Phosphorylation Generates ATP during Glycolysis. in *Molecular Cell Biology* (ed. Freeman, W. H.) (2000).

110. Silva, A. C. *et al.* Three-dimensional scaffolds of fetal decellularized hearts exhibit enhanced potential to support cardiac cells in comparison to the adult. *Biomaterials* **104**, 52–64 (2016).

111. Hirschy, A., Schatzmann, F., Ehler, E. & Perriard, J. C. Establishment of cardiac cytoarchitecture in the developing mouse heart. *Dev. Biol.* **289**, 430–441 (2006).

112. Tan, C. M. J. & Lewandowski, A. J. The Transitional Heart: From Early Embryonic and Fetal Development to Neonatal Life. *Fetal Diagn. Ther.* **47**, 373–386 (2020).

113. Brand, T. Heart development: Molecular insights into cardiac specification and early morphogenesis. *Dev. Biol.* **258**, 1–19 (2003).

114. Ieda, M. *et al.* Cardiac fibroblasts regulate myocardial proliferation through beta1 integrin signaling. *Dev Cell* **16**, 233–244 (2009).

115. Fong, A. H., Heylman, C. M., Keating, M., Gershon, P. D. & Botvinick, E. L. Three-Dimensional Adult Cardiac Extracellular Matrix Promotes Maturation of Human Induced Pluripotent Stem Cell-Derived Cardiomyocytes. **22**, 1016–1025 (2016).

116. Jacot, J. G., Martin, J. C. & Hunt, D. L. Mechanobiology of cardiomyocyte development. *J Biomech* **43**, 93–98 (2010).

117. Kolwicz, S. C., Purohit Jr, S. & Tian, R. Cardiac Metabolism and its Interactions With Contraction, Growth, and Survival of Cardiomyocytes. *Circ. Res.* **113**, 603–616 (2013).

118. Ahmed, R. E., Anzai, T., Chanthra, N. & Uosaki, H. A Brief Review of Current Maturation Methods for Human Induced Pluripotent Stem Cells-Derived Cardiomyocytes. *Front. Cell Dev. Biol.* **8**, 1–9 (2020).

119. DeLaughter, D. M. *et al.* Single-Cell Resolution of Temporal Gene Expression during Heart Development. *Dev Cell* **39**, 480–490 (2016).

120. Simpson, D. G. *et al.* Modulation of Cardiac Myocyte Phenotype In-Vitro by the Composition and Orientation of the Extracellular-Matrix. *J. Cell. Physiol.* **161**, 89–105 (1994).

121. Lundy, S. D., Zhu, W. Z., Regnier, M. & Laflamme, M. A. Structural and functional maturation of cardiomyocytes derived from human pluripotent stem cells. *Stem Cells Dev* **22**, 1991–2002 (2013).

122. Squire, J. M. Muscle contraction: Sliding filament history, sarcomere dynamics and the two Huxleys. *Glob. Cardiol. Sci. Pract.* **2016**, (2016).

123. Peter, A. K., Cheng, H., Ross, R. S., Knowlton, K. U. & Chen, J. The costamere bridges sarcomeres to the sarcolemma in striated muscle. *Prog. Pediatr. Cardiol.* **31**, 83–88 (2011).

124. Bedada, F. B., Wheelwright, M. & Metzger, J. M. Maturation status of sarcomere structure and function in human iPSC-derived cardiac myocytes ☆. *Biochim. Biophys. Acta - Mol. Cell Res.* **1863**, 1829–1838 (2016).

125. Karbassi, E. *et al.* Cardiomyocyte maturation: advances in knowledge and implications for regenerative medicine. *Nat. Rev. Cardiol.* **17**, 341–359 (2020).

126. Ribeiro, A. J. S. *et al.* Contractility of single cardiomyocytes differentiated from pluripotent stem cells depends on physiological shape and substrate stiffness. *Proc. Natl. Acad. Sci.* **112**, 12705–12710 (2015).

127. Rampazzo, A., Calore, M., Van Hengel, J. & Van Roy, F. Intercalated discs and arrhythmogenic cardiomyopathy. *Circ. Cardiovasc. Genet.* **7**, 930–940 (2014).

128. Lo, C. W. Role of gap junctions in cardiac conduction and development: Insights from the connexin knockout mice. *Circ. Res.* **87**, 346–348 (2000).

129. Rohr, S. Role of gap junctions in the propagation of the cardiac action potential. *Cardiovasc. Res.* **62**, 309–322 (2004).

130. Jongsma, H. J. & Wilders, R. Gap junctions in cardiovascular disease. *Circ. Res.* **86**, 1193–1197 (2000).

131. Grossmann, K. S. *et al.* Requirement of plakophilin 2 for heart morphogenesis and cardiac junction formation. *J. Cell Biol.* **167**, 149–160 (2004).

132. Cerrone, M. *et al.* Plakophilin-2 is required for transcription of genes that control calcium cycling and cardiac rhythm. *Nat. Commun.*

133. Jacot, J. G. *et al.* Cardiac Myocyte Force Dvelpoment during Differentiation and maturation. *Ann. N. Y. Acad. Sci.* **1188**, 121–127 (2010).

134. Morita, N., Mandel, W. J., Kobayashi, Y. & Karagueuzian, H. S. Cardiac fibrosis as a determinant of ventricular tachyarrhythmias. *J. Arrhythmia* **30**, 389–394 (2014).

135. Lahmers, S., Wu, Y., Call, D. R., Labeit, S. & Granzier, H. Developmental Control of Titin Isoform Expression and Passive Stiffness in Fetal and Neonatal Myocardium. *Circ. Res.* **94**, 505–513 (2004).

136. Opitz, C. a., Leake, M. C., Makarenko, I., Benes, V. & Linke, W. a. Developmentally Regulated Switching of Titin Size Alters Myofibrillar Stiffness in the Perinatal Heart. *Circ. Res.* **94**, 967–975 (2004).

137. Galie, P. & Stegemann, J. Substrate Stiffness affects Sarcomere and Costamere Structure and Electrophysiological Function of Isolated Adult Cardiomyocytes. **4**, 219–227 (2011).

138. Ronaldson-Bouchard, Kacey, Ma, S. P. *et al.* Advanced maturation of human cardiac tissue grown from pluripotent stem cells. *Nature* **556**, 239–243 (2018).

139. Scuderi, G. J. & Butcher, J. Naturally Engineered Maturation of Cardiomyocytes. *Front. Cell Dev. Biol.* \ **5**, 1–28 (2017).

140. Kai, D., Prabhakaran, M. P., Jin, G. & Ramakrishna, S. Guided orientation of cardiomyocytes on electrospun aligned nanofibers for cardiac tissue engineering. *J. Biomed. Mater. Res. - Part B Appl. Biomater.* **98 B**, 379–386 (2011).

141. Huebsch, N. *et al.* Miniaturized iPS-Cell-Derived Cardiac Muscles for Physiologically Relevant Drug Response Analyses. *Sci Rep* **6**, 24726 (2016).

142. Yoshida, S. *et al.* Maturation of Human Induced Pluripotent Stem Cell-Derived Cardiomyocytes by Soluble Factors from Human Mesenchymal Stem Cells. *Mol. Ther.* **26**, 2681–2695 (2018).

143. Li, M. X. & Hwang, P. M. Structure and function of cardiac troponin C (TNNC1): Implications for heart failure, cardiomyopathies, and troponin modulating drugs. *Gene* **571**, 153–166 (2015).

144. Jiang, Y., Park, P., Hong, S. M. & Ban, K. Maturation of cardiomyocytes derived from human pluripotent stem cells: Current strategies and limitations. *Mol. Cells* **41**, 613–621 (2018).

145. Goversen, B., van der Heyden, M. A. G., van Veen, T. A. B. & de Boer, T. P. The immature electrophysiological phenotype of iPSC-CMs still hampers in vitro drug screening: Special focus on IK1. *Pharmacol. Ther.* **183**, 127–136 (2018).

146. Kaestner, L. *et al.* Genetically encoded Ca2+ indicators in cardiac myocytes. *Circ. Res.* **114**, 1623–1639 (2014).

147. Chen, T. W. *et al.* Ultrasensitive fluorescent proteins for imaging neuronal activity. *Nature* **499**, 295–300 (2013).

148. Frazier, S. B., Roodhouse, K. a, Hourcade, D. E. & Zhang, L. The Quantification of Glycosaminoglycans: A Comparison of HPLC, Carbazole, and Alcian Blue Methods. *Open Glycosci.* **1**, 31–39 (2008).

149. Sambandamoorthy, S. *et al.* Matrix compliance and the regulation of cytokinesis. *Biol. Open* **4**, 885–892 (2015).

150. Sastry, S. K. *et al.* Quantitative changes in integrin and focal adhesion signaling regulate myoblast cell cycle withdrawal. *J. Cell Biol.* **144**, 1295–309 (1999).

151. Couchman, J. R., Rees, D. a., Green, M. R. & Smith, C. G. Fibronectin has a dual role in locomotion and anchorage of primary chick fibroblasts and can promote entry into the division cycle. *J. Cell Biol.* **93**, 402–410 (1982).

152. Klein, E. a *et al.* Cell-Cycle Control by Physiological Matrix Elasticity and In Vivo Tissue Stiffening. *Curr. Biol.* **19**, 1511–1518 (2009).

153. Williams, C., Sullivan, K. & Black, L. D. Partially Digested Adult Cardiac Extracellular Matrix Promotes Cardiomyocyte Proliferation In Vitro. *Adv. Healthc. Mater.* **4**, 1545–1554 (2015).

154. Morikawa, Y., Heallen, T., Leach, J., Xiao, Y. & Martin, J. F. Dystrophin glycoprotein complex sequesters Yap to inhibit cardiomyocyte proliferation. *Nature* **547**, 1–21 (2017).

155. Wu, C.-C., Jeratsch, S., Graumann, J. & Stainier, D. Modulation of Mammalian Cardiomyocyte Cytokinesis by the Extracellular Matrix. *Circ. Res.* (2020).

156. Blanco, A. & Blanco, G. Carbohydrate Metabolism. in *Medical Biochemistry* 283–323 (Elsevier, 2017).

157. Hu, D. *et al.* Metabolic Maturation of Human Pluripotent Stem Cell-Derived Cardiomyocytes by Inhibition of HIF1α and LDHA. *Circ. Res.* **123**, 1066–1079 (2018).

158. Yang, X. *et al.* Fatty Acids Enhance the Maturation of Cardiomyocytes Derived from Human Pluripotent Stem Cells. *Stem Cell Reports* **13**, 657–668 (2019).

159. Urciuolo, A. *et al.* Collagen VI regulates satellite cell self-renewal and muscle regeneration. *Nat. Commun.* **4**, 1–13 (2013).

160. Irwin, W. A. *et al.* Mitochondrial dysfunction and apoptosis in myopathic mice with collagen VI deficiency. *Nat. Genet.* **35**, 367–371 (2003).

161. Fontes-Oliveira, C. C., Steinz, M., Schneiderat, P., Mulder, H. & Durbeej, M. Bioenergetic Impairment in Congenital Muscular Dystrophy Type 1A and Leigh Syndrome Muscle Cells. *Sci. Rep.* **7**, 1–16 (2017).

162. Kamdar, F. & Garry, D. J. Dystrophin-Deficient Cardiomyopathy. *J. Am. Coll. Cardiol.* **67**, 2533–2546 (2016).

163. Kelly-Worden, M. & Thomas, E. Mitochondrial Dysfunction in Duchenne Muscular Dystrophy. *Open J. Endocr. Metab. Dis.* **04**, 211–218 (2014).

164. Dubinin, M. V. *et al.* Duchenne muscular dystrophy is associated with the inhibition of calcium uniport in mitochondria and an increased sensitivity of the organelles to the calcium-induced permeability transition. *Biochim. Biophys. Acta - Mol. Basis Dis.* **1866**, 165674 (2020).

165. Lajiness, J. D. & Conway, S. J. Origin, development, and differentiation of cardiac fibroblasts. *J Mol Cell Cardiol* **70**, 2–8 (2014).

166. Snider, P. *et al.* Origin of cardiac fibroblasts and the role of periostin. *Circ. Res.* **105**, 934–947 (2009).

167. Moore-morris, T., Cattaneo, P., Puceat, M. & Evans, S. M. Origins of Cardiac Fibroblasts. 1–5 (2017).

168. Hinz, B. *et al.* The Myofibroblast. *Am. J. Pathol.* **170**, 1807–1816 (2007).

169. Travers, J. G., Kamal, F. A., Robbins, J., Yutzey, K. E. & Blaxall, B. C. Cardiac fibrosis: The fibroblast awakens. *Circ. Res.* **118**, 1021–1040 (2016).

170. Zeisberg, E. M. & Kalluri, R. Origins of cardiac fibroblasts. *Circ. Res.* **107**, 1304–1312 (2010).

171. Hortells, L., Johansen, A. K. Z. & Yutzey, K. E. Cardiac Fibroblasts and the Extracellular Matrix in Regenerative and Nonregenerative Hearts. *J. Cardiovasc. Dev. Dis.* (2019).

172. Kong, P., Christia, P. & Frangogiannis, N. G. The pathogenesis of cardiac fibrosis. *Cell.*

Mol. Life Sci. **71**, 549–574 (2014).

173. Camelliti, P., Borg, T. K. & Kohl, P. Structural and functional characterisation of cardiac fibroblasts. *Cardiovasc. Res.* **65**, 40–51 (2005).

174. LaFramboise, W. A. *et al.* Cardiac fibroblasts influence cardiomyocyte phenotype in vitro. *Am. J. Physiol. - Cell Physiol.* **292**, 1799–1808 (2007).

175. Pedrotty, D. M., Klinger, R. Y., Kirkton, R. D. & Bursac, N. Cardiac fibroblast paracrine factors alter impulse conduction and ion channel expression of neonatal rat cardiomyocytes. *Cardiovasc. Res.* **83**, 688–697 (2009).

176. Frangogiannis, N. G. The extracellular matrix in myocardial injury, repair, and remodeling. *J. Clin. Invest.* **127**, 1600–1612 (2017).

177. Eyden, B. The myofibroblast: Phenotypic characterization as a prerequisite to understanding its functions in translational medicine: Translational Medicine. *J. Cell. Mol. Med.* **12**, 22–37 (2008).

178. Fan D et al. Cardiac fibroblasts, fibrosis and extracellular matrix remodeling in heart disease. *Fibrogenesis Tissue Repair* **5**, 1–13 (2012).

179. Segura, A. M., Frazier, O. H. & Buja, L. M. Fibrosis and heart failure. *Heart Fail. Rev.* **19**, 173–185 (2014).

180. Bhandary, B. *et al.* Cardiac Fibrosis in Proteotoxic Cardiac Disease is Dependent Upon Myofibroblast TGF-β Signaling. *J. Am. Heart Assoc.* **7**, 1–18 (2018).

181. Li, X., Zhu, L., Wang, B., Yuan, M. & Zhu, R. Drugs and targets in fibrosis. *Front. Pharmacol.* **8**, (2017).

182. Gyöngyösi, M. *et al.* Myocardial fibrosis: biomedical research from bench to bedside. *Eur.*

J. Heart Fail. **19**, 177–191 (2017).

183. Luther, D. J. *et al.* Absence of Type VI Collagen Paradoxically Improves Cardiac Function, Structure, and Remodeling After Myocardial Infarction. *Circ. Res.* **110**, 851–856 (2012).

184. Kohan, M., Muro, A. F., White, E. S. & Berkman, N. EDA-containing cellular fibronectin induces fibroblast differentiation through binding to alpha4beta7 integrin receptor and MAPK/Erk 1/2-dependent signaling. *FASEB J.* **24**, 4503–4512 (2010).

185. Arslan, F. *et al.* Lack of fibronectin-EDA promotes survival and prevents adverse remodeling and heart function deterioration after myocardial infarction. *Circ. Res.* **108**, 582–592 (2011).

186. Rozario, T. & DeSimone, D. W. The extracellular matrix in development and morphogenesis: A dynamic view. *Dev. Biol.* **341**, 126–140 (2010).

187. Sasse, P. *et al.* Perlecan is critical for heart stability. *Cardiovasc. Res.* **80**, 435–44 (2008).

188. Mellman, K., Huisken, J., Dinsmore, C., Hoppe, C. & Stainier, D. Y. Fibrillin-2b regulates endocardial morphogenesis in zebrafish. *Dev. Biol.* **372**, 111–119 (2012).

189. Kim, P. G. *et al.* Flow-induced protein kinase A-CREB pathway acts via BMP signaling to promote HSC emergence. *J. Exp. Med.* **212**, 633–48 (2015).

190. Astrof, S., Kirby, A., Lindblad-Toh, K., Daly, M. & Hynes, R. O. Heart development in fibronectin-null mice is governed by a genetic modifier on chromosome four. *Mech. Dev.* **124**, 551–558 (2007).

191. Doppler, S. A. *et al.* Cardiac fibroblasts: more than mechanical support. *J. Thorac. Dis.* **9**, S36–S51 (2017).

192. Freshney RI. *Culture of animal cells: a manual of basic technique and specialized applications.* (2010).

193. Kleinman, H. K. *et al.* Isolation and Characterization of Type IV Procollagen, Laminin, and Heparan Sulfate Proteoglycan from the EHS Sarcomat. *Biochemistry* **21**, 6188–6193 (1982).

194. Kaiser, N. J., Kant, R. J., Minor, A. J. & Coulombe, K. L. K. Optimizing Blended Collagen-Fibrin Hydrogels for Cardiac Tissue Engineering with Human iPSC-derived Cardiomyocytes. *ACS Biomater. Sci. Eng.* **5**, 887–899 (2019).

195. Mi, L., Fischer, S., Chung, B., Sundelacruz, S. & Harden, J. L. Self-assembling protein hydrogels with modular integrin binding domains. *Biomacromolecules* **7**, 38–47 (2006).

196. Caliari, S. R. & Burdick, J. A. A practical guide to hydrogels for cell culture. *Nat. Methods* **13**, 405–414 (2016).

197. Cukierman, E., Pankov, R., Stevens, D. R. & Yamada, K. M. Taking cell-matrix adhesions to the third dimension. *Science* **294**, 1708–1712 (2001).

198. Crapo, P. M., Gilbert, T. W. & Badylak, S. F. An overview of tissue and whole organ decellularization processes. *Biomaterials* **32**, 3233–3243 (2011).

199. Gillies, A. R., Smith, L. R., Lieber, R. L. & Varghese, S. Method for decellularizing skeletal muscle without detergents or proteolytic enzymes. *Tissue Eng. Part C. Methods* **17**, 383–389 (2011).

200. Choi, J. S., Kim, J. D., Yoon, H. S. & Cho, Y. W. Full-thickness skin wound healing using human placenta-derived extracellular matrix containing bioactive molecules. *Tissue Eng. - Part A* **19**, 329–339 (2013).

201. Urciuolo, A. & De Coppi, P. Decellularized tissue for muscle regeneration. *Int. J. Mol. Sci.*

19, 1–11 (2018).

202. Bejleri, D. & Davis, M. E. Decellularized Extracellular Matrix Materials for Cardiac Repair and Regeneration. *Adv. Healthc. Mater.* **8**, 1–29 (2019).

203. Hong, X. *et al.* Skeletal Extracellular Matrix Supports Cardiac Differentiation of Embryonic Stem Cells: A Potential Scaffold for Engineered Cardiac Tissue. *Cell. Physiol. Biochem.* **45**, 319–331 (2018).

204. Faulk, D. M., Wildemann, J. D. & Badylak, S. F. Decellularization and cell seeding of whole liver biologic scaffolds composed of extracellular matrix. *J. Clin. Exp. Hepatol.* **5**, 69–80 (2015).

205. Pecha, S., Eschenhagen, T. & Reichenspurner, H. Myocardial tissue engineering for cardiac repair. *J. Hear. Lung Transplant.* **35**, 294–298 (2016).

206. Saldin, L. T., Cramer, M. C., Velankar, S. S., White, L. J. & Badylak, S. F. Extracellular Matrix Hydrogels from Decellularized Tissues: Structure and Function. *Acta Biomater.* (2016).

207. Johnson, T. D., Braden, R. L. & Christman, K. L. Injectable ECM Scaffolds for Cardiac Repair. *Methods Mol Biol* **1181**, 109–120 (2014).

208. Spang, M. T. & Christman, K. L. Extracellular matrix hydrogel therapies: In vivo applications and development. *Acta Biomater.* **68**, 1–14 (2018).

209. Hocking, D. C., Sottile, J. & McKeown-Longo, P. J. Fibronectin's III-1 module contains a conformation-dependent binding site for the amino-terminal region of fibronectin. *J. Biol. Chem.* **269**, 19183–19191 (1994).

210. Zhong, C. *et al.* Rho-mediated contractility exposes a cryptic site in fibronectin and induces fibronectin matrix assembly. *J. Cell Biol.* **141**, 539–551 (1998).

211. Prewitz, M. C. *et al.* Tightly anchored tissue-mimetic matrices as instructive stem cell microenvironments. *Nat. Methods* **10**, 788–794 (2013).

212. Cheng, H. W., Yuan, M. T., Li, C. W. & Chan, B. P. Cell-derived matrices (CDM)—Methods, challenges and applications. in *Methods in Cell Biology* **156**, 235–258 (2020).

213. Kaukonen, R., Jacquemet, G., Hamidi, H. & Ivaska, J. Cell-derived matrices for studying cell proliferation and directional migration in a complex 3D microenvironment. *Nat. Protoc.* **12**, 2376–2390 (2017).

214. Raghunathan, V. K. *et al.* Transforming Growth Factor Beta 3 Modifies Mechanics and Composition of Extracellular Matrix Deposited by Human Trabecular Meshwork Cells. *ACS Biomater. Sci. Eng.* **1**, 110–118 (2015).

215. Fitzpatrick, L. & McDevitt, T. C. Cell-derived matrices for tissue engineering and regenerative medicine applications. *Biomater. Sci* **3**, 12–24 (2015).

216. Hwang, J. *et al.* Molecular assessment of collagen denaturation in decellularized tissues using a collagen hybridizing peptide. *Acta Biomater.* 268–278 (2017).

217. Lee, H., Scherer, N. F. & Messersmith, P. B. Single-molecule mechanics of mussel adhesion. *Proc. Natl. Acad. Sci.* **103**, 12999–13003 (2006).

218. Lee, H., Dellatore, S. M., Miller, W. M. & Messtersmith, P. B. Mussel-Inspired Surface Chemistry for Multifunctional Coatings. *Science* **318**, 426–430 (2008).

219. Lee, H., Rho, J. & Messersmith, P. B. Facile conjugation of biomolecules onto surfaces via mussel adhesive protein inspired coatings. *Adv. Mater.* **21**, 431–434 (2009).

220. Xu, H. *et al.* Comparison of decellularization protocols for preparing a decellularized porcine annulus fibrosus scaffold. *PLoS One* **9**, 1–13 (2014).

221. Kumar, P. *et al.* Macromolecularly crowded in vitro microenvironments accelerate the production of extracellular matrix-rich supramolecular assemblies. *Sci. Rep.* **5**, 8729 (2015).

222. Chen, C., Loe, F., Blocki, A., Peng, Y. & Raghunath, M. Applying macromolecular crowding to enhance extracellular matrix deposition and its remodeling in vitro for tissue engineering and cell-based therapies. *Adv. Drug Deliv. Rev.* **63**, 277–290 (2011).

223. Zeiger, A. S., Loe, F. C., Li, R., Raghunath, M. & Van Vliet, K. J. Macromolecular crowding directs extracellular matrix organization and mesenchymal stem cell behavior. *PLoS One* **7**, e37904 (2012).

224. Hata, R.-I. & Senoo, H. L-ascorbic Acid 2-phosphate Stimulates Collagen Accumulation, Cell Proliferation, and Formation of a Three-Dimensional Tissuelike Substance by Skin Fibroblasts. *J Cell Physiol.* **16**, (1989).

225. Pelyak, M. R. & Welter, J. F. Macromolecular Crowding Accelerates Extracellular Matrix Deposition by Differentiating MSCs. *Group* **581**, 50802–50802

226. Lareu, R. R. *et al.* Collagen matrix deposition is dramatically enhanced in vitro when crowded with charged macromolecules: The biological relevance of the excluded volume effect. *FEBS Lett.* **581**, 2709–2714 (2007).

227. Shendi, D. *et al.* Hyaluronic acid as a macromolecular crowding agent for production of cell-derived matrices. *Acta Biomater.* (2019).

228. Püspöki, Z., Storath, M., Sage, D. & Unser, M. Transforms and Operators for Directional Bioimage Analysis : A Survey. in *Advances in Anatomy, Embryology and Cell Biology* (eds. Vos, W. H. De, Munck, S. & Timmermans, J.-P.) 69–93 (Springer International Publishing, 2016).

229. Skardal, A., Mack, D., Atala, A. & Soker, S. Substrate elasticity controls cell proliferation, surface marker expression and motile phenotype in amniotic fluid-derived stem cells. *J. Mech. Behav. Biomed. Mater.* **17**, 307–316 (2013).

230. Schwanhäusser, B. *et al.* Global quantification of mammalian gene expression control. *Nature* **473**, 337–342 (2011).

231. Choi, M. *et al.* MSstats: an R package for statistical analysis of quantitative mass spectrometry-based proteomic experiments. *Bioinformatics* **30**, 2524–2526 (2014).

232. de Castro Brás, L. *et al.* Texas 3-step decellularization protocol: looking at the cardiac extracellular matrix. *J Proteomics* 43–52 (2013).

233. Naba, A. *et al.* The Matrisome: In Silico Definition and In Vivo Characterization by Proteomics of Normal and Tumor Extracellular Matrices. *Mol. Cell. Proteomics* **11**, M111.014647 (2012).

234. Garlíková, Z. *et al.* Generation of a close-to-native in vitro system to study lung cells-extracellular matrix crosstalk. *Tissue Eng. - Part C Methods* **24**, 1–13 (2018).

235. Hielscher, A., Ellis, K., Qiu, C., Porterfield, J. & Gerecht, S. Fibronectin deposition participates in extracellular matrix assembly and vascular morphogenesis. *PLoS One* **11**, 1–27 (2016).

236. Sottile, J. & Hocking, D. C. Fibronectin Polymerization Regulates the Composition and Stability of Extracellular Matrix Fibrils and Cell-Matrix Adhesions. *Mol. Biol. Cell* **13**, 3546–3559 (2002).

237. Seluanov, A., Vaidya, A. & Gorbunova, V. Establishing Primary Adult Fibroblast Cultures From Rodents. *J. Vis. Exp.* 1–4 (2010).

238. Ivey, M. J. & Tallquist, M. D. Defining the Cardiac Fibroblast: A New Hope. *Circ J.* **80**,

2269–2276 (2017).

239. Furtado, M. B., Nim, H. T., Boyd, S. E. & Rosenthal, N. A. View from the heart: cardiac fibroblasts in development, scarring and regeneration. *Development* **143**, 387–397 (2016).

240. Acharya, A. *et al.* The bHLH transcription factor Tcf21 is required for lineage-specific EMT of cardiac fibroblast progenitors. *Development* **139**, 2139–2149 (2012).

241. Yata, Y. DNase I–hypersensitive sites enhance α1(I) collagen gene expression in hepatic stellate cells. *Hepatology* **37**, 267–276 (2003).

242. Hookway, T. A. *et al.* Phenotypic Variation Between Stromal Cells Differentially Impacts Engineered Cardiac Tissue Function. *Tissue Eng. - Part A* **25**, 773–785 (2019).

243. Ek, B. & Heldin, C. Characterization of a Tyrosine-specific Kinase Activity in Human Fibroblast Membranes Stimulated by Platelet-derived Growth Factor alpha. *J. Biol. Chem.* **257**, 10486–10492 (1982).

244. Coornaert, B., Duys, I., Schueren, J. Van Der, Aar, E. Van Der & Heckmann, B. *Autotaxin Inhibitor GLPG1690 Affects TGFβ -induced Production of the Pro-Fibrotic Mediators CTGF , IL-6 and ET-1 in Fibroblasts*. (2017).

245. Franco-barraza, J., Beacham, D. A., Amatangelo, M. D. & Cukierman, E. Preparation of Extracellular Matrices Produced by Cultured and Primary Fibroblasts. *Curr Protoc Cell Biol* **71**, 1–44 (2017).

246. Hayman, E. G. & Ruoslahti, E. Distribution of fetal bovine serum fibronectin and endogenous rat cell fibronectin in extracellular matrix. *J. Cell Biol.* **83**, 255–259 (1979).

247. Rodríguez-Ares, M. T. *et al.* Effects of lyophilization on human amniotic membrane. *Acta Ophthalmol.* **87**, 396–403 (2009).

248. Trnka, H., Rantanen, J. & Grohganz, H. Well-plate freeze-drying: A high throughput platform for screening of physical properties of freeze-dried formulations. *Pharm. Dev. Technol.* **20**, 65–73 (2015).

249. Pegg, D. E. The relevance of ice crystal formation for the cryopreservation of tissues and organs. *Cryobiology* **60**, S36–S44 (2010).

250. Crowe, L. M., Reid, D. S. & Crowe, J. H. Is trehalose special for preserving dry biomaterials? *Biophys. J.* **71**, 2087–2093 (1996).

251. Zhang, J. *et al.* Functional cardiac fibroblasts derived from human pluripotent stem cells via second heart field progenitors. *Nat. Commun.* (2019).

252. Zhang, H. *et al.* Generation of Quiescent Cardiac Fibroblasts From Human Induced Pluripotent Stem Cells for In Vitro Modeling of Cardiac Fibrosis. 552–566 (2019).

253. Brade, T., Pane, L. S., Moretti, A., Chien, K. R. & Laugwitz, K. Embryonic Heart Progenitors and Cardiogenesis. 1–17 (2013).

254. Buckingham, M. First and Second Heart Field. in *Congenital Heart Diseases: The Broken Heart: Clinical Features, Human Genetics and Molecular Pathways* (eds. Rickert-Sperling, S., Kelly, R. G. & Driscoll, D. J.) 25–40 (Springer Vienna, 2016).

255. Leask, a. TGFβ signaling and the fibrotic response. *FASEB J.* **18**, 816–827 (2004).

256. Erdogan, B. *et al.* Cancer-associated fibroblasts promote directional cancer cell migration by aligning fibronectin. *J. Cell Biol.* **216**, 3799–3816 (2017).

257. Prewitz, M. C. *et al.* Extracellular matrix deposition of bone marrow stroma enhanced by macromolecular crowding. *Biomaterials* **73**, 60–69 (2015).

258. Schönfeld, P., Schild, L. & Bohnensack, R. Expression of the ADP/ATP carrier and

expansion of the mitochondrial (ATP + ADP) pool contribute to postnatal maturation of the rat heart. *Eur. J. Biochem.* **241**, 895–900 (1996).

259. Kreipke, R. *et al.* Metabolic Remodeling in early development and cardiomyocyte maturation. *Semin Cell Dev Biol* **52**, 84–92 (2017).

260. Hynes, R. O. & Yamada, K. M. Fibronectins: Multifunctional modular glycoproteins. *J. Cell Biol.* **95**, 369–377 (1982).

261. Gold, L. I. & Pearlstein, E. Fibronectin-collagen binding and requirement during cellular adhesion. *Biochem. J.* **186**, 551–559 (1980).

262. Bowers, S. L. K., Banjeree, I. & Baudino, T. A. The Extracellular Matrix: At the Center of it All. *J Mol Cell Cardiol* **48**, 474–482 (2011).

263. Huang, G. *et al.* Functional and Biomimetic Materials for Engineering of the Three-Dimensional Cell Microenvironment. (2017).

264. Camci-Unal, G., Annabi, N., Dokmeci, M. R., Liao, R. & Khademhosseini, A. Hydrogels for cardiac tissue engineering. *NPG Asia Mater.* **6**, (2014).

265. Chablais, F. & Jaźwińska, A. The regenerative capacity of the zebrafish heart is dependent on TGFβ signaling. *Development* **139**, 1921–1930 (2012).

266. Porter, K. E. & Turner, N. A. Cardiac fibroblasts: At the heart of myocardial remodeling. *Pharmacol. Ther.* **123**, 255–278 (2009).

267. Pawelec, G., Goldeck, D. & Derhovanessian, E. Inflammation, ageing and chronic disease. *Curr. Opin. Immunol.* **29**, 23–28 (2014).

268. Schwarz, B., Hollfelder, D., Scharf, K., Hartmann, L. & Reim, I. Diversification of heart progenitor cells by EGF signaling and differential modulation of ETS protein activity. *Elife*

7, 1–36 (2018).

269. Meloni, M. *et al.* Nerve growth factor promotes cardiac repair following myocardial infarction. *Circ. Res.* **106**, 1275–1284 (2010).

270. Oxlund, H. & Andreassen, T. T. The roles of hyaluronic acid, collagen and elastin in the mechanical properties of connective tissues. *J. Anat.* **131**, 611–20 (1980).

271. Cox, J. & Mann, M. MaxQuant Enables High Peptide Identification Rates, Individualized p.p.b.-range Mass Accuracies and Proteome-Wide Protein Quantification. *Nat Biotechnol* **26**, 1367–1372 (2008).

272. Snel, B., Lehmann, G., Bork, P. & Huynen, M. A. STRING: a web-server to retrieve and display the repeatedly occurring neighbourhood of a gene. **28**, 3442–3444 (2000).

273. Edmunds, K. J., Williams, C. & Black III, L. D. Promoting neonatal cardiomyocyte proliferation using a cryptic peptide derived from fibrillin-1. *Tissue Eng. - Part A* **20**, S-53 (2014).

274. Quondamatteo, F. *et al.* Fibrillin-1 and fibrillin-2 in human embryonic and early fetal development. *Matrix Biol.* **21**, 637–646 (2002).

275. Cohen, E. D., Miller, M. F., Wang, Z., Moon, R. T. & Morrisey, E. E. Wnt5a and Wnt11 are essential for second heart field progenitor development. **1940**, 1931–1940 (2012).

276. Kami, D. *et al.* Gremlin Enhances the Determined Path to Cardiomyogenesis. **3**, 1–10 (2008).

277. Deng, K. *et al.* Restoration of Circulating MFGE8 (Milk Fat Globule-EGF Factor 8) Attenuates Cardiac Hypertrophy Through Inhibition of Akt Pathway. *Hypertension* **70**, 770–779 (2017).

278. Atabai, K. *et al.* Mfge8 diminishes the severity of tissue fibrosis in mice by binding and targeting collagen for uptake by macrophages. **119**, 3713–3722 (2009).

279. Wang, Z. *et al.* Cardiac fibrosis can be attenuated by blocking the activity of transglutaminase 2 using a selective small-molecule inhibitor. *Cell Death Dis.* **9**, 613 (2018).

280. Sane, D. C., Kontos, J. L. & Greenberg, C. S. Roles of transglutaminases in cardiac and vascular diseases. *Front Biosci.* **12**, 2530–2545 (2009).

281. Wirrig, E. E. *et al.* Cartilage link protein 1 (Crtl1), an extracellular matrix component playing an important role in heart development. *Dev Bio.* **310**, 291–303 (2008).

282. Kang, Q. *et al.* TGF-β2 induces transdifferentiation and fibrosis in human lens epithelial cells via regulating gremlin and CTGF. *Biochem. Biophys. Res. Commun.* (2014).

283. Enomoto, Y. *et al.* LTBP2 is secreted from lung myofibroblasts and is a potential biomarker for idiopathic pulmonary fibrosis. *Clin. Sci.* **132**, 1565–1580 (2018).

284. Januzzi, J. L. J. *et al.* IGFBP7 (Insulin-Like Growth Factor–Binding Protein-7) and Neprilysin Inhibition in Patients With Heart Failure. *Circ. Hear. Fail.* **7**, 1–9 (2018).

285. Whellan, D. J., Donahue, M. P., Kitzman, D. W. & Piña, I. L. Utility of Growth Differentiation Factor-15, A Marker of Oxidative Stress and In fl ammation, in Chronic Heart Failure. *J. Am. Coll. Cardiol. Hear. Fail.* **5**, (2017).

286. Bouwens, E. *et al.* Temporal Patterns of 14 Blood Biomarker candidates of Cardiac Remodeling in Relation to Prognosis of Patients With Chronic Heart Failure—The Bio-SHiFT Study. *J. Am. Heart Assoc.* **8**, (2019).

287. Wu, C. *et al.* Galectin-3 level and the severity of cardiac diastolic dysfunction using cellular and animal models and clinical indices. *Nat. Publ. Gr.* 1–10 (2015).

288. Koshy, S. K. G., Reddy, H. K. & Shukla, H. H. Collagen cross-linking: new dimension to cardiac remodeling. *Cardiovasc. Res.* **57**, 594–598 (2003).

289. Le, S., Li, S., Hao, X., Zhang, Y. & Deng, W. Perindopril and a Galectin-3 inhibitor improve ischemic heart failure in rabbits by reducing gal-3 expression and myocardial fibrosis. *Front. Physiol.* **10**, 1–8 (2019).

290. Suthahar, N. *et al.* Galectin-3 activation and inhibition in heart failure and cardiovascular disease: An update. *Theranostics* **8**, 593–609 (2018).

291. Cescon, M., Gattazzo, F., Chen, P. & Bonaldo, P. Collagen VI at a glance. *J. Cell Sci.* **128**, 3525–3531 (2015).

292. Fitch, J. M., Birk, D. E., Linsenmayer, C. & Linsenmayer, T. F. Stromal assemblies containing collagen types IV and VI and fibronectin in the developing embryonic avian cornea. *Dev. Biol.* **144**, 379–391 (1991).

293. Santamaria-kisiel, L., Rintala-dempsey, A. C. & Shaw, G. S. Calcium-dependent and -independent interactions of the S100 protein family. **214**, 201–214 (2006).

294. Peuch, J. L. E. *et al.* Cardiac calmodulin and its role in the regulation of metabolism and contraction. *J. Mol. Cell. Cardiol.* **12**, 1091–1101 (1980).

295. Grabarek, Z. Insights into Modulation of Calcium Signaling by Magnesium in Calmodulin, Troponin C and Related EF-hand Proteins. *Biochim Biophys Acta* **1813**, 913–921 (2012).

296. Donato, R. S100: a multigenic family of calcium-modulated proteins of the EF-hand type with intracellular and extracellular functional roles. *Int. J. Biochem. Cell Biol.* **33**, 637–668 (2001).

297. Gerke, V. & Moss, S. E. Annexins: From Structure to Function. *Physiol. Rev.* **82**, 331–371 (2002).

298. Camors, E. & Monceau, V. Annexins and Ca2+ handling in the heart. **65**, 793–802 (2005).

299. Liu, Y., Myrvang, H. K. & Dekker, L. V. Annexin A2 complexes with S100 proteins: structure, function and pharmacological manipulation. *Br. J. Pharmacol.* **172**, 1664–1676 (2015).

300. Chang, N. *et al.* Identification of a novel interaction between the Ca 2+-binding protein S100A11 and the Ca 2+- and phospholipid-binding protein annexin A6. **1**, 1417–1430 (2020).

301. Farhadian, F., Contard, F., Sabri, A., Samuel, J. L. & Rappaport, L. Fibronectin and basement membrane in cardiovascular organogenesis and disease pathogenesis. *Cardiovasc. Res.* **32**, 433–442 (1996).

302. Qasim, M., Haq, F., Kang, M. H. & Kim, J. H. 3D printing approaches for cardiac tissue engineering and role of immune modulation in tissue regeneration. *Int. J. Nanomedicine* **14**, 1311–1333 (2019).

303. Kagemoto, T., Li, A., dos Remedios, C. & Ishiwata, S. Spontaneous oscillatory contraction (SPOC) in cardiomyocytes. *Biophys. Rev.* **7**, 15–24 (2015).

304. Kleber, A. G. & Saffitz, J. E. Role of the intercalated disc in cardiac propagation and arrhythmogenesis. *Front. Physiol.* **5**, 1–9 (2014).

305. Hong, T. T. & Shaw, R. M. *Ion Channel Trafficking*. *Ion Channels in Health and Disease* (Elsevier Inc., 2016).

306. Salameh, A. *et al.* Cyclic mechanical stretch induces cardiomyocyte orientation and polarization of the gap junction protein connexin43. *Circ. Res.* **106**, 1592–1602 (2010).

307. Kolodziejczyk, S. M. *et al.* MEF2 is upregulated during cardiac hypertrophy and is

required for normal post-natal growth of the myocardium. *Curr. Biol.* **9**, 1203–1206 (1999).

308. Rodriguez, M. L. *et al.* Measuring the contractile forces of human induced pluripotent stem cell-derived cardiomyocytes with arrays of microposts. *J. Biomech. Eng.* **136**, 1–10 (2014).

309. Grant, A. O. Cardiac Ion Channels. *Circulation* **2**, 185–194 (2009).

310. Zhang, J. & Zhang, Q. *Cancer Metabolism: Using Seahorse Machine to Measure OCR and ECAR in Cancer Cells. In: Haznadar M. (eds) Cancer Metabolism. Methods in Molecular Biology*. (Humana Press, 2019).

311. Peat, R., Goemans, N., North, K. N., Baker, N. L. & Mo, M. Dominant collagen VI mutations are a common cause of Ullrich congenital muscular dystrophy. **14**, 9–11 (2005).

312. Flöck, A. *et al.* Progressive Cardiac Dysfunction in Bethlem Myopathy During Pregnancy. *Obstet. Gynecol.* **123**, 436–438 (2014).

313. Ulmer, B. M. *et al.* Contractile Work Contributes to Maturation of Energy Metabolism in hiPSC-Derived Cardiomyocytes. *Stem Cell Reports* **10**, 834–847 (2018).

314. Sager, H. B. *et al.* Proliferation and recruitment contribute to myocardial macrophage expansion in chronic heart failure. *Circ. Res.* **176**, 139–148 (2017).

315. Zhang, Y. *et al.* Dedifferentiation and proliferation of mammalian cardiomyocytes. *PLoS One* **5**, 1–13 (2010).

316. Chen, W. C. W. *et al.* Decellularized zebrafish cardiac extracellular matrix induces mammalian heart regeneration. *Sci. Adv.* **2**, (2016).

317. Brown, N. H. Extracellular matrix in development: Insights from mechanisms conserved between invertebrates and vertebrates. *Cold Spring Harb. Perspect. Biol.* **3**, 1–13 (2011).

318. Hamill, K. J., Kligys, K., Hopkinson, S. B. & Jones, J. C. R. Laminin deposition in the extracellular matrix: a complex picture emerges. (2009).

319. Hyysalo, A. *et al.* Laminin α5 substrates promote survival, network formation and functional development of human pluripotent stem cell-derived neurons in vitro. *Stem Cell Res.* **24**, 118–127 (2017).

320. Shibata, S. *et al.* Selective Laminin-Directed Differentiation of Human Induced Pluripotent Stem Cells into Distinct Ocular Lineages. *Cell Rep.* **25**, 1668-1679.e5 (2018).

321. Laperle, A. *et al.* alpha5 Laminin Synthesized by Human Pluripotent Stem Cells Promotes Self-Renewal. *Stem Cell Reports* **5**, 195–206 (2015).

322. Rodin, S., Antonsson, L., Hovatta, O. & Tryggvason, K. Monolayer culturing and cloning of human pluripotent stem cells on laminin-521-based matrices under xeno-free and chemically defined conditions. *Nat. Protoc.* **9**, 2354–2368 (2014).

323. Miner, J. H. *et al.* The laminin alpha chains: expression, developmental transitions, and chromosomal locations of alpha1-5, identification of heterotrimeric laminins 8-11, and cloning of a novel alpha3 isoform. *J. Cell Biol.* **137**, 685–701 (1997).

324. Belkin, A. M. *et al.* β1D integrin displaces the β1A isoform in striated muscles: Localization at junctional structures and signaling potential in nonmuscle cells. *J. Cell Biol.* **132**, 211–226 (1996).

325. Belkin, A. M. & Retta, S. F. b1D integrin inhibits cell cycle progression in normal myoblasts and fibroblasts. *J. Biol. Chem.* **273**, 15234–15240 (1998).

326. Gimond, C., Baudoin, C. & Sonnenberg, a. Defects in adhesion and migration, but not in

proliferation and differentiation, of embryonic stem cells upon replacement of integrin subunit beta1A by beta1D. *Differentiation* **66**, 93–105 (2000).

327. Baudoin, C., Goumans, M. J., Mummery, C. & Sonnenberg, A. Knockout and knockin of the beta1 exon D define distinct roles for integrin splice variants in heart function and embryonic development. *Genes Dev.* **12**, 1202–1216 (1998).

328. Bernardi, P. & Di Lisa, F. The mitochondrial permeability transition pore: Molecular nature and role as a target in cardioprotection. *J. Mol. Cell. Cardiol.* **78**, 100–106 (2015).

329. Kwong, J. Q. & Molkentin, J. D. Physiological and Pathological Roles of the Mitochondrial Permeability Transition Pore in the Heart. *Cell Metab.* **21**, 206–214 (2015).

330. Marini, J. C., Cabral, W. A., Barnes, A. M. & Chang, W. Components of the collagen prolyl 3-hydroxylation complex are crucial for normal bone development. *Cell Cycle* **6**, 1675–1681 (2007).

331. Lipson, K. E., Wong, C., Teng, Y. & Spong, S. CTGF is a central mediator of tissue remodeling and fibrosis and its inhibition can reverse the process of fibrosis. *Fibrogenesis Tissue Repair* **5**, 2–9 (2012).

332. Dorn, L. E., Petrosino, J. M., Wright, P. & Accornero, F. CTGF/CCN2 is an autocrine regulator of cardiac fibrosis. *J. Mol. Cell. Cardiol.* **121**, 205–211 (2018).

333. Tsukui, T. *et al.* Collagen-producing lung cell atlas identifies multiple subsets with distinct localization and relevance to fibrosis. *Nat. Commun.* **11**, 1–16 (2020).

334. Zhang, Y. *et al.* GDF15 is an epithelial-derived biomarker of idiopathic pulmonary fibrosis. *Am. J. Physiol. Lung Cell. Mol. Physiol.* **317**, L510–L521 (2019).

335. Jovic, S. *et al.* The neutrophil-recruiting chemokine GCP-2/CXCL6 is expressed in cystic fibrosis airways and retains its functional properties after binding to extracellular DNA.

Mucosal Immunol. **9**, 112–123 (2016).

336. Lai, T. S. & Greenberg, C. S. TGM2 and implications for human disease: Role of alternative splicing. *Front. Biosci.* **18**, 504–519 (2013).

337. Vainio, L., Szabo, Z. & Kerkela, R. Connective Tissue Growth Factor Inhibition Enhances Cardiac Repair and Limits Fibrosis After Myocardial Infarction. *J Am Coll Cardiol Basic Trans Sci.* **4**, (2019).

338. Zhang, P. *et al.* Protein Analysis of Atrial Fibrosis via Label-Free Proteomics in Chronic Atrial Fibrillation Patients with Mitral Valve Disease. *PLoS One* **8**, (2013).

339. Kim, Y. S. & Ahn, Y. Functional Relevance of Macrophage-mediated Inflammation to Cardiac Regeneration. *Chonnam Med. J.* **54**, 10–16 (2018).

340. Plow, E. F. & Hoover-Plow, J. The functions of plasminogen in cardiovascular disease. *Trends Cardiovasc. Med.* **14**, 180–186 (2004).

341. Lo, R. *et al.* Plasmin activity is required for myogenesis in vitro and skeletal muscle regeneration in vivo. **99**, 2835–2845 (2019).

342. Roig-borrellas, A., Garcı, A., Llorens, A. & Lo, R. Requirement of Plasminogen Binding to Its Cell-Surface Receptor a -Enolase for Efficient Regeneration of Normal and Dystrophic Skeletal Muscle. **7**, (2012).

343. Takeshita, K. *et al.* Increased Expression of Plasminogen Activator Inhibitor-1 in Cardiomyocytes Contributes to Cardiac Fibrosis after Myocardial Infarction. **164**, 449–456 (2004).

344. Gupta, K. K., Donahue, D. L., Sandoval-cooper, M. J. & Francis, J. Plasminogen Activator Inhibitor-1 Protects Mice Against Cardiac Fibrosis by Inhibiting Urokinase- type Plasminogen Activator- mediated Plasminogen Activation. *Sci. Rep.* 1–11 (2017).

345. Hohensinner, P. J. *et al.* Urokinase plasminogen activator protects cardiac myocytes from oxidative damage and apoptosis via hOGG1 induction. *Apoptosis* **22**, 1048–1055 (2017).

346. Cho, H. *et al.* ENOblock, a unique small molecule inhibitor of the non-glycolytic functions of enolase, alleviates the symptoms of type 2 diabetes. *Sci. Rep.* **7**, 1–16 (2017).

347. Gao, S., Liu, X. P., Wei, L. H., Lu, J. & Liu, P. Upregulation of α-enolase protects cardiomyocytes from phenylephrine-induced hypertrophy. *Can. J. Physiol. Pharmacol.* **96**, 352–358 (2018).

348. Marcinkiewicz, M. & Gordon, P. V. A role for plasmin in platelet aggregation: Differential regulation of IGF release from IGF – IGFBP complexes. **18**, 325–334 (2008).

349. Bloor, C. M., Nimmo, L., Mckiman, M. D., Zhang, Y. & White, F. C. Increased gene expression of plasminogen activators and inhibitors in left ventricular hypertrophy. 265–271 (1997).

350. Chapin, J. C. & Hajjar, K. A. Fibrinolysis and the control of blood coagulation. *Blood Rev.* **29**, 17–24 (2015).

351. Liu, J. *et al.* Current Methods for Skeletal Muscle Tissue Repair and Regeneration. *Biomed Res. Int.* **2018**, (2018).

352. Parsa, H., Ronaldson, K. & Vunjak-Novakovic, G. Bioengineering methods for myocardial regeneration. *Adv. Drug Deliv. Rev.* (2015).

353. Kc, P., Hong, Y. & Zhang, G. Cardiac tissue-derived extracellular matrix scaffolds for myocardial repair: Advantages and challenges. *Regen. Biomater.* **6**, 185–199 (2019).

354. Iozzo, R. V & Gubbiotti, M. A. Extracellular matrix: The driving force of mammalian diseases. **71**–**72**, 1–9 (2018).

355. Delaughter, D. M. *et al.* Single-Cell Resolution of Temporal Gene Expression During Heart Development. **39**, 275–292 (2017).

356. Dunn, K. K. & Palecek, S. P. Engineering scalable manufacturing of high-quality stem cell-derived cardiomyocytes for cardiac tissue repair. *Front. Med.* **5**, (2018).

357. McDevitt, T. C. *et al.* In vitro generation of differentiated cardiac myofibers on micropatterned laminin surfaces. *J. Biomed. Mater. Res.* **60**, 472–479 (2002).

358. Hom, J. R. *et al.* The Permeability Transition Pore Controls Cardiac Mitochondrial Maturation and Myocyte Differentiation. *Dev. Cell* **21**, 469–478 (2011).

359. Cho, S. W. *et al.* Dual modulation of the mitochondrial permeability transition pore and redox signaling synergistically promotes cardiomyocyte differentiation from pluripotent stem cells. *J. Am. Heart Assoc.* **3**, (2014).

360. Martin, P. T. Dystroglycan glycosylation and its role in matrix binding in skeletal muscle. **13**, 55–66 (2003).

361. Yamada, A. & Kamijo, R. Nephronectin: An Extracellular Matrix Protein with Diverse In Vivo Functions. *J. Dent. Oral Disord.* **2**, 1–5 (2016).

362. Montanaro, F., Lindenbaum, M. & Carbonetto, S. alpha-Dystroglycan Is a Laminin Receptor Involved in Extracellular Matrix Assembly on Myotubes and Muscle Cell Viability. **145**, 1325–1340 (1999).

363. Assoian, R. K. & Klein, E. A. Growth control by intracellular tension and extracellular stiffness. *Trends Cell Biol.* **18**, 347–352 (2008).

364. Pfaff, M., Liu, S., Erle, D. J. & Ginsberg, M. H. Integrin B1 cytoplasmic domains differentially bind to cytoskeletal proteins. *J. Biol. Chem.* **273**, 6104–6109 (1998).

365. Manabe, R. I., Oh-E, N., Maeda, T., Fukuda, T. & Sekiguchi, K. Modulation of cell-adhesive activity of fibronectin by the alternatively spliced EDA segment. *J. Cell Biol.* **139**, 295–307 (1997).

366. Fukuda, T. *et al.* Mice lacking the EDB segment of fibronectin develop normally but exhibit reduced cell growth and fibronectin matrix assembly in vitro. *Cancer Res.* **62**, 5603–5610 (2002).

367. Chen, W. & Culp, L. a. Adhesion mediated by fibronectin's alternatively spliced EDb (EIIIB) and its neighboring type III repeats. *Exp Cell Res* **223**, 9-19. (1996).

368. Nishiuchi, R. *et al.* Ligand-binding specificities of laminin-binding integrins: A comprehensive survey of laminin-integrin interactions using recombinant α3β1, α6β1, α7β1 and α6β4 integrins. *Matrix Biol.* **25**, 189–197 (2006).

369. Perez-riverol, Y. *et al.* The PRIDE database and related tools and resources in 2019 : improving support for quantification data. **47**, 442–450 (2019).

370. Kim, D., Langmead, B. & Salzberg, S. L. HISAT: a fast spliced aligner with low memory requirements. *Nat. Methods* **12**, (2015).

371. Robinson, M. D., Mccarthy, D. J. & Smyth, G. K. edgeR: a Bioconductor package for differential expression analysis of digital gene expression data. *Bioinformatics* **26**, 139–140 (2010).

372. Law, C. W., Chen, Y., Shi, W. & Smyth, G. K. voom: precision weights unlock linear model analysis tools for RNA-seq read counts. *Genome Biol.* 1–17 (2014).

373. Zhang, Z. *et al.* Novel Data Transformations for RNA-seq Differential Expression Analysis. *Sci. Rep.* **9**, 1–12 (2019).

Publishing Agreement

It is the policy of the University to encourage open access and broad distribution of all theses, dissertations, and manuscripts. The Graduate Division will facilitate the distribution of UCSF theses, dissertations, and manuscripts to the UCSF Library for open access and distribution. UCSF will make such theses, dissertations, and manuscripts accessible to the public and will take reasonable steps to preserve these works in perpetuity.

I hereby grant the non-exclusive, perpetual right to The Regents of the University of California to reproduce, publicly display, distribute, preserve, and publish copies of my thesis, dissertation, or manuscript in any form or media, now existing or later derived, including access online for teaching, research, and public service purposes.

DocuSigned by:
Mara Ariel Kauss
FC0D5CB41CE74D3...
Author Signature

8/29/2020
Date